LARGE SCALE PARAMETER ESTIMATION THROUGH THE INVERSE PROCEDURE AND UNCERTAINTY PROPAGATION IN THE COLUMBUS BASIN, NEW MEXICO

by

T. Neil Blandford

Submitted in Partial Fulfillment
of the Requirements for the
Degree of Master of Science

NEW MEXICO INSTITUTE OF MINING AND TECHNOLOGY

Socorro, New Mexico

June, 1987

ACKNOWLEDGMENTS

I would like to thank my friend and advisor Dr. John Wilson for his help and guidance throughout the course of this work. Swen Magnuson wrote many of the preprocessors used during this study and conducted the parameter estimation over zones analysis; his contribution is gratefully acknowledged. Dr. John Hawley generously provided data and insights regarding the geology and hydrology of the Columbus Basin region. Dr. Allan Gutjahr was a great help during the geostatistical phase of this research.

Thanks are due to Debbie Hathaway and Louise Putnam of the State Engineer Office for providing information during the early phases of this project. Lee Case, Roger Miller, and others of the USGS (Albuquerque) also provided useful information. In particular, John McLean's detailed review of this manuscript is appreciated.

Debbie Brook typed and edited many editions of this manuscript and her efforts are greatly appreciated.

Finally, I would like to thank my wife, Diana, for her continual support.

This project was funded by the U.S. Geological Survey through the New Mexico Water Resources Research Institute under contracts 14236356 and 1423652, and by the U.S. Department of Energy Thesis Research Program on Nuclear Waste Management (funds administered through Argonne National Laboratory).

ABSTRACT

Estimates of the aquifer parameters storativity, transmissivity, boundary heads and fluxes were made for the Columbus Basin, New Mexico. A two-dimensional groundwater flow code called CERT was used. CERT employs a non-linear unconstrained generalized weighted least squares minimization algorithm to obtain optimal aquifer parameters from historic observations of hydraulic head. An initial or prior estimate of the aquifer parameters was obtained using kriging and other geostatistical tools. The record of historic observed head data from 1930 to 1975 was used for the least squares fit. Optimal parameter estimates for transmissivity, storativity and fluxes were reasonable. Nodal and zoned values of the parameters were estimated. The algorithm had difficulty estimating realistic boundary heads for conceptualization and data for the Columbus Basin.

A validation study of CERT was conducted by estimating transmissivity and/or nodal fluxes using portions of the observed head data set divided in space or time. A posterior linearized estimate of the parameter covariance matrices was also conducted. These results were used as input to the uncertainty propagation algorithm coded into CERT, and predictions of heads and head standard deviations were made over the time period 1930 to 1975. Model heads matched well with observed heads when the model input parameters were conditioned only on a portion of the observed head data. Values of the standard deviation on heads were reasonable once boundary node correlation was accounted for.

Key words: groundwater, water management, modeling, parameter estimation, inverse problem, uncertainty, finite elements

TABLE OF CONTENTS

Table of Contents (con't.)

Table of Contents (con't.)

Table of Contents (con't.)

LIST OF TABLES

LIST OF FIGURES

List of Figures (con't.)

List of Figures (con't.)

List of Figures (con't.)

List of Figures (con't.)

List of Figures (con't.)

List of Figures (con't.)

List of Figures (con't.)

List of Figures (con't.)

List of Figures (con't.)

List of Figures (con't.)

List of Figures (con't.)

INTRODUCTION

The primary purpose of this research was to conduct a validation study of CERT; a computer code for two-dimensional groundwater flow modeling and parameter estimation which includes a methodology for unCERTainty propagation (Townley and Wilson 1985). An ancillary purpose of this research was to provide usable aquifer parameter estimates and an enhanced knowledge of a groundwater flow system somewhere in New Mexico. The regional aquifer in the vicinity of Columbus, New Mexico was chosen as the study area because an extensive record of water level measurements was available, a fair amount of aquifer conductivity data was available and the groundwater flow was thought to be approximately two-dimensional. The modeled area, located along the U.S.-Mexico border, and important geographic features are shown in figure 1.

The validation study consisted of three main parts. First, data and information pertaining to the geology and hydrology of the Columbus area and adjoining regions was collected. The information was analyzed and digitized where appropriate. Next the parameter estimation algorithms in CERT were used to identify the aquifer parameters storativity, transmissivity, and boundary fluxes and heads. A posterior covariance estimation on the model estimated parameter set was conducted in some cases. This posterior covariance estimation gave an indication of 'how good' the model estimated parameters were. The results of the parameter estimation efforts for each of the four parameter types are presented individually in the following chapters. Finally, the observed head data set was divided in time and space and parameter estimates were made using the observed head sub-sets. These parameter estimates (and estimates of their uncertainty) were then input to CERT uncertainty propagation runs, and predictions of model heads and head

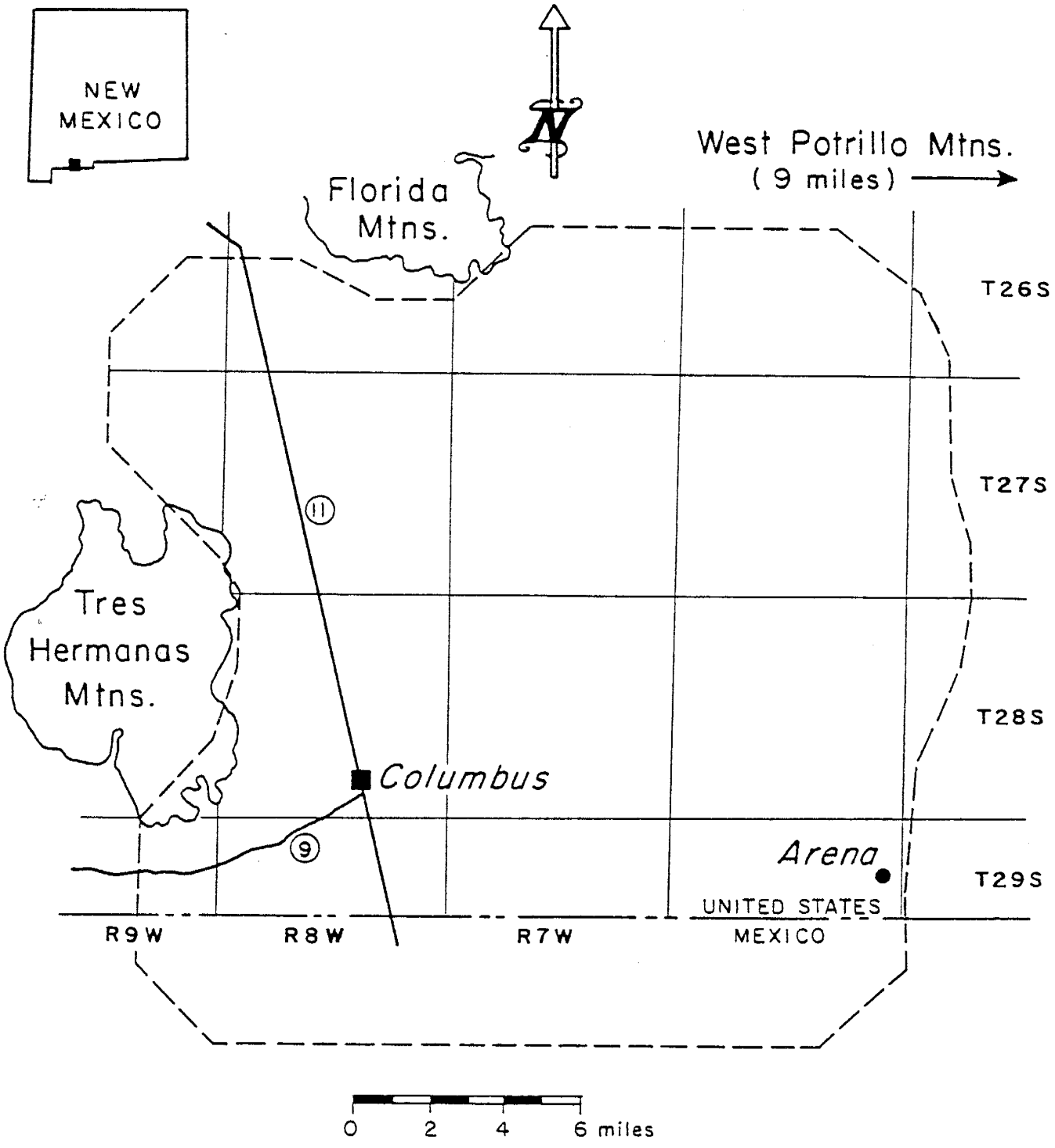

Fig. 1. Location map of Columbus Basin and important geographic features. Dashed line indicates model grid boundary.

uncertainties were made. The model heads were then compared to the observed heads at measurement locations throughout the Columbus Basin.

The Columbus Basin study is an ongoing project which will continue after publication of this report. Although new insights pertaining to the hydrogeology of the basin were gained through this modeling study, some as yet unanswered questions were raised as well. A primary directive of future research will be a more detailed investigation into the nature of the basin's storage parameters and boundary conditions.

LITERATURE REVIEW

There has been a proliferation of papers addressing the inverse parameter estimation problem over the past twenty years. Neuman (1973) divided the two categories of methods into "direct" and "indirect" approaches. Direct methods require the calculation of head gradients from observed heads over the modeled domain. Combining the derivative information with the appropriate boundary conditions it is in some cases possible to solve for the unknown parameters directly using the governing partial differential equation. Indirect approaches compare aquifer model output with observed heads and if the sum of the residuals is too large the aquifer parameter values are changed until some convergence criteria is met. The objective function to be minimized is most commonly the sum of (weighted) least squares with an added term for stabilization purposes. The computer code CERT (Townley 1983 and Townley and Wilson 1985) embodies an indirect approach to the inverse problem. Yeh (1986) provides a detailed summary of previous and current inverse problem techniques.

Examples of large scale inverse parameter estimation models successfully applied to natural systems are relatively rare. Neuman and Yakowitz (1979), Neuman et al. (1980), Cooley (1979, 1983), and Cooley et al. (1983) applied inverse procedures to model steady state systems. Better parameter estimates should be obtained for a transient system (Wilson and Dettinger 1979), but examples of such models are few. Carrera and Neuman (1986) present one of the most significant works to date.

There are several obvious "gaps" in reported research which this study was designed to address. First of all, most of the inverse algorithms presented thus far are only capable of estimating one or two of the parameters which affect the flow model. The estimation of boundary

conditions has almost universally been neglected, although Wilson and Harper (1983) did address this issue using CERT. Secondly, one of the advantages of many of the inverse algorithms used currently is that a linearized estimate of the uncertainty of the posterior parameters can be made. This posterior uncertainty estimate lends itself well to uncertainty propagation algorithms, but reported examples of uncertainty propagation studies are relatively few (e.g. Wilson et al. 1979 and Townley 1983) and more research is needed. Finally, the issue of inverse model validation has not been previously addressed. The primary goal of this research was to look at the model validation issue. Specifically, model parameters were estimated through the inverse procedure using some portion of the available observed head data, and then model heads obtained using these parameters were compared to the withheld observations. An uncertainty propagation algorithm was subsequently used to obtain error bounds on the predicted heads.

OVERVIEW OF CERT CAPABILITIES AND SOLUTION ALGORITHMS

General Flow Equation and Boundary Conditions

The flow code in CERT is a Galerkin finite element algorithm which utilizes linear triangular elements. The two-dimensional, vertically integrated groundwater flow equation modeled is:

$$\frac{\partial}{\partial x}\left(T \frac{\partial h}{\partial x} \right) + \frac{\partial}{\partial y}\left(T \frac{\partial h}{\partial y} \right) + Q = S \frac{\partial h}{\partial t} \qquad (1)$$

where:

- $h(x,y,t)$ = piezometric head [L]
- $T(x,y)$ = transmissivity [L^2/T]
- $S(x,y)$ = storage coefficient [L/L]
- $Q(x,y,t)$ = source/sink term [L/T]
- x,y = cartesian coordinates [L]
- t = time

The parameter T in equation (1) is a vertically integrated permeability:

$$T = Kb \qquad (2)$$

where:

- K = effective horizontal hydraulic conductivity [L/T]
- b = saturated thickness [L]

The boundary conditions for equation (1) are written in a generalized form. The term "generalized boundary condition" refers to a single equation from which the three boundary types can be derived. The boundary equation

is

$$(-T\nabla h) \cdot \vec{n} = \frac{K'W'}{B'} (h^* - h) + \delta \left[\frac{K'W'}{B'} \right] q^* \qquad (3)$$

where $\vec{n}$ is a unit inward pointing vector normal to the boundary, $K'W'/B'$ is a leakage coefficient, h^* is some known piezometric head and q^* is a known flux into the aquifer. The function δ has the value of unity when $K'W'/B'$ is zero, and is zero otherwise. To simplify notation the following representations are defined:

$$A = \frac{K'W'}{B'} \qquad (4)$$

and

$$B = \begin{cases} h^* \text{ if } A \neq 0 \\ q^* \text{ if } A = 0 \end{cases} \qquad (5)$$

A and B are the two boundary parameters implemented into CERT. B is time varying, A is not.

The three standard boundary types are derived as follows. If A is zero, B simply becomes a flux value, and the boundary is a second type, known flux or Neuman boundary. If A is non-zero, h^* must be specified and the boundary is a third type, mixed or Cauchy boundary condition. A first type, constant head or Dirichlet boundary condition is obtained when the A parameter approaches infinity (in practice this boundary type is obtained by setting A equal to some large finite number). In this case h^* is the prescribed head value.

The finite element formulation of equation 1 is discussed in detail by Wilson et al. (1979). A discussion of the generalized boundary condition

and its implementation can be found in Townley (1983) and Townley and Wilson (1985).

Generalized Weighted Least Squares Procedure

CERT uses a generalized weighted least squares (WLS) algorithm to obtain optimal aquifer parameter estimates. The algorithm is based upon the minimization of the following objective function:

$$\min_{\hat{\underline{u}}} J(\hat{\underline{u}}) = \sum_{k=0}^{N} [\underline{H}(k)\hat{\underline{h}}(k) - \underline{h}(k)]^T \underline{R}^{-1}(k)[H(k)\hat{\underline{h}}(k) - \underline{h}(k)]$$

$$+ [\hat{\underline{u}} - \underline{u}]^T \underline{U}^{-1}[\hat{\underline{u}} - \underline{u}] \qquad (6)$$

where:

J = objective function (scalar)

$\underline{H}$ = sparse interpolation matrix of nodal values onto observation points

$\hat{\underline{h}}$ = vector of model calculated nodal heads

$\underline{h}$ = vector of observed heads

$\underline{R}$ = covariance matrix of observed heads

$\hat{\underline{u}}$ = vector of model parameters

$\underline{u}$ = vector of observed parameters

$\underline{U}$ = covariance matrix of parameters

k = time index

N = total number of time steps

The superscript T denotes the transpose of the matrix.

The objective function, J, in the above equation is composed of two parts - a 'head' part (J_h) and a 'parameter' part (J_u).

$$J = J_h + J_u \tag{7}$$

Both portions of J are time dependent. It is desirable to know the values of J_h and J_u as well as J.

The sparse interpolation matrix $\underline{H}(k)$ contains the integration weights of elements which contain a head measurement (observation) point. When $\underline{H}(k)$ is multiplied by $\hat{\underline{h}}(k)$, the model calculated heads are interpolated onto the measurement points inside specified elements. This procedure allows the model calculated heads to be compared directly to the vector of observed heads, $\underline{h}(k)$. With this methodology the observed head values do not have to be interpolated onto the model grid nodal points.

The squared differences between the model calculated and observed heads are weighted by the inverse of the observed head covariance matrix, $\underline{R}$. Hence the head observations assigned a high variance are given a small weight during the minimization procedure. In theory, $\underline{R}$ could be banded or full, but in practice it is often diagonal since head measurement errors are generally considered uncorrelated (statistically) in space.

The vector of observed, or prior, parameter values can be defined at nodal points, over individual elements, or over groups (zones) of elements. The method of generalized kriging is commonly used to assign spatially varying data (e.g. T or S) to specified points or zones, and it is especially suited to CERT's methodology because Kriging variances and covariances can also be easily calculated. Therefore portions of the prior parameter covariance matrix, $\underline{U}$, are often banded or full in practice. It may be difficult to derive spatial or temporal correlation relationships for some model parameters (e.g. the 'B' boundary parameter), and therefore the portions of $\underline{U}$ which correspond to these parameters are often diagonal.

The minimization of equation 6 is performed using a numerical non-linear unconstrained search procedure in u parameter space (u = number of uncertain parameters). Many methods have been developed to solve this problem, and a description of those coded into CERT can be found in Luenberger (1984), and Townley and Wilson (1985). Briefly, the most efficient non-linear search algorithms are those which belong to a category called quasi-Newton methods. Quasi-Newton methods utilize full first derivative information combined with approximated second derivative information. The Davidon-Fletcher-Powell method was used to minimize J for the WLS parameter estimation runs in this report.

The minimization of J is an iterative procedure and therefore it is necessary to specify some convergence criterion. When the difference between successive values of J is smaller than the convergence criterion, the minimization process is stopped and the "optimal" parameter estimates can be examined. The multi-level convergence criteria presented by Townley and Wilson (1985) was used initially for all runs in this report. Some simulations which ran for excessive periods of time were stopped and restarted with a larger specified convergence criterion (usually 1.0) to insure their convergence upon the next iteration.

Uncertainty Propagation

Once the optimal $\underline{u}$ is found from equation 6, a linearized estimate of its accuracy is given by the covariance

$$\underline{P}_{uu} = E\{[\underline{u} - E(\underline{u})]\ [\underline{u} - E(\underline{u})]^T\}$$

$$= \left\{ \sum_{k=0}^{N} \left[\underline{H}(k) \frac{d\underline{h}(k)}{d\underline{u}^T} \right]^T \underline{R}^{-1}(k) \left[\underline{H}(k) \frac{d\underline{h}(k)}{d\underline{u}^T} \right] + \underline{U}^{-1} \right\}^{-1} \qquad (8)$$

where E{ } is the expected value. Using this posterior estimate of the parameter covariance matrix a covariance matrix for the model calculated heads can be obtained from

$$\underline{P}_{hh}(k) = \left[\frac{d\underline{h}(k)}{d\underline{u}'}\right] \underline{P}_{uu} \left[\frac{d\underline{h}(k)}{d\underline{u}'}\right]^T \tag{9}$$

given that $\underline{h}(k)$ is a function of the uncertain parameter set $\underline{u}$ only (Dettinger and Wilson 1981), or by other specialized means (Townley and Wilson 1985). Using this methodology CERT not only can calculate an optimal parameter set $\underline{u}$ and the heads $\underline{h}$ which result from those parameters, but it can also calculate an uncertainty (in terms of a variance) associated with the predicted heads. The CERT user's manual (Townley and Wilson 1985) provides several examples of uncertainty propagation, as does Townley (1983), Townley and Wilson (1983), and Wilson and Harper (1983).

CLIMATE

The Columbus Basin is characterized by an arid climate. Records of the Columbus weather station indicate the mean annual rainfall to be 9.2 inches, with about 65 percent of the rainfall occurring during the months of July, August, September and October. Gabin and Lesperance (1977), using the Blaney-Criddle method with a crop coefficient for alfalfa, calculated potential evapotranspiration for the Columbus area to be 52.85 inches per year, thereby leaving a water budget deficit of 44 inches per year. This large deficit is exemplified by the fact that there are no perennial streams in the Columbus Basin.

Mean monthly temperatures for Columbus range from 43° F in January to 81° F in July, with a mean annual temperature of 61.7° F. The high and low daily temperatures, however, show significant variation about these mean values.

GEOLOGY

The Columbus Basin is located in the Basin and Range physiographic province of the United States. Much of the area to be modeled is underlain by the Mimbres Graben or Basin (the word "basin" here is used in a geological, not hydrological, sense) which has a north-south orientation. The Florida and Tres Hermanas mountains (see figure 1), and the uplift which forms the base and flanks of the West Potrillo Mountains, are north-south aligned range features which lie on the east and west sides of the graben respectively. Swanberg et al. (1981) deduced the location of the western fault using gravity profiling, and the eastern fault, which is known as the Camel Mountain Fault, has a clearly defined surface expression (figure 2). The extensional faulting that is responsible for the basin and range structure of the region is Quaternary or possibly Neogene in age (Swanberg et al. 1981 and Cordell 1978).

The basin and range structure is complicated somewhat in that it is superimposed on older northwest-southeast trending high angle faults, thought to be boundary faults in the Laramide overthrust structure of the region (Seager 1983). Strike slip along the boundary faults probably accounts for the apparent lateral offset between the Florida and Tres Hermanas ranges.

The mountain rocks and sediments that compose the ranges and intermontane basin fill (bolson) of the Columbus region exhibit a diverse lithology (figure 2). The Tres Hermanas Mountains consist primarily of Tertiary andesite, quartz monzanite, rhyolite, latite and conglomerate (Seager 1982). The southern portion of the Florida Mountains consist of Precambrian granite, syenite and quartz syenite, and Ordovician and Silurian

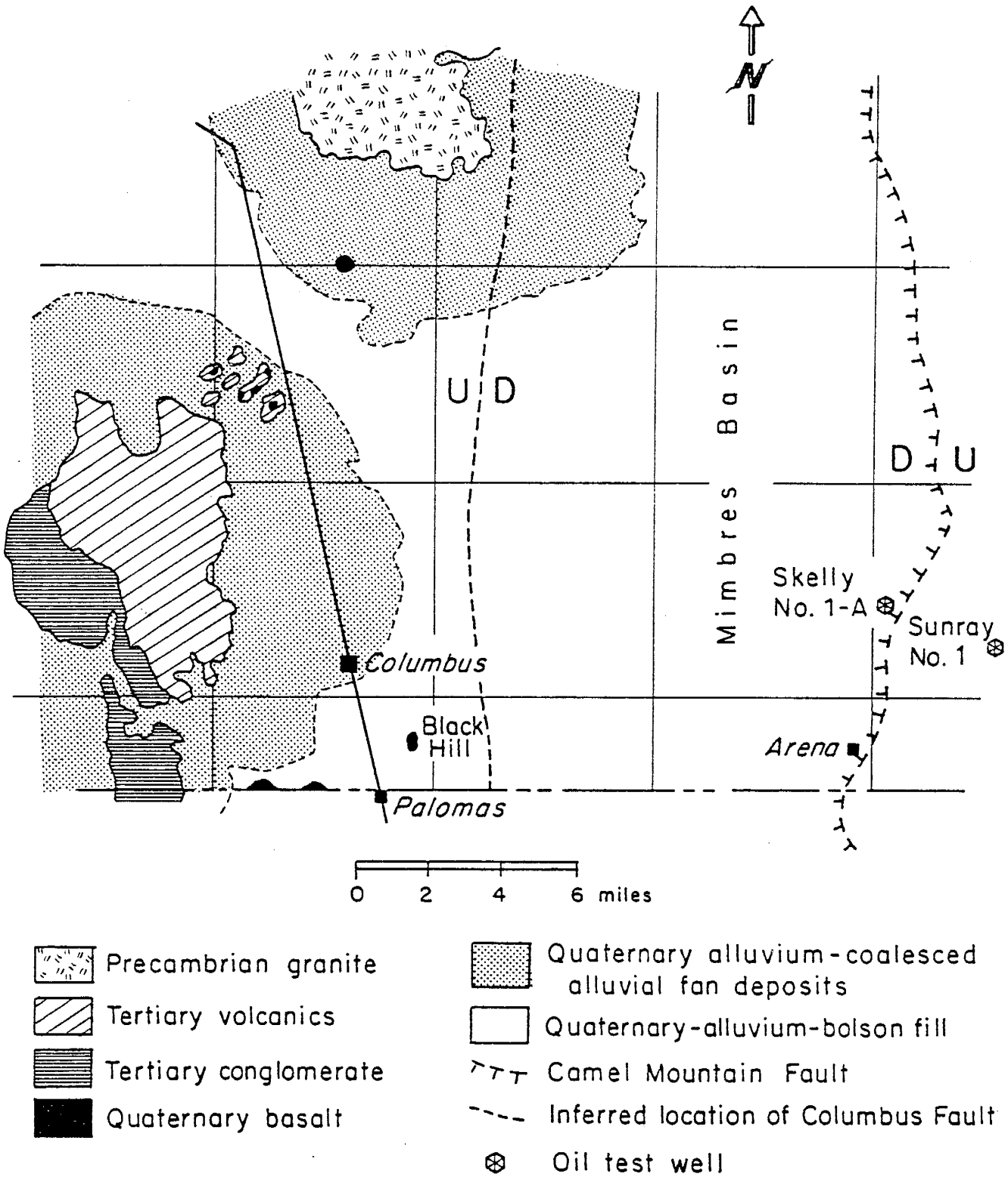

Fig. 2. Simplified geologic map of the Columbus Basin.

dolomites (Clemons et al. 1983 and Darton 1916). Dikes of varying lithology and faults are also common in the aforenamed ranges.

The rock types that compose the western flanks of the West Potrillo Mountains are somewhat obscure. The Camel Mountain Fault has a surface expression on the east side of the Mimbres Basin, but the aggregate Quaternary basalt flows, that form the West Potrillos, outcrop about 8 mi farther east. The surficial deposits between these two landmarks consist of bolson fill type material, but the thickness of the Quaternary sediment is uncertain. Kottlowski et al. (1969) report a bolson fill thickness of 520 ft at the Sunray No. 1 test hole (figure 2). Several small masses of intrusive igneous rocks outcrop through the Quaternary sediment in this area. Basalt flows of the West Potrillo Mountains probably extend westward beyond their surface exposures and are covered by a thin veil of alluvium, however there is no indication that they extend to the fault boundary. It is also important that the West Potrillo Mountains in themselves are not a range feature; a considerable portion of their relief is due to the constructional process of piling up volcanic ejecta and basalt flows (King et al. 1971). The quaternary basalts and alluvium probably overlie a horst feature, however, and the question becomes what type of geology exists below the relatively thin veil of alluvium and basalt. The answer to this question is unknown, but King et al. (1971) postulize:

> ...It is not known whether the basalts are underlain by a thick section of basin fill deposits or by Tertiary and other bedrock units. Isolated exposures of middle Tertiary volcanic rocks and older sedimentary rocks on the flank of the West Potrillo Mountains do indicate that the latter alternative is probably more likely.

The intermontane basin fill, which is primarily alluvial in nature, is often referred to as "bolson fill" and consists of layered gravels, sands, silts and clays. Conspicuous alluvial fans flank the Tres Hermanas and Florida ranges (figure 2). In addition to ephemeral drainages originating in the highlands surrounding the Columbus Basin, the Mimbres River has deposited fluvial sediments in the basin as well. In the recent geologic past the river flowed into the Columbus Basin through the gap between the Tres Hermanas and the Florida mountains (Hawley 1975), but the present course of the river terminates in a shallow depression north of the Columbus Basin and east of the Florida Mountains. River water reaches this point, however, only when rainfall is exceptionally heavy (Darton 1916).

Basalt flows, generally 10 to 90 ft thick, are common on the western fault escarpement of the Mimbres Basin, especially in the vicinity of Columbus. Basalt layers are not discernible from well logs within the Mimbres Basin; flows possibly exist but have been vertically displaced to such a degree that they are not penetrated by wells. Several small surface exposures of basalt occur in the Columbus region, the most notable of which is Black Hill, two miles southeast of Columbus. The basalt flows and interbedded bolson sediments are late Tertiary in age (Seager et al. 1984).

The thickness of the bolson fill varies with proximity to the ranges and depth of the down-faulted basement rock. Wilkins (report in press) used seismic data to estimate bolson fill thicknesses in the Columbus area. His interpretations are presented in figure 3, which is reproduced from his report. The deepest fill sequences reported by Wilkins, about 3000 ft, occur in the Mimbres Basin. However, the Skelly No. 1A test well (figure 2) reportedly penetrated over 4500 ft of valley-fill sediments at the eastern margin of the Mimbres Basin (Kottlowski et al. 1969). Perhaps the discrepancy is due to the uncertain nature of geophysical methods. Wilkens

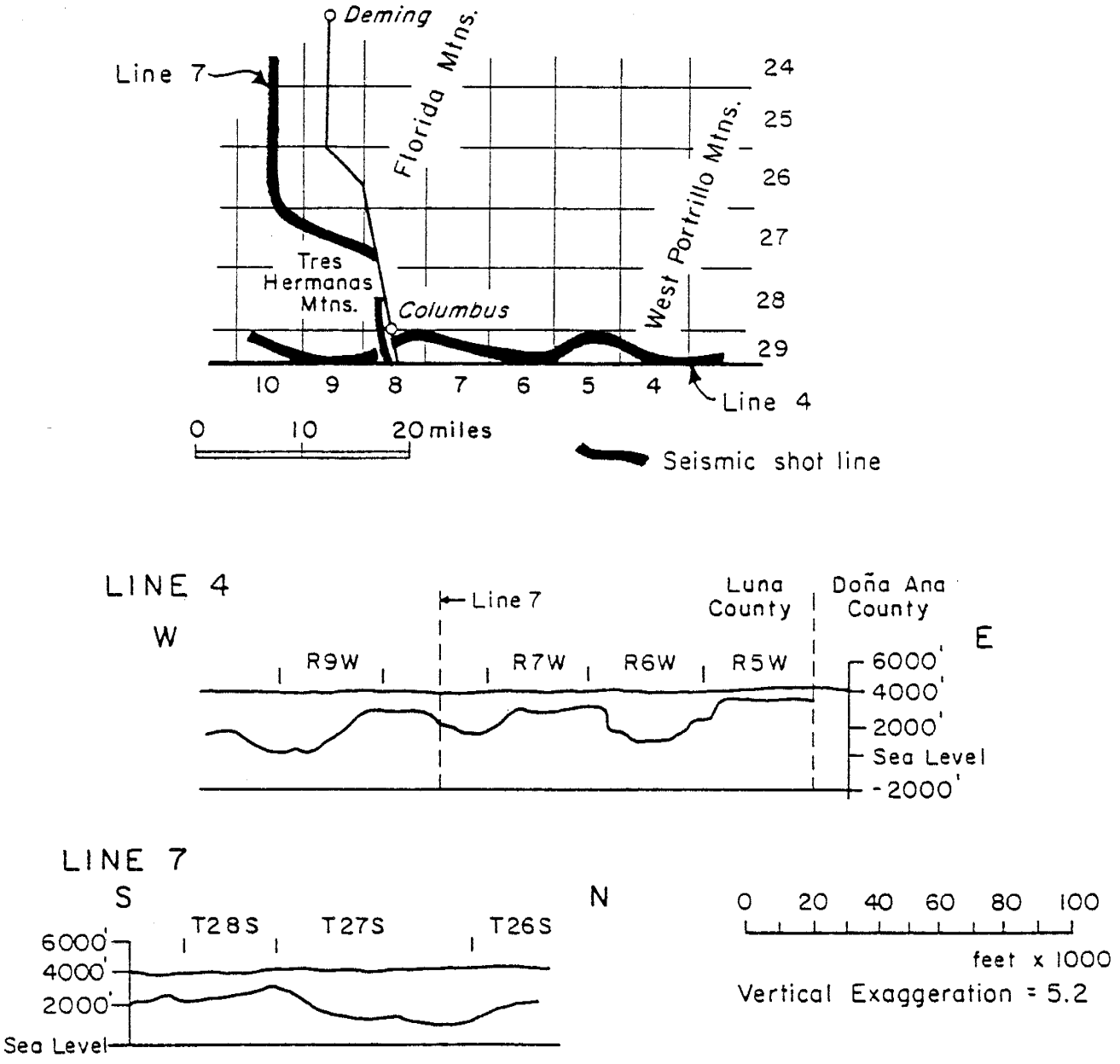

Fig. 3. Location of seismic shot lines in Columbus area and corresponding interpretations from Wilkins (in press). Cross sections show approximate depth of alluvial sediments.

data also indicates the presence of a bedrock high in the center of the Columbus Basin, a contention that is supported by gravity data compiled by Birch (1980).

Reeves (1969) puts forth substantial evidence that indicates the existence of a Quaternary pluvial lake, Lake Palomas, which covered a large portion of the Columbus Basin. Hawley (1975) supports this contention and outlines an even larger portion of the Columbus Basin which has lake and playa deposits (figure 4). The existence of Quaternary pluvial lakes in the Columbus region would help to explain the massive clay layers found over much of the area, some of which are hundreds of feet thick.

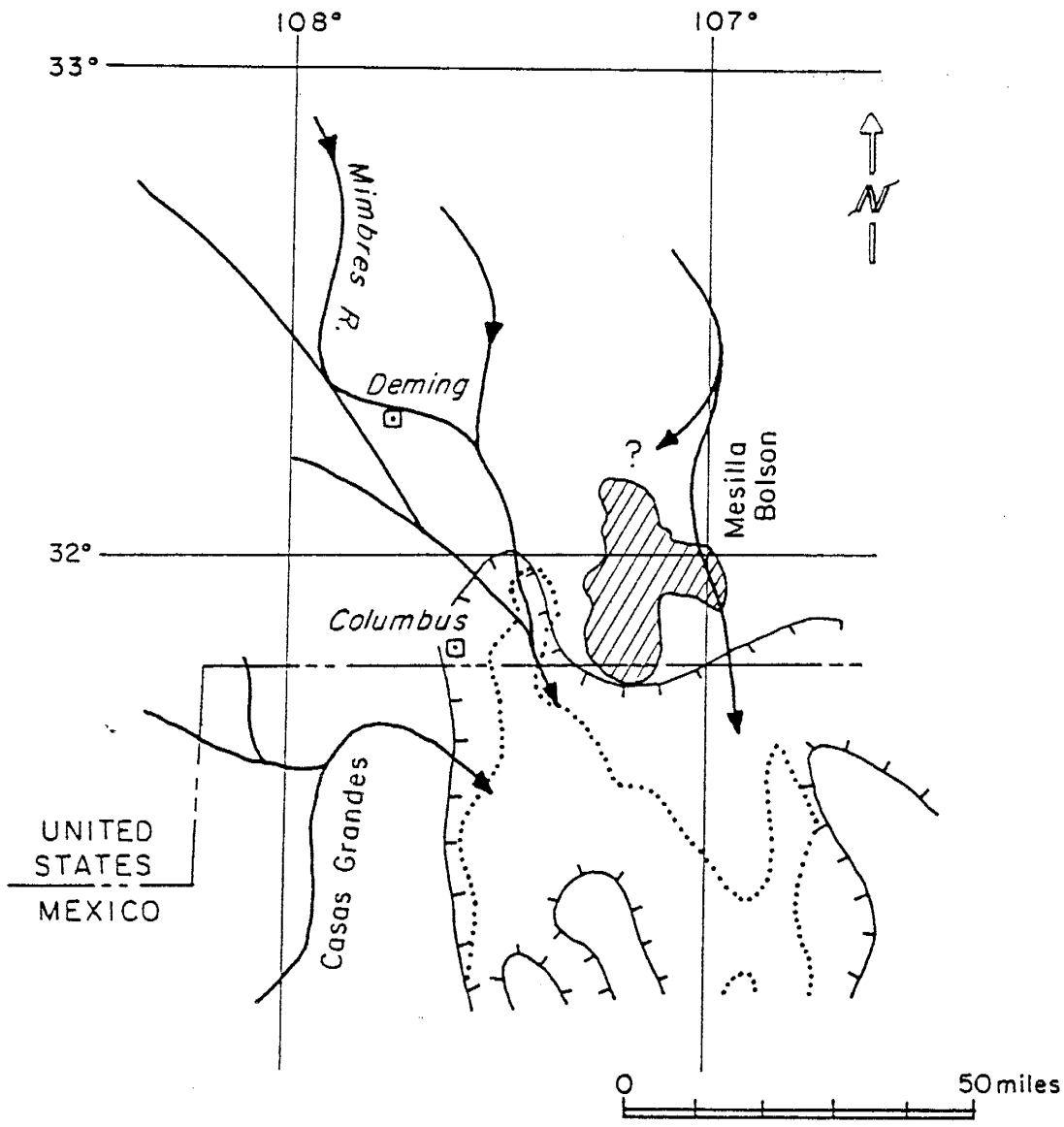

Fig. 4. Early and middle Quaternary paleodrainage, undrained depressions and pluvial lake basins of Columbus region (from Hawley, 1975).

HYDROGEOLOGY

General Flow Conditions

The bolson sediments of the Columbus Basin contain enormous amounts of groundwater. Due to its comparatively large porosity and permeability, most of the groundwater movement occurs within the bolson fill and not in the ranges, that are composed primarily of igneous rocks. For this reason, the mountains that partially outline the Columbus Basin are conceptualized as low permeability 'islands' that deflect and partially direct the flow field. Note that the ranges were not said to be no-flow hydrologic boundaries.

N. H. Darton (1916) was the first researcher to study the geology and hydrology of the Columbus Basin and large adjoining areas to the north in detail. He derived an equipotential map of the Columbus Basin which can be considered a steady state representation of the flow system (figure 5). The groundwater supply had not been developed substantially at that time (1911). If flow lines are drawn perpendicular to Darton's equipotential lines, the indicated flow within the basin is generally north to south. The Columbus Basin receives underflow from two sources; the gap between the Tres Hermanas and the Florida mountains that connects the Columbus bolson to the bolson centered about Deming, and the wide, gently sloping valley east of the Florida Mountains. Underflow travels out the southern end of the basin into Mexico and may at least partially discharge at a series of playas about 50 miles south of the international border. Although the flow system is believed to behave as described above, Darton's water-level map is subject to some reinterpretation. His data for the central and northern portions of the basin was sparse or nonexistent and many of the wells measured were quite shallow (<100 ft) and probably did not sample the primary aquifer of the Columbus Basin that is utilized today.

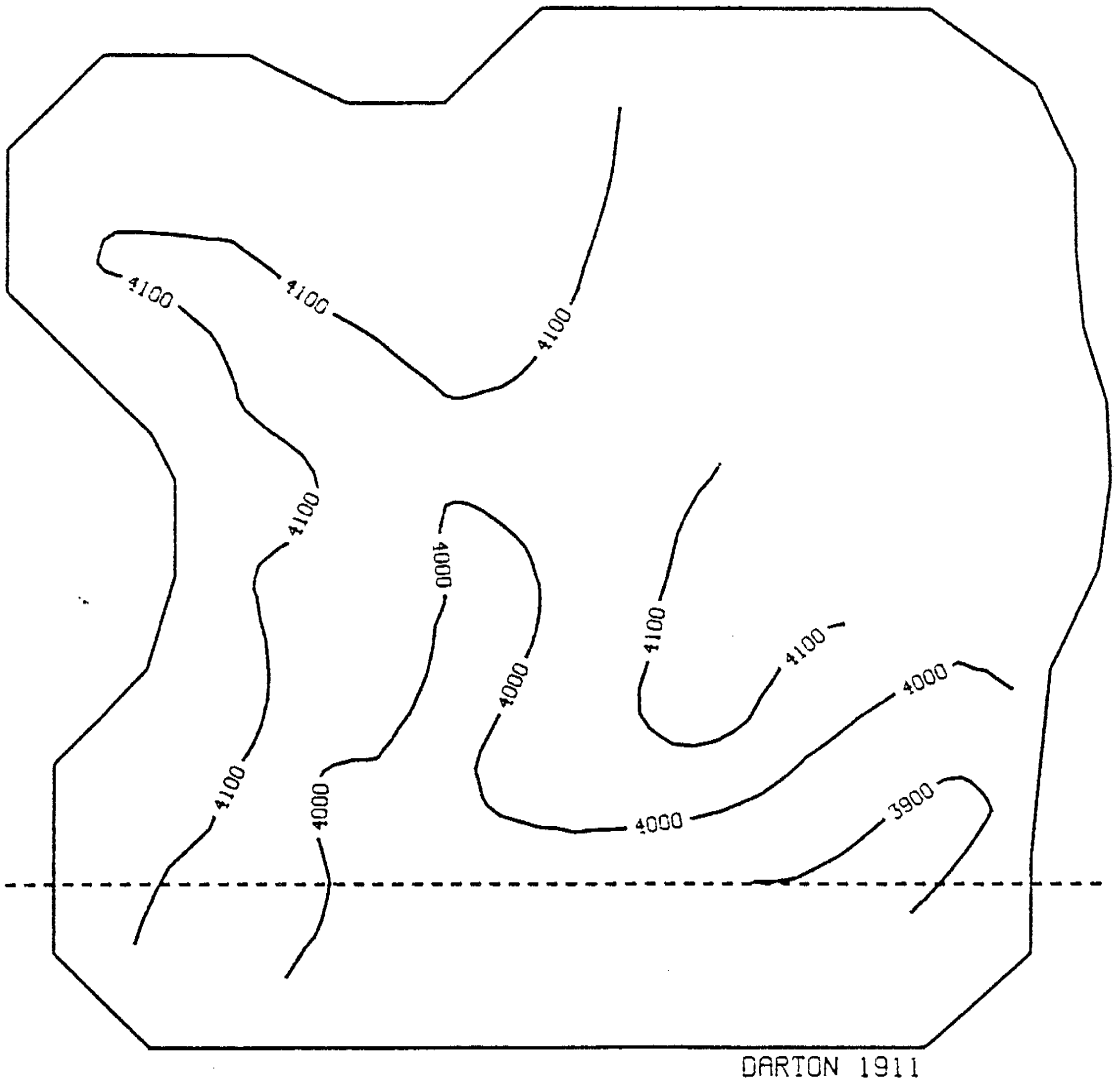

Fig. 5. Columbus Basin 1911 head field presented by Darton (1916).

Recharge

While discussing the groundwater resources of Luna County in general, Darton (1916) states that the infiltration of rainfall and the flows of the Mimbres River and San Vicente Arroyo are the major sources of recharge to the groundwater system. Because neither of the above streams support flow that reaches the Columbus Basin (with the possible exception of the Mimbres River after extreme freshets), it is clear that the major source of areal recharge for the Columbus Basin is rainfall. The rainfall that reaches the groundwater reservoir may do so in two ways; direct infiltration and mountain front recharge. The latter process is dominant. Darton (1916) states, "There is no run-off in the bolson except after cloud bursts, when small amounts of water may flow to the lower ground, where it either evaporates or sinks. On the mountain slopes there is considerable run-off which flows out upon the bolsons."

Mountain front recharge is a general term commonly used in hydrological studies of desert groundwater basins. It refers to the process in which mountain ranges serve as recharge areas for the groundwater reservoirs of the adjoining sediment filled basins. Due to their topographic relief the mountain ranges surrounding the desert basins receive greater amounts of rain and snow than does the adjacent valley floor. This water may recharge the valley aquifers in two ways. Rainwater or snowmelt may percolate into the fractured mountain rocks and under the influence of gravity eventually recharge the basin fill, or runoff from storms may flow out upon the bolson and infiltrate into the sediments directly. The rate of mountain front recharge is often considered to be independent of aquifer exploitation, but the precise estimation of this flux is difficult.

Groundwater Development

Although the groundwater resources of the Columbus Basin have been exploited since about 1910, the Columbus Basin did not experience major groundwater development until 1952 (New Mexico State Engineer 1956). The bulk of the groundwater withdrawn has been and is presently used for irrigation, but the town of Columbus also depends on groundwater for its municipal needs.

McLean (1977) constructed maps of hydraulic head decline in the Columbus Basin (see our figure 99, p. 194). The area just east of Columbus has exhibited the most extensive drop, about 140 ft as of 1970. This 'mining' of groundwater is to be expected, since only a small portion of the annual rainfall recharges the aquifer. The post-development cones of depression plotted by McLean also indicate that in addition to storage depletion, a source of water for wells in the Columbus Basin is reduced underflow toward the basin's southern boundary. The cone of depression has locally induced flow from south to north - the opposite of pre-development conditions. The quantity of reduced underflow is unknown.

Aquifer Storativity and Hydrostratigraphy

The major aquifer in the Columbus Basin is confined, but locally water table conditions may exist. The largest thicknesses of clay are reported in the logs of wells in the Mimbres Graben (log T27S.R6W.20 reports over 400 ft of continuous clay), but the majority of well logs west of the graben also indicate clay layers of 50 ft or more in thickness. Several cross-sections have been constructed from water well logs for different segments of the Columbus Basin (figure 6). These cross-sections were drawn with the hydrogeology of the basin in mind- not detailed geology. An examination of figures 7 through 9 shows a permeable aquifer of sand, gravel and basalt overlain by a thick confining layer throughout much of the basin. At

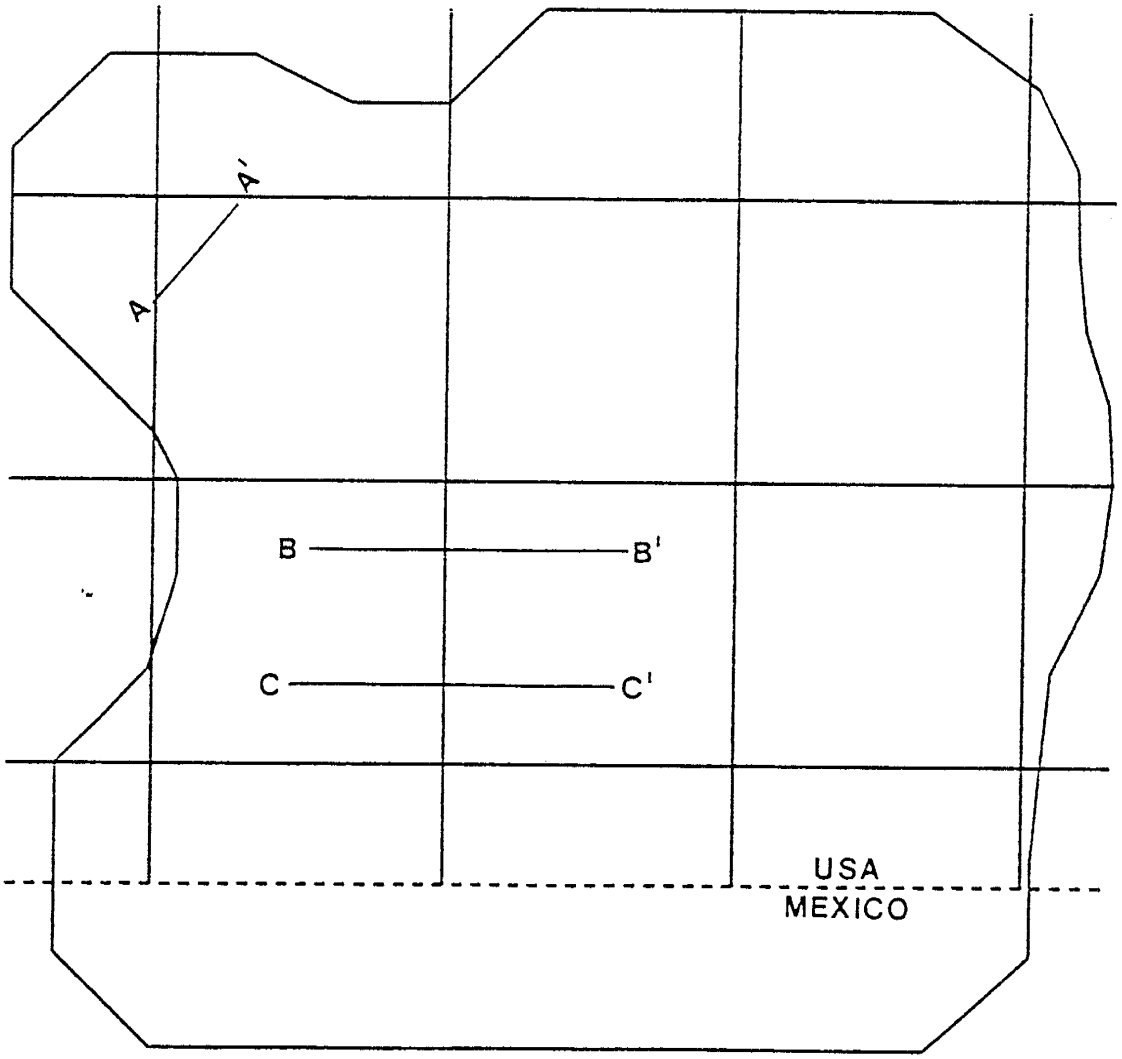

Fig. 6. Locations of hydrostratigraphic cross sections constructed for the Columbus Basin.

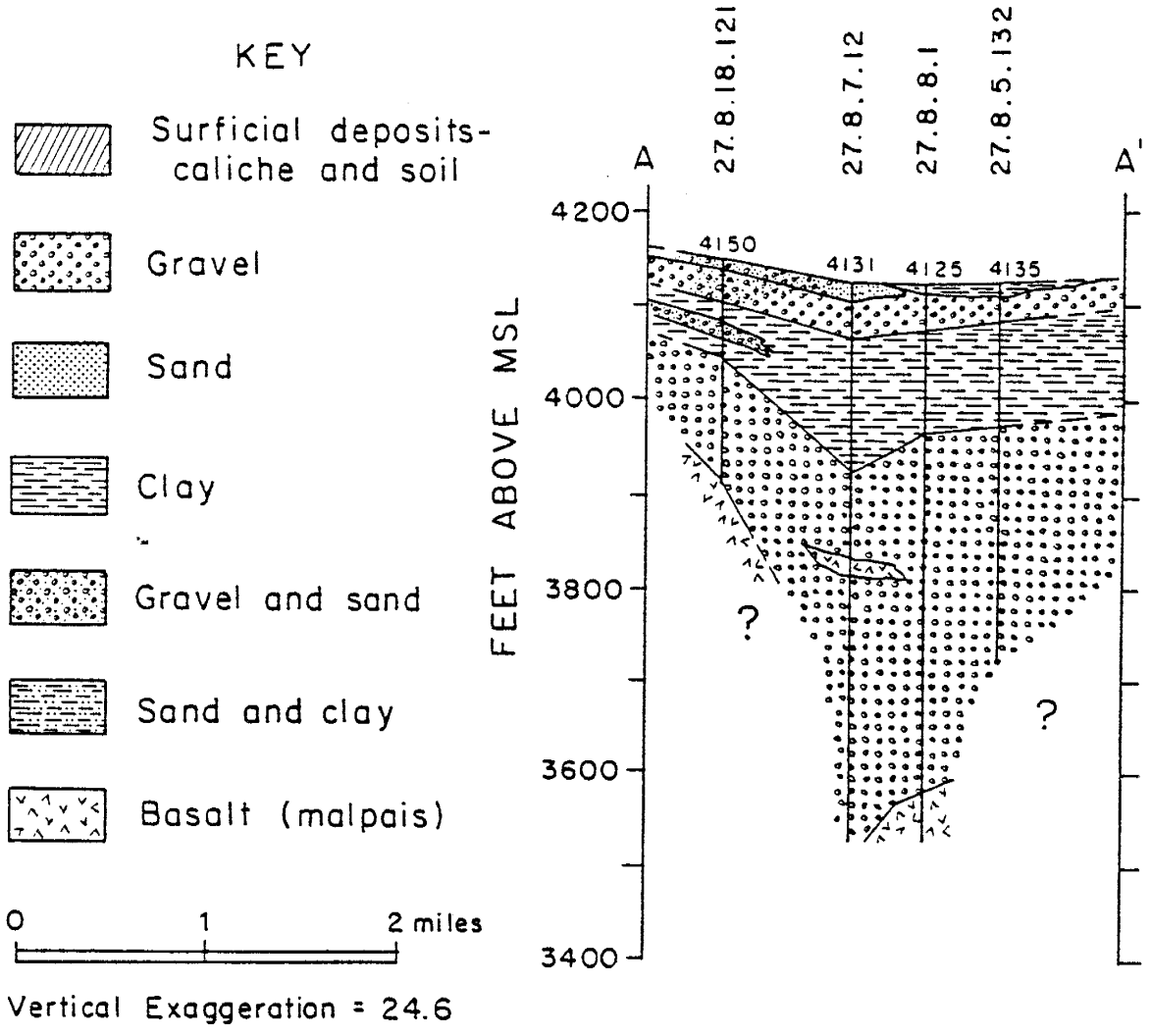

Fig. 7. Simplified geologic cross section A to A'.

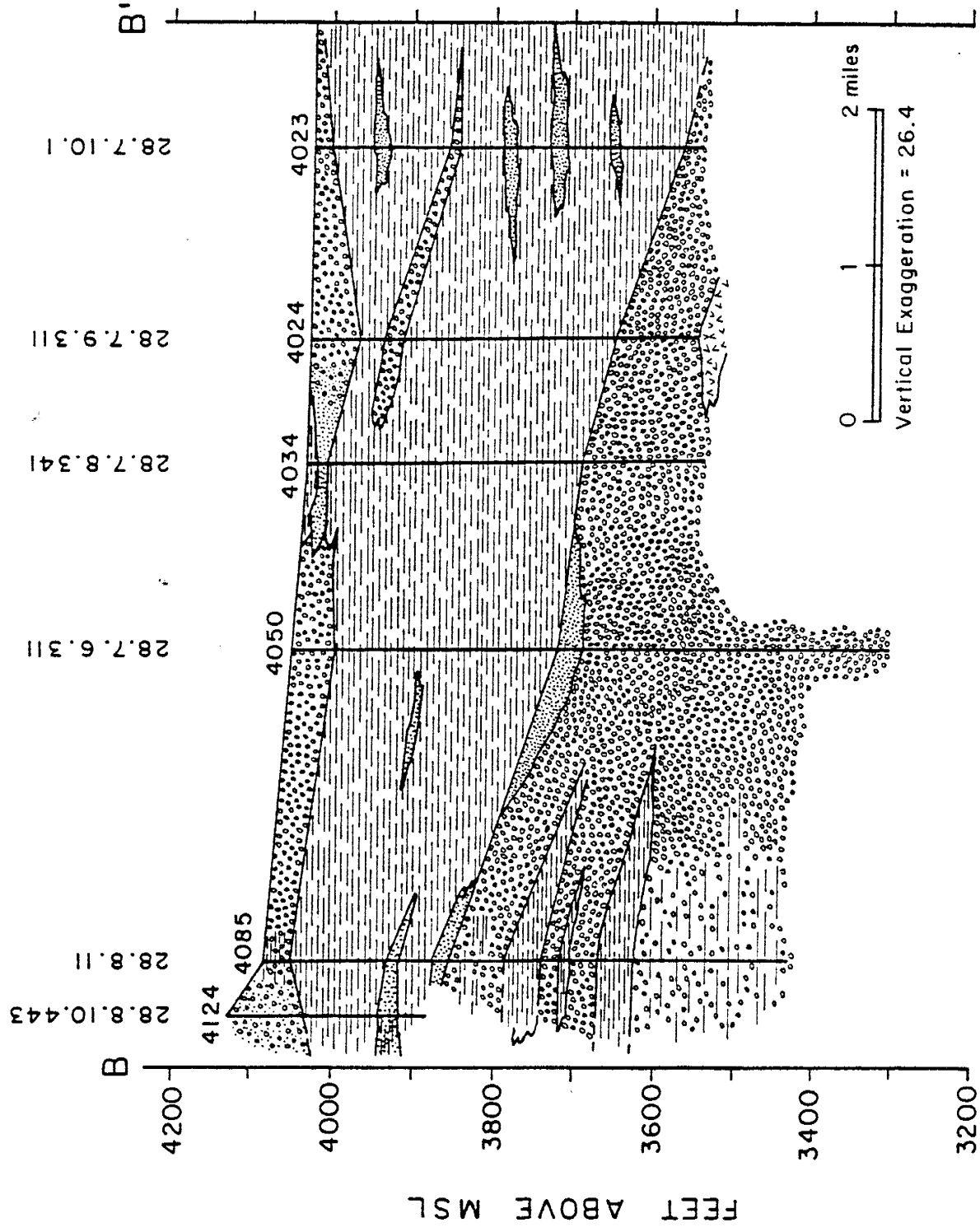

Fig. 8. Simplified geologic cross section B to B'.

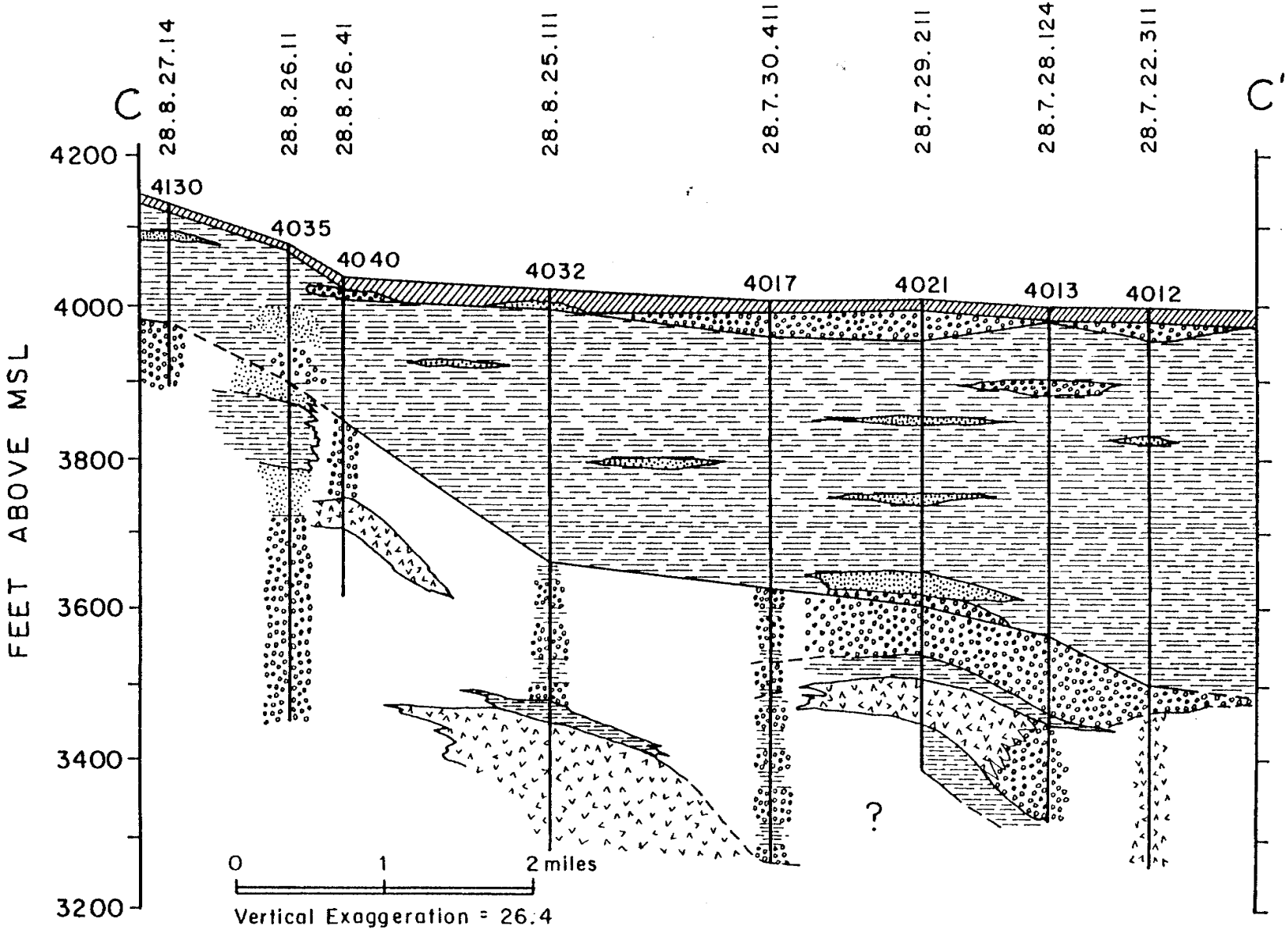

Fig. 9. Simplified geologic cross section C to C'.

several places in the basin, most notably at the western margin, the aquifer-aquitard sequence is not so clearly defined. In these areas the principal aquifer may be unconfined or partially confined.

Aside from the presence of clay layers, there is other evidence indicating confined flow in the Columbus Basin. In a report about groundwater in the vicinity of Arena (see figure 1), Doty (1969) observed that the water levels in two 700-foot-deep wells about 6 mi west of Arena had declined substantially within the period 1952 to 1969. The water level in one well had declined over 68 ft during this period, and the water level in the other declined over 136 ft. These declines occurred despite the fact that water in the Arena area was pumped for stock and domestic purposes only - these uses cause almost negligible stress on the bolson flow system. Doty comes to the conclusion:

> The water level changes in the two wells west of the Arena area probably reflect the effects of pumping for irrigation in the farmed area near Columbus about 4 miles to the west. The large water-level declines in these two wells suggest that the aquifers at depth beneath the Arena area are effectively confined so that the effects of pumping in the Columbus area may extend over wide areas in relatively short periods of time.

Comparisons of deep and shallow wells in the western portion of the basin also indicate a confined flow system. The shallow wells obtain water from relatively thin sand and gravel lenses which occur within or above the extensive confining layer. The deeper wells in this portion of the basin (approximately greater than 450 to 500 ft) tap the main aquifer (see figures 8 and 9). Early in the basin development, the measured head in the deep wells was greater than that in the shallow wells. This condition reversed itself in some areas as the water levels in the deep wells fell due to the

effects of pumping. Water levels in the shallow wells have remained essentially constant through time. Comparisons of the following pairs of hydrographs illustrate these observations: 26.7.26.224 with 26.7.24.424, 27.6.31.333 with 27.6.26.120, 27.7.31.231 with 27.7.31.411, and 28.6.10.311 with 28.6.2.212 (Appendix I).

Regrettably, there are no aquifer tests for the Columbus Basin for which a storage coefficient is indicated. Two aquifer tests were conducted north of the Columbus Basin (24.7.9.24112A and 25.6.3.121A) however, and these tests indicate storage coefficients on the order of 10^{-4}, which is a number indicative of confined conditions.

Two-Dimensional Flow Condition

Groundwater flow systems in arid fault-block basins, such as the Columbus Basin, are unquestionably three-dimensional. This three dimensional (3-D) nature of flow is most pronounced in the recharge and discharge areas of the system, which are the mountain ranges and the playas respectively. Because CERT is a two-dimensional (2-D) groundwater flow model, it makes little sense to use it in a 3-D flow situation. For this reason, the finite element grid boundaries were placed in such a way as to minimize inclusion in the solution domain of highly 3-D flow areas. This task was simplified by the fact that a playa does not exist in the Columbus Basin. The model grid does extend approximately five miles south of the border into Mexico (to assure that the cone of depression about Columbus did not intersect the grid edge), but this southern grid boundary is still tens of miles north of possible discharge areas of the flow system. The boundary nodes along the Tres Hermanas and Florida mountain ranges were positioned at the mountain/alluvial fan junction as determined from a topographic map. Groundwater flow near these boundaries may contradict the 2-D assumption

somewhat, but it was not believed that the error incurred would have a major effect on the numerical simulations.

At certain locations within the modeled area it was possible to check the 2-D flow assumption by comparing the hydrographs of wells that are close to one another but have different depths. If the heads in both wells were approximately the same, then the equipotentials were nearly vertical and the 2-D flow assumption was a good one for that region. One must keep in mind, however, that most wells in the Columbus Basin are screened at varying intervals over much of their depth, and hence the head measured in a well is the "average" head over the different intervals. The 2-D flow assumption, therefore, was best checked by well pairs with a maximum difference in depth. In most cases the hydrographs of neighboring wells of different depth in the Columbus Basin compared very favorably. The well pair 28.7.22.311 (depth = 917 ft) and 28.7.28.124 (depth = 723 ft) is a typical example (Appendix I).

Leakage

Because a shallow aquifer exists above the confining layer in the basin, the occurrence of leakage through the aquitard recharging or discharging the primary aquifer is highly probable if not certain. CERT does not account for this type of areal leakage explicitly, and therefore the effects of such leakage are 'incorporated' into the areal values of parameters A and B. Leakage was explicitly ignored in the following analyses, leading to the belief that, for example, pumping rates estimated by CERT may be biased low at late times to account for the "missing" leakage.

DATA AQUISITION AND ANALYSIS

Aquifer Properties

Specific Capacity and Transmissivity Data. Within the region delineated in figure 1 there were only three transmissivity (T) values obtained from pumping tests, but there were 38 specific capacity (C_s) values available (McLean 1977). Analytical methods exist to determine T from C_s data (see Walton 1970), but these methods are highly uncertain in that the well is assumed to be fully penetrating, well diameter must be known or assumed, and the pumping period must be known or assumed. None of these conditions were known for the Columbus Basin C_s data, and therefore it was decided to fit a regression line to the plot of log T vs. log C_s with hopes that correlation would be significant. If such was indeed the case, T could then be determined from C_s using the regression analysis.

The logarithm of T and C_s was used because the system of equations being solved is sensitive to the log of T and the problem of negative T estimates is avoided (Townley and Wilson 1985). Additionally, previous research has shown that aquifer permeabilities often have a log-normal statistical distribution. The assumption that the uncertain parameter types have a normal distribution was a key one during the development of the first order second moment analysis embodied in CERT.

More than three pairs of points are needed to conduct a regression analysis. In addition to the three T values available for the Columbus Basin (which had corresponding C_s values), 14 points that had reported T (from pumping tests) and C_s values were selected from the adjoining Mimbres Basin to the north and Deming Basin to the northwest. The justification for the selection of the additional points was that the geology and hydrology of the adjoining basins was believed to be similar to, if not the same as, that

of the Columbus Basin. A listing of the data used in the regression analysis is provided in table 1.

The regression line (figure 10) has a correlation coefficient of 0.71 which is significant, and the following regression equation was used to determine log T from log C_s within the Columbus Basin.

$$\log T = 0.80 (\log C_s) + 3.22 \qquad (10)$$

$$r = 0.71$$

$$\sigma^2 = 0.0625$$

Note that there was a variance of 0.0625 associated with the regression analysis, and consequently the accuracy of any log T prediction was not expected to be greater than this value. One data pair (marked by an * in table 1) was not used in the regression analysis because the point appeared to be an anomalous value.

The units of the T and C_s values used in the above analysis were ft^2/day. The units used for CERT input were ft^2/year. To convert a log (T) or log (C_s) value from one set of units to the other, it is only necessary to add to or subtract from that value the constant log (365). When estimating the correlation structure (i.e. the variogram or generalized covariance) the units of measure make no difference.

Storativity Data. There were no storativity (S) values available for the Columbus Basin. As discussed previously (Hydrogeology section), a large portion of the major aquifer was believed to be confined with S on the order of 10^{-4}. Parts of the Columbus Basin (most notably the extreme western and north-western regions) may be unconfined or only partially confined, and a S value representative of these areas is a question that was addressed during the modeling study.

Table 1

Transmissivity and specific capacity data used in regression analysis

	Well Location	T (ft^2/day)	C_s (ft^2/day)	Log T	Log C_s
	23S.9W.35.34333	1,500	1.8	3.18	0.26
	24S.7W.9.24112A	2,400	1.4	3.38	0.15
	24S.7W.10.11111	2,100	3.5	3.32	0.54
	24S.9W.1.21134	16,000	9.6	4.20	0.98
	24S.9W.1.22232	2,000	2.1	3.30	0.32
	24S.9W.6.431	2,900	1.9	3.46	0.28
	24S.9W.7.211	5,300	4.2	3.72	0.62
	24S.9W.21.131	2,300	3.3	3.36	0.52
	24S.10W.12.41111	7,800	6.4	3.89	0.81
	25S.6W.3.121A	3,080	1.25	3.49	0.10
	25S.6W.8.112	1,100	1.2	3.04	0.08
	25S.9W.28.21113	8,700	6.4	3.94	0.81
	25S.10W.36.222	5,200	7.3	3.72	0.86
	26S.10W.11.11211	8,700	5.0	3.94	0.70
	27S.8W.8.31111	7,900	1.35	3.90	0.13
*	28S.7W.21.21113	50,000	2.5	4.70	0.34
	28S.8W.25.311111	10,450	4.8	4.02	0.68

* Did not use this data point in the regression analysis because it appears to be anomalous

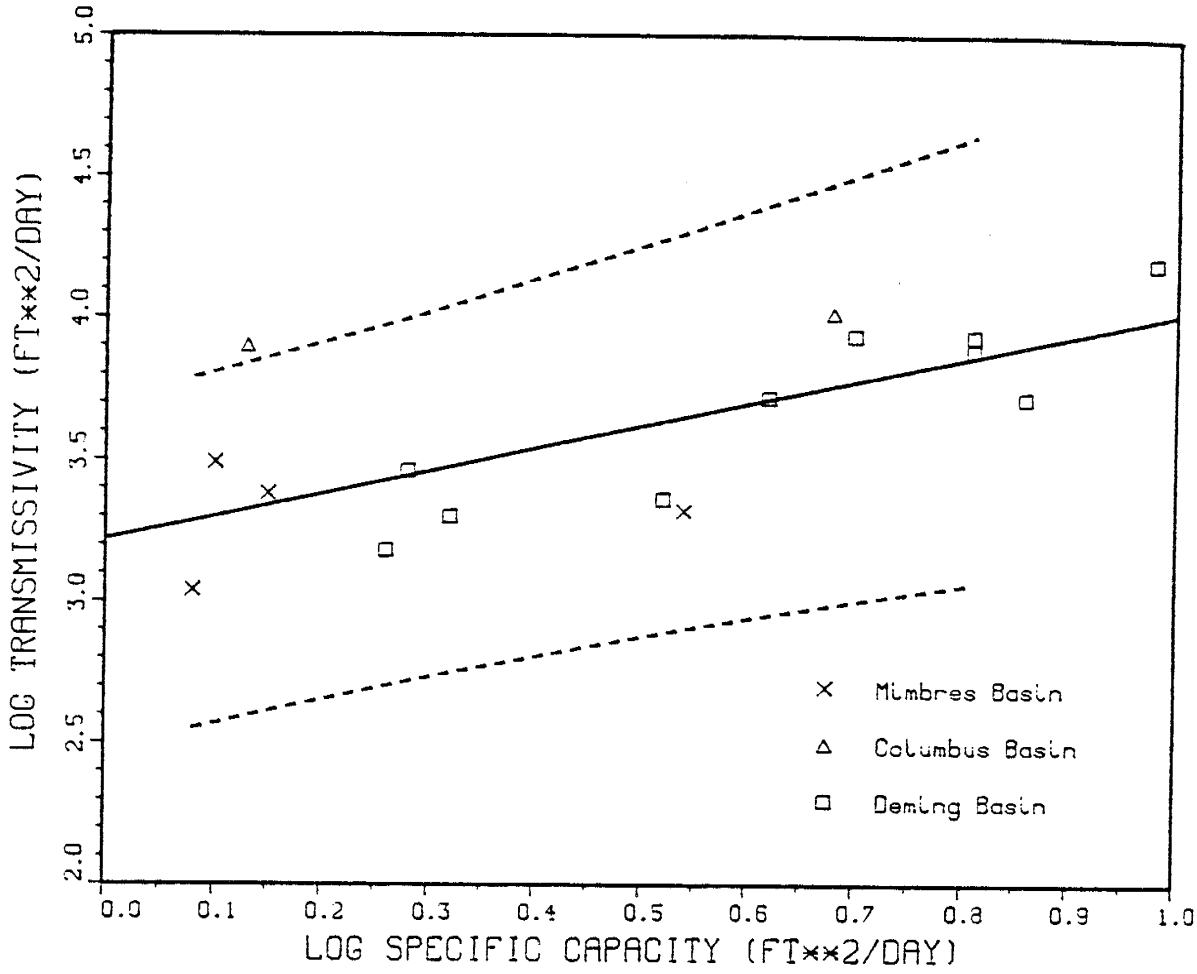

Fig. 10. Linear regression of log C_s vs. log T. Solid line is the regression line, dashed lines are the 95% confidence intervals.

Observed Head Data

Sources. Water level data for the Columbus area was obtained from the Albuquerque office of the U. S. Geological Survey (USGS) in digitized form. Measurements for wells in the Columbus Basin were extracted from a large data file containing historical head data for all of Luna County. The Columbus Basin portion of the file consisted primarily of data reported by McLean (1977), but some more recent measurements had been added. The collection and recording of water levels has traditionally been a joint effort between the USGS and the New Mexico State Engineer Office (SEO). The digitized record was checked against records available at the SEO in Deming, and the USGS file included the most recent measurements.

Screening. Hydrographs for the Columbus Basin wells display a seasonal fluctuation which is caused primarily by the presence or absence of pumping for irrigation (figure 11). There was no intention of modeling this seasonal behavior using CERT, and therefore head measurements were screened to get a representation of declining water levels within the basin not complicated by a superimposed seasonal trend.

To facilitate the screening process, the calendar year was divided into tenths and each water level measurement was assigned to one of the ten divisions. If there was more than one measurement per division, the measurements were averaged arithmetically. Next, the hydrographs of several wells with a good record of seasonal fluctuation were plotted with different portions of the year omitted. The goal was to define a portion of the year for which water levels seemed to be relatively unaffected by pumping. Several of the wells analyzed were from the Deming Basin because wells with a high number of yearly measurements were fairly scarce in the Columbus Basin. There should be essentially no difference in the seasonal

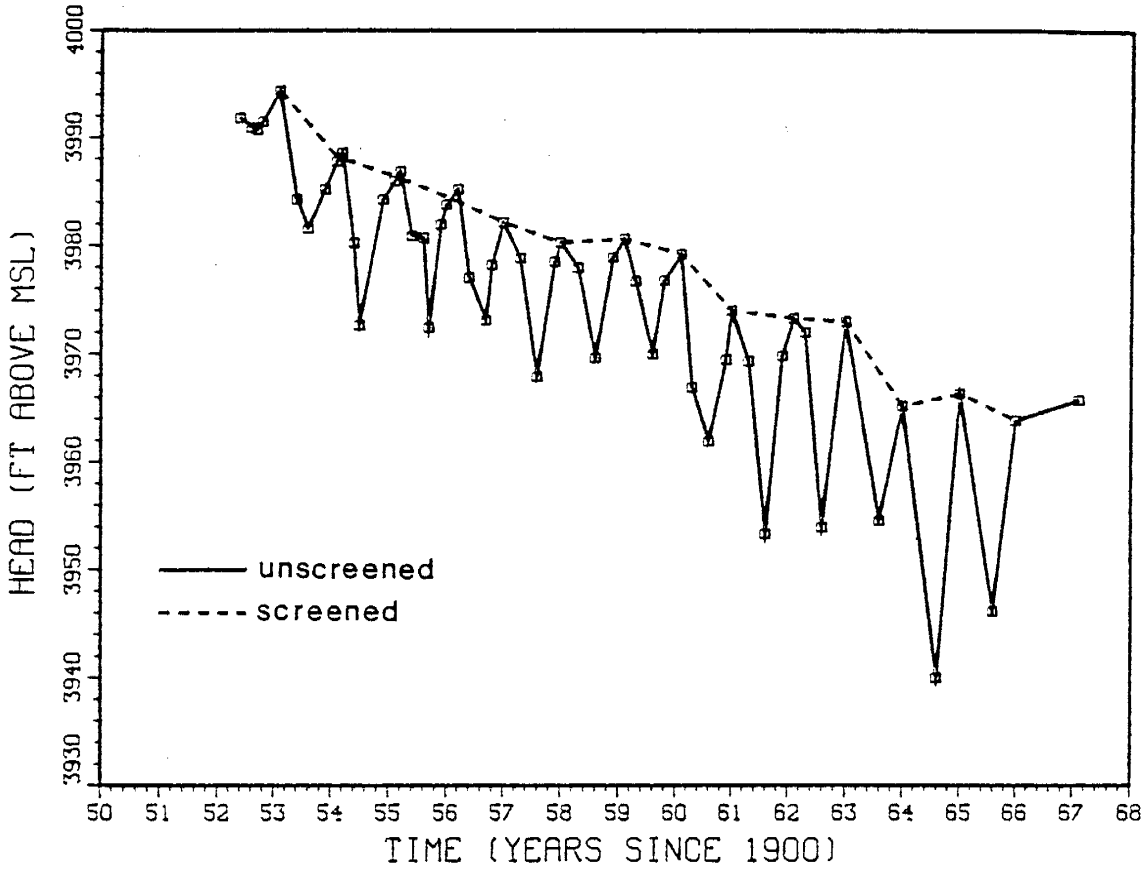

Fig. 11. Screened and unscreened measured water levels for well 28.8.36.111 in the Columbus Basin, New Mexico.

distribution of pumping between the two basins since both use water for the same type of agriculture.

It was decided by inspection that when measurements during the interval 0.2 to 0.9 of any year were screened out the observed seasonal fluctuations of the hydrographs were diminished sufficiently (figure 11). This approximately corresponds to the period of mid March to late November.

A relatively small number of water level measurements were taken in wells that were pumping or near other wells that were pumping. These measurements were not used in this investigation.

Once the water level measurements falling within the period of mid March to late November and those measurements known to be influenced by pumping were screened from the data file, the hydrographs for all of the wells in the Columbus Basin were plotted. Based on these hydrographs, an additional screening process was conducted by inspection. Specifically, the identification of anomalous wells and/or anomalous measurements was attempted. A listing of the deleted wells and measurements, along with the reason for the deletion, is provided in Appendix I. Many of the deleted wells are of shallow depth and located in the western portion of the basin. They appeared not to be in connection with the major regional aquifer. Some other measurements seemed to be slightly anomalous but their deletion would have been difficult to justify objectively. These measurements were given an increased uncertainty or variance, as is described below.

Measurement Error and Biasedness. Recall that the first term of the objective function, equation 6, is weighted by the inverse of the measured head covariance matrix. Only the main diagonal of this matrix, which is the variance of the head measurements, was used in this study. To fill these diagonal terms required an estimate of the head measurement variances.

There are primarily two sources of uncertainty associated with measured hydraulic head in the Columbus Basin. First of all, the actual measurement of depth to water has some associated error. However, most measurements in the basin were obtained by steel tape and the error margin is probably negligible. Secondly, the conversion of depth to water to hydraulic head required that the surface elevation at the well bore be known. These elevations were interpolated from USGS 7.5 minute topographic sheets. The elevation estimates for wells in gently sloping or flat regions of the basin were believed to be quite good. In these regions the contour intervals were only 5 or 10 ft, providing for a detailed interpolation. In areas near the mountains the topography becomes steeper and the contour intervals were often 20 or 40 ft. In these areas elevation interpolation was more uncertain. Finally, it must be kept in mind the well location was not specified exactly in the records. It was only known that the well lies within a square unit of some finite size. This is due to the nature of the well numbering system used in New Mexico (Appendix I).

Based on the above considerations, a subjective estimate of the standard deviation of water level measurements was made. Measurements made at locations in gently sloping regions of the basin (contour intervals of 5 or 10 ft) were given a standard deviation of 5 ft (this was the majority of the measurements), and measurements made at locations in rugged regions (contour interval 20 or 40 ft) were assigned a standard deviation of 9 ft. These values imply that recorded water level values were expected, with approximately a 95 percent degree of confidence, to lie within ±10 ft and ±18 ft of the "true" value for the plains and mountainous regions respectively. Observations assigned a higher standard deviation because they appeared somewhat anomalous were assigned a value of 7 ft. All of

these locations were in gently sloping regions. This analysis assumed a normal distribution of measurement error.

Some types of errors were not considered in the above analysis because they are extremely difficult if not impossible to detect. For example, the distance from the measuring point to the ground surface is supposed to be subtracted from the depth to water value before it is recorded in the field. There could be mistakes in identifying the actual location of a well, and so on. Errors such as these were not believed to be a significant problem with the Columbus Basin data set.

Pumping Data

The pumping rates used in this study were obtained from and compiled by the SEO in Santa Fe. They were used as input to the SEO uncalibrated groundwater management model of the Mimbres Hydrologic Basin. The pumping data represented an average discharge over five year periods (1930-1974) for 4 sq mi administrative blocks. The finite difference blocks of the SEO uncalibrated model grid were equivalent to the administrative units. The administrative blocks are the result of dividing each township and range block into 9 equal squares.

The pumping rates were calculated by the SEO using power consumption records and irrigated acreages where available. When such data was not available, consumptive use was taken to be 70 percent of the duty or official allocation for that area.

There is much inherent uncertainty in estimating pumping rates in an indirect manner. The power consumption method requires a knowledge of pumping lifts, pressure heads and pumping efficiency factors. Often the calculations are based on average values of these parameters for the basin of interest. This procedure could lead to large deviations from the actual

values in areas of the basin which are not characterized well by the averaged parameters.

Crop consumptive-use factors may overestimate pumping rates because they are determined from lysimeter studies under ideal situations where the soil has been disturbed during construction (Sammis 1979). Results calculated from crop consumptive-use factors also assume proper irrigation practices - a condition probably often not met in the Columbus Basin.

Perhaps the most uncertain discharge estimates arise from taking 70 percent of the official allocation for some area. The entire duty is probably almost never used, but how can the proper percentage be determined?

A cross-validation of the SEO pumping estimates was attempted using reported irrigated acreages for the years 1973, 1974 and 1975 obtained from the Deming office of the SEO. The pumping rates estimated from the irrigated acreages ranged from 20 percent to 175 percent of the SEO estimates. So many factors could have affected the comparison of the pumping estimates, however, that the cross-validation results were viewed as inconclusive. It would have been very labor intensive to compile new pumping estimates for the Columbus Basin, and therefore the SEO pumping estimates were used without modification.

A 3-D view of the nodal pumping estimates (see next section) are presented later for the two years 1955 and 1970 in figure 14 (see page 49). Note that the major pumping center is located due east of Columbus.

It was difficult to conclude whether the SEO pumping estimates were biased high or low. There were numerous factors for which there was insufficient data to evaluate. For example, overestimation due to consumptive-use factors could have been offset by underestimation of pumping lifts or over-irrigation to prevent crop-loss. For the purposes of this

study it was assumed that the estimated pumping values were distributed normally about the estimated values.

As a conservative subjective estimate, 25 percent of the pumping value was used as the standard deviation for that discharge estimate. The 95 percent confidence interval then consisted of plus or minus 50 percent of the pumping estimate.

MODELING STRATEGY

Finite Element Grid

The finite element grid used for the Columbus Basin study is shown in figure 12. The grid consisted of 356 triangular elements and 201 nodal points. The uniform pattern of the grid interior was a direct consequence of the form of the available pumping data. The SEO estimated discharge rates for the Columbus Basin over 'administrative units', each unit consisting of four sections (there are nine administrative units in any township and range). The interior nodal points of the grid mimicked this system, thereby facilitating assignment of the SEO areally averaged discharges to nodal points.

The density of the grid was primarily controlled by computer storage and computational limitations. Before access was available to a virtual memory Digital MICROVAX computer, some pilot runs were made on a DECSYSTEM 20 computer with a limited 140 megaword extended memory. Because increasing the number of nodes in a grid directly increases the number of parameters for the parameter estimation and uncertainty propagation problems when a nodal parameterization is employed, one can see why grid size is an important consideration when machine storage and computational capacity is limited.

Boundary Node Locations

The boundary nodes for the Columbus Basin grid were placed in such a way as to minimize the probability of two possible problems occurring:

1) Three-dimensional flow, and

2) Extension of drawdown through prescribed head boundary nodes

The subject of three-dimensional flow in the Columbus Basin was addressed in a previous section. The extent of drawdown in the Columbus area was

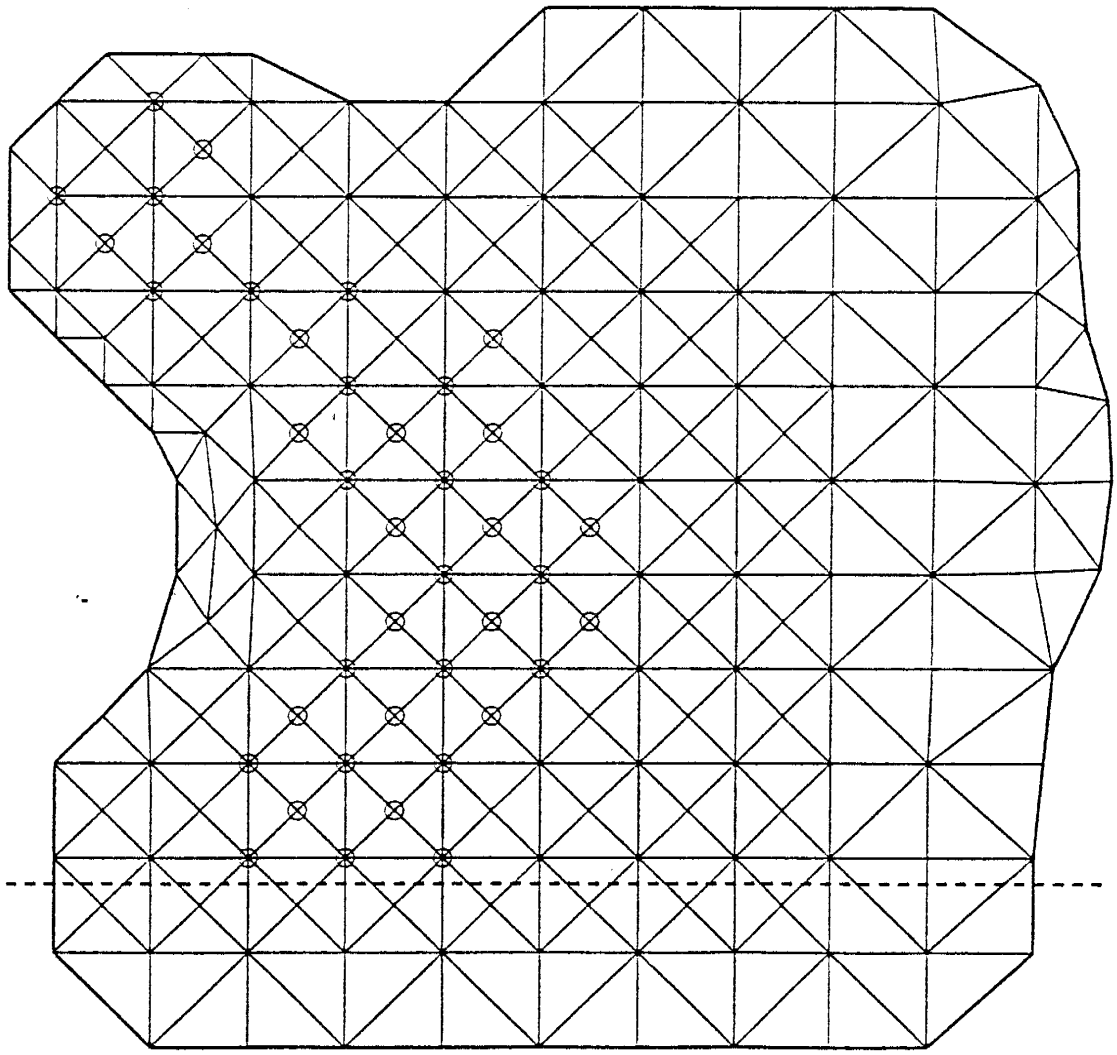

Fig. 12. Finite element grid composed of 201 nodes and 356 linear triangular elements used for the Columbus Basin study. Circles indicate pumping nodes.

initially assessed using the maps compiled by McLean (1977) (see our figure 99 on p. 194). Boundary nodes on the north, east and south sides of the basin were easily placed far enough from the centers of pumping so as not to be effected. Problem areas may exist at the gap between the Tres Hermanas and Florida mountains and due south of the Tres Hermanas Mountains. In these areas pumping centers outside the basin may have a minor effect on water levels inside the basin. Drawdown at these boundary nodes would only occur during later development, however, and the error incurred through the prescribed head assumption should be small.

Boundary Type. As was implied in the previous paragraph, a first type boundary head was prescribed for all of the boundary nodes in the Columbus Basin. A detailed description of how the prescribed heads were chosen and what their values were is presented in the "Estimation of Boundary Conditions Through the Inverse Procedure" section of this report. The prescribed head boundary type was chosen because there was little or no T or head data near most of the boundary nodes. It was felt that water levels could be interpolated out to the boundary node locations fairly accurately, but T values would have been much more difficult to estimate. Because the estimation of second and third type boundary conditions requires T estimates, and because the cone of depression should not reach the boundary nodes within the simulation period, first type boundary nodes were used.

Distribution of Pumping

A program was written to distribute the SEO pumping data to the node points marked by circles in figures 12 and 13. These nodes were chosen to be pumping nodes because they most clearly outline the irrigated areas observed on areal photographs taken in November of the years 1960 and 1969. Of course, the pumping wells might not have been in close proximity to the irrigated acreage, but it was assumed that they were. A listing of the

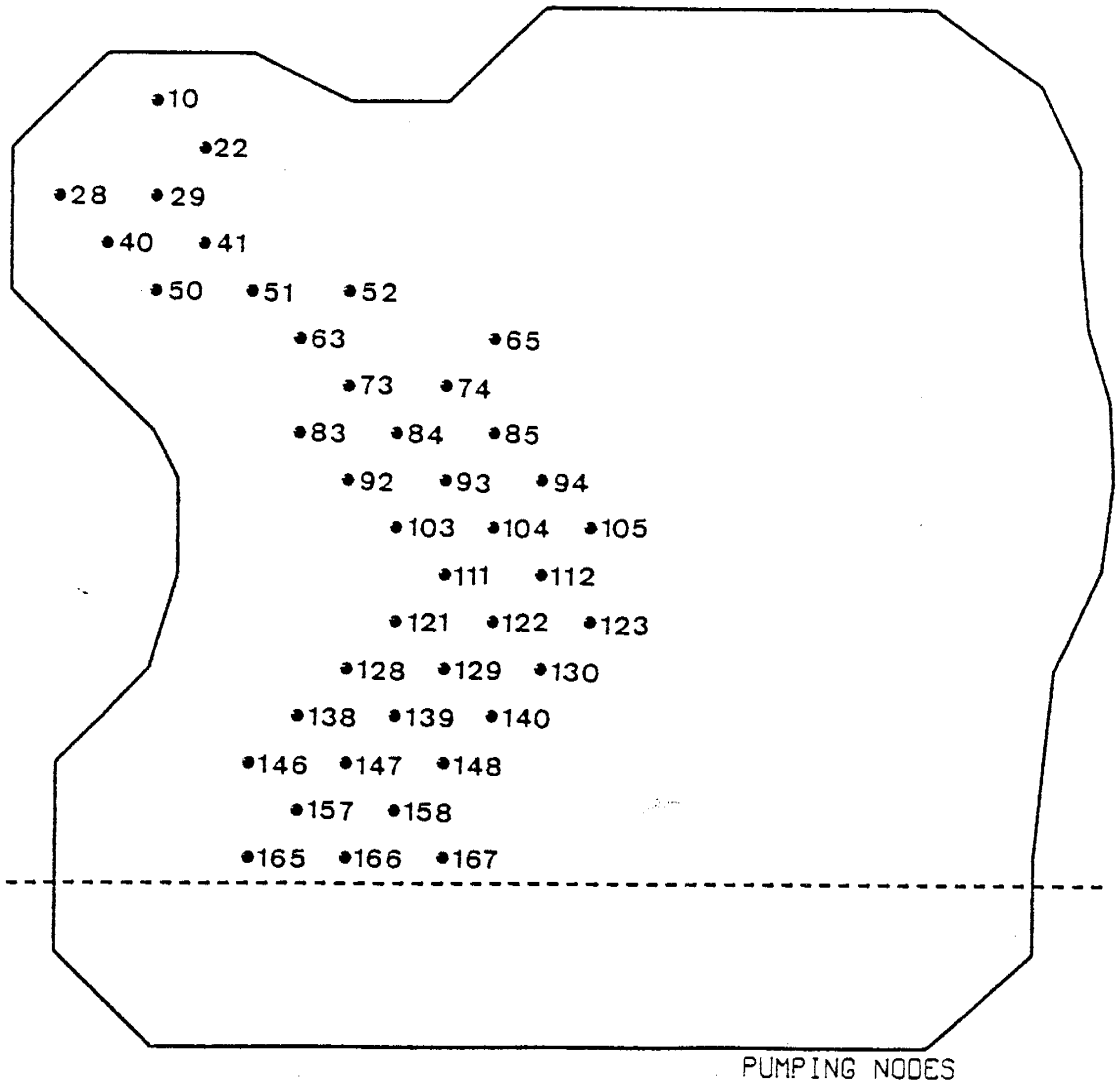

Fig. 13. Location and node numbers of 41 pumping nodes used in the Columbus Basin study.

percentage of the SEO areally averaged pumping estimate assigned to each pumping node in the CERT grid is provided in table 2. The nodal pumping estimates for the two years 1955 and 1970 are shown in figure 14.

The total Columbus Basin SEO estimated average pumping for five-year periods is shown in figure 15. As is explained in the next section, a one-year time step was used for the Columbus Basin simulations. The lumped five-year pumping estimates of the SEO were distributed to one-year periods using a mass conservative interpolation algorithm (dashed line, figure 15).

Time Period

The maximum time period over which simulations were made was 1930 to 1975. The year 1930 was chosen as a starting point for three reasons. First, the SEO compilation of pumping data began with this year. Secondly, the Columbus Basin did not experience significant groundwater development until the early 1950s (see figure 15). Starting the simulations 20 years prior to the heaviest development within the basin allowed the model ample time to "smooth out" possible erratic numerical behavior associated with the first few time steps of the finite difference scheme used for the time domain. Finally, data available prior to 1930 is very unreliable. Aside from Darton's 1911 survey of the basin, hydrologic data is nonexistent for the basin prior to 1930 and water levels, discharge rates, etc., would have had to have been interpolated through time.

The time step used for all of the CERT simulations was one year. This value was believed to be small enough to adequately simulate the observed water level behavior after screening. An additional consideration was the fact that the 'B' boundary parameter is time varying, and therefore an increase in the number of time steps causes an increase in the number of model parameters. An increase in the number of model parameters induces larger storage and computational time requirements on the computer.

Table 2

Portion of SEO block pumpage assigned to nodal points of finite element grid

Node	State Engineer Model Block (I,J)	Portion of Block Pumpage Assigned to Node
10	18,33	1/3
22	18,33	1/2
28	20,34	1
	19,34	1/6
29	18,33	1/6
	18,34	1/6
	19,34	1/6
40	19,34	1/2
41	18,34	1/2
50	19,34	1/6
	18,34	1/6
	18,35	1/2
51	18,34	1/6
	18,35	1/2
	17,35	1/6
52	17,35	1/6
63	17,35	1/2
73	17,35	1/6
	17,36	1/6
	16,36	1/6
74	16,36	1/6
	15,36	1/6
	15,35	1/2
65	15,35	1/2
83	17,36	1/2
84	16,36	1/3
85	15,36	1/2
92	17,36	1/3
	16,36	1/6
	16,37	1/6
93	16,36	1/6
	15,36	1/6
	16,37	1/6
	15,37	1/6
94	15,36	1/6
	15,37	1/6
	14,37	1/3
103	16,37	1/2
104	15,37	1/3
105	14,37	1/3
111	16,37	1/6
	15,37	1/6

Table 2 Contd.

	16,38	1/6
	15,38	1/6
112	15,37	1/6
	14,37	1/3
	15,38	1/6
	14,38	1/3
121	16,38	1/2
122	15,38	1/3
123	14,38	1/2
128	16,38	1/6
	16,39	1/6
	17,39	1/6
129	16,38	1/6
	15,38	1/6
	16,39	1/6
	15,39	1/6
130	15,38	1/6
	14,38	1/6
	15,39	1/6
	14,39	1
138	17,39	1/2
139	16,39	1/3
140	15,39	1/2
146	17,39	1/6
	17,40	1/6
147	17,39	1/6
	16,39	1/6
	17,40	1/6
	16,40	1/6
148	16,39	1/6
	15,39	1/6
	16,40	1/6
157	17,40	1/3
158	16,40	1/3
165	17,40	1/6
	18,41	1
166	17,40	1/6
	16,40	1/6
	16,41	1/2
167	16,40	1/6
	16,41	1/2

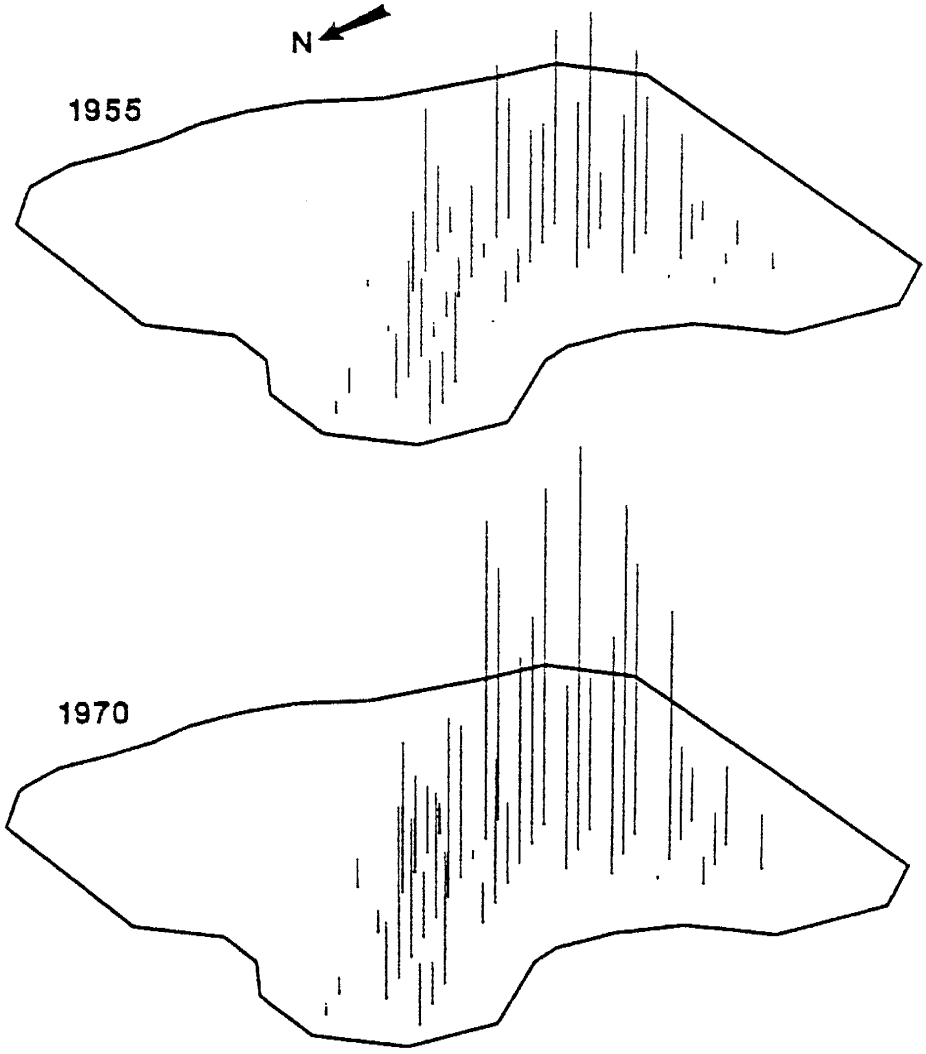

Fig. 14. Spatial distribution of pumping by node for the years 1955 and 1970. To give some idea of scale, the tallest spike for the year 1970 is 50 million ft^3/year. View from NW looking SE.

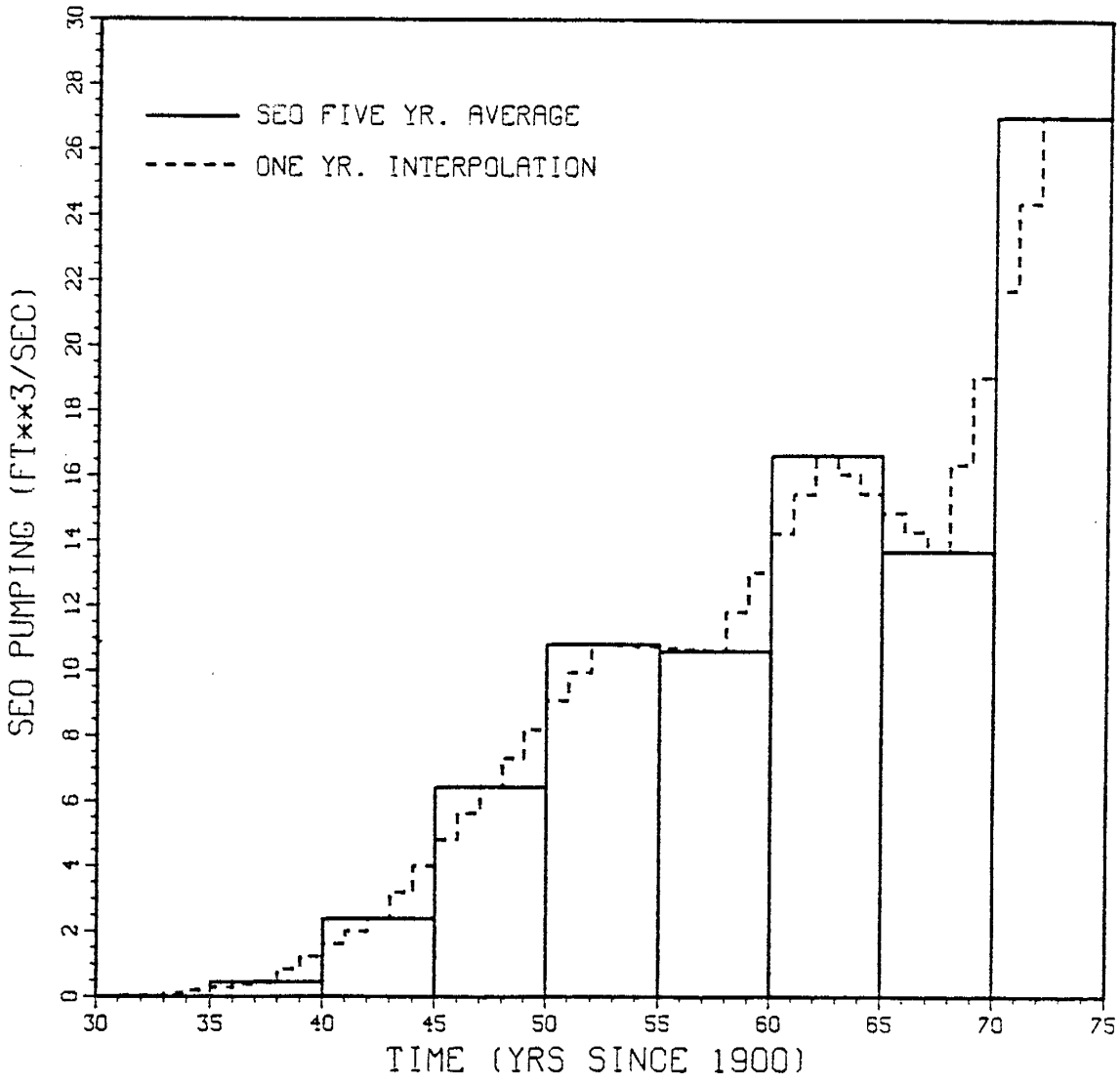

Fig. 15. Total SEO pumping estimates for the Columbus Basin and the interpolation scheme used to divide the five year averages into annual values.

Observed Head Data

Only water level measurements that remained after the screening process were used for simulations. A program was written to select the appropriate measurements for any specified time period from the water level measurement data file. If there were multiple measurements at any one location for any one year, the measurements were consolidated to one value by arithmetic averaging and were subsequently assigned to the appropriate time period. The number of "yearly measurements" at each location are shown later in figure 20d.

Final Comment

In the previous sections the central strategy for modeling the Columbus Basin was outlined. This strategy was followed for all simulations using CERT unless noted otherwise.

PRIOR INFORMATION ON T AND ESTIMATION OF T THROUGH THE INVERSE PROCEDURE

Geostatistics

An important phase of the parameter estimation procedure utilized in CERT is the estimation of aquifer parameters a priori. The "prior" information determines the starting point in u-dimensional parameter space (u = number of parameters) from which the search algorithm begins its search for the global minimum of the objective function, J. As the minimization procedure takes place, the value of J is directly dependent upon the prior estimates of the system parameters and the estimated covariance matrix of those parameters. The prior information also helps to stabilize the estimation procedure. For these reasons it is important to make the best possible initial estimates of the model parameters so that the convergence of the inverse problem is enhanced.

Given an irregularly spaced network of observed parameter values (e.g. T) over some area, kriging is a particularly convenient method of obtaining parameter estimates at the nodes of some grid and a corresponding covariance matrix. The theory of kriging requires that the variable under consideration be random and that some spatial derivative of it be statistically homogeneous (stationary). The conditions of stationarity (Intrinsic Random Field (IRF) of order - 1) for T are as follows:

1. The mean (expected value) is constant (or known)

$$E[T(\underline{x})] = m = \text{constant}$$

2. The auto-covariance (or the variogram or generalized covariance) is a function of the separation vector only

$$\text{Cov}[T(\underline{x}_1), T(\underline{x}_2)] = R(\underline{\ell})$$

$$\text{where } \underline{\ell} = (\underline{x}_1 - \underline{x}_2)$$

The random field is statistically isotropic if the auto-covariance is a function of the magnitude of the separation vector only:

$$\text{cov}[T(\underline{x}_1),\ T(\underline{x}_2)] = R(|\underline{\ell}|)$$

Kriging is a two-part process. First, structural analysis is conducted to determine the characteristics of the covariance between data points. At this stage a theoretical variogram or covariance model is chosen that best matches the experimental data. Secondly, this observed covariance behavior is used to estimate random variables at specified locations (in this case the nodal points of a finite element grid). In addition to estimating "point" values of a random field, kriging can also be used to estimate randomly distributed parameters over 'blocks' or 'zones' of finite elements. To do this the point process must be averaged over some area and the appropriate integrals must be implemented in the kriging equations (see Townley 1973). For a detailed explanation of structural analysis and kriging see Journel and Huijbregts (1978).

Structural analysis and the subsequent kriging of T in the Columbus Basin is discussed in the next two sections. S could not be kriged because there were no S measurements within the basin. Observed head values were not kriged because in contrast to previous research (e.g. Neumann and Yakowitz 1979), CERT does not require that head observations be located at or interpolated onto nodal points. To interpolate model calculated heads onto some observation point within a triangular finite element, CERT uses the three nodal heads and the basis functions of that element.

Structural Analysis

Variogram. Although CERT requires the covariance structure of a given random field to be expressed in the form of a generalized covariance (IRF of order 0, 1 or 2), a less complex variogram estimation (IRF or order -1 or 0) was conducted initially to get a general idea of covariance behavior. This

method assumes that T or its first derivative is stationary. The variogram, $\gamma(\underline{h})$, is defined by

$$\gamma(\underline{h}) = \frac{1}{2} \mathrm{Var}[T(\underline{x} + \underline{\ell}) - T(\underline{x})]$$
$$= \frac{1}{2} E[(T(\underline{x} + \underline{\ell}) - T(\underline{x}))^2] \qquad (11)$$

where E[ ] denotes the expected value, $\underline{x}$ is a coordinate vector in two-space, and $\underline{\ell}$ and T are as defined previously.

The first step in determining the experimental variogram for any random variable is to collect the data set of observed values. As discussed earlier, there were 38 C_s and two T observations for the Columbus Basin. The regression equation (10) was used to estimate log T values from the 38 log C_s values, and all 40 log T values were then used in the experimental variogram estimation (table 3).

The locations of the 38 C_s values and the two T values are shown in figure 16. Note that two C_s observations are located at the extreme eastern edge of the basin, while the other observations are in the western half of the basin. These two locations are further distinguished from the others in that their measured C_s values are significantly lower than any of the other points. Well depth data for these two wells is not available, but there are few wells in the eastern half of the Columbus Basin that are deep enough to tap the primary aquifer. If these wells do not tap the primary aquifer, they are drawing water from thin sand and gravel layers separated by thick beds of clay, which would explain their low C_s values. For the above reasons, the use of the two outlying points during the structural analysis phase was suspect, and their effect on the variogram (or generalized covariance) deserved scrutiny.

Table 3

Locations of Log T values used in variogram and generalized covariance estimation (cartesian coordinate origin at intersection of R9W-R10W boundary and international border)

Location	x (ft)	y (ft)	Log T (ft^2/day)
27.7.19.13332	63608.	58578.	3.091
27.7.31.21111	66083.	50328.	2.965
27.8.5.31211	37703.	74088.	3.337
27.8.8.31111	37043.	68808.	3.898
27.8.15.13111	47603.	64848.	3.443
27.8.18.12132	33248.	65838.	3.538
27.8.18.12333	33083.	65013.	3.443
27.8.22.13333	47603.	58413.	3.142
27.8.25.11114	58328.	55443.	2.902
27.8.25.21312	60968.	54948.	2.765
27.8.25.41112	60968.	52968.	2.902
27.8.27.41221	51233.	52968.	2.979
27.8.35.11331	52883.	49338.	3.693
27.8.35.12213	54863.	50163.	3.180
27.8.36.11122	58658.	50328.	3.478
28.5.19.43132	129608.	24918.	2.179*
28.7.17.41113	71363.	31683.	3.383
28.7.19.22111	67403.	29208.	3.443
28.7.20.31112	68888.	26568.	3.494
28.7.20.42222	73838.	26568.	3.538
28.7.21.21113	76643.	29043.	3.538
28.7.22.11113	79283.	29043.	3.819
28.7.29.21114	71528.	23763.	3.679
28.7.30.21313	66083.	23103.	3.253
28.8.1.11113	58163.	44883.	2.902
28.8.2.11312	53048.	44388.	3.404
28.8.24.11121	58493.	29208.	3.311
28.8.24.11134	58328.	28713.	3.565
28.8.24.13111	58163.	27888.	3.043
28.8.24.21211	61463.	29208.	3.012
28.8.24.31112	58328.	26568.	2.999
28.8.24.3130	58410.	25660.	3.142
28.8.25.31111	58163.	21288.	4.019
28.8.34.2440	52470.	16420.	3.693
28.8.36.41112	60968.	16008.	2.802
29.6.12.41114	124328.	5283.	2.483*
29.8.2.11113	52883.	13203.	3.911
29.8.4.21131	44963.	13038.	3.750
29.8.9.41111	44963.	5448.	3.404
29.8.17.2310	39930.	1240.	3.565

* outlying data points not used in some estimations

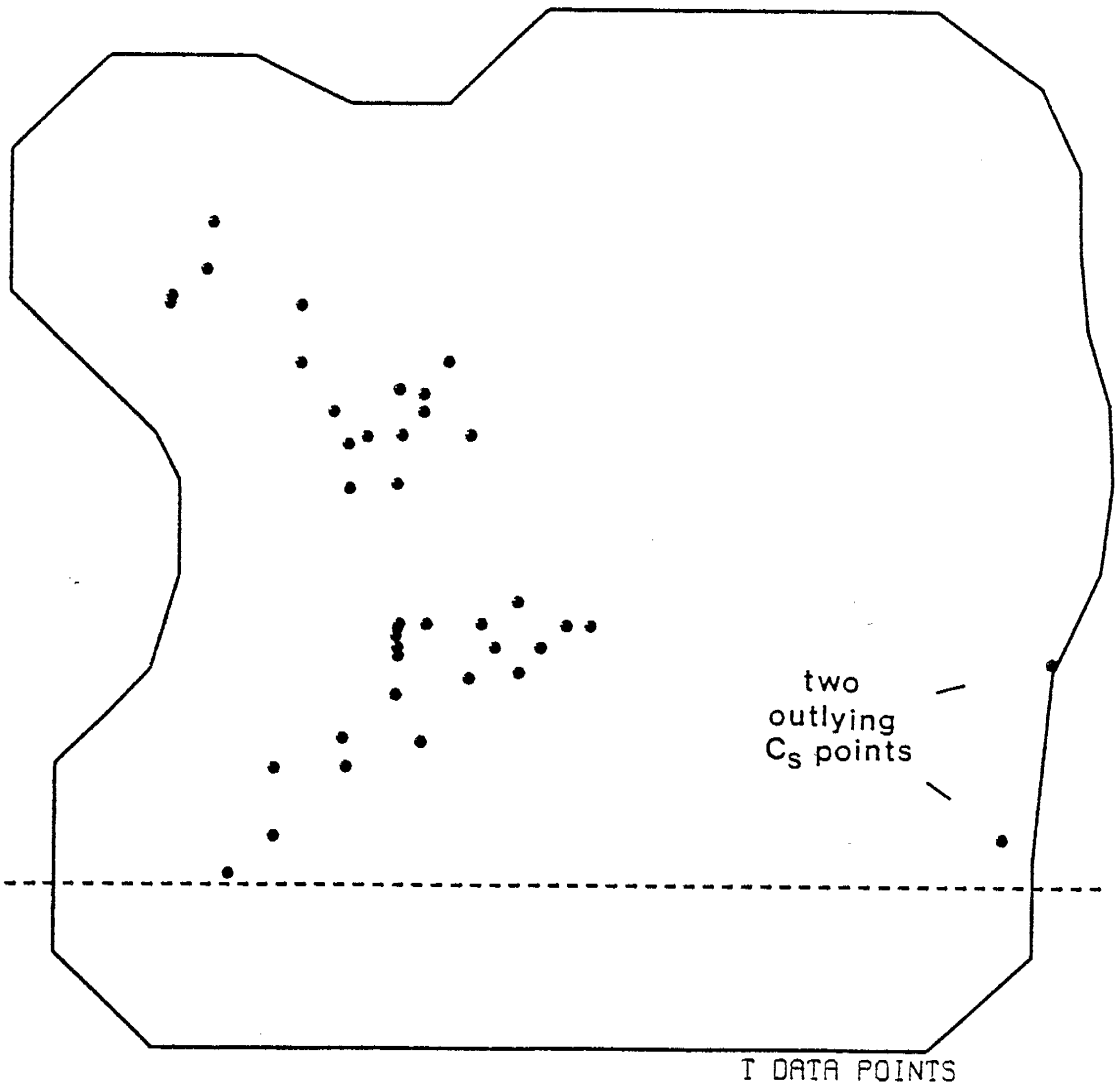

Fig. 16. Locations of 38 C_s and two T measurements available for the Columbus Basin.

Isotropic experimental variogram estimates were made with VGRAM, a Fortran program developed at the New Mexico Institute of Mining and Technology. In practice, the expected value of a random variable is approximated by the arithmetic mean of some number of observations of the variable. Once some range or step size of separation distances is defined within which the random field will be averaged, equation 11 can be solved approximately for $\gamma(\underline{h})$ of the field. This is the alogrithm coded into VGRAM.

There is some subjectivity involved in choosing the step size α. If α is small, there may not be many T observations to be averaged and a poor estimate of the expected value will be obtained. As α becomes large the mean of the random field is approached and the estimated covariance structure becomes increasingly smoothed. Based on some preliminary investigations a step size of 5,000 ft was used to estimate the variogram for the Columbus Basin log T data.

Two variogram estimates are presented in figure 17. The variogram which increases after a separation distance of 50,000 ft was estimated using all 40 data points. The variogram which decreases after 50,000 ft was estimated with the two outlying log T values excluded. The two curves diverge at separation distances greater than 51,000 ft - a distance which corresponds to the minimum separation distance between the westernmost outlying point and the easternmost point within the cluster of 38.

It was obvious that the two outlying C_s points significantly effected the variogram estimate at large distances. The validity of the "hump" which arose in the upper curve of figure 17 at about 70,000 ft was questioned for two reasons: (1) the number of data pairs composing the variogram estimates at separation distances greater than about 70,000 ft was small, and (2) most of these data pairs were a product of the two outlying C_s points

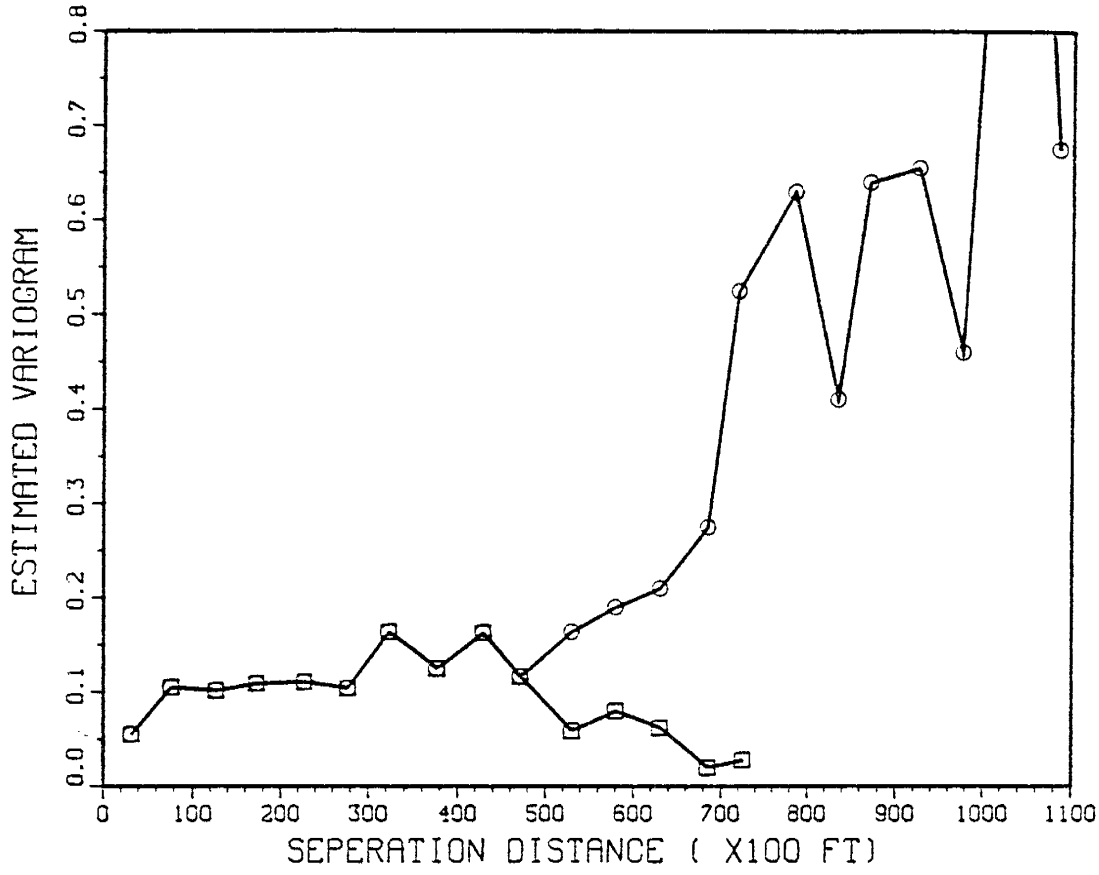

Fig. 17. Experimental isotropic variogram estimates for 40 (circles) and 38 (boxes) log T values. The difference between the two curves is due to the two outlying C_s points.

exclusively. For these reasons a variogram model was fit to the first 12 points of the upper variogram estimate only. Several different spherical and linear models were tested, but the best results were obtained from a linear variogram with a slope of 1.81×10^{-6} and a nugget value equal to 0.072 (figure 18).

The estimated linear variogram was influenced by the two extreme C_s points because the eleventh and twelfth points of the variogram estimate were partially composed of data pairs which included them. The lower curve of figure 17 is a variogram estimate conducted with the outlying points excluded from the analysis. The theoretical variogram which best seemed to match this curve was simply a nugget value (horizontal line) of approximately 0.08 (figure 18).

Finally, the statistically isotropic assumption was checked for the log T data set using VGRAM. Directional variogram estimates were made for the angles of 0, 45 and 110 degrees relative to east. With the two outlying log T points omitted, the three directional variograms matched favorably with the bottom curve of figure 17. When all 40 data values were used, the 45 and 110 degree directional variograms matched favorably with the lower curve of figure 17, but the 0 degree directional variogram mimicked the upper curve of figure 17. These results indicated that the Columbus Basin data is isotropic if the two outlying low log T points are omitted, but the data is anisotropic otherwise.

Generalized Covariance. CERT uses a class of correlation structures which can be considered a generalization of variogram theory, hence the name generalized covariance. The theory is briefly outlined here, but more extensive discussions can be found in Krafistas and Bras (1981), Delhomme (1978), or Delfiner (1976).

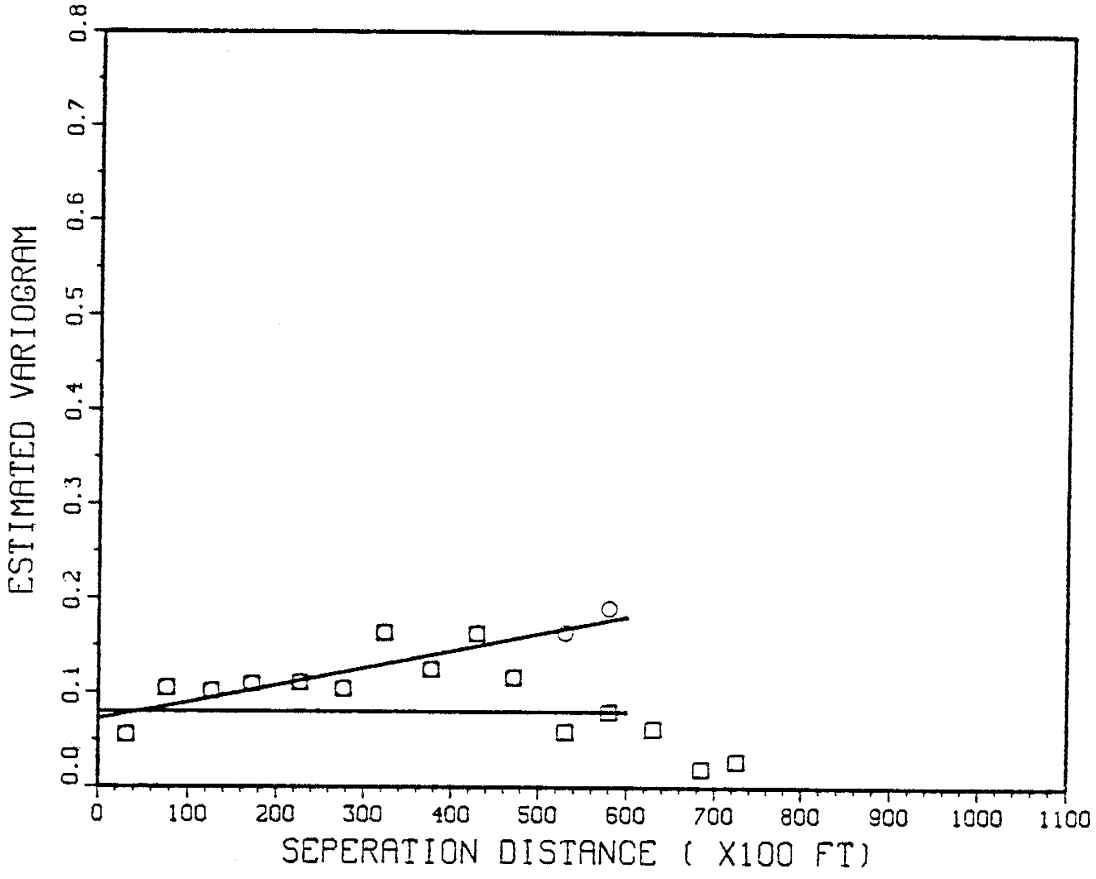

Fig. 18. Linear and nugget variogram models fit to the experimental variogram curves.

First note that the variogram defined by equation 11 is the product of first order differences, or the variance of increments of order one. Also note the ability of first-order differences to filter out constants, because if the assumption of constant expected value is true ($E[Z(\underline{x})] = m$), then the increments $Z(\underline{x}+\underline{h}) - Z(\underline{x})$ have zero expectation, independent of the value of m.

Delhomme (1978) states the next step, "... for phenomena in which the intrinsic hypothesis is not relevant (mean is not constant, or the variance is not finite), the idea is to use second, third or higher order differences which have the power to filter out polynomials of degrees 1, 2, ... etc. This procedure is currently used in the study of non-stationary time series: one calculates successive finite differences until an approximately stationary result is reached." That is, one looks for the order of the first stationary derivative of the field.

The particulars of developing the generalized covariance of order K, denoted by the function $K(\underline{\ell})$, can be found in the references cited above. K can be thought of as the degree of drift in the data. Therefore if $K = 0$, the generalized covariance function $K(\underline{\ell})$ will filter only a constant m, and is identical to the variogram $\gamma(\underline{\ell})$ except in sign. If $K = 1$, the $K(\underline{\ell})$ function will filter a polynomial of order 1, and so on. Because the variances of the increments must always be positive, only certain functions are admissible for use as generalized covariances. The polynomial models available for use in CERT can be found in Krafistas and Bras (1981) on page 42.

The coefficients of the polynomials listed in Krafistas and Bras (1981) are obtained by regression of the experimental variances of the K^{th} order increments. The theoretical model that best fits the data is then picked using either a lowest average rank or a minimum mean squared error criteria.

Two generalized covariances were estimated using CERT. The first estimate was made using all 40 of the available data points, and the second estimate was made using 38 points (two points on the eastern edge of the basin deleted). The generalized covariances are listed and compared to the previously estimated VGRAM variograms in table 4. Recall that for zero order differences, the generalized covariance differs from the variogram only in sign.

Because the order of both generalized covariances estimated for the Columbus Basin is zero, the assumption of stationarity of the data was validated; a substantial drift or trend in the data was not detected. The nugget values for each model agree well also. They all have a magnitude greater than or nearly equal to 0.0625, the variance of the log T - log C_s regression. The linear variogram and the zero order linear generalized covariance can be compared directly by changing the sign of either model. The slope of $K(\underline{\ell})$ is roughly twice that of $\gamma(\underline{\ell})$. This is because during the estimation of $K(\underline{\ell})$ all of the T data pairs were used (up to the largest possible separation distance), but when a variogram model was chosen only data pairs with a separation of 50,000 ft or less were used. Referring to figure 17, the large "jump" starting around 60,000 ft influenced the generalized covariance estimate.

Kriging and Inverse Estimates of T

Once the covariance structure of a random field is expressed appropriately in either variogram or generalized covariance form, it is a simple matter to krige (interpolate) the observed data values onto the nodal points of some specified grid. A prediction variance is also easily calculated at each node, and an additional feature implemented in CERT allows calculation of the covariance between nodes. This latter option is not available in many standard kriging codes, but it is important for CERT

Table 4

Comparison of VGRAM estimated variograms and CERT estimated generalized covariances

	# Points Used	Order	Nugget Value	Slope
Generalized Covariance	40	0	5.91×10^{-2}	-3.71×10^{-6}
Variogram	40	0	7.2×10^{-2}	1.81×10^{-6}
Generalized Covariance	38	0	0.10	0
Variogram	38	0	0.08	0

applications because an entire covariance matrix is obtained after kriging instead of only a diagonal. This covariance matrix constitutes a portion of the weighting matrix for the parameter half of the objective function, J_u.

Of the four possible covariance structures indentified in the previous two sections, one had to be selected for use during kriging to obtain the prior estimates of log T for subsequent CERT runs. The kriged fields obtained using the estimated linear generalized covariance and the estimated linear variogram (with sign on the slope changed), along with the corresponding kriging standard deviations, are shown in figure 19. The effect of the two low log T points at the eastern edge of the basin is clearly evident - they produced an east-west trend of log T across the basin. The kriged field using the nugget generalized covariance of 0.1 results in a constant value of log T (=5.916) and a constant standard deviation (=0.3229) over the entire basin.

Before deciding which kriged field to use, a series of simulations was made to determine if the different priors significantly affected inverse parameter estimates. With each of the three kriged fields above used as prior input into CERT, the code was run for the period 1930 to 1975 and log T was estimated at the 201 nodal points using CERT's WLS parameter estimation algorithm. S was a constant 5.0×10^{-4} over the entire basin, and the pumping and boundary conditions were the standard input. The results of this set of simulations as well as the observed head measurement locations and the number of measurements at each location are shown in figure 20.

The estimated log T fields in figures 20a and 20b are very similar. This was not surprising given the similarity of the priors for these two fields. The log T field in figure 20c is similar to the other two in the western half of the basin, but some major differences exist in the eastern

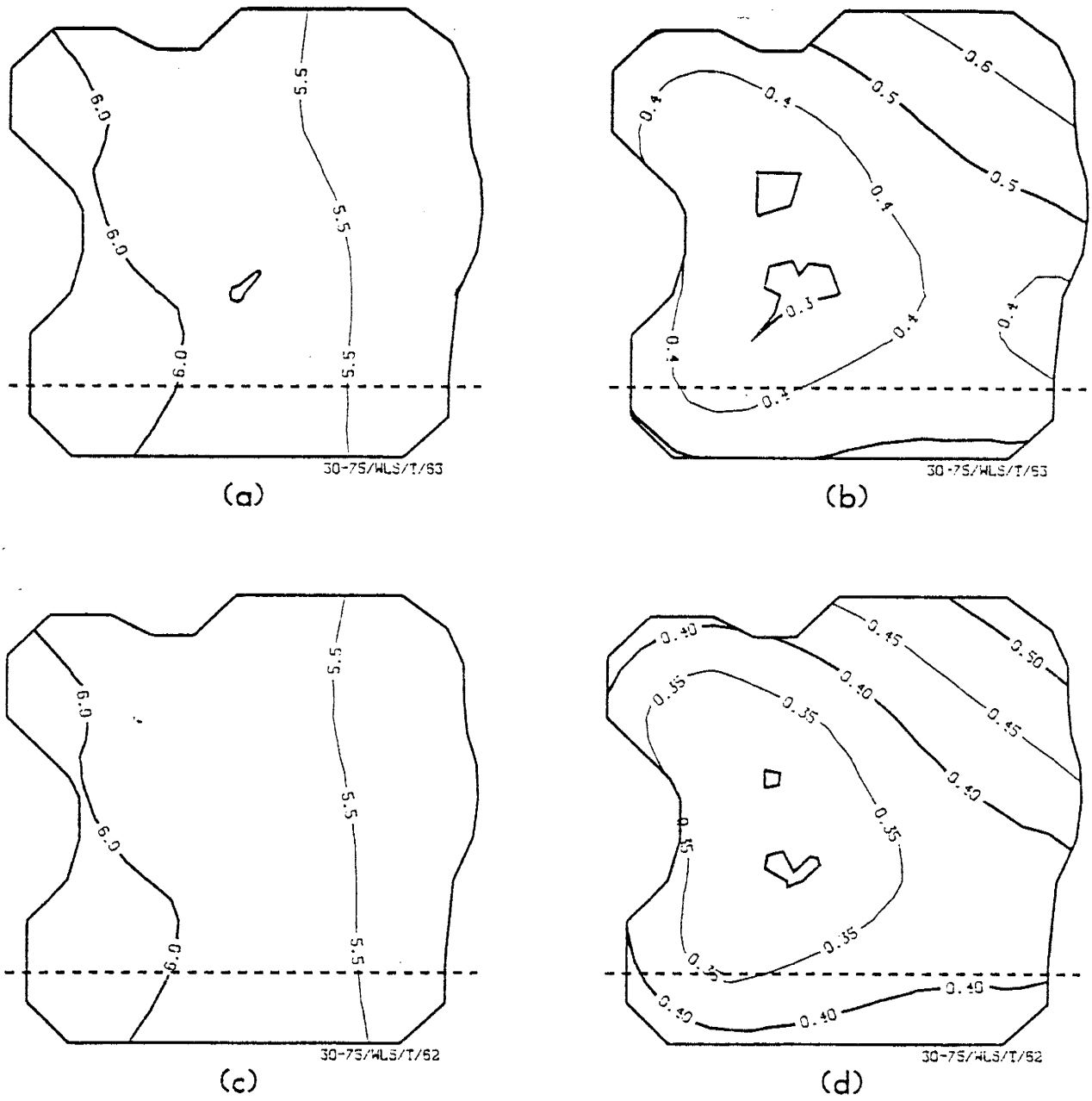

Fig. 19. Kriged log T field and corresponding σ_T field for linear generalized covariance (a and b) and linear variogram (c and d).

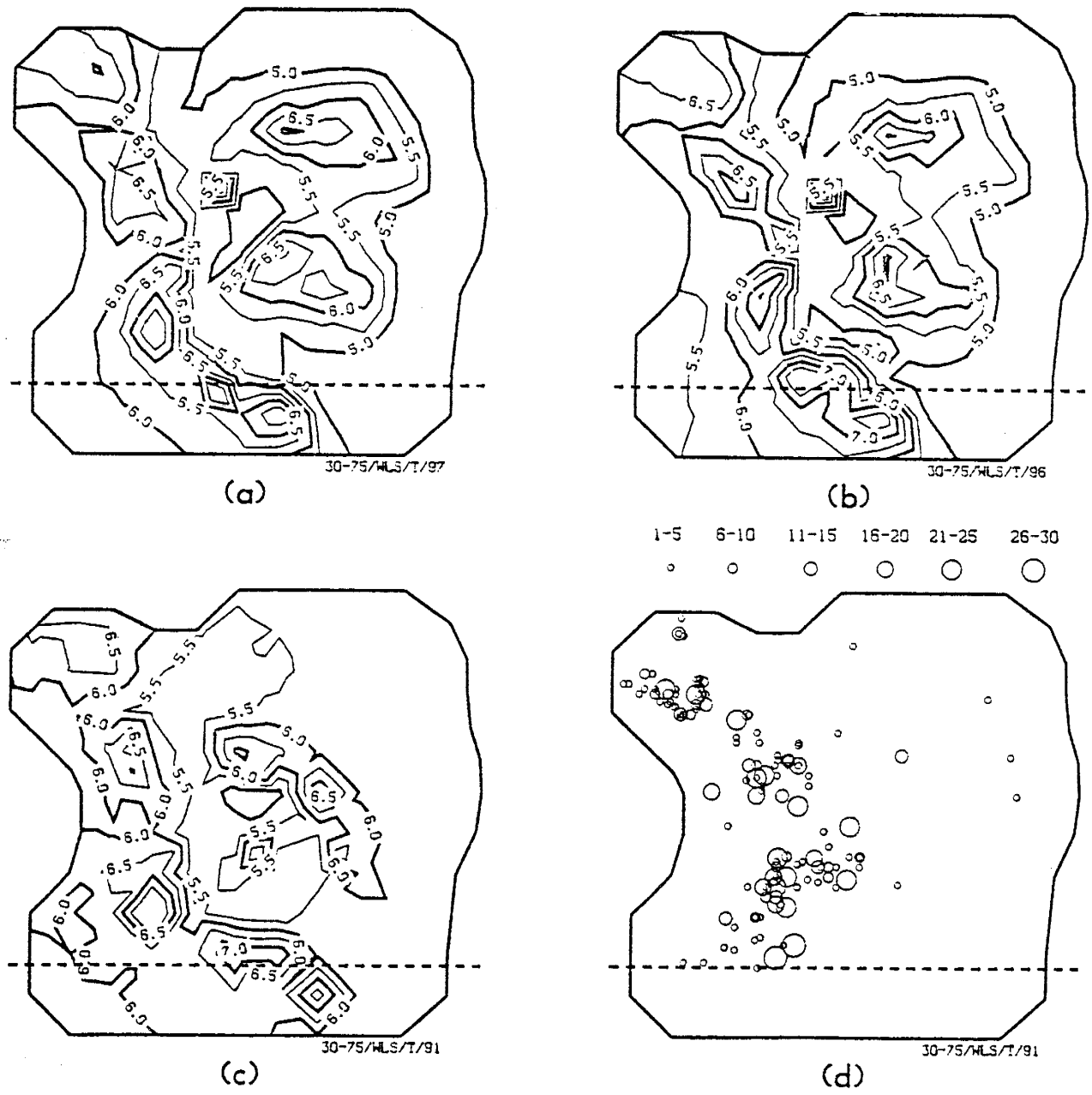

Fig. 20. WLS log T parameter estimates for prior log T values obtained from linear generalized covariance (a), linear variogram (b), and nugget generalized covariance (c). The locations and number of yearly head measurements are illustrated in (d).

half. In general, the location and configuration of high log T zones differs somewhat between the two sets of figures.

Figure 20d shows the location and number of head observations used in the WLS runs. Note that the major differences between the three log T fields occur in areas of the basin that did not have a large number of head measurements. It would seem that where a large number of head observations was available the estimated log T field tended to be unique regardless of the prior log T values. In areas of the basin where observed heads were sparse or nonexistent, the estimated log T values are strongly conditioned on the supplied prior information.

The three estimated log T fields in the western portion of the basin make good sense geologically. A high T "corridor" that begins at the gap between the Tres Hermanas and Florida mountains and continues south through Columbus is possible for two reasons. First, this high T zone approximates the course of the ancestral Mimbres River when it flowed to the west of the Florida Mountains instead of around the north end of them as it does today (figure 4). It is very possible that the Mimbres River deposited very transmissive beds of sands and gravels in this region. Secondly, well logs indicate numerous basalt layers in the subsurface of the region outlined above. Fractured basalt aquifers can have very high Ts, and there is no evidence to indicate that this is not the case in the Columbus Basin as well.

The estimated log T fields in the eastern portion of the basin are difficult to explain geologically. Since there were few head observations in this area, CERT may have adjusted the log T parameters arbitrarily to aid in the minimization of J. A high log T zone was consistently estimated due east of Columbus and north of the international border. This zone may have been dependent upon the pumping center as much as anything. The high log T

zone that trends northwest-southeast and is located south of the international border was probably a function of the imposed prescribed head boundary conditions on the basin's southern boundary (see figure 22). The high log T zone was required to channel flow east so that it could exit the basin. If the boundary conditions on the basin's southern boundary were changed, the position of this high log T zone would probably change also.

Due to the similarities of the three log T fields estimated for the western portion of the basin, and because the two outlying C_s points were believed to be unreliable, a constant value of log T equal to 5.916 and a constant σ_T equal to 0.3229 was used as the prior estimate of log T for all subsequent CERT runs described in this report. This prior corresponds to the nugget generalized covariance of 0.1. The simulated head fields for four years that were obtained using the log T field in figure 20b are shown in figure 21. These head surfaces are typical of those obtained throughout this study.

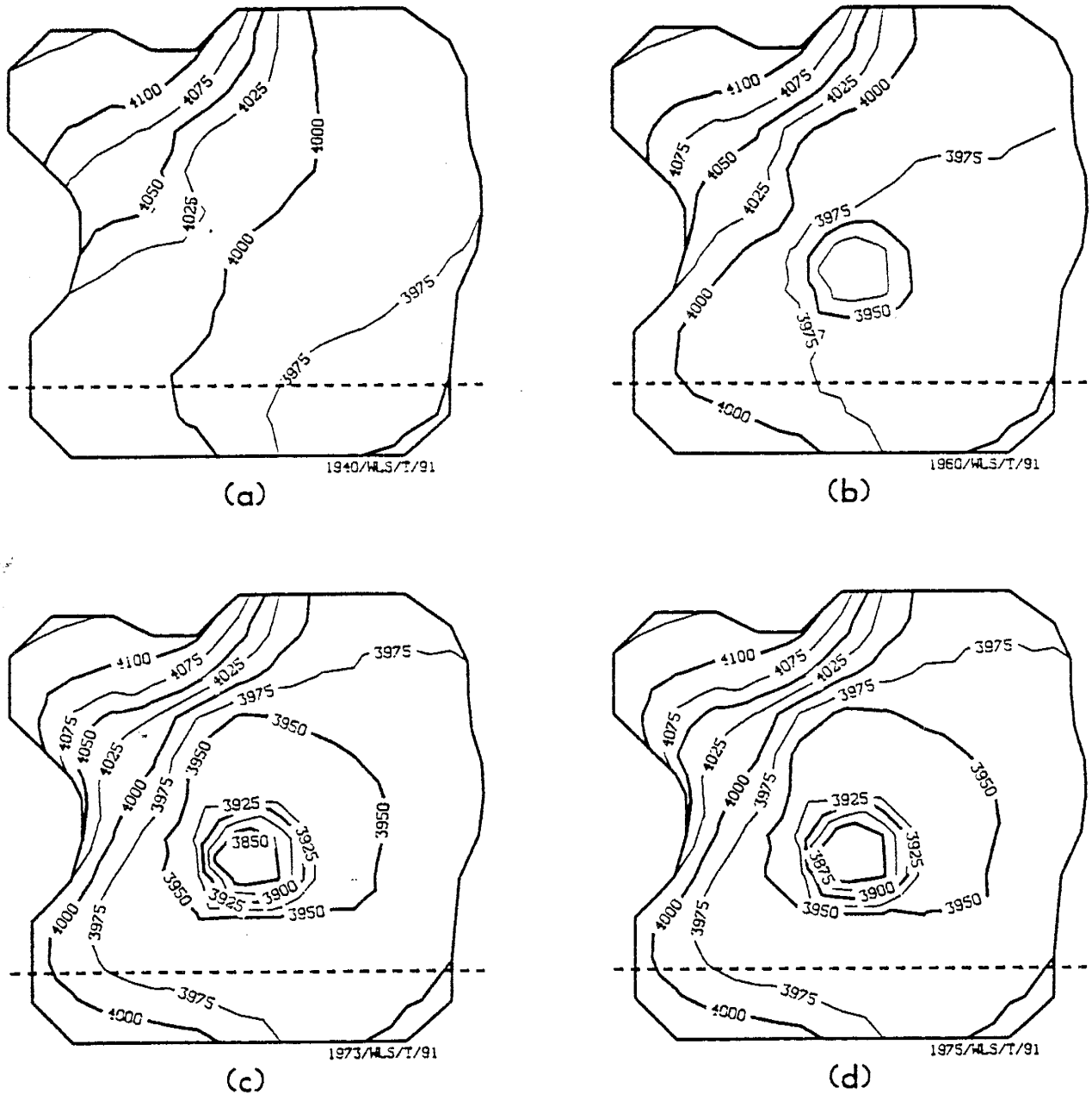

Fig. 21. Head surfaces for run 91 for years 1940, 1960, 1973 and 1975.

ESTIMATION OF BOUNDARY CONDITIONS THROUGH THE INVERSE PROCEDURE

Prior Information

A pre-development hydraulic head map was constructed for the Columbus Basin using the available water level measurements near the basin boundaries and qualitative knowledge of the basin hydrogeology (figure 22). Most of the measurements used were made prior to 1955; a time at which water levels near the Columbus Basin boundaries were not affected by pumping. Several of the measurements used in the eastern portion of the basin were taken around 1970. These measurements were used to help construct the pre-development map because they were the only measurements available for the area and they were probably only minimally affected by the cone of depression at that time (see figure 99 p. 194).

Using the pre-development hydraulic head map a first type boundary head was estimated for all of the boundary nodes of the finite element mesh. The term boundary nodes is used in reference to those nodes which define the external boundary of the finite element grid. When using the generalized boundary condition internal nodes with some prescribed flux (i.e. pumping nodes) can also be considered boundary nodes, but in this report such "internal" boundary nodes will be referenced as flux nodes or pumping nodes.

A standard deviation (σ_B) was subjectively assigned to each boundary node estimate. Any one σ_B value directly reflected the availability of observed head data in the vicinity of that node. The estimated boundary heads north of the international border and on the west and northwest edges of the grid were felt to be the most certain. The nodal boundary heads were assumed to be uncorrelated in space during the WLS estimation procedure.

The first type boundary heads and their assigned standard deviations are listed in table 5. The locations of the boundary nodes are shown in

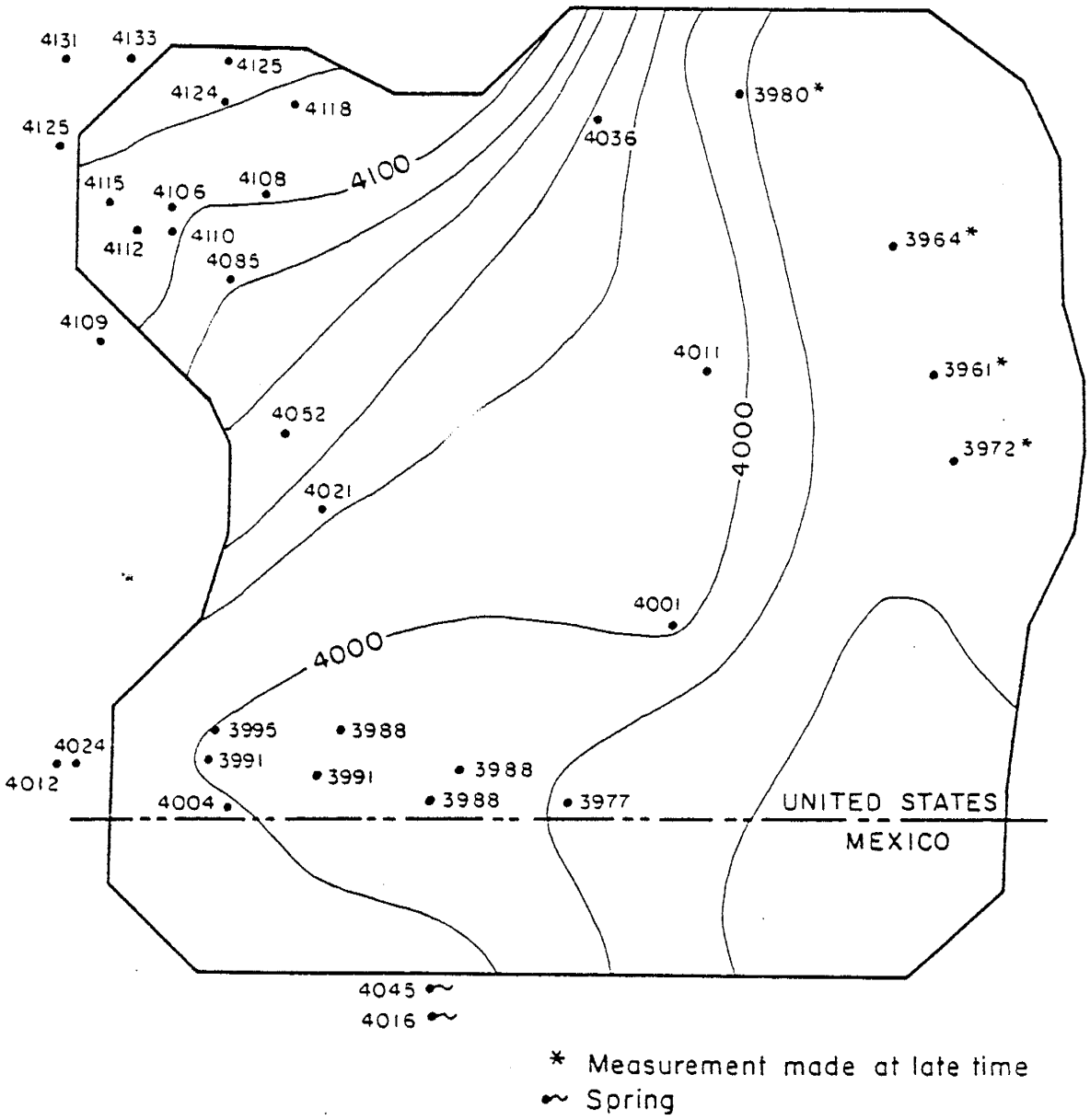

Fig. 22. Subjective pre-development head contour map for Columbus Basin used to obtain estimates of boundary heads. Head in feet above MSL.

Table 5

Prior estimates of A and B boundary paramaters

Node	A	B	Standard Deviation
1	1E+15	4132.	10.
2	1E+15	4126.	15.
3	1E+15	4124.	15.
12	1E+15	4115.	15.
13	1E+15	4105.	20.
4	1E+15	4095.	20.
5	1E+15	4025.	20.
6	1E+15	3990.	30.
7	1E+15	3978.	30.
8	1E+15	3977.	30.
19	1E+15	3976.	30.
9	1E+15	4127.	10.
20	1E+15	4125.	10.
39	1E+15	4117.	15.
48	1E+15	4115.	15.
60	1E+15	4111.	15.
70	1E+15	4095.	15.
81	1E+15	4070.	15.
90	1E+15	4060.	15.
108	1E+15	4051.	15.
126	1E+15	4025.	15.
136	1E+15	4015.	15.
144	1E+15	4008.	10.
163	1E+15	4007.	10.
182	1E+15	4009.	10.
193	1E+15	4025.	25.
194	1E+15	4022.	25.
195	1E+15	4015.	25.
196	1E+15	4010.	25.
197	1E+15	3991.	25.
198	1E+15	3975.	30.
199	1E+15	3960.	35.
200	1E+15	3950.	35.
201	1E+15	3945.	40.
192	1E+15	3948.	40.
173	1E+15	3950.	40.
154	1E+15	3960.	35.
27	1E+15	3975.	35.
47	1E+15	3975.	35.
69	1E+15	3975.	35.
89	1E+15	3975.	35.
100	1E+15	3975.	35.
118	1E+15	3974.	35.
135	1E+15	3970.	35.

figure 23. The heads and standard deviations in table 5 represent the prior information for the boundary node parameters.

Estimation of Boundary Parameters

Estimation of B. Using the boundary heads in table 5, a constant value of S (= 5×10^{-4}), a constant prior of log T (= 5.916 ft^2/year) and standard input as described previously, a series of runs was made to estimate the generalized boundary parameters A and B for the boundary nodes. Each run was made for the time period 1930 to 1975. For each run the nodal values of log T, as well as the boundary parameters, were allowed to vary. This facilitated the convergence of the parameter estimation algorithm since it was unreasonable to expect a good match between interior nodal heads and observed heads during a transient run when only the boundary heads (constant through time) were permitted to vary. For this set of runs a posterior covariance estimation was not conducted on the estimated parameters due to the computational intensity of the algorithm and the large number of parameters.

For the next three runs the results are presented in a table comparing the prior and post estimates of the boundary parameters, a posterior log T contour map with the most significant changes in boundary heads, B, marked at the appropriate nodes, and a contour map of the steady state hydraulic head field obtained using the posterior (estimated) log T and boundary parameters.

The first run (50) was conducted using the prior boundary parameters listed in table 5. The log T and B parameters were considered uncertain. The results are presented in table 6 and figures 24a and 24b.

Looking at table 6, there are two nodes, 12 and 6, for which the posterior head estimate moved more than two standard deviations away from the prior estimate. There are also two regions of the boundary which seem

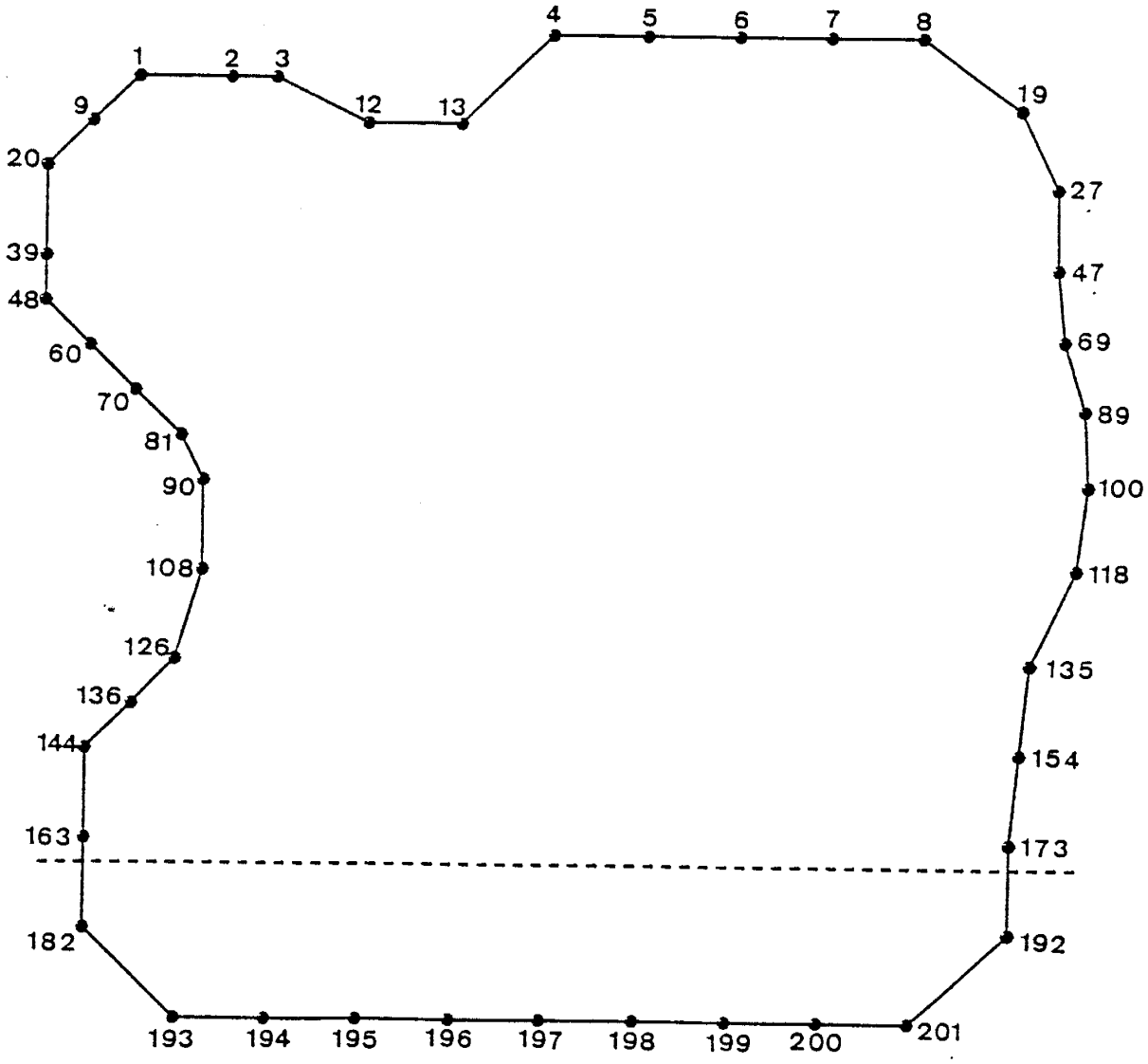

Fig. 23. Boundary node numbers and locations for the Columbus Basin grid.

Table 6

Post and prior estimates of boundary heads (B) for simulation 50 (units = ft)

Node	Prior	Post	Difference
1	4.1320E+03	4.1310E+03	-1.00E+00
2	4.1260E+03	4.1330E+03	7.00E+00
3	4.1240E+03	4.1510E+03	2.70E+01
12	4.1150E+03	4.1490E+03	3.40E+01
13	4.1050E+03	4.1100E+03	5.00E+00
4	4.0950E+03	4.1020E+03	7.00E+00
5	4.0250E+03	3.9990E+03	-2.60E+01
6	3.9900E+03	3.9020E+03	-8.80E+01
7	3.9780E+03	3.9480E+03	-3.00E+01
8	3.9770E+03	3.9810E+03	4.00E+00
19	3.9760E+03	3.9800E+03	4.00E+00
9	4.1270E+03	4.1340E+03	7.00E+00
20	4.1250E+03	4.1430E+03	1.80E+01
39	4.1170E+03	4.1190E+03	2.00E+00
48	4.1150E+03	4.1090E+03	-6.00E+00
60	4.1110E+03	4.1020E+03	-9.00E+00
70	4.0950E+03	4.0960E+03	1.00E+00
81	4.0700E+03	4.0810E+03	1.10E+01
90	4.0600E+03	4.0780E+03	1.80E+01
108	4.0510E+03	4.0770E+03	2.60E+01
126	4.0250E+03	4.0350E+03	1.00E+01
136	4.0150E+03	3.9750E+03	-4.00E+01
144	4.0080E+03	3.9990E+03	-9.00E+00
163	4.0070E+03	4.0070E+03	0.00E+00
182	4.0090E+03	4.0080E+03	-1.00E+00
193	4.0250E+03	4.0200E+03	-5.00E+00
194	4.0220E+03	4.0200E+03	-2.00E+00
195	4.0150E+03	3.9970E+03	-1.80E+01
196	4.0100E+03	3.9700E+03	-4.00E+01
197	3.9910E+03	3.9900E+03	-1.00E+00
198	3.9750E+03	4.0100E+03	3.50E+01
199	3.9600E+03	4.0190E+03	5.90E+01
200	3.9500E+03	3.9970E+03	4.70E+01
201	3.9450E+03	3.9760E+03	3.10E+01
192	3.9480E+03	3.9750E+03	2.70E+01
173	3.9500E+03	4.0070E+03	5.70E+01
154	3.9600E+03	4.0090E+03	4.90E+01
27	3.9750E+03	3.9810E+03	6.00E+00
47	3.9750E+03	3.9850E+03	1.00E+01
69	3.9750E+03	3.9730E+03	-2.00E+00
89	3.9750E+03	3.9620E+03	-1.30E+01
100	3.9750E+03	3.9810E+03	6.00E+00
118	3.9740E+03	3.9810E+03	7.00E+00
135	3.9700E+03	4.0010E+03	3.10E+01

to have a greater change in head than other areas. These regions are defined (moving counter-clockwise) by nodes 195 to 135 and nodes 7 to 5. Nodes 3 and 136 also show significant changes. Finally, note (figure 24a) that high log T zones are estimated adjacent to the boundary nodes with the greatest decrease in boundary head values (nodes 136, 196 and 6).

The increases at boundary nodes 3 and 12 are not disturbing. These nodes are located on the proximal alluvial fans of the Florida Mountains and gradients in this area could logically be steeper than predicted.

The changes in boundary heads on the southern boundary may not represent reality but were not surprising. The standard deviation of these heads was high due to their inherent uncertainty (no data in Mexico), and therefore these nodes were not tightly constrained during the search procedure. The estimated log T field is "flat" and maintains the prior value on the east side of the basin primarily due to the lack of data, but a high log T "corridor" trending north-south was estimated on the west side of the basin. CERT simply channeled water out of the southern boundary (see heads in figure 23b) by increasing T and decreasing the boundary heads (figure 24a).

The scenario described above is not believed to be realistic judging from regional water level trends but it is hard to tell due to the lack of data. The same process, however, seems to be occurring at two additional locations in the basin: at node 136 located on the southeastern flank of the Tres Hermanas Mountains and at nodes 5, 6 and 7, located on the northern basin boundary in the bolson east of the Florida Mountains. At these two locations the model has channeled water out of the basin by decreasing the boundary head(s) and locating a high log T zone adjacent to it(them).

The model predictions at these two locations are absurd. Groundwater is not moving northward out of the basin and it certainly is not moving west

into the bulk of the Tres Hermanas Mountains. The model seems to be moving water out of the basin along a path of minimal energy expenditure, within the constraints, of course, of observed head measurements and provided prior information. For example, CERT allowed recharge from the Florida Mountains to flow out the northern basin boundary, as opposed to directing this water along a longer flow path east and then south down the Mimbres Graben, which is believed to be the case in reality. The unrealistic nature of the boundary parameter estimates becomes readily apparent upon inspection of figure 24b. This head map is the steady state solution for the Columbus Basin given the posterior estimates of the log T and B parameters from run 50.

Given the unrealistic and sometimes drastic change in boundary heads during the previous run, another run was conducted where the 'problem' boundary nodes where constrained through the assignment of small σ_B (run 52). The standard deviation on boundary nodes 5 through 8 and 195 through 135 was changed to 5 ft. The results of this run are presented in table 7 and figures 24c and 24d.

The constraints on the northern and southern boundary nodes worked and no significant changes occurred at these locations. However, the remaining estimated boundary heads were still no more realistic than before. The standard deviation for node 136 was not reduced and CERT channelled an even larger amount of water through this node than previously. This is because flow could no longer conveniently exit the southwestern portion of the boundary. Note also that a high log T zone trending northwest-southeast was estimated south of the international border - presumably to move water towards the southeastern discharge area of the basin. This effect was also noted in the previous section.

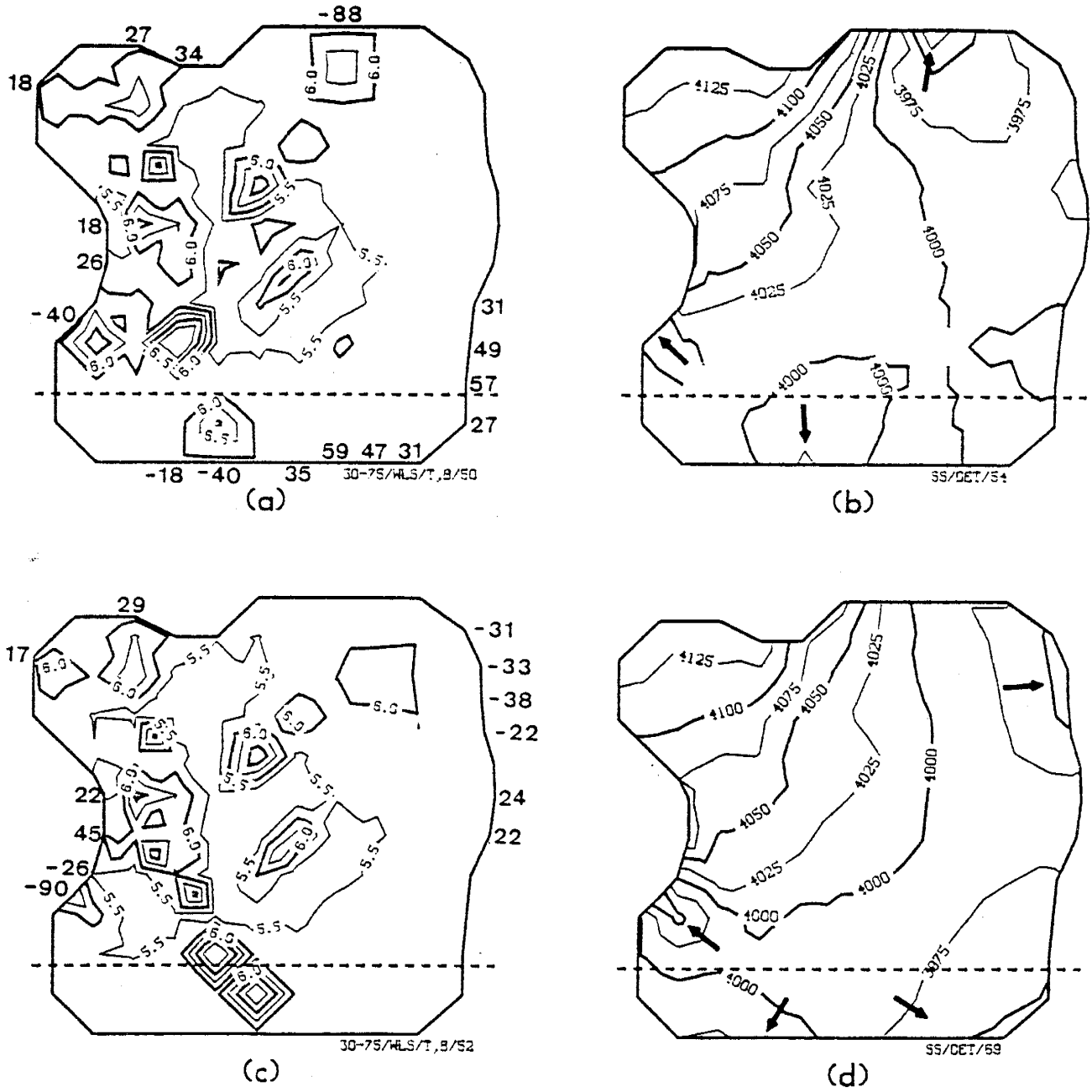

Fig. 24. Posterior log T field with greatest changes in boundary heads and steady state head field from posterior log T and B parameter estimates for runs 50 (a and b) and 52 (c and d). Head in feet above MSL.

Table 7

Prior and post estimates of boundary heads (B) for simulation 52 (units = ft)

Node	Prior	Post	Difference
1	4.1320E+03	4.1300E+03	-2.00E+00
2	4.1260E+03	4.1280E+03	2.00E+00
3	4.1240E+03	4.1530E+03	2.90E+01
12	4.1150E+03	4.1440E+03	2.90E+01
13	4.1050E+03	4.0800E+03	-2.50E+01
4	4.0950E+03	4.0830E+03	-1.20E+01
5	4.0250E+03	4.0230E+03	-2.00E+00
6	3.9900E+03	3.9880E+03	-2.00E+00
7	3.9780E+03	3.9760E+03	-2.00E+00
8	3.9770E+03	3.9760E+03	-1.00E+00
19	3.9760E+03	3.9450E+03	-3.10E+01
9	4.1270E+03	4.1320E+03	5.00E+00
20	4.1250E+03	4.1420E+03	1.70E+01
39	4.1170E+03	4.1170E+03	0.00E+00
48	4.1150E+03	4.1070E+03	-8.00E+00
60	4.1110E+03	4.0980E+03	-1.30E+01
70	4.0950E+03	4.0900E+03	-5.00E+00
81	4.0700E+03	4.0750E+03	5.00E+00
90	4.0600E+03	4.0820E+03	2.20E+01
108	4.0510E+03	4.0960E+03	4.50E+01
126	4.0250E+03	3.9990E+03	-2.60E+01
136	4.0150E+03	3.9250E+03	-9.00E+01
144	4.0080E+03	4.0040E+03	-4.00E+00
163	4.0070E+03	4.0030E+03	-4.00E+00
182	4.0090E+03	4.0080E+03	-1.00E+00
193	4.0250E+03	4.0250E+03	0.00E+00
194	4.0220E+03	4.0290E+03	7.00E+00
195	4.0150E+03	4.0150E+03	0.00E+00
196	4.0100E+03	4.0100E+03	0.00E+00
197	3.9910E+03	3.9870E+03	-4.00E+00
198	3.9750E+03	3.9750E+03	0.00E+00
199	3.9600E+03	3.9610E+03	1.00E+00
200	3.9500E+03	3.9510E+03	1.00E+00
201	3.9450E+03	3.9460E+03	1.00E+00
192	3.9480E+03	3.9490E+03	1.00E+00
173	3.9500E+03	3.9510E+03	1.00E+00
154	3.9600E+03	3.9610E+03	1.00E+00
27	3.9750E+03	3.9420E+03	-3.30E+01
47	3.9750E+03	3.9370E+03	-3.80E+01
69	3.9750E+03	3.9530E+03	-2.20E+01
89	3.9750E+03	3.9710E+03	-4.00E+00
100	3.9750E+03	3.9990E+03	2.40E+01
118	3.9740E+03	3.9960E+03	2.20E+01
135	3.9700E+03	3.9710E+03	1.00E+00

In the northeastern quarter of the basin, because heads on the northern boundary were constrained, flow was directed due east. The east boundary nodes 89 through 19 were decreased and a large increased log T zone (6.0 contour, figure 24c) was estimated between them and the Florida Mountains. CERT was 'chasing' the boundary around - the model forced the discharge of source water from the Floridas through the first sequence of boundary nodes on which it could decrease the heads enough to do so. The fallacy of the estimated parameters again became apparent when the steady state head map produced using the the parameter estimates was plotted (figure 24d).

Finally, a new hypothesis was tried to see if a more realistic set of boundary conditions could be estimated. The hydraulic head contours in figure 22 indicate the possible presence of a groundwater flow divide, oriented north-south, approximately 3 mi west of the eastern basin boundary. Due to the close proximity of the divide to the eastern boundary, it seemed reasonable to approximate the eastern boundary nodes (192 through 19) as no-flow boundaries with an assigned variance. This special case of the second type boundary condition was implemented by setting the A and B boundary parameters to zero. The B parameters of these second type boundary nodes were given a standard deviation of 6.81×10^6 ft^3/year, and the northern and southern first type boundary nodes were left constrained by a 5 ft σ_B as in the previous run. Results of this run (53) are presented in table 8 and figure 25.

The new conceptualization did not help matters and the picture was basically the same (figure 25a). A flux was estimated out the northeast corner of the basin, which was the same effect of course as decreasing the constant head boundaries in this region. Flow was also directed due south through nodes 193 and 194 on the southern boundary. High log T zones were estimated adjacent to each of these areas to facilitate the outward fluxes.

Table 8

Post and prior estimates of boundary heads (ft) and fluxes (ft**3/year) for simulation 53 (* indicate flux nodes)

Node	Prior	Post	Difference
1	4.1320E+03	4.1310E+03	-1.0000E+00
2	4.1260E+03	4.1330E+03	7.0000E+00
3	4.1240E+03	4.1510E+03	2.7000E+01
12	4.1150E+03	4.1460E+03	3.1000E+01
13	4.1050E+03	4.0910E+03	-1.4000E+01
4	4.0950E+03	4.0880E+03	-7.0000E+00
5	4.0250E+03	4.0240E+03	-1.0000E+00
6	3.9900E+03	3.9890E+03	-1.0000E+00
7	3.9780E+03	3.9640E+03	-1.4000E+01
8	3.9770E+03	3.9770E+03	0.0000E+00
19*	0.0000E+00	-1.9020E+06	-1.9020E+06
9	4.1270E+03	4.1340E+03	7.0000E+00
20	4.1250E+03	4.1430E+03	1.8000E+01
39	4.1170E+03	4.1180E+03	1.0000E+00
48	4.1150E+03	4.1090E+03	-6.0000E+00
60	4.1110E+03	4.1010E+03	-1.0000E+01
70	4.0950E+03	4.0950E+03	0.0000E+00
81	4.0700E+03	4.0740E+03	4.0000E+00
90	4.0600E+03	4.0680E+03	8.0000E+00
108	4.0510E+03	4.0780E+03	2.7000E+01
126	4.0250E+03	4.0500E+03	2.5000E+01
136	4.0150E+03	4.0190E+03	4.0000E+00
144	4.0080E+03	4.0080E+03	0.0000E+00
163	4.0070E+03	4.0080E+03	1.0000E+00
182	4.0090E+03	4.0090E+03	0.0000E+00
193	4.0250E+03	4.0140E+03	-1.1000E+01
194	4.0220E+03	3.9580E+03	-6.4000E+01
195	4.0150E+03	4.0110E+03	-4.0000E+00
196	4.0100E+03	4.0050E+03	-5.0000E+00
197	3.9910E+03	3.9870E+03	-4.0000E+00
198	3.9750E+03	3.9740E+03	-1.0000E+00
199	3.9600E+03	3.9600E+03	0.0000E+00
200	3.9500E+03	3.9510E+03	1.0000E+00
201	3.9450E+03	3.9460E+03	1.0000E+00
192*	0.0000E+00	3.3410E+06	3.3410E+06
173*	0.0000E+00	4.5610E+06	4.5610E+06
154*	0.0000E+00	5.4560E+06	5.4560E+06
27*	0.0000E+00	-1.6250E+06	-1.6250E+06
47*	0.0000E+00	-7.8480E+05	-7.8480E+05
69*	0.0000E+00	1.2270E+06	1.2270E+06
89*	0.0000E+00	3.9150E+06	3.9150E+06
100*	0.0000E+00	6.5850E+06	6.5850E+06
118*	0.0000E+00	6.2860E+06	6.2860E+06
135*	0.0000E+00	5.7360E+06	5.7360E+06

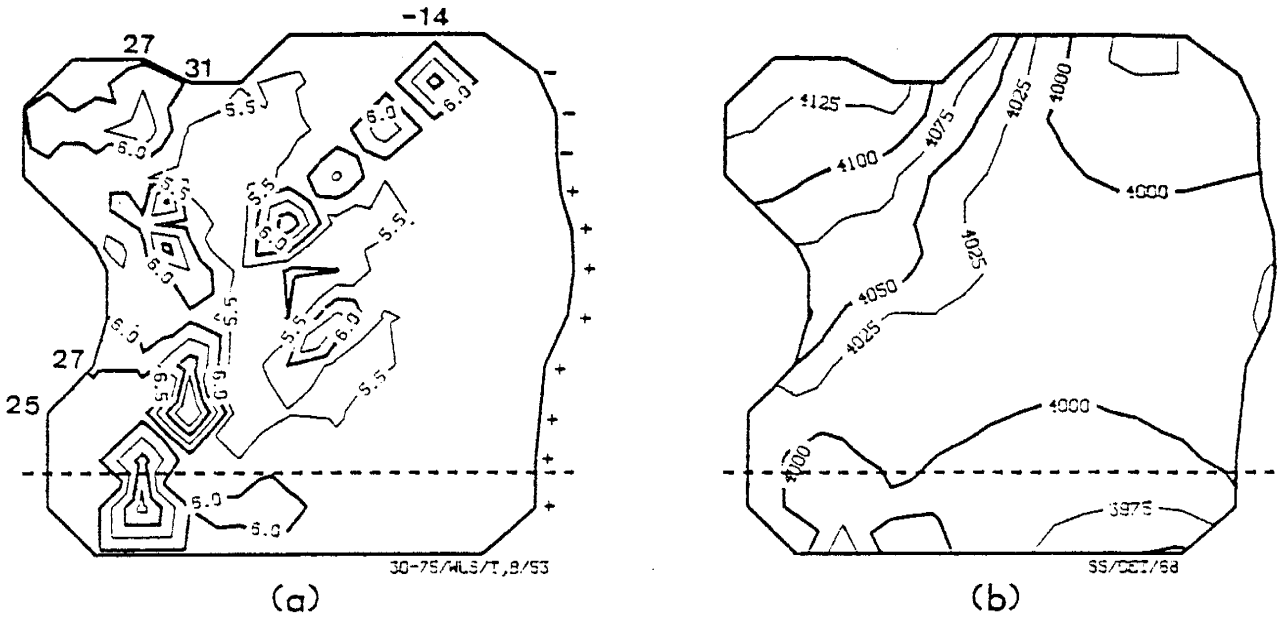

Fig. 25. Posterior log T field with changes in boundary heads and sign of boundary fluxes marked at appropriate nodes for run 53 (a), and steady state head field obtained using parameter estimates from run 53 (b). Head in feet above MSL.

No new insights were gained from implementing the no-flow boundary, and this observation added to the fact that every zero-flux node changed significantly indicted that this new conceptualization was probably not a sound one.

Estimation of A. One CERT run was made to estimate the A parameter of the Columbus Basin boundary nodes. This run was identical to the first run described in the previous section (table 6 and figures 24a and 24b), the only difference being that the A as well as the B parameters were considered uncertain. The prior estimate of the A parameters for the first type boundary nodes was 1.0×10^{15} with an associated σ_A of 0.5×10^{15}. This standard deviation was large enough to allow A to approach zero, which would indicate a movement towards a flux type boundary condition. The results from this run are not presented because they are essentially the same as those in figure 24 and table 6. The changes in the boundary heads were within several feet of those observed previously, and with the exception of node 108 where A was estimated as 4.9×10^{11}, all of the A parameters were estimated to be on the order of 10^{14}. None of the changes were of sufficient magnitude to suggest a different boundary type, which in any case is arbitrary for this conceptualization.

Discussion

The attempt to estimate boundary conditions from prior information using CERT obviously failed. There are several plausible reasons for the failure, some of which could possibly be fixed by additional modeling and/or programming effort, and some of which can not be adequately handled by a computer model. First of all, CERT input routines do not allow for correlation between boundary parameters (i.e. boundary head, flux, or type), although the inverse solution does. This lack of correlation structure allowed some parameters to oscillate a great deal while adjacent parameters

remained stationary. Boundary parameter correlation could be added to CERT input, but such an option would probably only reduce the extreme oscillations of the parameter estimates, not lead to a more realistic situation. An added problem would also arise of estimating the correlation structure between boundary parameters for areas where data is sparse or nonexistent, since model boundaries are often far removed from the area of interest to minimize their effect on model predictions. Never-the-less this approach should be explored in future work.

The above statement leads directly to another problem with the estimation of boundary parameters- boundaries often are arbitrarily placed and hence boundary parameters are not readily identifiable. If data is not available in the vicinity of the boundaries (e.g., water level measurements), good parameter estimates should not be expected. This leads to a "Catch 22" situation, since if data were available near or on the boundary points, the prior estimates of the parameters should be good anyway. In short, CERT cannot estimate something with nothing. This task falls to the hydrogeologist (who does this all the time).

Finally, there is subjective information and real data outside the basin boundary which CERT cannot incorporate. For the Columbus Basin study there was no way to tell the code that flow was north to south through the northern boundary, or that the Tres Hermanas Mountains existed west of node 136. There was also no way for CERT to assess the plausibility of a high T zone within the Mimbres Graben due to an increased thickness of the bolson sediments. There was no log T and virtually no head measurement data for this eastern portion of the study area.

Some of these problems might be partially rectified by the addition of constraints to the search procedure. The algorithm currently used by CERT is an entirely unconstrained search. For example, a constraint could be

added to the code which would specify that flux through the northern boundary nodes would have to be positive into the basin. Run 52 was effectively an attempt to use small parameter variances to implement such a constraint. Obviously, as the results of that attempt show, constraints alone can not do the job.

Another approach would be to increase the size of the domain, to seek more natural boundaries. A similar concern was raised for the Palo Duro Basin application of CERT several years ago (Wilson and Harper 1983). The Columbus Basin grid could easily be extended on the northern and southern boundaries. Data in these regions (east of the Florida Mountains to the north and in Mexico to the south), however, is sparse or non-existent. The Camel Mountain Fault on the east side of the basin and the Florida and Tres Hermanas mountains on the west side of the basin should provide good natural boundaries. The boundary nodes in the gap between the Tres Hermanas and Florida mountains and due south of the Tres Hermanas Mountains present a unique problem because they separate the Columbus Basin from adjoining basins where groundwater development is substantial. The grid boundary at these locations could not be extended without attempting to model entire basins which adjoin the Columbus Basin.

In light of the previous discussion it is of paramount importance that code users view all output with a critical eye, and users should keep in mind that although CERT, or similar codes, can greatly reduce the effort involved with some parameter estimates, it cannot work wonders. The prior estimates of the boundary parameters listed in table 5 were used for all of the following CERT simulations presented in this study.

ESTIMATION OF STORATIVITY THROUGH THE INVERSE PROCEDURE

Constant Prior of S Over Entire Basin

Storativity was assumed constant over the entire basin (value = 5.0×10^{-4}) during the previous analysis. However, geologic evidence indicated that some areas of the basin, most notably those regions adjacent to the Tres Hermanas and Florida mountain ranges, may be only partially confined or unconfined. A run was made to see if CERT would identify these potentially high S zones (run 66). A constant prior S and σ_s value of 5.0×10^{-4} and 5.0×10^{-3} respectively was assigned to each node in the basin. S was assumed uncorrelated between nodes. The large standard deviation indicated that the prior was essentially non-informative. The prior values of the other parameters were the same as previous runs. Both S and log T were permitted to vary during the WLS search procedure.

Output from run 66 is presented in figure 26. One can see from a comparison of figure 26a, the contoured S field, and figure 26c, the 1973 head field, that CERT estimated a high S zone almost directly over the center of pumping in the basin. This region of the basin was believed to be confined, although the large prior σ_s did not insure this. CERT also estimated a high log T zone at the center of pumping (figure 26b).

The S field estimated by CERT is obviously unrealistic. Because no recharge was considered in this model, water pumped from the aquifer was obtained either from storage or inflow (or decreased outflow) through the boundaries. When S was left unconstrained (high prior variance), CERT simply increased S in and about the center of pumping to create a readily available source of water.

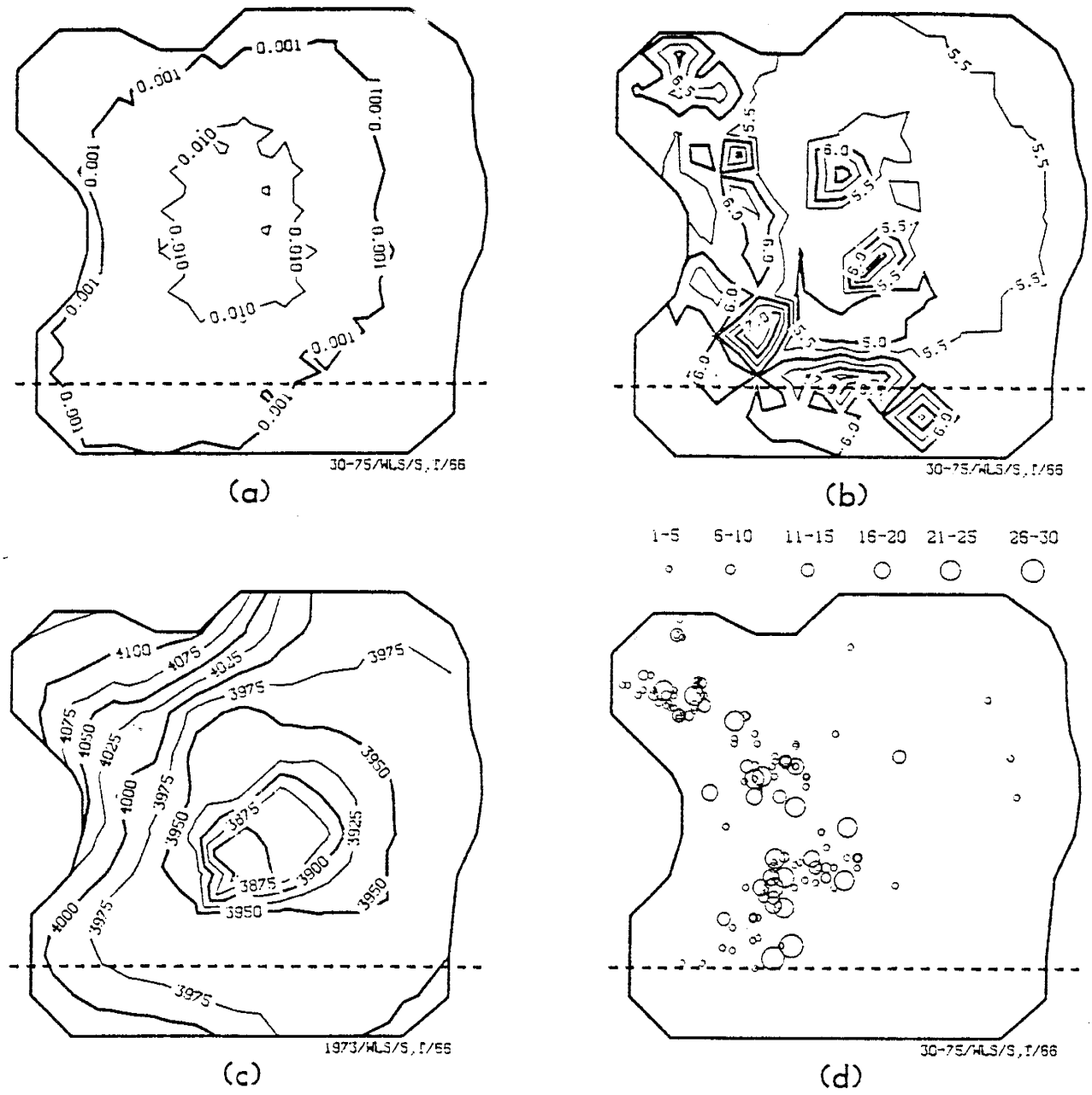

Fig. 26. Estimated S field (a), log T field (b), 1973 head field (c), and observations used (d) for WLS run 66. Head in feet above MSL.

Zoned Storativity

Since a reasonable configuration of the storage coefficient was not estimated in the previous run, a new prior for S was input into CERT and another WLS run was conducted (run 67). The new nodal values of S were based on the hydrogeological cross sections in figures 7 through 9. For this run 64 nodes on the west and northwest margins of the basin were assigned an S value of 0.05 and a σ_s of 0.01, while the remaining nodes were assigned an S value of 5.0×10^{-4} and a σ_s of 1.0×10^{-4}. The basic outline of the two S zones is shown in figure 27. Log T was again allowed to vary.

For this run the prior values of S were tightly constrained over the region of the basin believed to be confined, but the prior values over regions of the basin where the value of S was more uncertain were given quite a bit of freedom to move. The results of this run are not presented in a figure because the values of S at nodes exhibited only minor changes. All S values in the 5×10^{-2} zone remained on the order of 10^{-2}, and all S values in the 5×10^{-4} zone remained close to this value. These results indicated that either the two zone parameterization is a good one for S, or that the model heads are relatively insensitive to the S parameter. Recall that in run 66, many nodal S values increased by more than two orders of magnitude, but these changes were still within one standard deviation of the prior values. This fact lends credence to the possibility of insensitivity.

The above estimations of S by CERT were either improbable or inconclusive. No new insights regarding S values in the Columbus Basin were obtained through the inverse procedure. However, the zoning of S was also addressed using CERT following a slightly different procedure. A set of runs was conducted where S was not permitted to vary during the parameter search, but log T was still considered uncertain and could change. Different sets of prior S values and a constant convergence criteria of 1.0

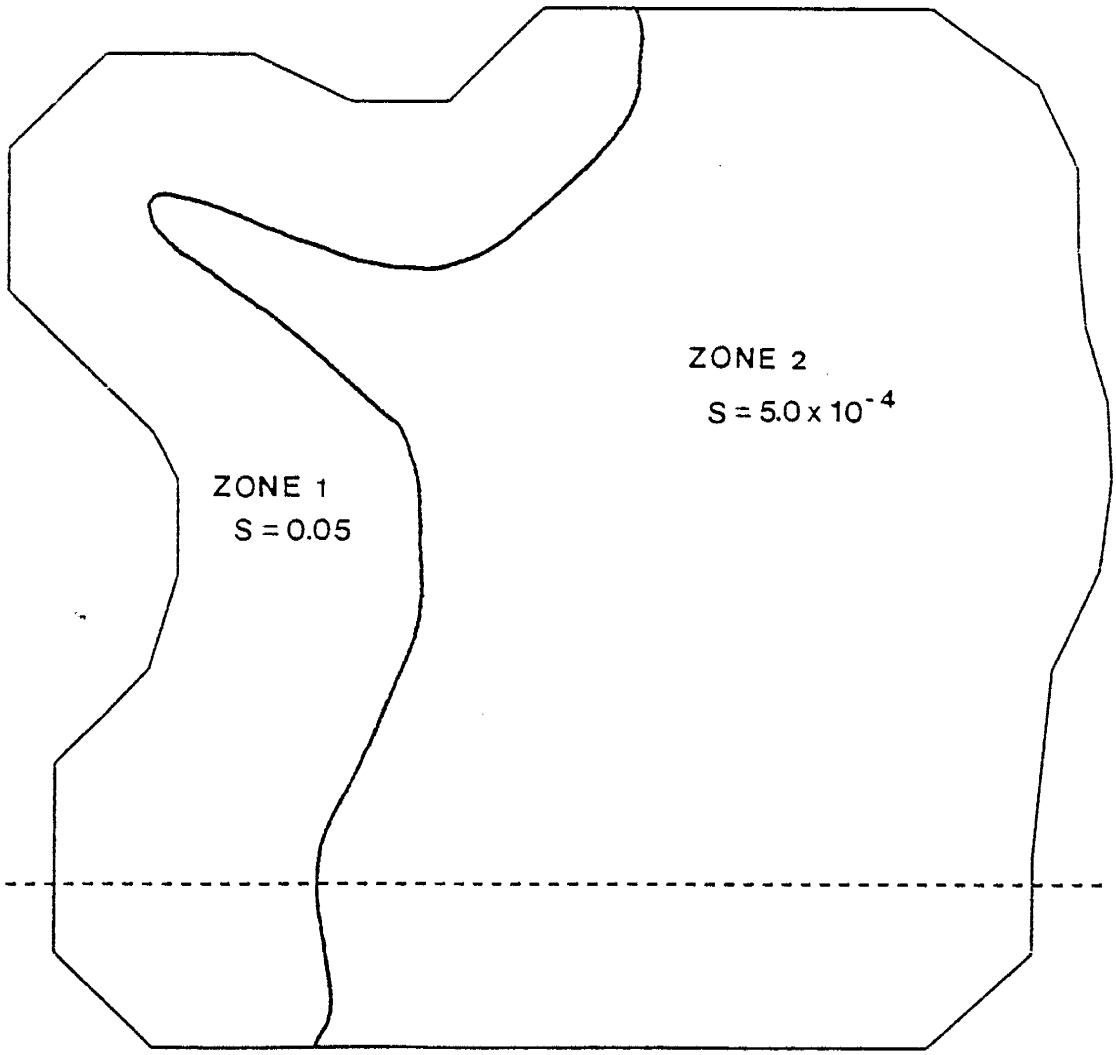

Fig. 27. Approximate outline of nodal zonation used for run 67.

(Townley and Wilson 1985) was specified for all runs. The final objective function values from each run were then compared. A smaller J_h value for any run should indicate a more optimal parameterization of S.

This set of runs is presented in table 9. The zoned S values in run 61 result in the lowest value of J_h. These values tend to confirm that zone 1 may be unconfined or only partially confined.

The smallest J_h value was obtained when S in the unconfined zone was set at 0.3. This value seemed rather high, however, considering the geological setting of zone 1. It was decided that a more reasonable value might be 0.1.

Storage Depletion

A plot of time vs. total pumpage and storage depletion for run 107 is shown in figure 28. Run 107 used Log T and pumping parameters estimated during run 89, which will be discussed later. The results of run 107 are presented here because the two zones of S outlined in figure 27 were used with S = 0.1 in the unconfined zone and S = 5.0×10^{-4} in the confined zone.

One can see from figure 28 that storage depletion during run 107 accounted for less than half of the estimated withdrawals from the aquifer. The difference between the two curves must be accounted for by net inward flux through the prescribed head boundary nodes. The net flux through the basin boundary increased substantially with time, and hence the first type boundary nodes artificially restricted the cone of depression.

These results indicated that either the basin has a very small time constant and pumping effects the boundaries almost instantly, or that some significant sources of water were not being accounted for. With this thought in mind, simulation 107 was rerun with the highest S values believed to be possible for the Columbus Basin. S for the unconfined zone was set at

Table 9

Comparison of J for different values of S in zones 1 and 2. Only T uncertain for each run.

Run #	Values of S Zone 1	Zone 2	Convergence Criteria	J_h	J
59	5.0 x 10	5.0×10^{-4}	1.0	5.024×10^3	5.942×10^3
60	0.05	5.0×10^{-4}	1.0	4.563×10^3	5.085×10^3
61	0.3	5.0×10^{-4}	1.0	4.175×10^3	4.631×10^3

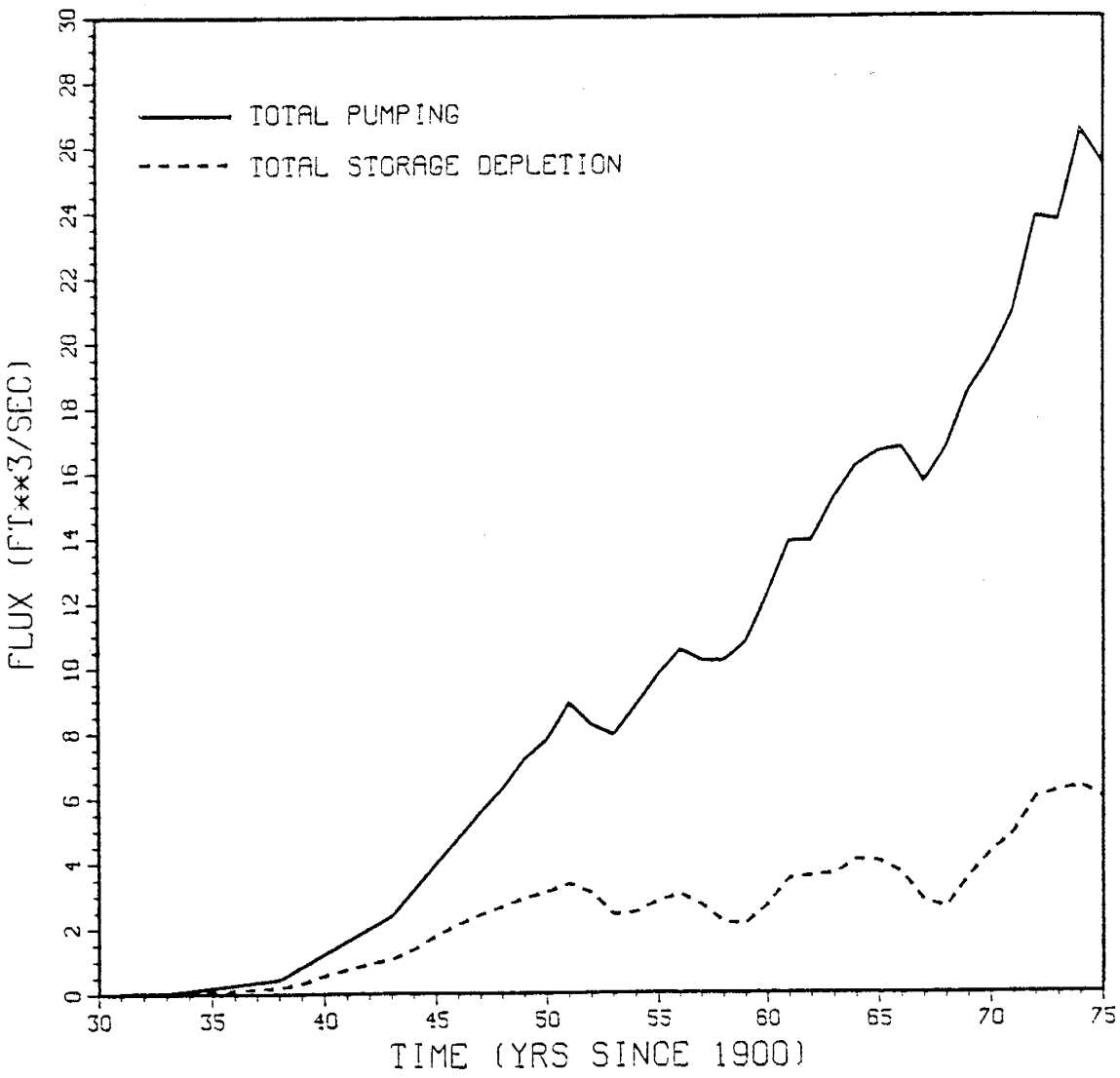

Fig. 28. Plot of time vs. total pumping and storage depletion for run 107. S was 0.1 and 5 x 10^{-4} in the unconfined and confined zones respectively.

0.3, while S in the confined zone was 5.0×10^{-2}. The results of this run are shown in figure 29.

Even with the increased S values the boundary nodes were still affected (figure 29). One source of water not accounted for was the decrease in discharge through the confining layer due to drawdown in the primary aquifer. This water budget component, however, was not believed to be large enough to account for the observed discrepencies. There is a strong possibility of vertical leakage from below which was not accounted for in the conceptual model of the basin. The examination of the plausibility and volume of such leakage is a topic for future research.

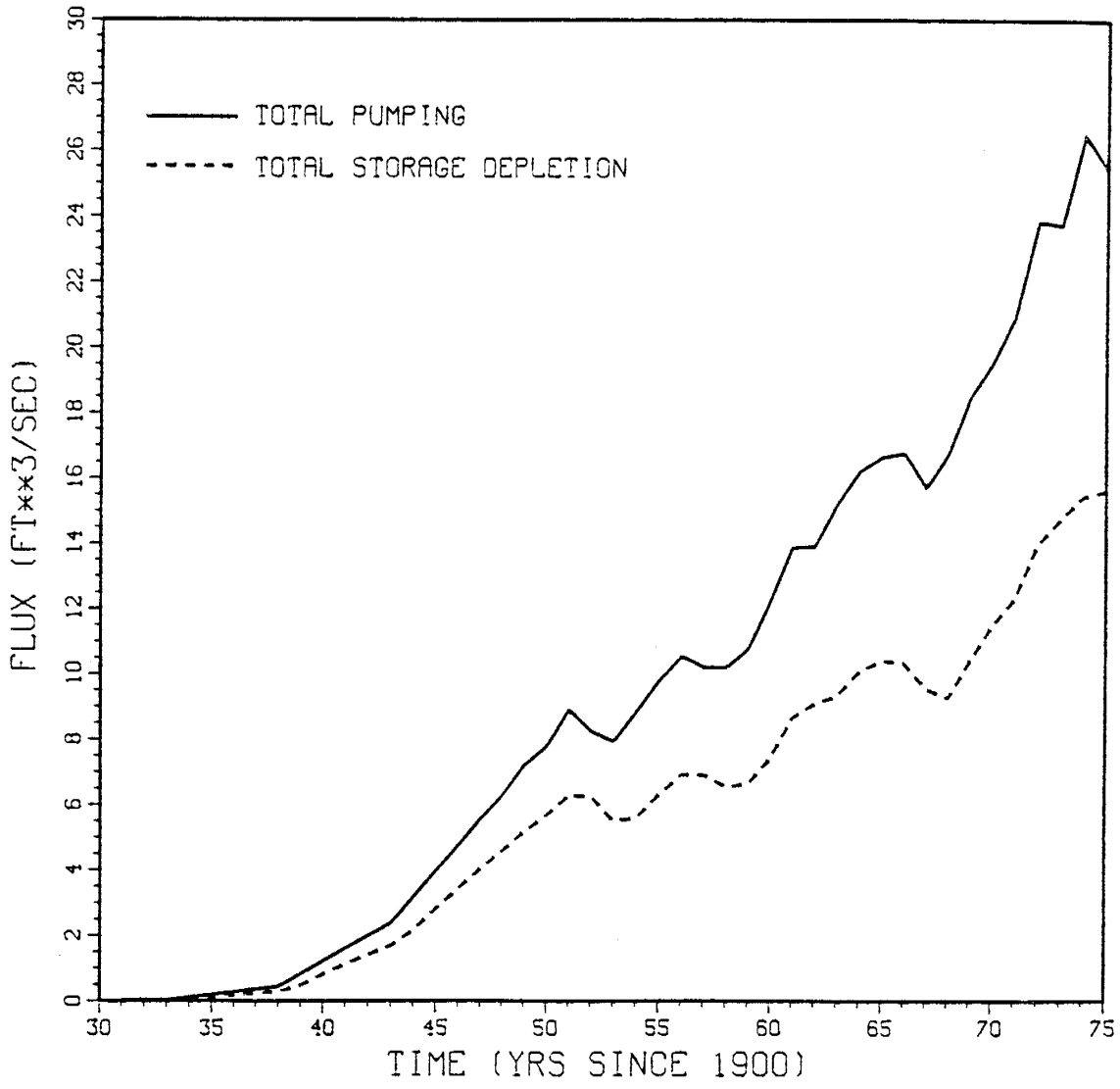

Fig. 29. Plot of time vs. total pumping and storage depletion for run 106. S was 0.3 and 5 x 10^{-2} in the unconfined and confined zones respectively.

ESTIMATION OF PUMPING THROUGH THE INVERSE PROCEDURE

Prior Information

The source of the pumping data used in this study and the way in which pumping values were assigned to nodes was described in the Data Aquisition and Analysis section of this report. Swen Magnuson attempted to find some correlation structure for the pumping data using multivariate regression and median polish (Cressie 1986). The variogram estimates for both methods showed no consistent structural behavior over space at a given time or over time at pumping locations.

The failure to find a spatial or temporal correlation between the pumping values may have been due to the failure of multivariate regression to estimate an accurate surface and a failure of median polish to remove trends in the data. Because pumping increased with time it was essential to estimate the trend accurately so that it could be removed prior to the variogram analysis.

The problem may also have been due to the nature of the data itself. The SEO pumping estimates were obtained through crude methods, and the estimates were further processed in this work to facilitate their assignment to nodes. Even if a true correlation of pumpage in the Columbus Basin existed, its character may have been seriously filtered during the various processing procedures.

Estimation of Pumping

WLS run 70 estimated log T and B (pumping) over the entire time period 1930 to 1975. All of the available head data was used, S was a constant 5.0×10^{-4}, and the boundary heads were those presented previously. The B parameters were estimated at the circled nodes of the finite element grid shown in figures 12 and 13. Recall that the flux at a node is the B

parameter of the generalized boundary condition when the A parameter is set to zero.

The nodal fluxes were uncorrelated and were assigned a σ_B of 25 percent of the B value for each node at each time. Therefore as the nodal fluxes increased through time, so did the estimate of their uncertainty. Pumping nodes assigned a zero B value (this was common for early time steps) were assigned a σ_B of 12,500 ft^3/year, which was approximately 25 percent of the average of the early pumping values.

The posterior log T field, and the head data used for run 70 are shown in figure 30. The posterior B values were analyzed by plotting the prior and posterior estimates of pumping versus time at individual nodes. These plots tended to fall into one of two classes: (1) the post and prior (SEO) estimates were nearly identical, or (2) the post estimates showed substantial fluctuations about the prior values. The nodes which fell into class 1 were located away from the pumping center, generally in the gap between the Tres Hermanas and Florida Mountains (e.g. nodes 22, 41 and 63). Withdrawals in this region were not substantial when compared to the area east of Columbus. The nodes which fell into class 2 were located within or near the pumping center due east of Columbus (e.g. nodes 112, 122, 123 and 129). The prior (SEO) and post pumping estimates are shown for four nodes in figure 31. There were no significant deviations between the prior and post B estimates for any pumping node prior to 1950. The typical fluctuations shown in figure 31d for node 112 may represent actual pumping fluctuations or the noise in estimates of uncorrelated parameters. The former was investigated by examining rainfall records.

Correlation with Precipitation

Because the only sources of water for crops in the Columbus Basin are groundwater withdrawals and rainfall, it was suspected that there might have

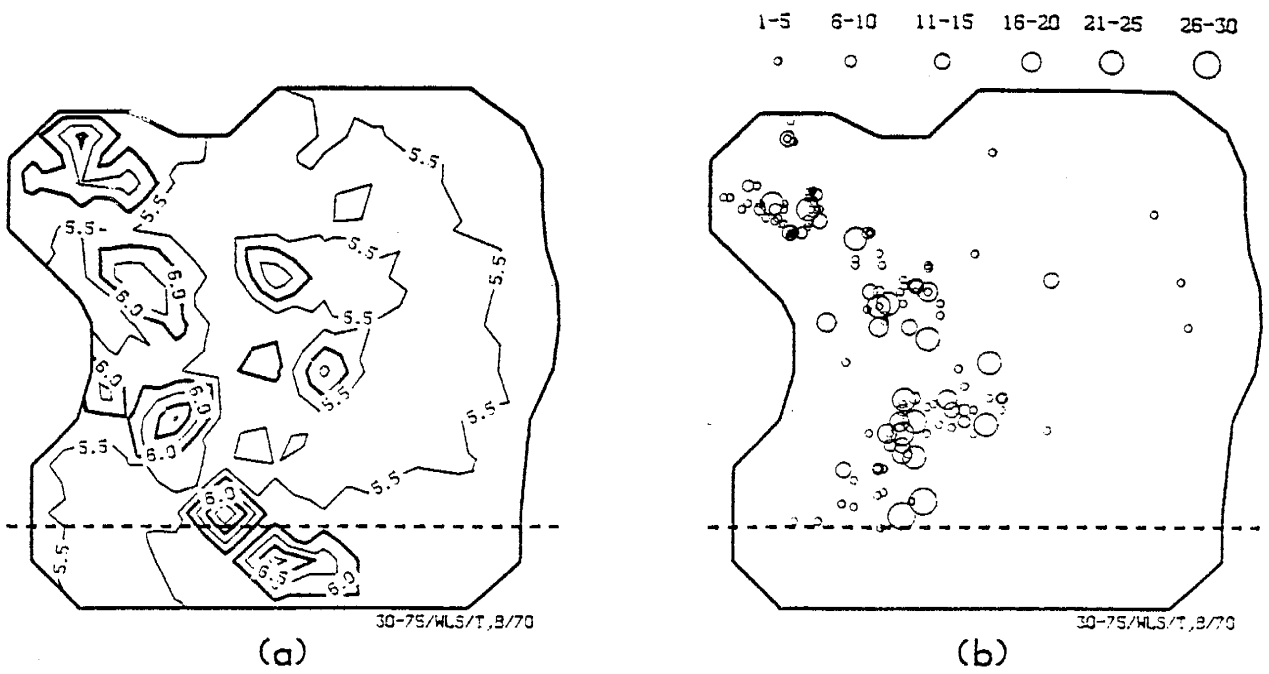

Fig. 30. Posterior log T field (a) and head observations (b) for run 70.

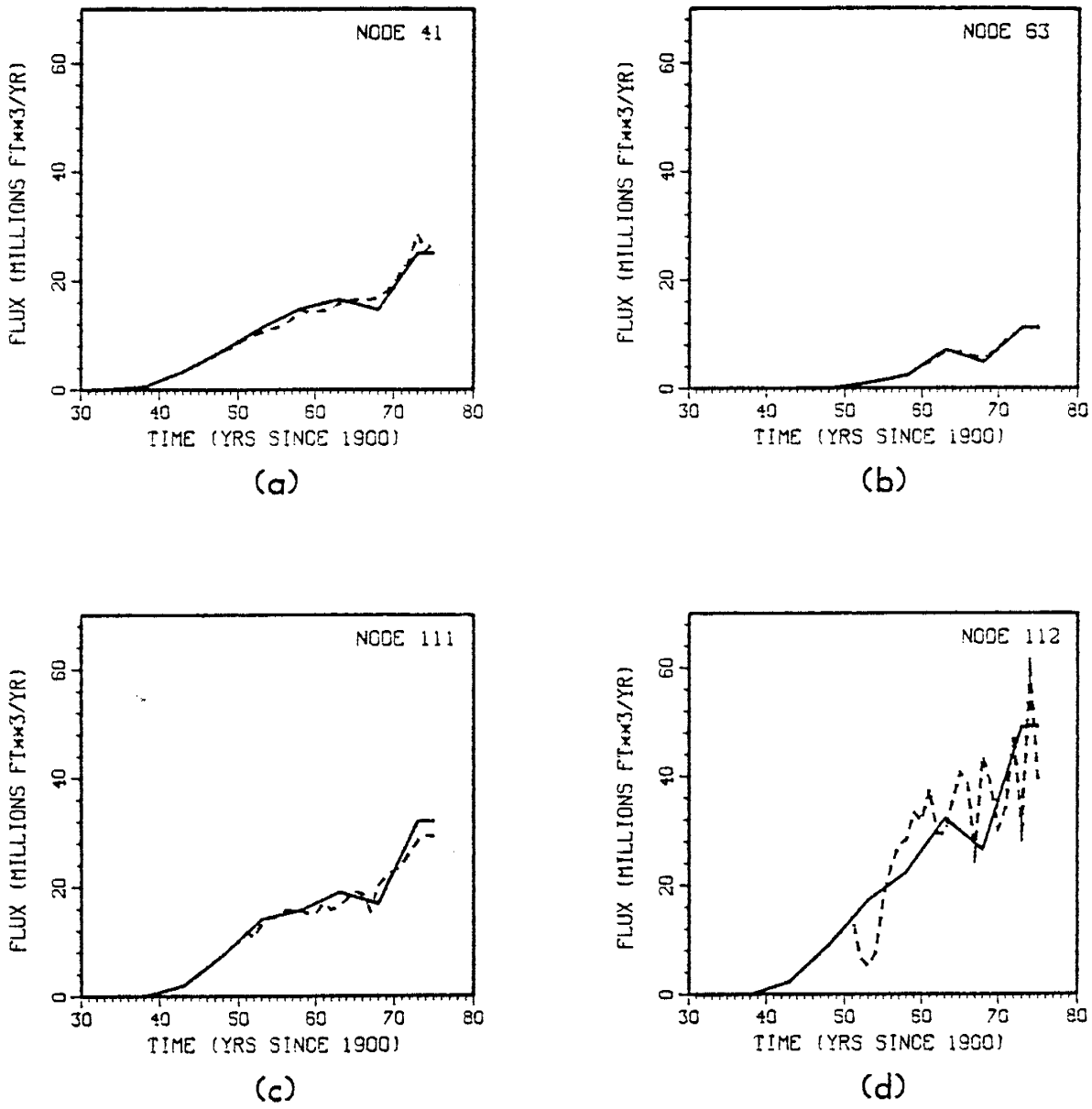

Fig. 31. SEO prior (solid) and post (dashed) pumping estimates for four nodes for run 70.

been some correlation between the two. A "wet" year should correspond to a decrease in pumping and a "dry" year should correspond to an increase in pumping. This basic inverse relationship would be complicated by a trend of increased withdrawals through time in the basin.

The prior and post B parameters for four nodes and annual precipitation reported by the Columbus weather station are plotted against time in figures 32 and 33. All four of the nodes were located within the pumping center. Many of the peaks and troughs of the posterior B estimates appear to be inversely correlated with rainfall, particularly for the time period 1965 to 1975.

A number of multiple linear regressions were run to see if the observed correlation could be defined statistically. The model used was

$$Q_t = a + bt + cP_t + \epsilon_t \qquad (15)$$

where

Q_t = posterior pumping (dependent variable)

t = time (independent variable)

P_t = precipitation (independent variable)

a,b,c = linear regression coefficients

ϵ_t = error term

The first two terms on the right hand side of equation 15 accounted for the trend of the posterior B estimates while the third term accounted for the deviations from the trend due to precipitation. With the third term neglected equation 15 becomes a simple linear regression model.

A series of regressions was performed for 7 nodes for the time period 1950 to 1975 since yearly fluctuations of B were not observed at times prior to 1950. The results of these regressions were nearly identical for any one

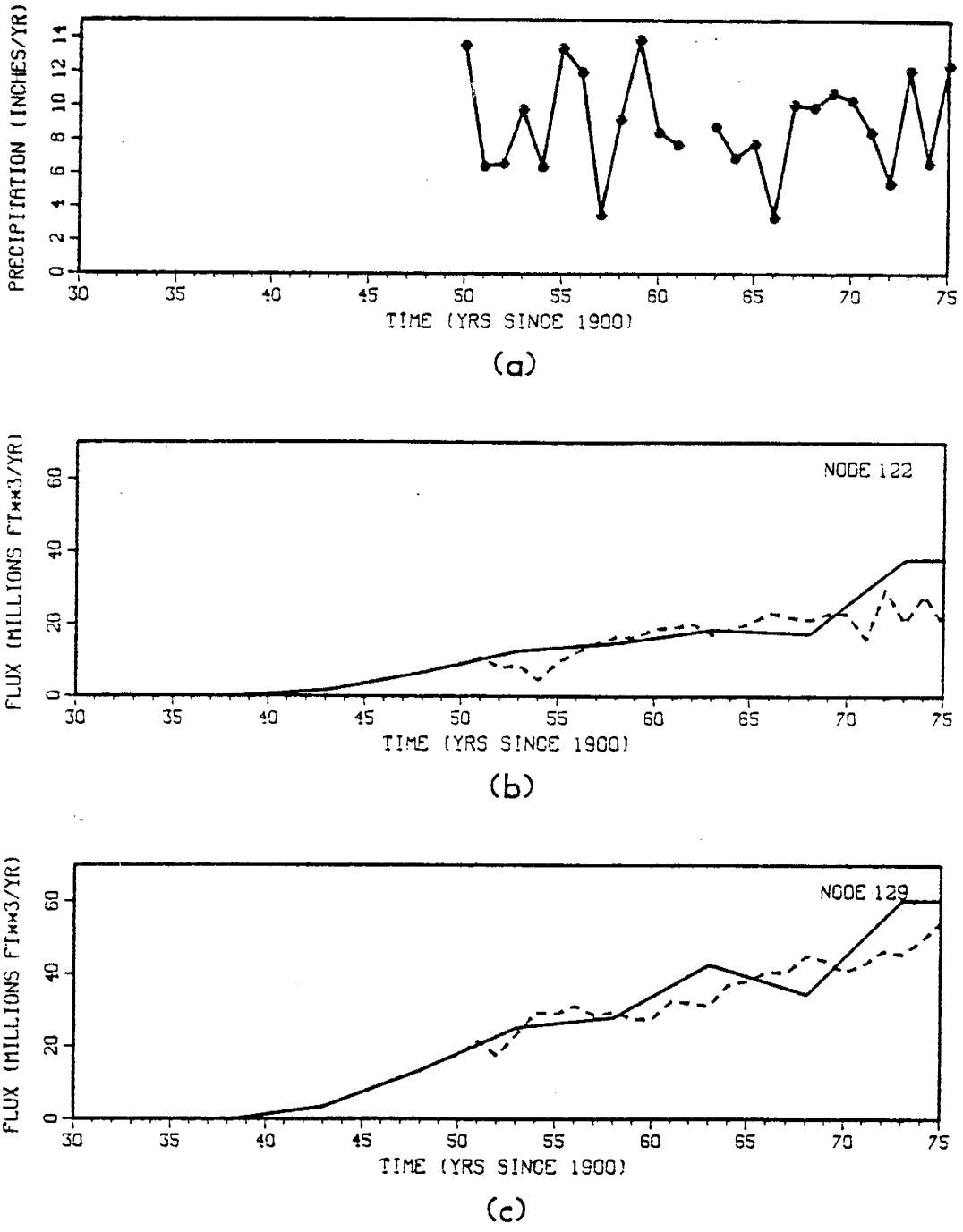

Fig. 32. Precipitation record (a) and prior (solid) and post (dashed) pumping estimates for nodes 122 (b) and 129 (c) for run 70.

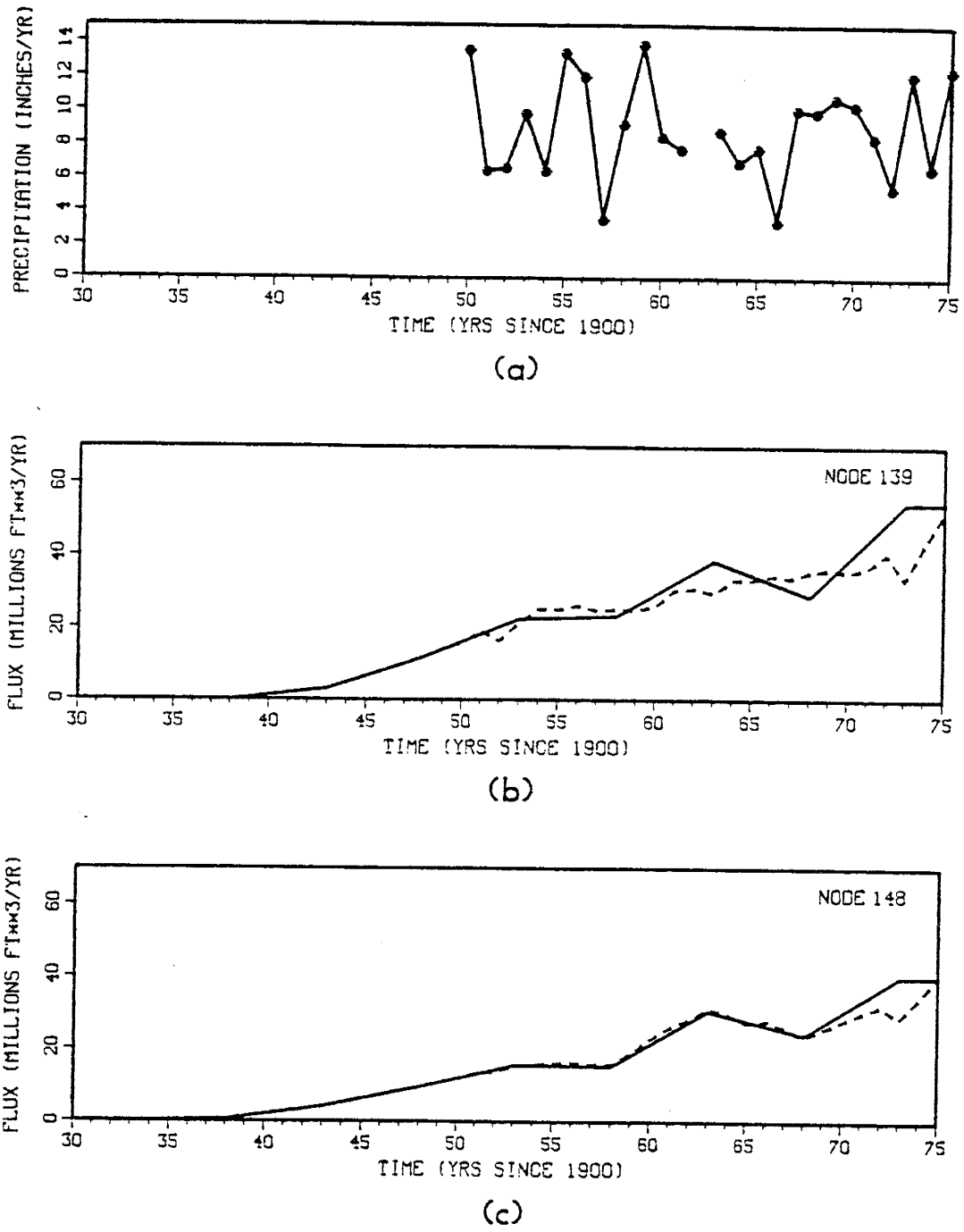

Fig. 33. Precipitation record (a) and prior (solid) and post (dashed) pumping estimates for nodes 139 (b) and 148 (c) for run 70.

node regardless of whether the precipitation term of equation 15 was included or not. Therefore another series of regressions was performed at the same nodes for the time period 1965 to 1975 since during these years Q_t and P_t seemed to be better correlated. The resulting correlation coefficients are shown in table 10, from which it is obvious that a significant statistical correlation between Q_t and P_t could not be found.

The residuals of precipitation and pumping for two nodes are shown in figure 34. The precipitation residuals were obtained by subtracting the mean precipitation from each rainfall value, while the residuals of pumping were obtained by subtracting the linear regression results from each posterior B value.

Graphically, at least, some correlation between pumping and rainfall does seem to exist. The possibility that the posterior pumping estimates are random fluctuations produced to minimize J can not be ignored however. The large year to year fluctuations observed at some nodes (e.g. 112) almost certainly could not be due entirely to rainfall variation. If some correlation structure could have been defined for the SEO pumping estimates the large fluctuations would have been subdued somewhat, and possibly more realistic estimates may have been obtained at these locations.

In summary, the posterior pumping estimates are believed to be a truer representation of yearly groundwater withdrawals for the Columbus Basin than are the SEO averaged values. CERT was able to identify fluctuations in the pumping record which can at least partially be attributed to fluctuations in yearly rainfall. At some nodal locations, the magnitude of the pumping fluctuations was greater than deemed probable, however. Implementation of a covariance structure for the pumping parameters would solve this problem, and the identification of such a structure could warrant future research.

Table 10

Correlation coefficients for multiple and linear regressions of seven nodes

Node	Multiple Regression (P and t vs. Q)	Linear Regression (t vs. Q)
84	0.4567	0.0796
112	0.6833	0.2959
122	0.6077	0.1939
123	0.2848	0.0150
129	0.8597	0.8596
139	0.7352	0.7292
147	0.9547	0.9392

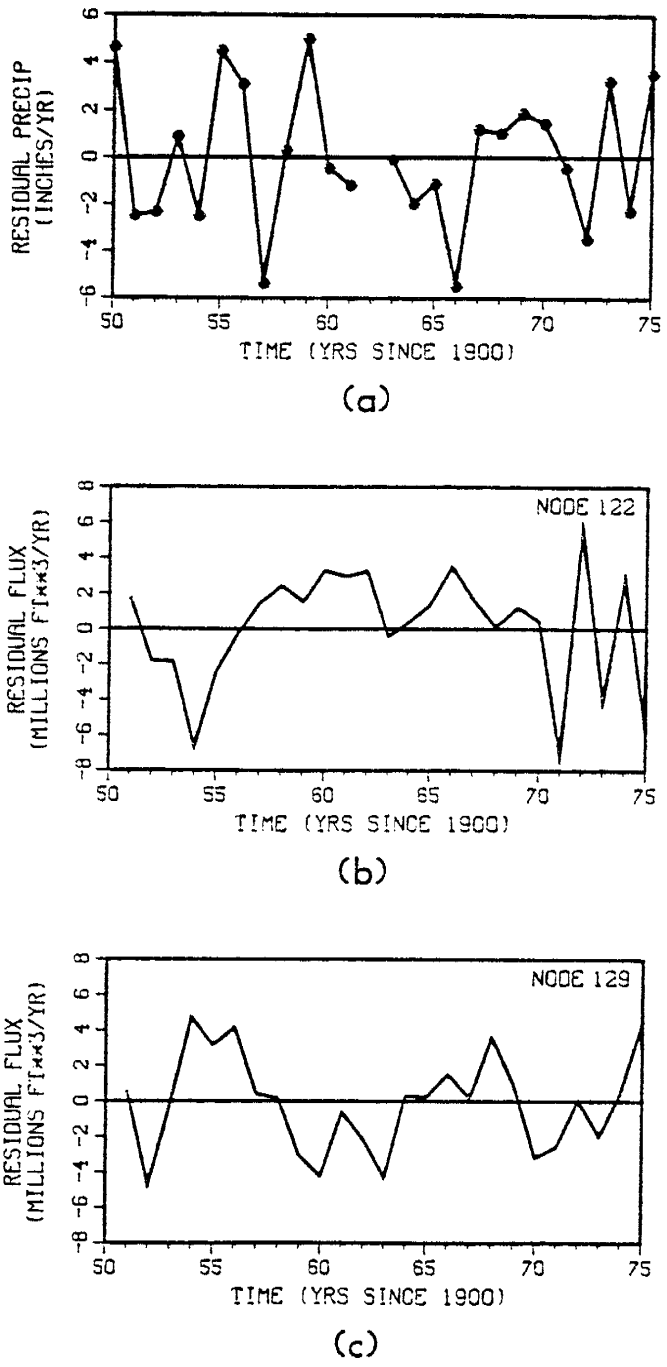

Fig. 34. Residual precipitation (a) and residual posterior pumping for nodes 122 (b) and 129 (c) for run 70.

PARAMETER ESTIMATION OVER ZONES THROUGH THE INVERSE PROCEDURE

Purpose

An identifiability problem may arise when the estimation of 201 nodal log T's is performed using a limited data set. The Columbus Basin head data consisted of 139 measurement locations with erratically spaced head measurements over the period 1930 to 1975. Additionally, the head information was concentrated in regions of the basin which experienced groundwater withdrawals. The log T estimates obtained from the nodal estimation exercise showed a relatively small variance reduction. If the number of parameters were to be reduced by grouping elements into zones, greater variance reduction would occur. The purpose of this section was to see if results similar to the nodal log T estimates could be obtained when log T was estimated over zones of elements. The work described in this section was performed by Swen Magnuson.

Zoned Log T Estimation

In the first zoning pattern tested the finite element grid was divided into 25 zones of approximately equal area (figure 35). A log T value of 5.916 and a σ_T of 0.3329 taken from the kriging exercise, were used as the prior estimates for each zone. The results of this run are shown in figure 31. The posterior covariance calculation was not performed for this run, and thus the σ_T's shown are the prior values.

The results of this run are fairly consistent with the log T pattern observed for the nodal estimation procedure. A high log T corridor exists in the western portion of the basin, and low log T's occur in the eastern portion of the basin. These results were not surprising since 25 zones was not a particularly small number of parameters.

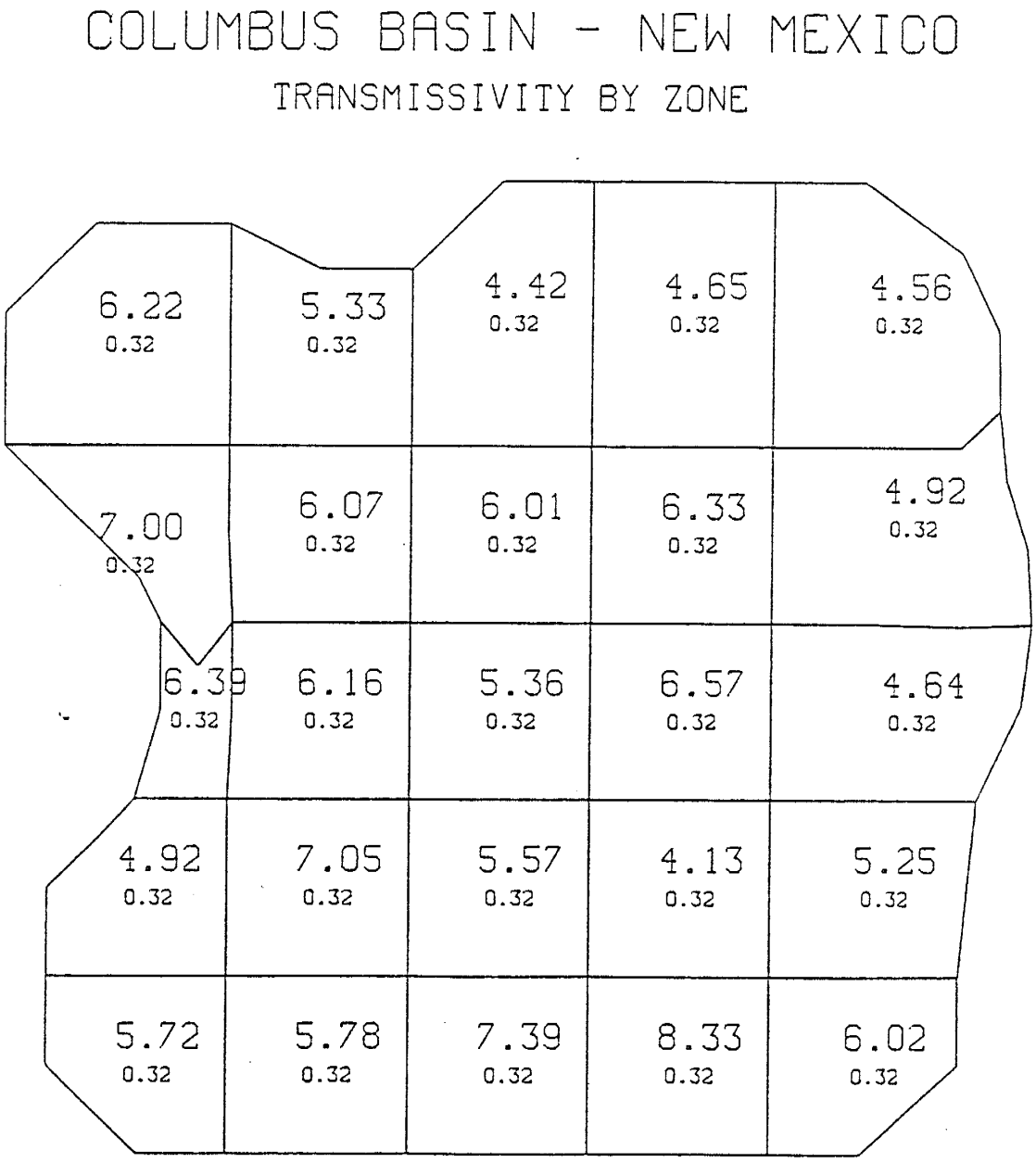

Fig. 35. Posterior log T estimates by zone, for 25 zones. Smaller numbers are prior standard deviation.

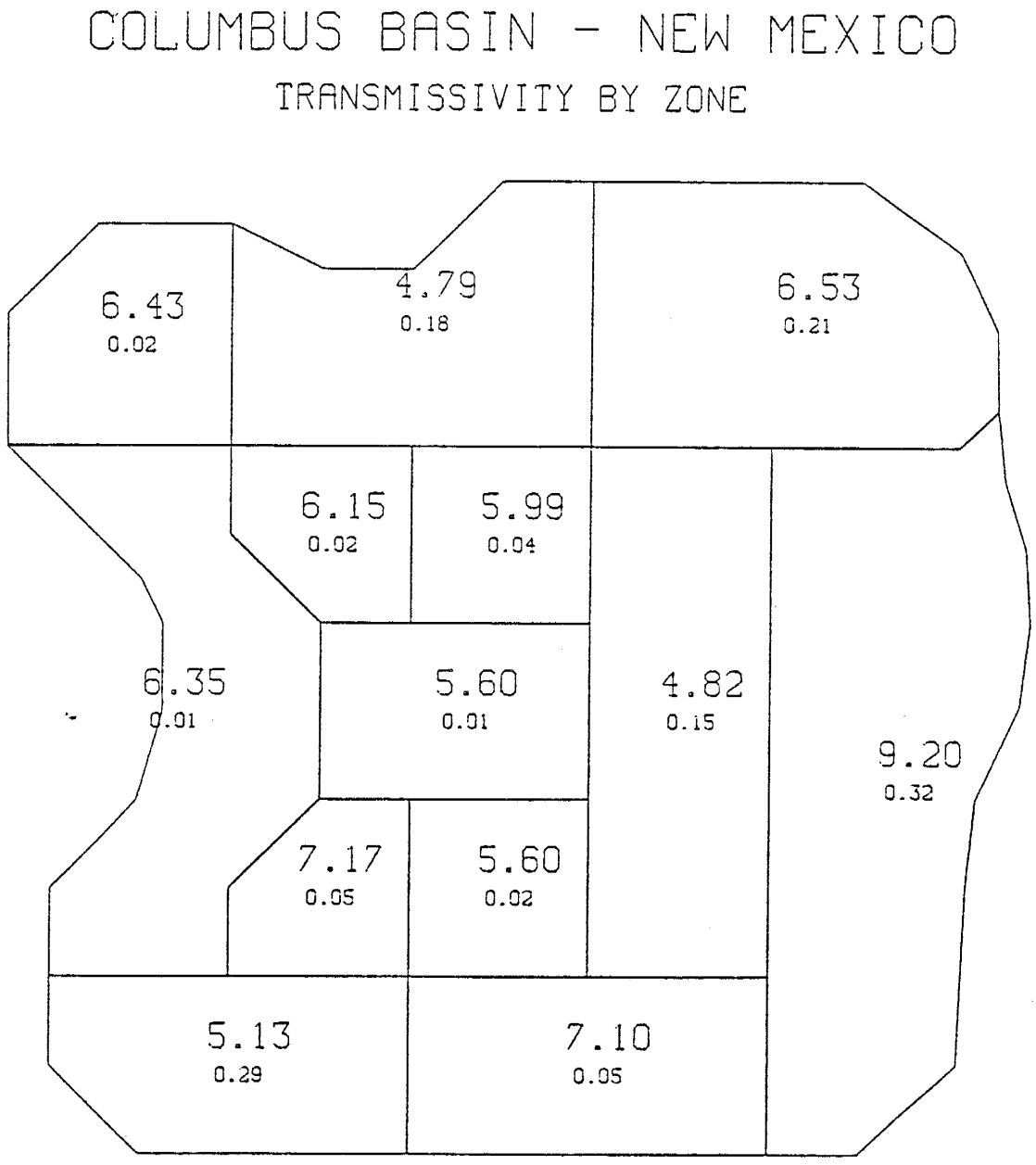

Fig. 36. Posterior log T estimates by zone, for 13 zones. Smaller numbers are posterior standard deviations.

To further decrease the number of parameters, a new pattern was constructed with 13 zones. The larger zones were constructed from those of the previous run by grouping zones in the alluvial fan regions of the Florida and Tres Hermanas Mountains, and by grouping zones on the eastern and southern boundaries which had similar log T estimates. Zones in the grid interior were left ungrouped to allow detail in the pumping region.

The results of the WLS run with 13 zones are shown in figure 36. The high log T zones on the eastern and south-eastern boundaries were likely a result of the zoning pattern. Two zones in this region were oriented north-south. The entire eastern region had a high estimated value of log T, possibly to allow an outlet of water from the basin.

The north-south orientation of the 13 zone run was eliminated in the next run which raised the number of zones to 15 (figure 37). These results show a high estimated log T zone along the southern boundary only. Again this zone was possibly required in order to provide an outlet for water from the basin.

One other run which estimated log T over zones was performed. The parameterization for this run consisted of 16 zones which were based exclusively on geologic features of the basin. One zone type consisted of alluvial fans on the flanks of the Tres Hermanas and Florida mountains. Two other zone types were created based on the hypothesized north-south trending Columbus Fault (figure 38). Each of these three geologic zones were further sub-divided into smaller zones. The results from this run remained significantly different from those obtained during the nodal log T WLS estimation.

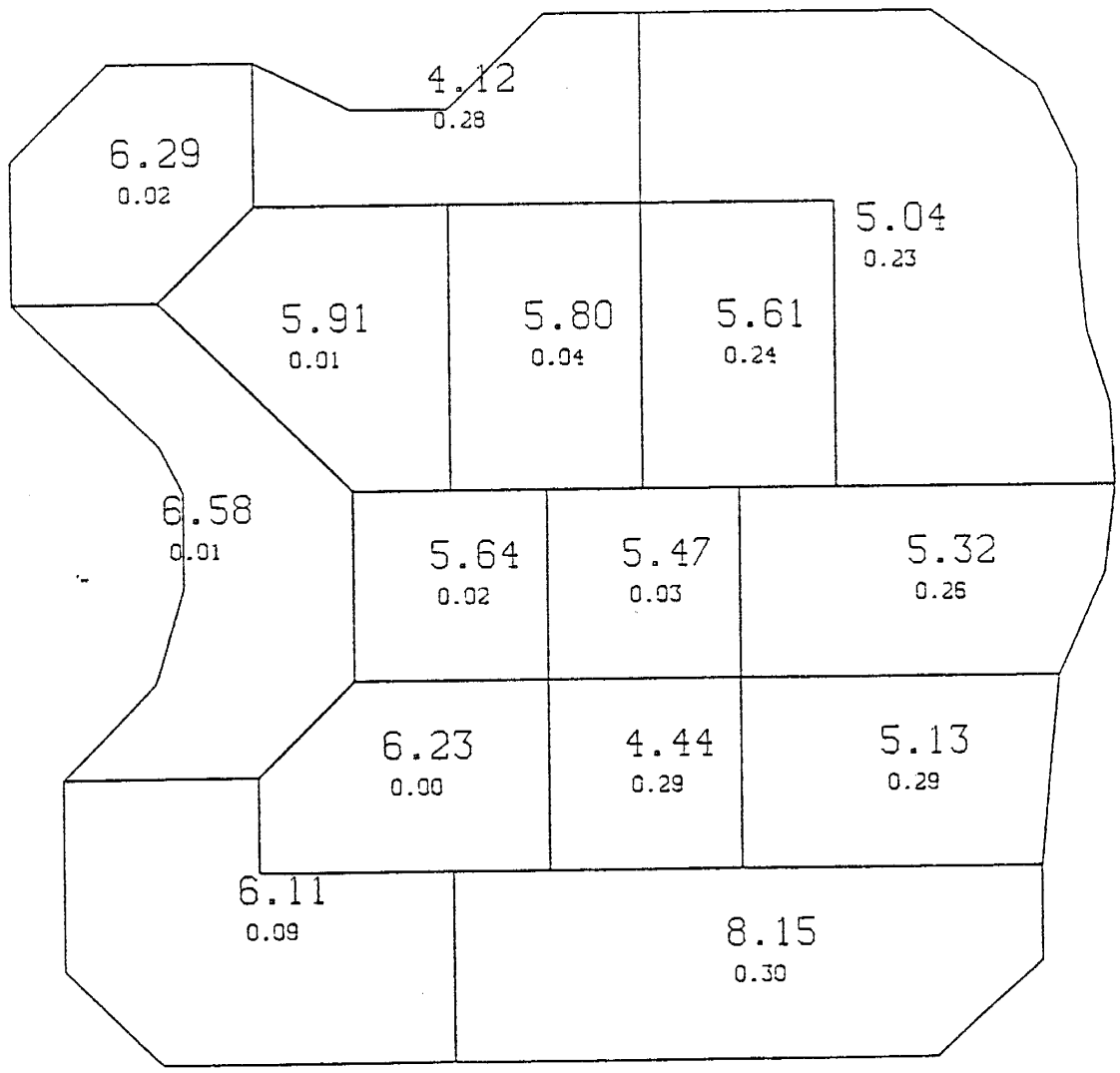

Fig. 37. Posterior log T estimates by zone, for 15 zones. Smaller numbers are posterior standard deviations.

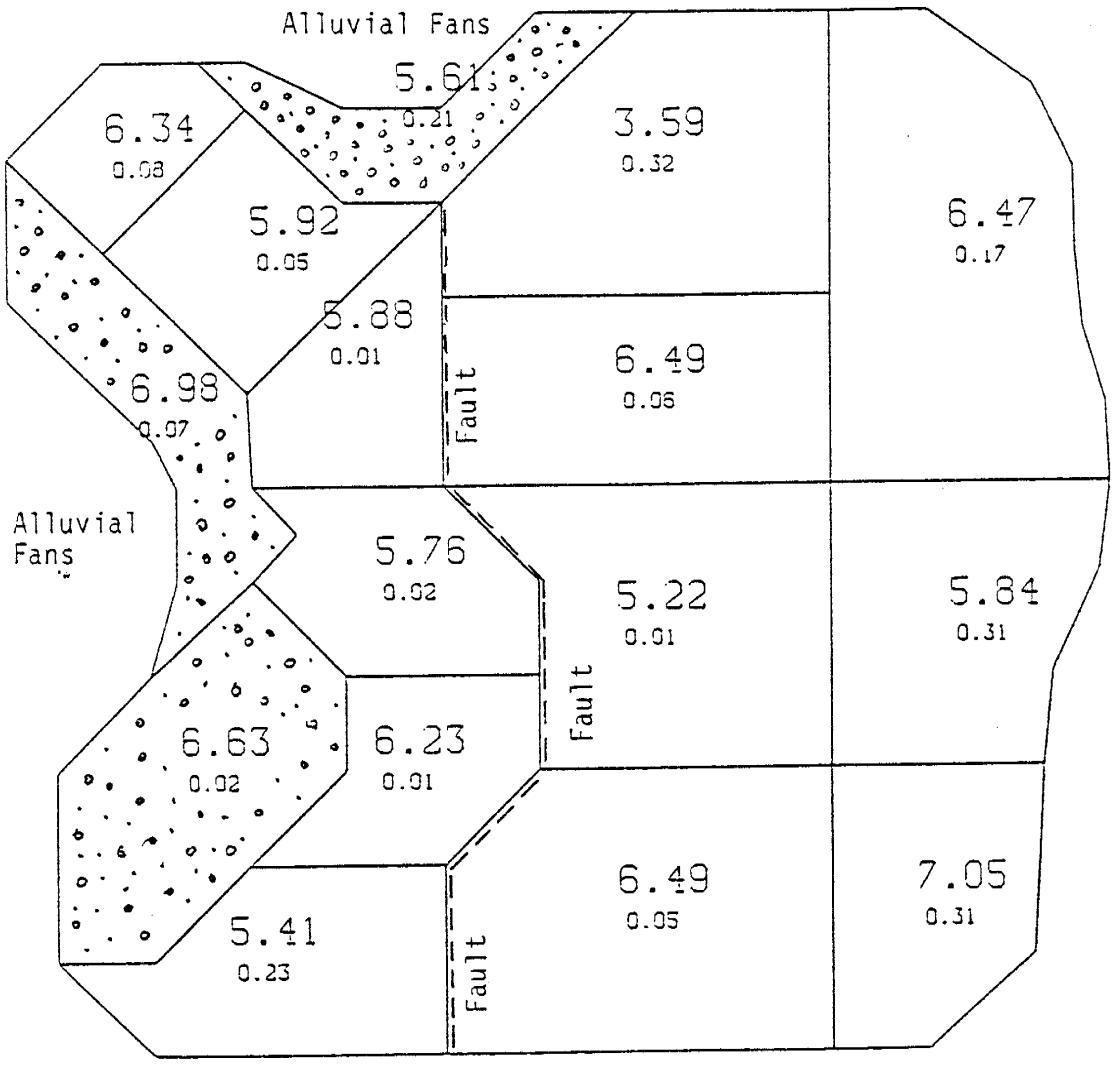

Fig. 38. Posterior log T estimates by zone, for 16 zones. Smaller numbers are posterior standard deviation.

Discussion

The variance reduction for the zoned parameter WLS runs was significantly greater than for the nodal parameter WLS runs. Only the run with 25 zones showed the high log T channel that was apparent when log T was estimated at nodes. It should be kept in mind that the log T values resulting from the zoned parameterization are estimates over an area, or an averaged value. They do not represent the true value at any point.

None of the WLS runs with less than 25 zones provided what was believed to be a reasonable log T field. For example, in figure 36 a high log T value of 9.2 ft^2/yr was estimated for a large zone that bordered the Camel Mountain Fault within the Mimbres Graben. The thicknesses of basin fill sediments in this region are substantial, and therefore a potential for high T values exists. However, a log T value of 4.8 ft^2/yr was estimated for an adjacent zone due west of the first zone that still lies within the graben (figure 36). There is no logical geological explanation for the sharp contrast of log T values between these zones. Similar discrepancies are evident in figures 37 and 38 as well. Therefore, one comes to the conclusion that the zoned log T estimates were conditioned on "artificial" modeling constraints, such as zoning pattern or boundary conditions, rather than upon hydrogeological relationships.

UNCERTAINTY PROPAGATION

Introduction

In addition to its "automated" parameter estimation procedure, one of CERT's greatest utilities is its ability to propagate the uncertainty of model parameters through the solution process. Input for the uncertainty propagation (UP) problem includes all of the model parameters previously discussed and some estimate of the associated parameter uncertainties (i.e. variances and covariances). The model parameters and associated covariance matrices may be subjective estimates, estimates obtained through geostatistics, estimates provided by a previous WLS parameter estimation run, or any combination of these procedures.

As indicated by equation 9, the uncertainty of model output (head) depends not only upon the variance of model parameters but also upon the derivative of heads with respect to the parameters. These derivatives are called the "sensitivities" of heads to parameters. Uncertain parameters with a large variance may contribute very little uncertainty to the predicted heads if the sensitivity of the heads to those parameters is small.

The uncertainty of the model calculated heads is expressed as a variance of head (σ_h^2) at the nodal points. Head variances can also be calculated for locations within finite elements. Output, therefore, from a UP run can be expressed as contour maps of σ_h^2 (or σ_h) for certain times or as well hydrographs with h and σ_h plotted for all times. These estimates of model output uncertainty are extremely useful in many engineering problems where a quantitative estimate of confidence intervals must be made. For detailed studies of sensitivity analysis as related to uncertainty propagation, see Sykes et al. (1985) and Wilson and Metcalf (1985).

Variance Reduction Inside Finite Elements

The head observation locations used in this study did not correspond to nodal point locations. Nodal heads were interpolated onto observation points inside elements using the following equation:

$$h_0^e = h_1 w_1 + h_2 w_2 + h_3 w_3 \tag{12}$$

where

h_0^e = head at observation point inside element e

h_i = head at node i of element e

i = 1,3

w_i = interpolation weight associated with nodal value i of element e

i = 1,3

The interpolation weights depend directly upon the position of the observation point within the finite element. A detailed description of their calculation and use can be found in Wilson et al. (1979).

Combining equation 12 and the variance of a sum formula, σ_h^2 at an observation point inside an element is calculated by:

$$\sigma_0^2 = \sigma_1^2 w_1^2 + \sigma_2^2 w_2^2 + \sigma_3^2 w_3^2 + 2w_1 w_2 \mathrm{Cov}(h_1,h_2) + 2w_1 w_3 \mathrm{Cov}(h_1,h_3) + 2w_2 w_3 \mathrm{Cov}(h_2,h_2) \tag{13}$$

where

σ_0^2 = head variance at observation point inside element e

σ_i^2 = head variance at node i of element e

i = 1,3

$\mathrm{Cov}(h_i,h_j)$ = covariance between heads at nodes i and j of element e

i,j = 1,3

The calculation of σ_0^2 using 13 yields a reduced variance for points inside the element. This variance reduction effect can only be avoided if the covariance terms exhibit perfect correlation between nodal heads. The magnitude of variance reduction is greatest for points at or near the element centroid and decreases as observation points are located closer to the nodal points.

The covariance between nodal heads in the Columbus Basin simulation was high, but not perfect. Hence the variance estimates at the observation locations were reduced a small amount from the corresponding nodal head variances.

Conditioning

When observed head data is used to assist in the model calibration procedure (as in WLS parameter estimation), the resulting parameter estimates are said to be "conditioned" on the observed heads. Conditioning usually results in a variance reduction of parameter estimates because as more information is used to estimate a parameter the more certain that estimate often becomes, depending on the non-linearity of the parameter-head relationship.

The results of conditioning in the Columbus Basin are clearly evident in the following sections. Contour plots of σ_T estimated from WLS runs show a clear variance reduction in the vicinity of available head data (e.g. figure 41b). Plots of σ_B would have displayed similar behavior had they been constructed.

Effects of Boundary Node Correlation

Run 73 was the first UP simulation made for the Columbus Basin. The results of this run are used here only to stress the importance of boundary node correlation, a more detailed analysis of UP results is presented in the next section. Input parameters for run 73 consisted of nodal log T values

and an associated covariance matrix ($\underline{P}_{TT}$) obtained from a previous WLS run for the time period 1930 to 1960 (run 71), and the S and B (boundary node and flux) parameters were the standard priors. The observed heads used in run 71 are shown in figure 41d. Recall that the covariance matrices associated with the S ($\underline{P}_{SS}$) and B ($\underline{P}_{BB}$) parameters were diagonal.

The results of run 73 at measurement location 168 are illustrated in figure 39a. Note that several of the observed head values lie outside of the $\pm 2\sigma_h$ lines. In fact, the confidence band seems quite narrow considering all of the uncertainties embedded in the Columbus Basin model. All of the model parameters (excluding A, boundary type) were considered uncertain. The relatively small estimates of σ_h led to the suspicion that much inherent uncertainty in the system was not being captured by the UP algorithm parameterization.

The uncertainty of T was obtained from WLS run 71. A covariance structure for the SEO pumping record could not be obtained through either multiple regression or median polish, which indicated that the portion of $\underline{P}_{BB}$ associated with the pumping nodes was correctly diagonal. A $\underline{P}_{SS}$ matrix could not be obtained since there were no recorded values of S in the basin. The assumed independence of the S parameters was partially responsible for the low σ_h estimates, but the fact that the model heads were relatively insensitive to S minimized this effect. It seemed probable, therefore, that a major source of uncertainty which should have affected the model predictions but did not was the error attributable to the constant boundary heads.

The portion of $\underline{P}_{BB}$ related to the boundary heads was diagonal because there was no quantitative way to estimate the appropriate correlation structure. The assumed statistical independence between boundary heads effectively negated the propagation of boundary condition uncertainty into

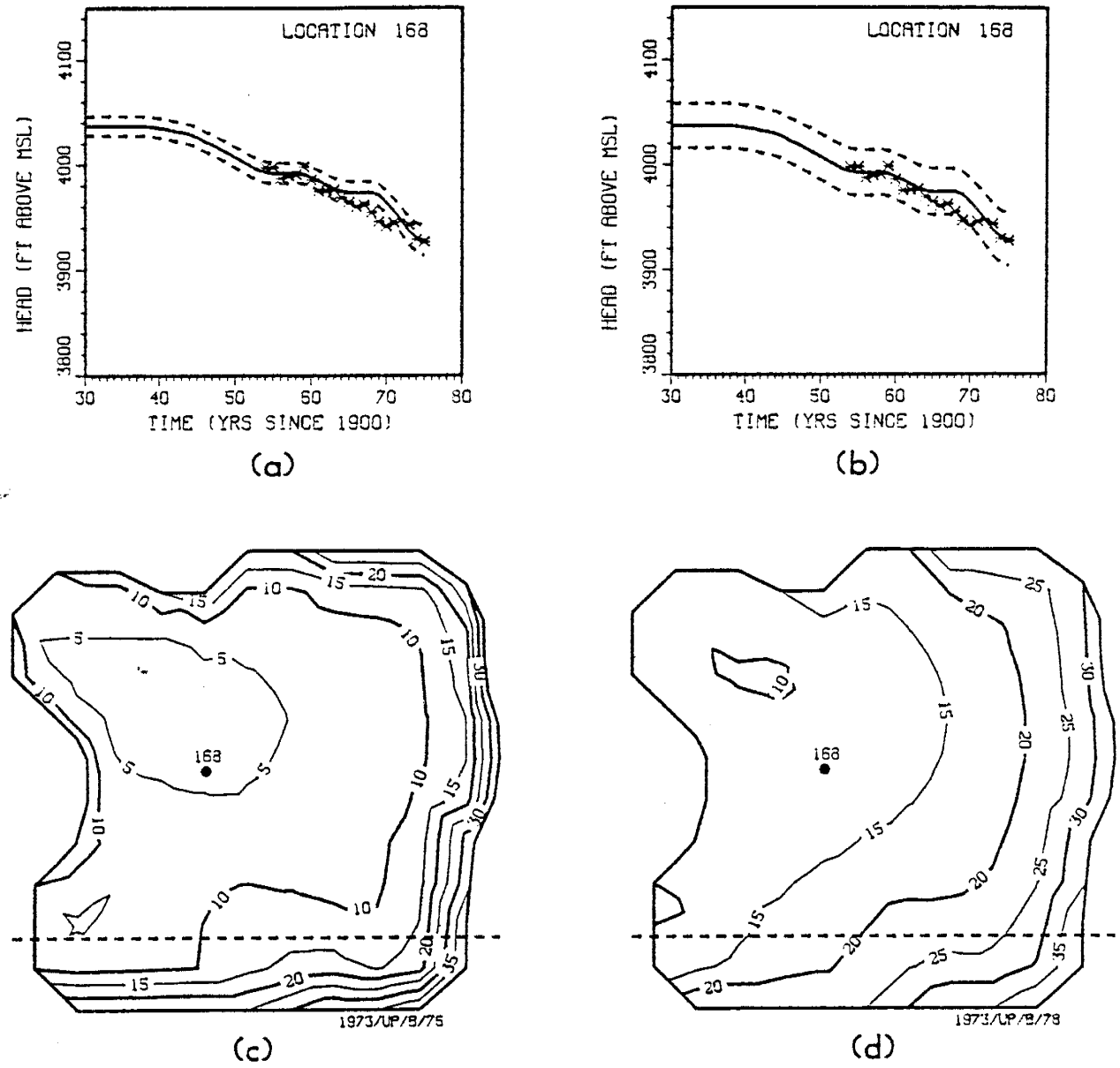

Fig 39. Hydrograph for measurement location 168 and 1973 σ_h field for run 76 (a and c) and run 78 (b and d). Run 78 incorporated boundary node correlation, run 76 did not. In the hydrographs the solid line is the model calculated head, the dashed lines are the $\pm 2\sigma_h$ values, and the asterisks are the observed head values.

the basin center. A plot of the portion of σ_h attributable to the uncertainty in the B boundary parameters is shown in figure 39c.

Because this estimate of σ_h in the basin interior attributable to the boundary heads was believed to be too small, and because the estimation of the boundary heads was a subjective process, a subjective covariance function was estimated for the boundary heads in order to fill the off-diagonal terms of $\underline{P}_{BB}$. The boundary heads were assumed to be correlated by an exponential covariance:

$$C(\underline{h}_1, \underline{h}_2) = \sigma_1 \sigma_2 e^{-\xi/\ell} \tag{14}$$

where

$C(\underline{h}_1, \underline{h}_2)$ = covariance

$\underline{x}_1$ = location of first boundary head ($|R^2$)

$\underline{x}_2$ = location of second boundary head ($|R^2$)

$\xi = |\underline{x}_1 - \underline{x}_2|$ = distance between points $\underline{x}_1$ and $\underline{x}_2$

σ_1 = standard deviation of head at location $\underline{x}_1$

σ_2 = standard deviation of head at location $\underline{x}_2$

ℓ = correlation length

The correlation length was estimated as 38,620 ft for the Columbus Basin boundary nodes. This is the mean distance over which the head estimate at one boundary node was believed to influence the head estimate at another boundary node.

Using equation 14, the off-diagonal terms of $\underline{P}_{BB}$ associated with the boundary nodes were filled and run 73 was conducted again. The results of this run are presented in figures 39b and 39d.

The effect of the boundary node correlation is immediately obvious. The $\pm 2\sigma$ lines at measurement location 168 are significantly widened and

include all of the observed head values. The correlation permits the boundary head uncertainty to be propagated into the basin center - the effect of the uncertain boundary nodes does not dissipate within several miles of the model boundary. The assumed boundary correlation was used as input to all subsequent UP runs because, otherwise, the estimates of σ_h were felt to be biased low.

Variogram analysis could also have been used to estimate head boundary condition correlation, as it was in Wilson and Harper (1983), but was not attempted here. The Palo Duro basin field examined by them was in steady state, while the Columbus head is transient. The few pre-development head measurements available were inadequate for a satisfactory variogram analysis.

Effects of S, T and B Parameters

The spatial pattern of σ_h estimated by any UP run can be decomposed into constituent parts, each part being a function of one uncertain parameter type. The σ_h field for one run, 79, was decomposed to illustrate the effect each uncertain parameter type had on the UP output. Run 79 used the same input parameters as run 73 described in the previous section, the only difference between the two runs being that the estimated boundary node correlation was implemented in run 79. The σ_h field was not decomposed for any other runs, but it is believed that the same general results would have been observed.

Figures 40a and 40b show the portion of σ_h due to the boundary parameters at times 1960 and 1973 respectively. The two figures are identical, indicating that the component of σ_h due to boundary condition uncertainty did not change with time, since the B boundary parameters and the associated $\underline{P}_{BB}$ matrix were not time dependent. Note that figures 40a and 40b are identical to figure 39d.

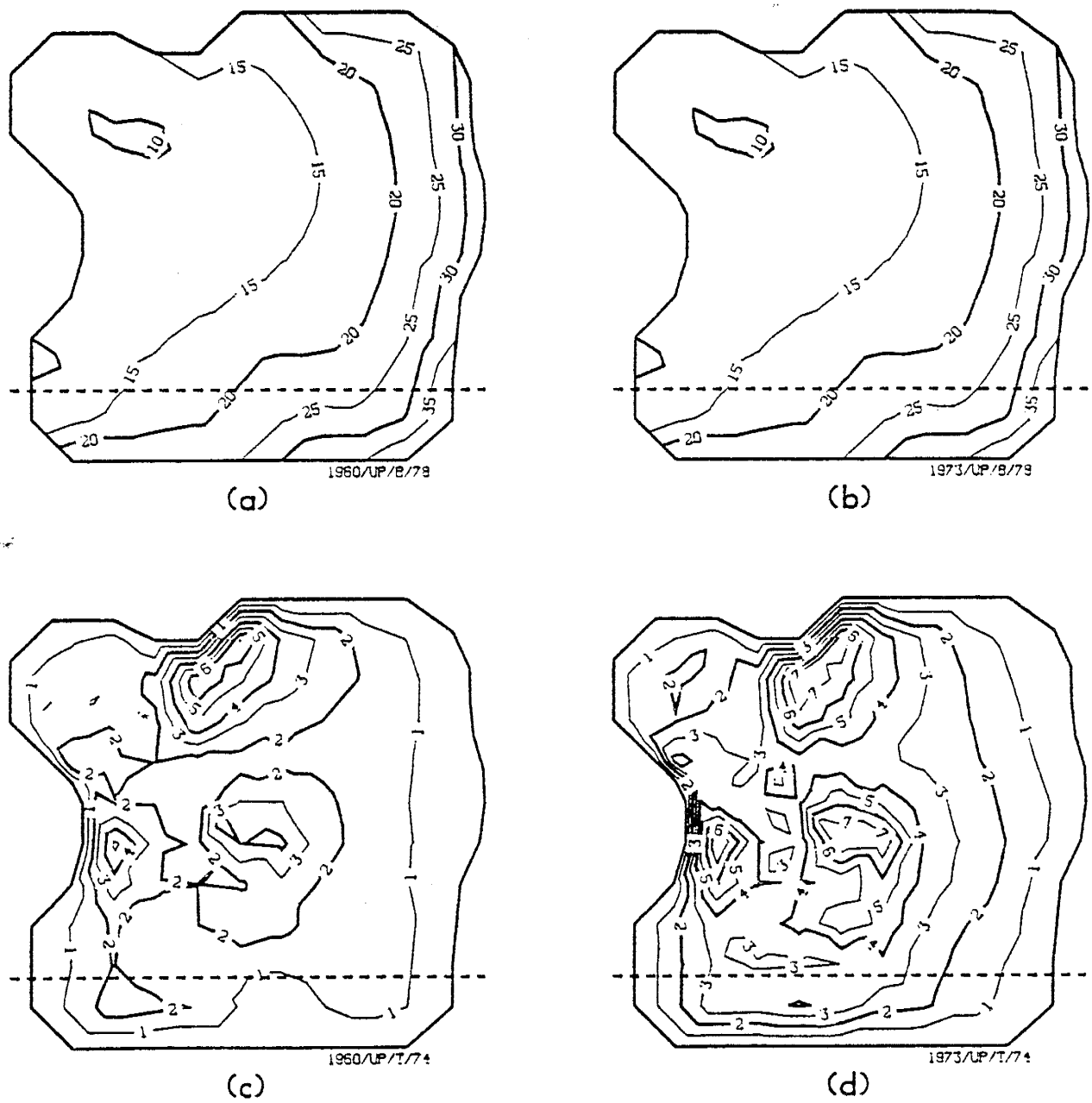

Fig. 40. The σ_h fields resulting from uncertain boundary heads only for 1960 (a) and 1973 (b) and the σ_h fields resulting from uncertain log T values only for 1960 (c) and 1973 (d) for run 79. Units in feet.

Figures 40c and 40d illustrate the portion of σ_h attributable to the WLS estimates of log T at 1960 and 1973 respectively. The σ_h values were obviously not constant in time, even though the log T parameters and the $\underline{P}_{TT}$ matrix were. This fact implies that the derivatives of heads to the log T values ($\partial h/\partial T$) changed through time, and the direction of change was positive since σ_h generally increased from 1960 to 1973.

There are three distinct areas of high uncertainty discernable from figures 40c and 40d. Two of the areas are adjacent to the Tres Hermanas and Florida Mountain ranges. The WLS estimates for log T in these areas were only poorly conditioned on observed heads since observations were not available (figure 41d), and consequently variance reduction in these areas was low (figure 41b). Because the variance of the log T values in these areas was reduced only slightly, these areas appear as zones of higher uncertainty during the UP run. Steep hydraulic gradients near the mountain fronts (see figures 43c and 44a) also contributed to the high variance of heads at these locations. Previous work has shown (Bakr et al. 1978) that the variance of predicted head increases with increasing head gradient. The third zone of high uncertainty, however, corresponds directly with the center of pumping (figures 40d and 41c). There was a good head record available for this area (figure 41d), and the WLS log T estimates were well conditioned on observed heads (figure 41b). This region of high uncertainty, therefore, could not be attributed to a lack of variance reduction but was rather due to an increase in the head sensitivities due to pumping. It makes intuitive and quantitative sense (Wilson and Dettinger 1979) that $\partial h/\partial T$ increased as heads fell relatively fast in the basin.

One might have expected that σ_h in the eastern third of the basin might have been high due to poor conditioning of the log T parameters on observed heads. The sensitivities of heads to log T in this region must have been

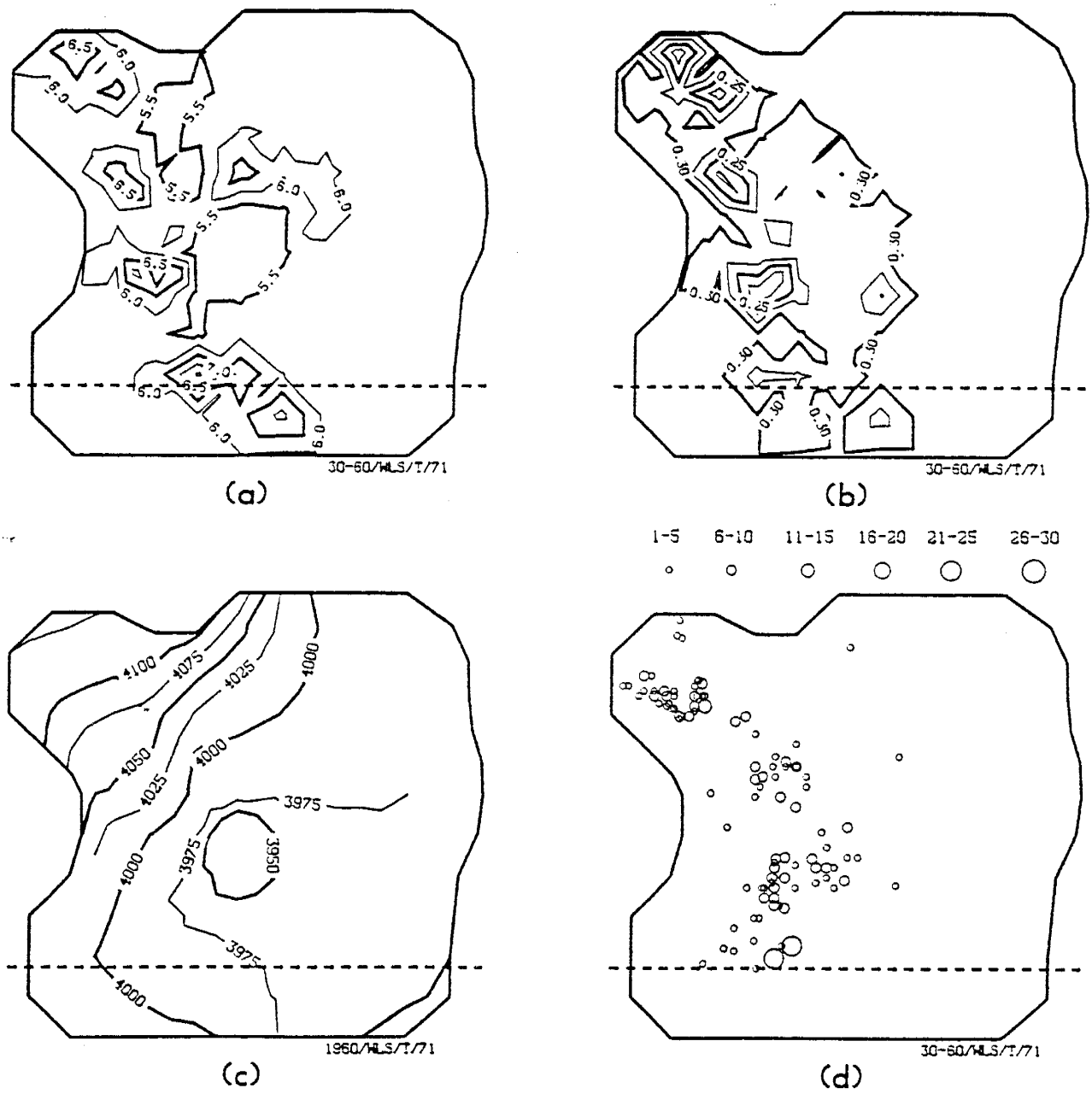

Fig. 41. Input log T field (a), associated σ_T field (b), 1960 head surface (c) and head observations that log T and σ_T were conditioned upon for run 79. Heads in feet above MSL.

small, thereby creating a zone of low σ_h. This result was not surprising considering that there is no pumping in this region and consequently drawdowns are not severe.

The portion of σ_h caused by uncertainty of the S parameters is shown in figures 42a and 42b. The pattern of σ_h in these figures is the result of two factors. First, σ_S for the unconfined nodes in the west and northwest regions of the basin was assigned as 0.1, and σ_S for the confined nodes was 5×10^{-4}. Secondly, the influence of pumping on the sensitivity derivatives $\partial h/\partial S$ is evident in both space and time. The combination of these factors creates a zone of high σ_h adjacent to the pumping center but offset to the west where the storage conditions change from confined to unconfined (figure 27). The increase of $\partial h/\partial S$ through time was expected because a transient system would obviously be more sensitive to S than one at quasi-steady state.

Finally, the portion of σ_h attributable to the uncertain B (pumping) parameters is depicted in figures 42c and 42d. As was expected the uncertainty contours are centered about the cone of depression and grow in areal extent and magnitude with time. This behavior has two explanations: (1) the actual B (pumping) parameters increase with time, and since σ_B was taken to be 25 percent of the pumping value σ_B increases with time also, and (2) the sensitivities $\partial h/\partial B$ increase as B increases. The pumping nodes located in the gap between the Tres Hermanas and Florida Mountains contributed very little to the σ_h map. These nodes tended to have small discharge values relative to nodes near the basin center, and their sensitivities must have been small as well.

One final point should be noted about figures 42c and 42d. These figures resulted from a $\underline{P}_{BB}$ matrix which was diagonal - no covariance structure could be found for the SEO pumping data in time or space.

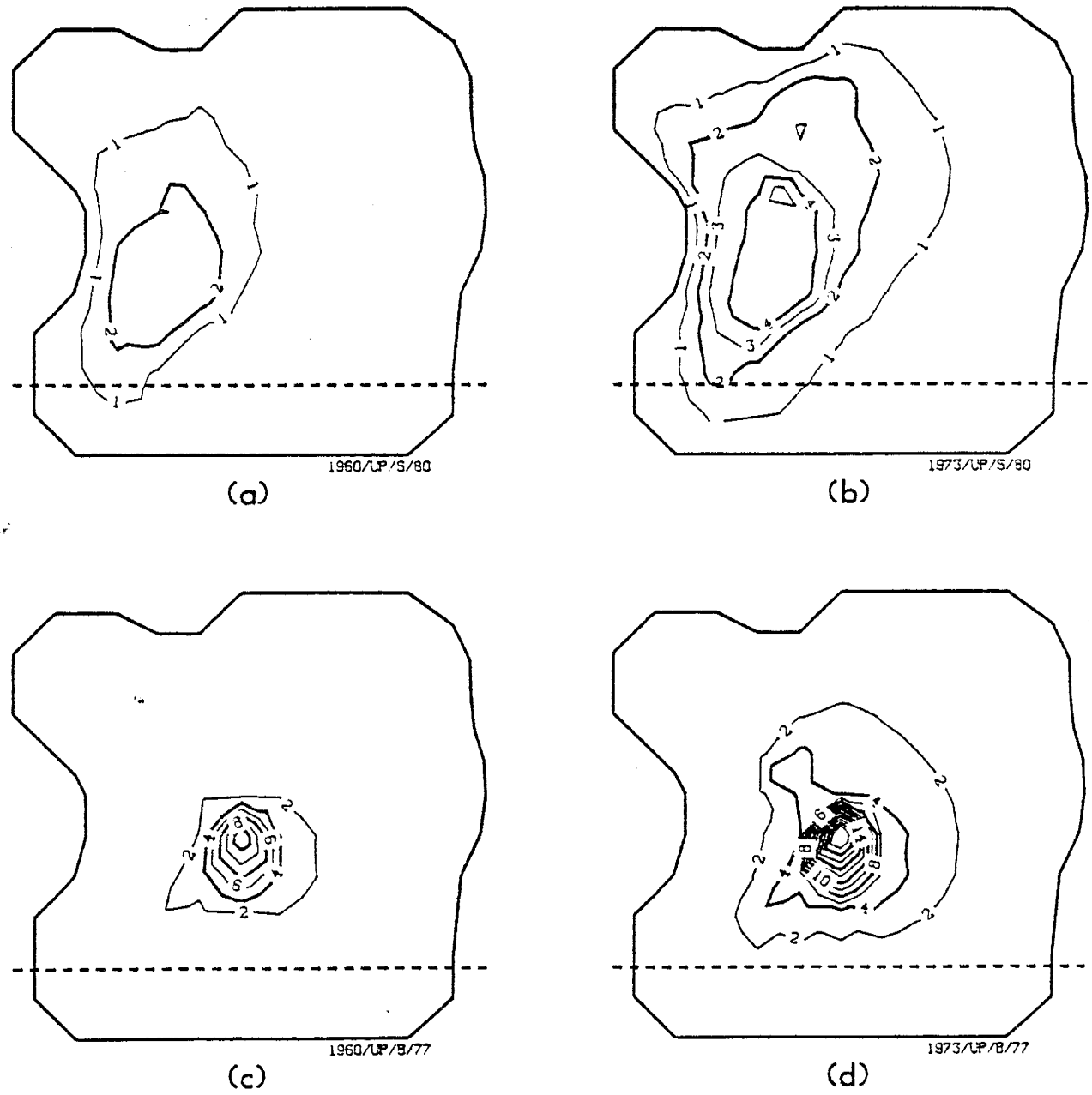

Fig. 42. The σ_h fields resulting from uncertain S parameters only for 1960 (a) and 1973 (b) and the σ_h fields resulting from uncertain pumping values only for 1960 (c) and 1973 (d) for run 79. Units in feet.

However, when the pumping parameters were estimated by WLS and equation 8 was used to calculate a linearized posterior covariance, this posterior $\underline{P}_{BB}$ matrix was no longer diagonal and consequently uncertainty due to pumping was propagated more easily through time and space (see the boundary node correlation section). The off-diagonal terms in the posterior $\underline{P}_{BB}$ matrix are created because the sensitivity matrices in equation 8 are in general full or banded, and when such matrices are multiplied by a diagonal matrix ($\underline{R}^{-1}$ in (8)), off-diagonal terms are generated. The effect of greater uncertainty propagation due to filling $\underline{P}_{BB}$ may have been offset to some degree by variance reduction of the B parameters due to the WLS estimation.

When the contributions to σ_h from each uncertain parameter type are added together, the resulting σ_h map represents the total modeled head uncertainty at any point in the basin. The head and σ_h contours for 1940, 1960, 1973 and 1975 from run 79 are shown in figures 43 and 44. Two aspects of the σ_h field are immediately obvious when viewing these figures. First, the character and to some extent the magnitude of σ_h over the basin is dominated by the boundary condition uncertainty. Secondly, σ_h at the basin center grows appreciably with time. This effect is primarily due to the uncertain pumping parameters and to a lesser extent the log T parameters. The standard deviation of head at locations outside the major pumping center, however, displayed a nearly stationary behavior in time.

Effect of Conditioned Parameters on Uncertainty Propagation

The input parameters to UP run 88 were not conditioned on observed heads at all. Input to this run consisted of the kriged log T estimates and the best estimates (not WLS) of S and B as described previously. It is tempting to believe that σ_h at all measurement locations for run 88 should be equal to or higher than the σ_h predicted for other runs since the input

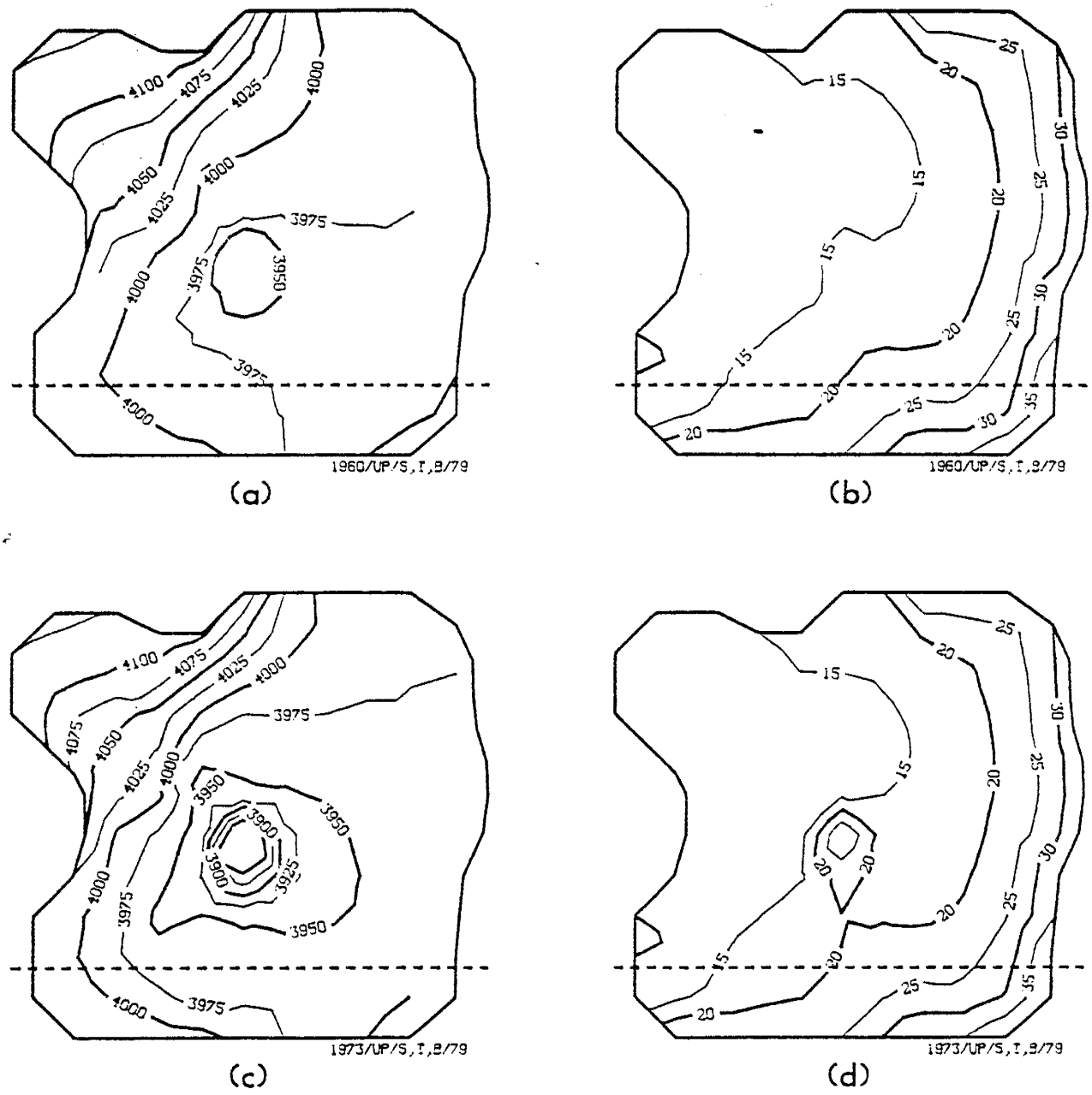

Fig. 43. Head fields (ft above MSL) and associated σ_h fields (ft) for run 79 for 1940 (a and b) and 1960 (c and d).

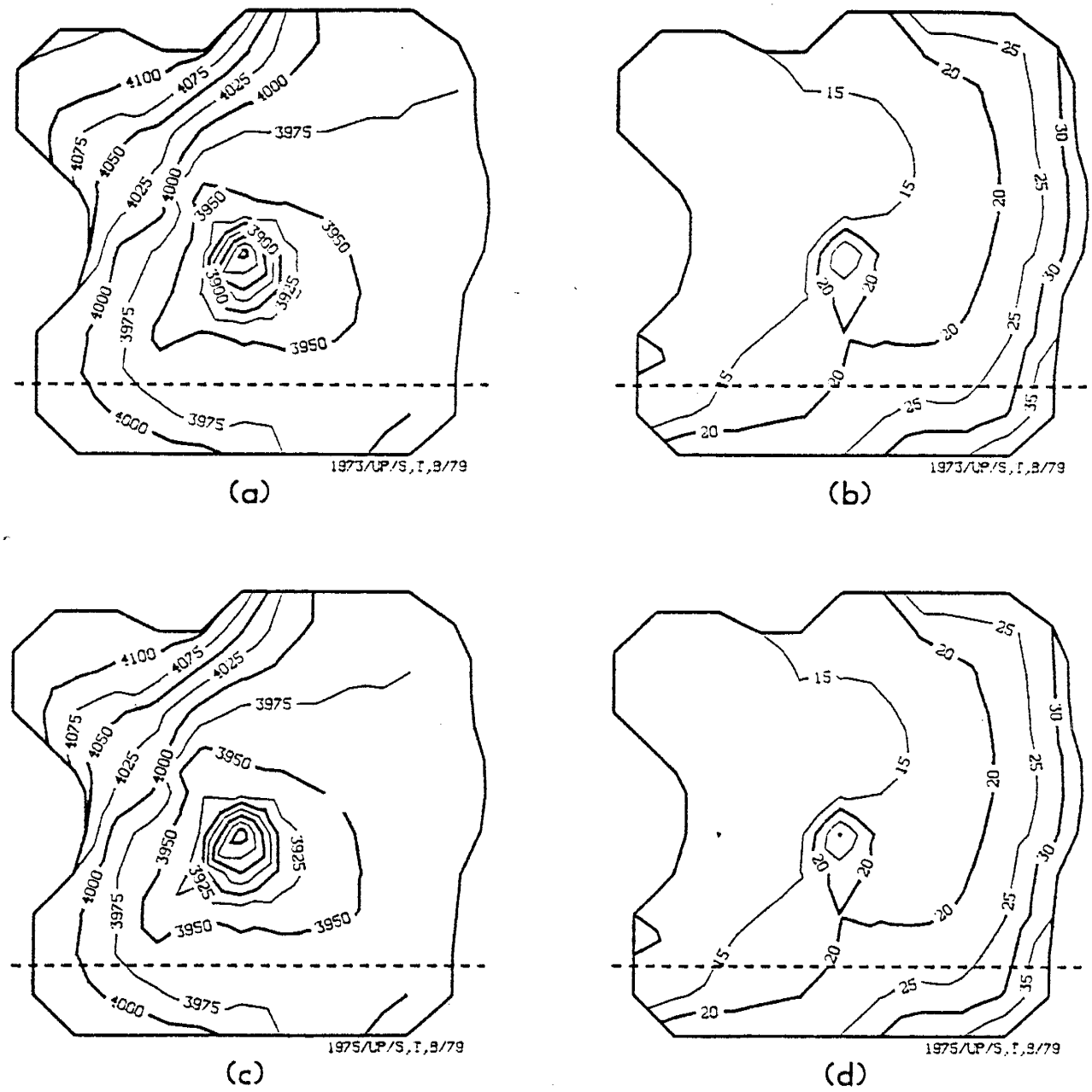

Fig. 44. Head fields (ft above MSL) and associated σ_h fields (ft) for run 79 for 1973 (a and b) and 1975 (c and d).

parameters experienced no variance reduction. In reality, however, this is not always the case.

Run 93 used WLS log T estimates conditioned on all of the available head data during the period 1930 to 1975. The input log T and σ_T values for run 93 are shown in figure 45, along with the 1930 σ_h fields for runs 93 and 88. All input parameters except for log T were identical for the two runs.

Comparison of the σ_h fields shows a variance reduction in the northern half of the basin for run 93 as expected. The 10 ft and 15 ft contours of σ_h were extended considerably compared to the equivalent contours for run 88. In the south-central region of the basin, however, the σ_h field for run 93 shows a significant variance increase over that of run 88. This increase occurs despite the fact that the σ_T's for run 93 were less than those of run 88 in this area.

The variance increase must be due to the boundary node uncertainty - no other parameters exhibited high enough standard deviations at 1930 to account for the observed "bulge" in the σ_h contours for run 93. A comparison of figure 45a with figure 45d shows that the area of increased variance is nearly coincident with a high log T zone estimated by WLS. The high log T zone effectively allowed a more efficient propagation of boundary node uncertainty into the basin, and subsequently σ_h actually increased where a decrease (due to variance reduction of the WLS parameter estimates) was expected. Note that the portion of σ_h due to the log T values did actually decrease for run 93, but the decrease was simply overshadowed by the increase in σ_h due to the boundary nodes.

This example indicates that the head variances depend not only upon the input parameter uncertainty, but upon the input parameters as well. The interaction between the model parameters, their covariance matrices and

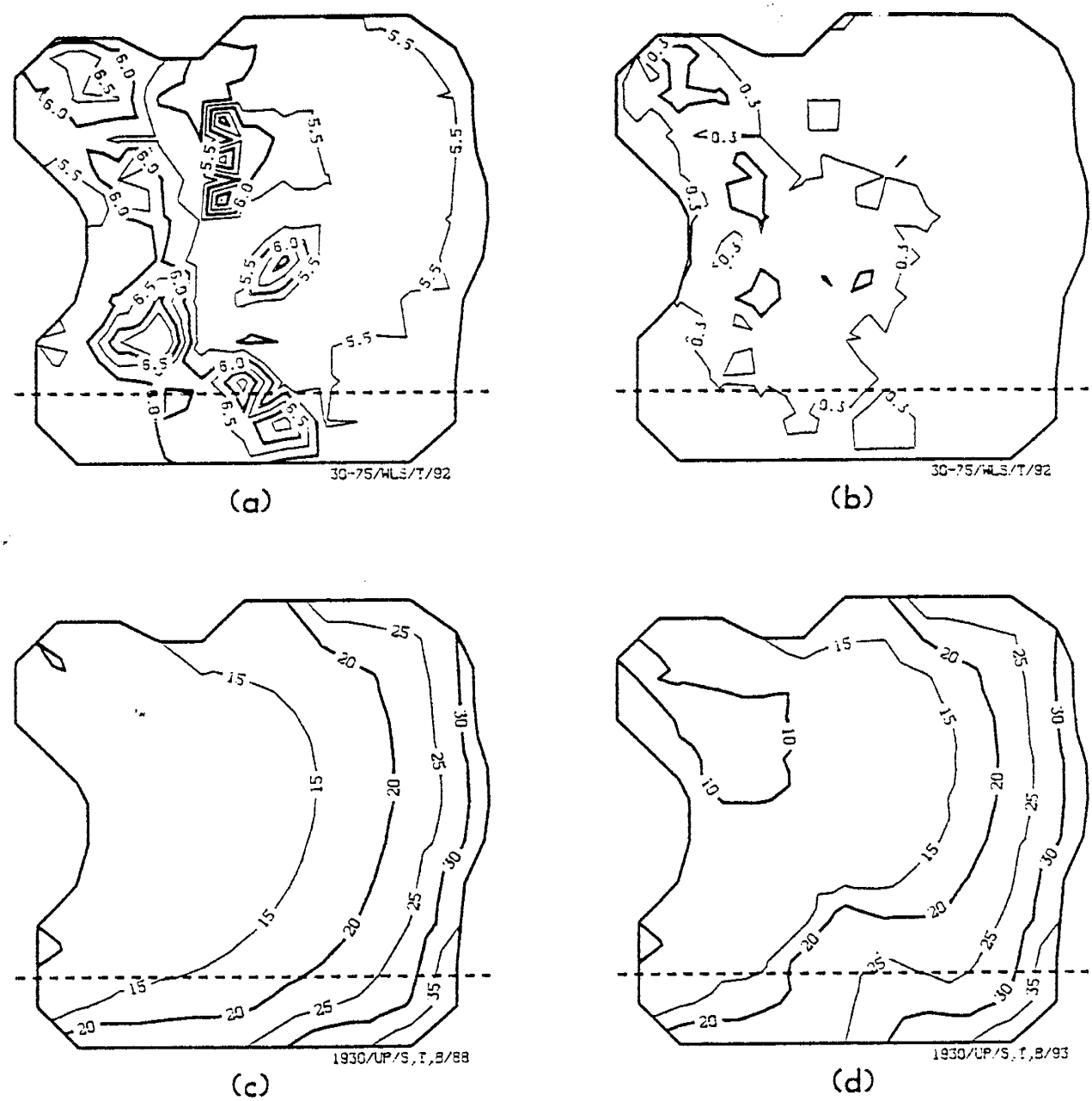

Fig. 45. Posterior log T (a), σ_T (b) and 1930 σ_h fields for runs 88 (c) and 93 (d). Standard deviations in feet.

uncertainty propagation is complex and may be counter-intuitive in some cases.

MODEL VALIDATION

In order to validate a numerical model it is necessary to somehow "check" the performance of model parameters estimated using one data set against a different data set for the same physical situation. If this task can be performed successfully with some degree of certainty then it is reasonable to use the model for predictive purposes. A validation of CERT was performed by withholding selected portions of the observed head data from the parameter estimation (calibration) process, and then output from the calibrated model was compared to the withheld data set.

The available data set can be divided into two or more subsets in time or space. Both techniques were used in this study. It was logical to only estimate log T for the validation study in time, but for the validation runs where the available head data was divided in space T and/or B (pumping) could have been estimated parameters. Boundary conditions and storage parameters were not estimated due to problems described previously.

A summary of the CERT simulations used during the validation study is provided in table 11. Table 11 should be a useful reference during the following discussion. The measurement locations used during the following discussion are shown in figure 46.

Standard Cases

To interpret the results of the validation runs, it was necessary to have some "base cases" to which they could be compared. Three CERT runs were conducted with this point in mind.

Best Fit. Run 92 was a WLS run where log T was the only estimated parameter. All of the available head measurements over the entire time period were used to condition the log T estimates. The S and B parameters were those described previously. The posterior log T parameters, σ_T's and

Table 11

Description of WLS and UP runs relevant to the validation study

Run #	Description
92	WLS run: log T conditioned on all available head data 1930 - 1975.
71	WLS run: log T conditioned on avilable head data 1930 - 1960.
82	WLS run: log T conditioned on observations at locations with less than 10 measurments 1930 - 1975.
84	WLS run: log T conditioned on observations at locations with more than 10 measurments 1930 - 1975.
89	WLS run: log T and B (pumping) conditioned on all available head data 1930 - 1975.
83	WLS run: log T and B (pumping) conditioned on observationes at locations with less than 10 measurments 1930 - 1975.
85	WLS run: log T and B (pumping) conditioned on observationes at locations with more than 10 measurments 1930 - 1975.
88	UP run: constant log T over basin. Standard input for B and S. S,T and B uncertain. 1930-1975.
93	UP run: used WLS estimates of log T from run 92 as input. S,T,B uncertain. 1930 - 1975.
79	UP run: used WLS estimates of log T from run 71 as input. S,T,B uncertain. 1930 - 1975.
86	UP run: used WLS estimates of log T from run 82 as input. S,T,B uncertain. 1930 - 1975.
87	UP run: used WLS estimates of log T from run 84 as input. S,T,B uncertain. 1930 - 1975.

Table 11 Contd.

94	UP run: used WLS estimates of log T and B from run 83 as input. S,T,B uncertain. 1930 - 1975.
95	UP run: used WLS estimates of log T and B from run 85 as input. S,T,B uncertain. 1930 - 1975.

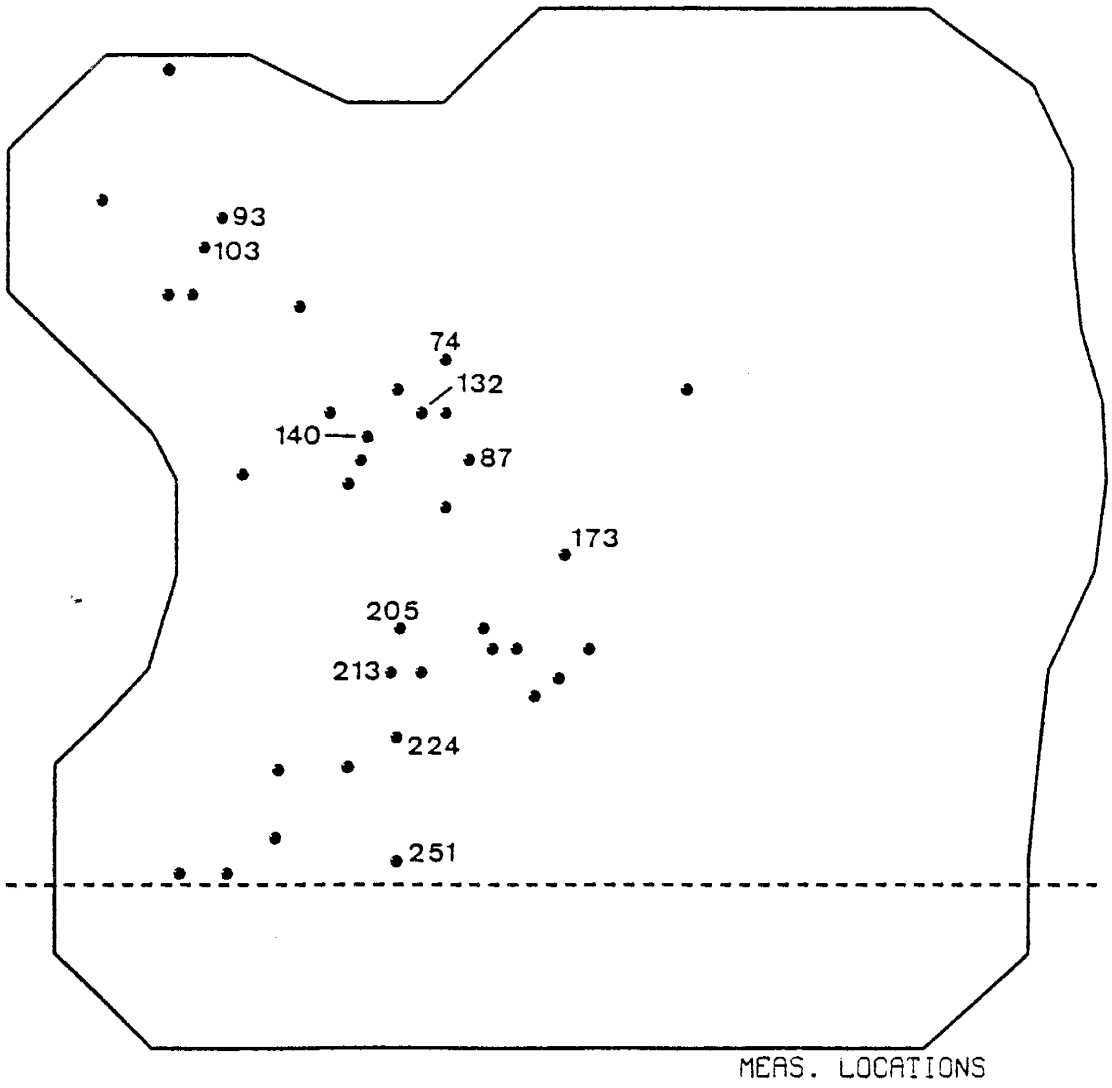

Fig. 46. Measurement locations inside finite elements where model h and σ_h were calculated for all UP runs. Labels indicate locations presented in this report.

the head data used as input to run 92 are shown in figure 47. The output from run 92 was used as input to UP run 93 where the T, S and B parameters were considered uncertain. The matches between observed and calculated heads produced by run 93 were considered optimal, or the best fit case, against which validation runs where only log T was estimated could be compared.

For validation runs where log T and B (pumping only) parameters were estimated, run 89 was the optimal case against which output could be compared. Run 89 estimated the parameters log T and B over the entire time period using all of the observed head data. The estimated log T values and the head data on which log T and B were conditioned during run 89 is shown in figure 48. The estimated B parameters for four pumping nodes for run 89 are shown in figure 49. Note that the posterior B estimates were essentially the same as those obtained from run 70 (see figure 31). Run 89 used two S zones, while run 70 used only one. The posterior covariance matrix of the uncertain parameter types in run 89 could not be obtained due to computer difficulties, and therefore variances on the heads output from run 89 could not be calculated.

One would expect a very good match between modeled heads from run 89 and observed heads. This was indeed the case, but the validity of the estimated B parameters may be questionable under some circumstances. This issue was discussed previously in this paper.

The head and σ_h contours for the four years 1940, 1960, and 1975 for run 93 are presented in figures 50 and 51. The head contours for the same four years for run 89 are presented in figure 52.

Worst Fit. In contrast to runs 93 and 89 described above, the results of run 88 can be considered a least optimal, or worst fit, solution against which to compare the validation runs. Run 88 used the kriged prior for

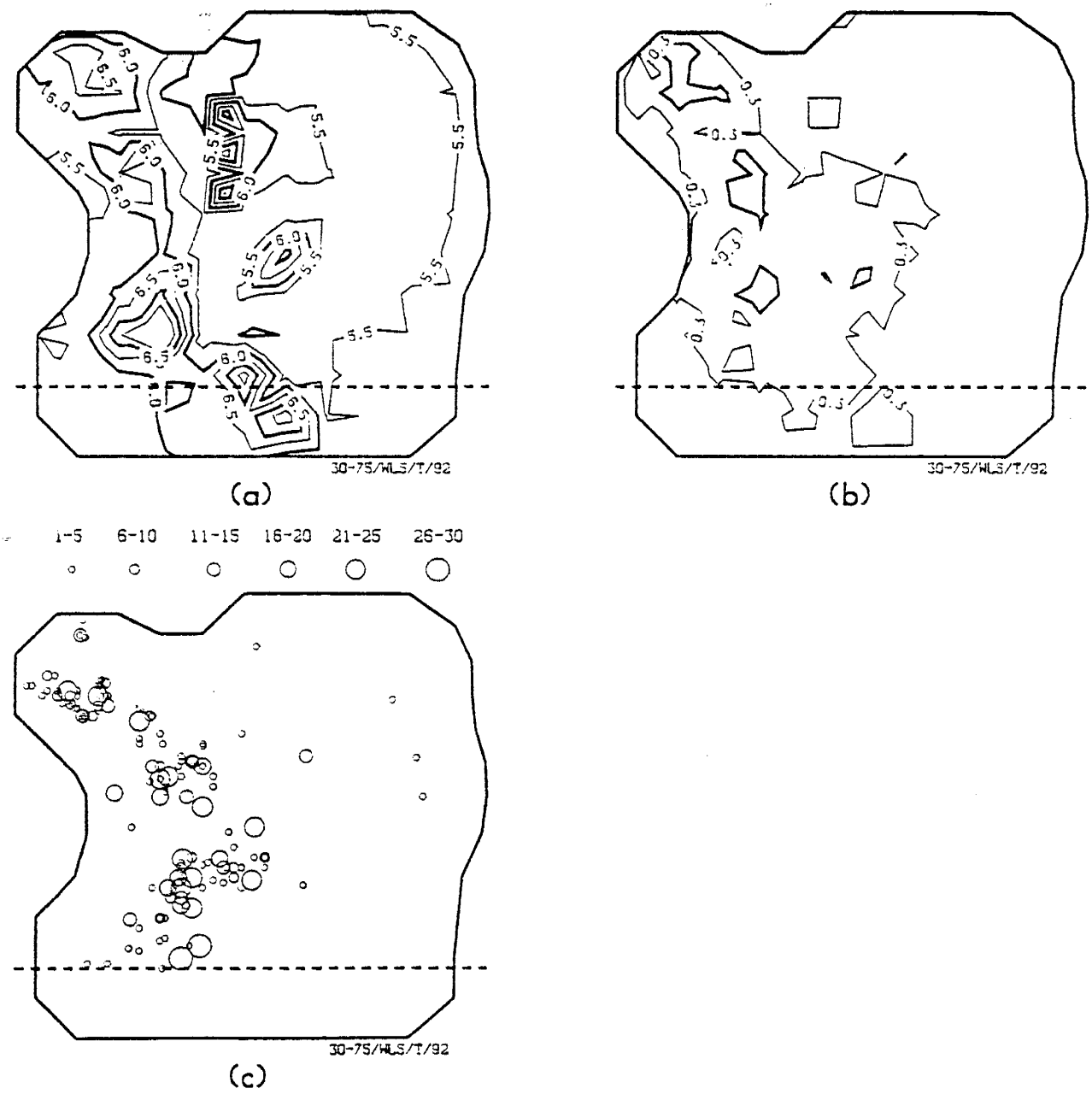

Fig. 47. Posterior log T (a) and σ_T (b) fields and location and frequency of observed head data for run 92.

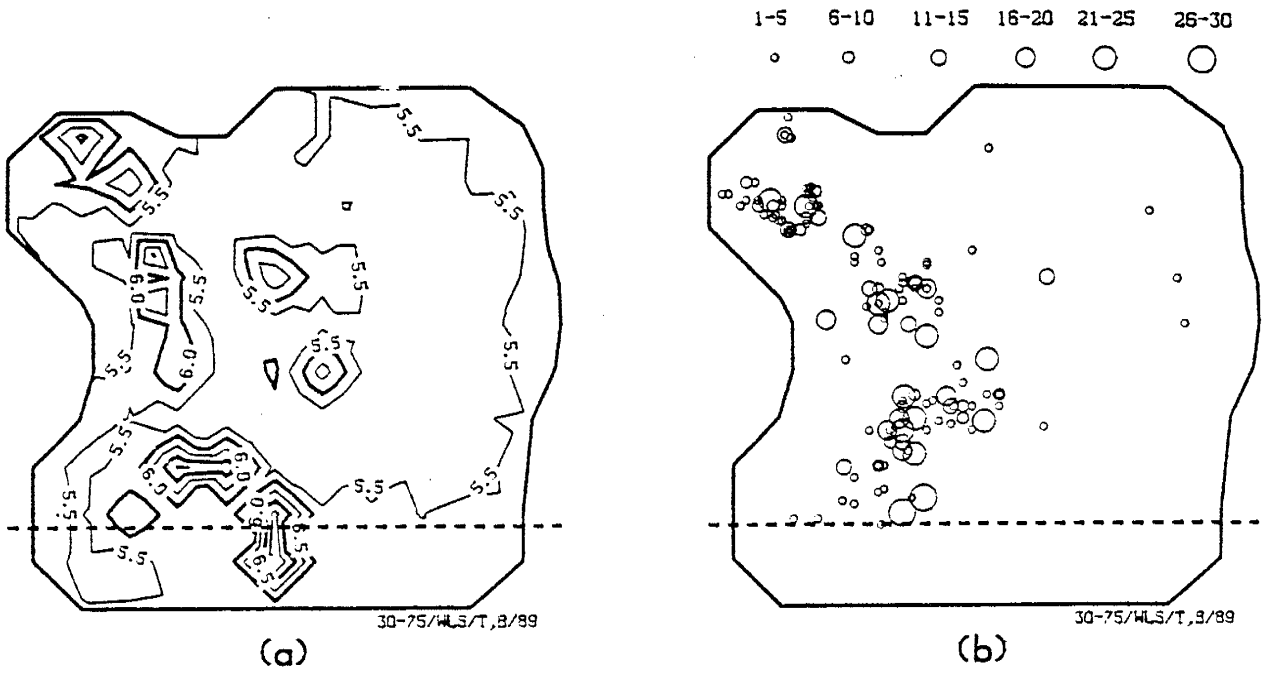

Fig. 48 Posterior log T field (a) and observations on which the field was conditioned (b) for run 89.

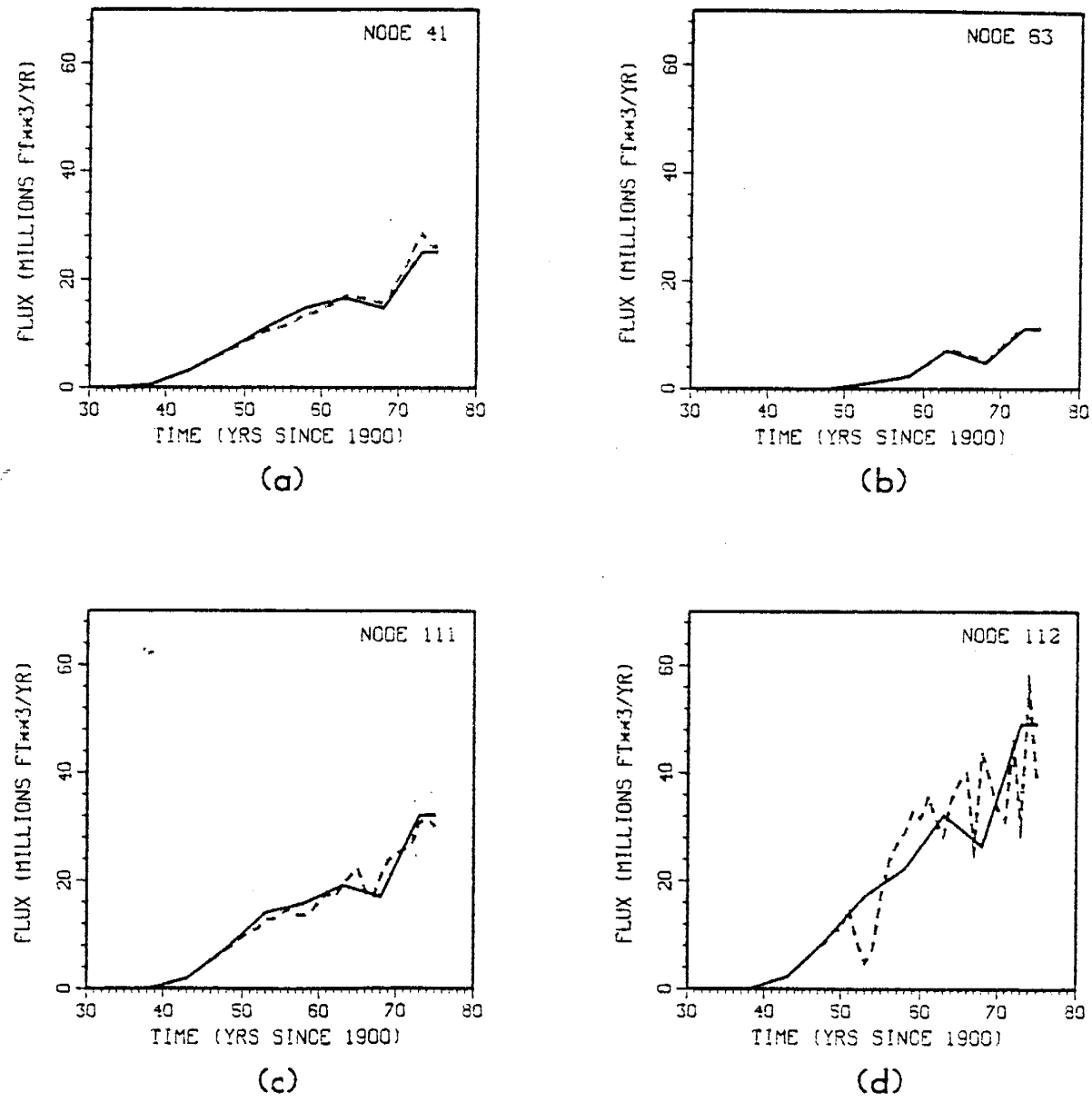

Fig. 49. Prior (solid) and post (dashed) pumping estimates for four nodes for run 89.

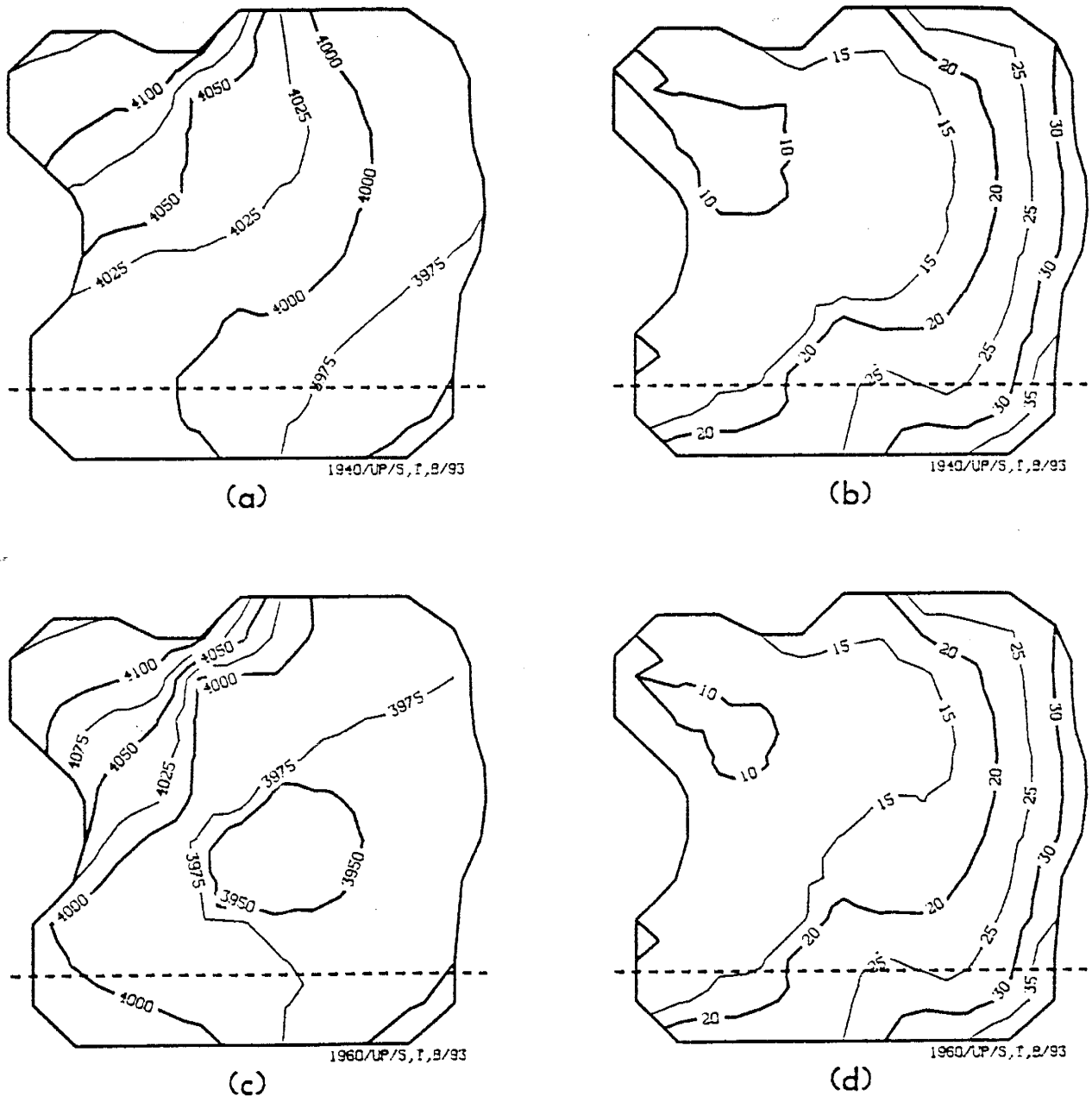

Fig. 50. Head fields (ft above MSL) and associated σ_h fields (ft) for run 93 for 1940 (a and b) and 1960 (c and d).

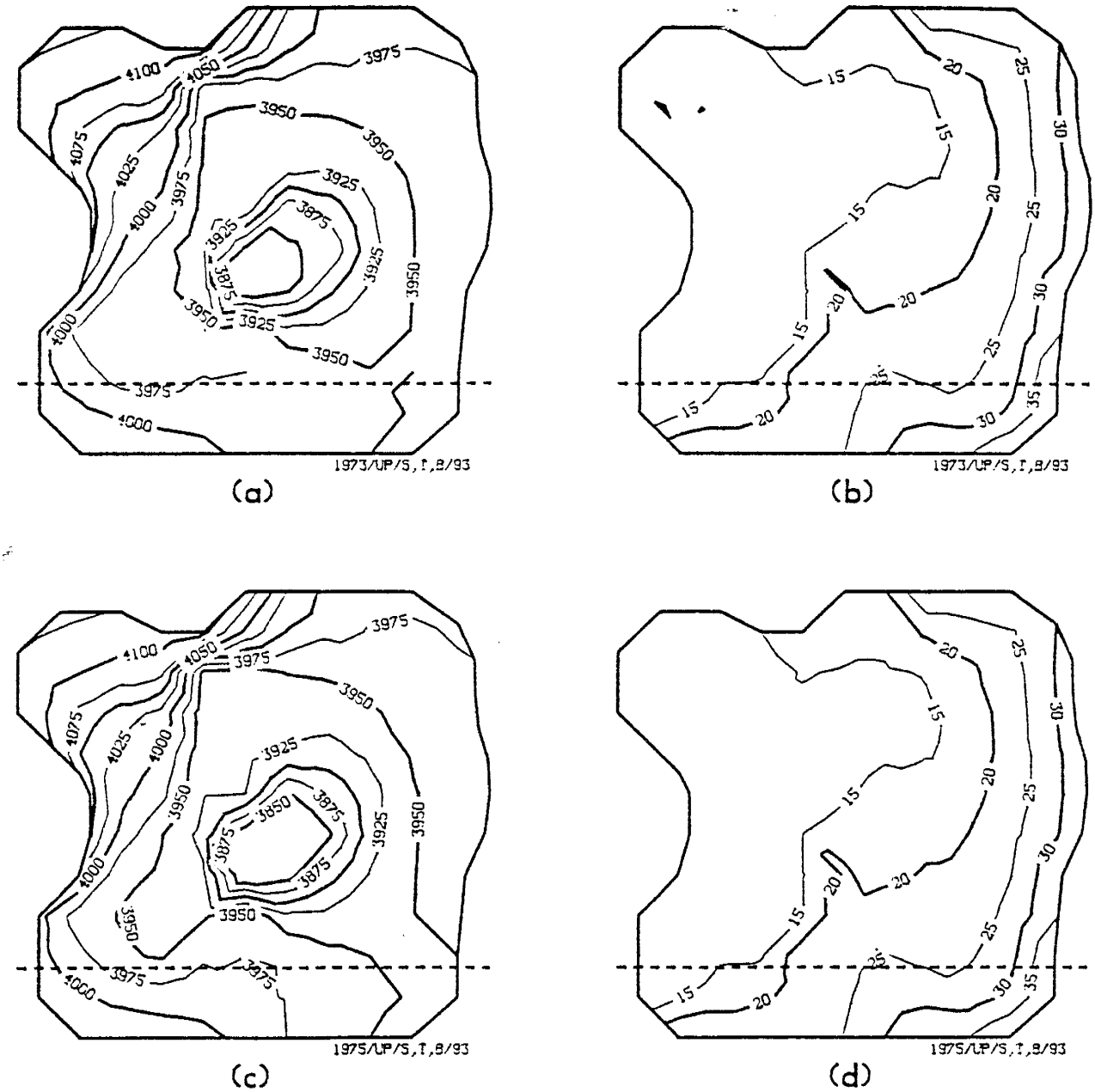

Fig. 51. Head fields (ft above MSL) and associated σ_h fields (ft) for run 93 for 1973 (a and b) and 1975 (c and d).

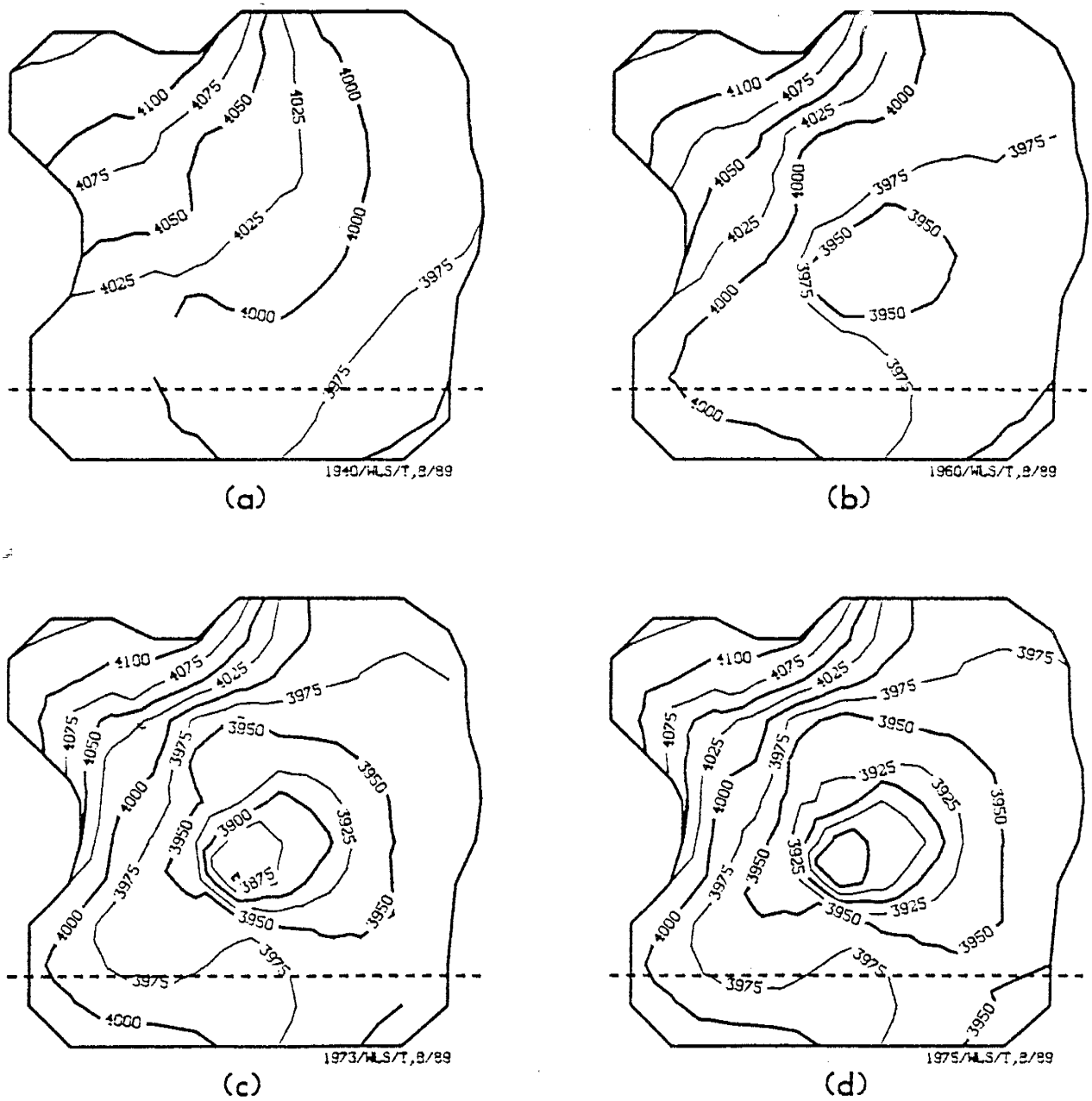

Fig. 52. Head fields (ft. above MSL) for run 89 for 1940 (a), 1960 (b), 1973 (c) and 1975 (d).

nodal log T values over the basin (log T = 5.916, σ_T = 0.3229), the standard SEO pumping record, and the subjectively estimated S and boundary parameters as input. The output from run 88 can be considered a "worst case" scenario where the input parameters were not conditioned at all using the available head data. Note that run 88 was discussed previously in the "Effect of Conditioned Parameters on Uncertainty Propagation" section. Head and σ_h contours for run 88 are presented in figures 53 and 54.

Model Validation in Time

The WLS log T estimates from run 71 are contoured in figure 55a. The associated estimation variances and the observations on which the estimates were conditioned are shown in figures 55b and 55c. Run 71 used all of the head observations available for the period 1930 to 1960. UP run 79 used the output from run 71 as input, but B and S as well as log T were considered uncertain parameters. The objective of this set of runs was to analyze how well log T parameters conditioned on early head data predicted future water levels in the Columbus Basin.

The results of run 79 are presented in figures 56 through 63 for eight measurement locations. In each of these figures, the sub-figures a and b represent the "worst" and "best" fit cases for log T model validation (runs 88 and 93) respectively. The c sub-figures are results from run 79.

In general, one would have expected that the fit between observed and calculated heads would be the worst for run 88 ('a' sub-figure), better for run 79 ('c' sub-figure) and the best for run 93 ('b' sub-figure). This is indeed the case at some locations throughout the basin, one of which is location 74 (figure 56). However, at many locations, such as those shown in figures 57 through 63, the results of run 79 are as good or even better than those of run 93. This indicates that a great deal of conditioning occurred using only an initial portion of the head record (1930-1960). This is an

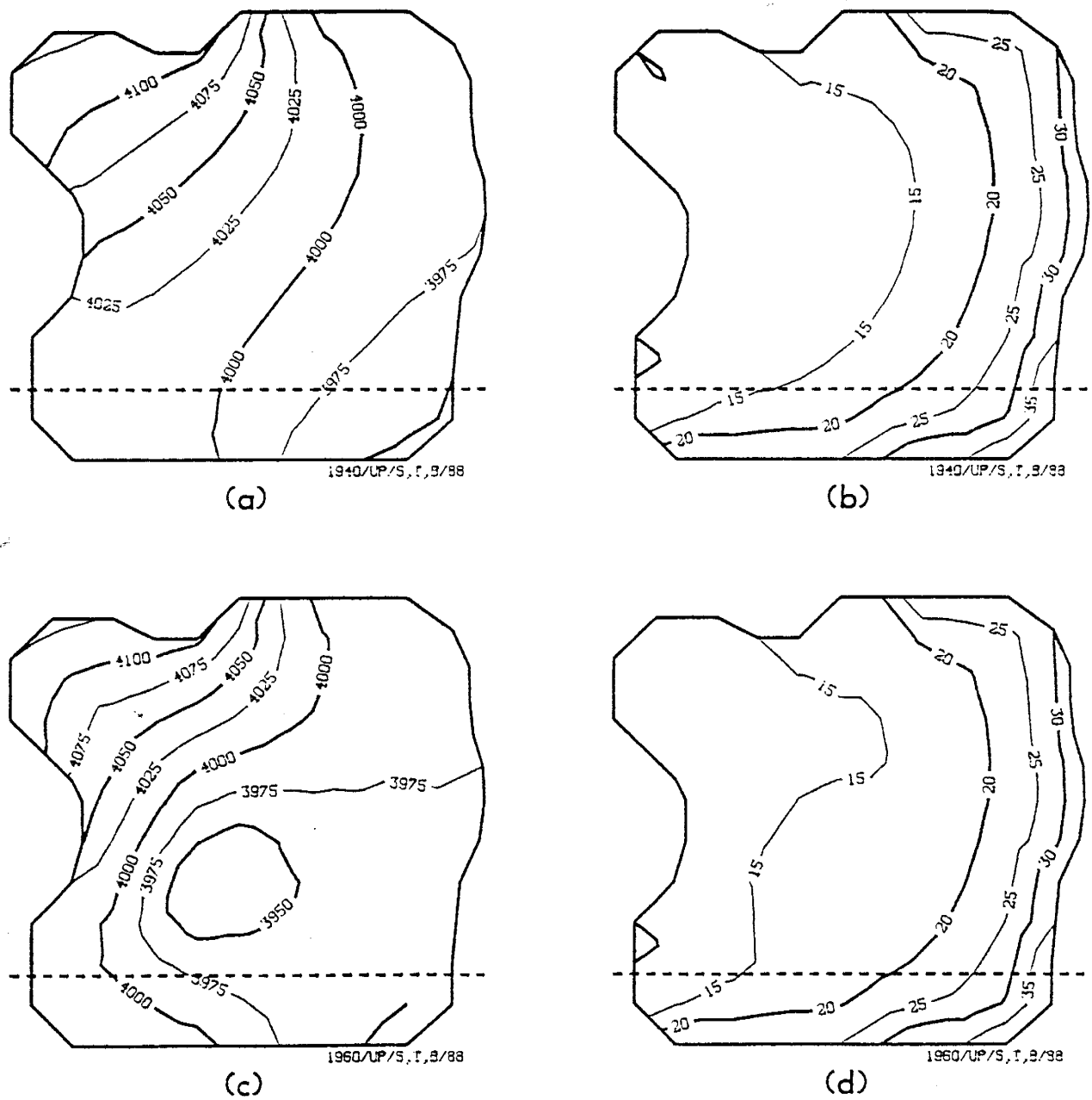

Fig. 53. Head fields (ft above MSL) and associated σ_h fields (ft) for run 88 for 1940 (a and b) and 1960 (c and d).

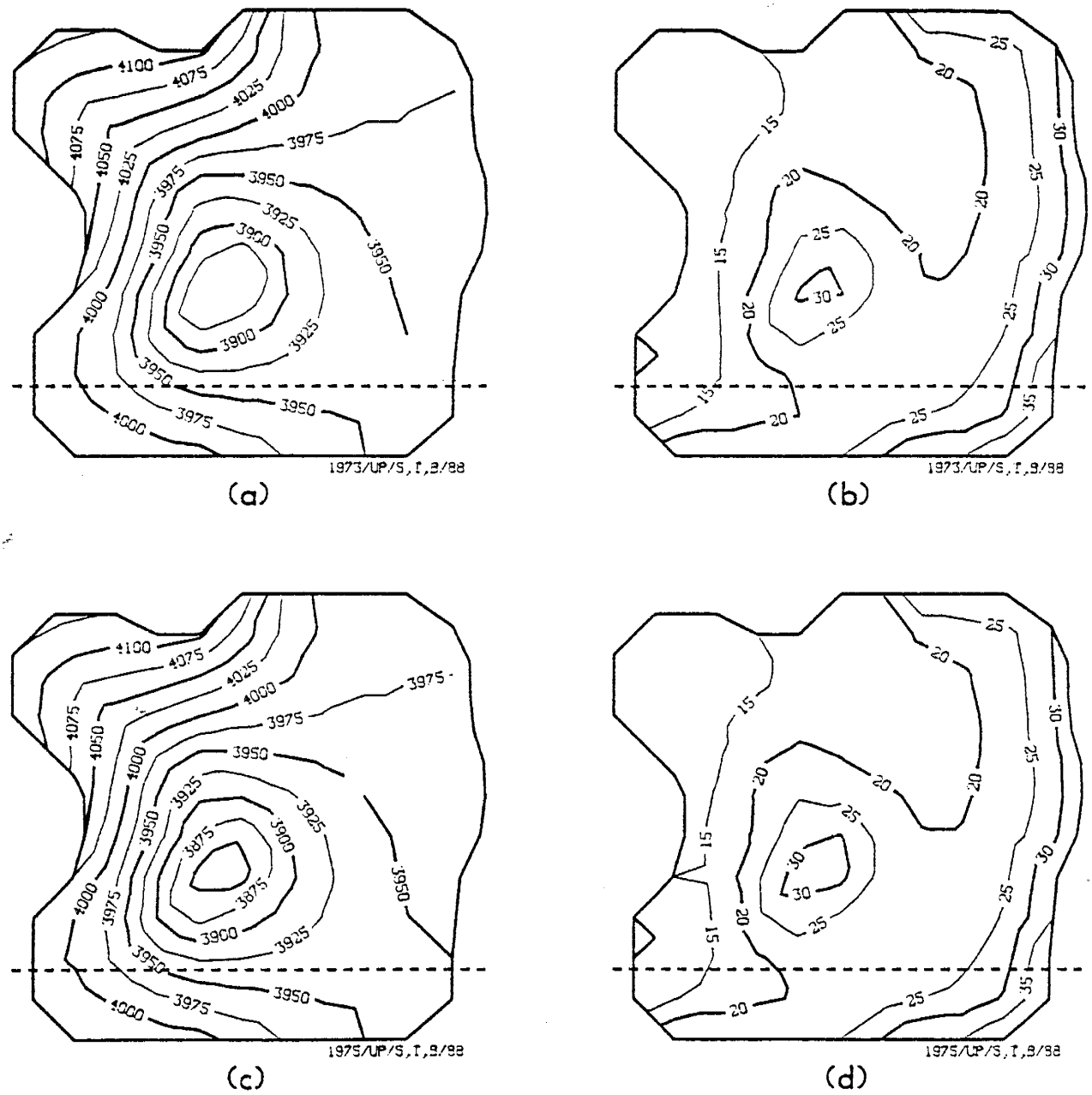

Fig. 54. Head fields (ft above MSL) and associated σ_h fields (ft) for run 88 for 1973 (a and b) and 1975 (c and d).

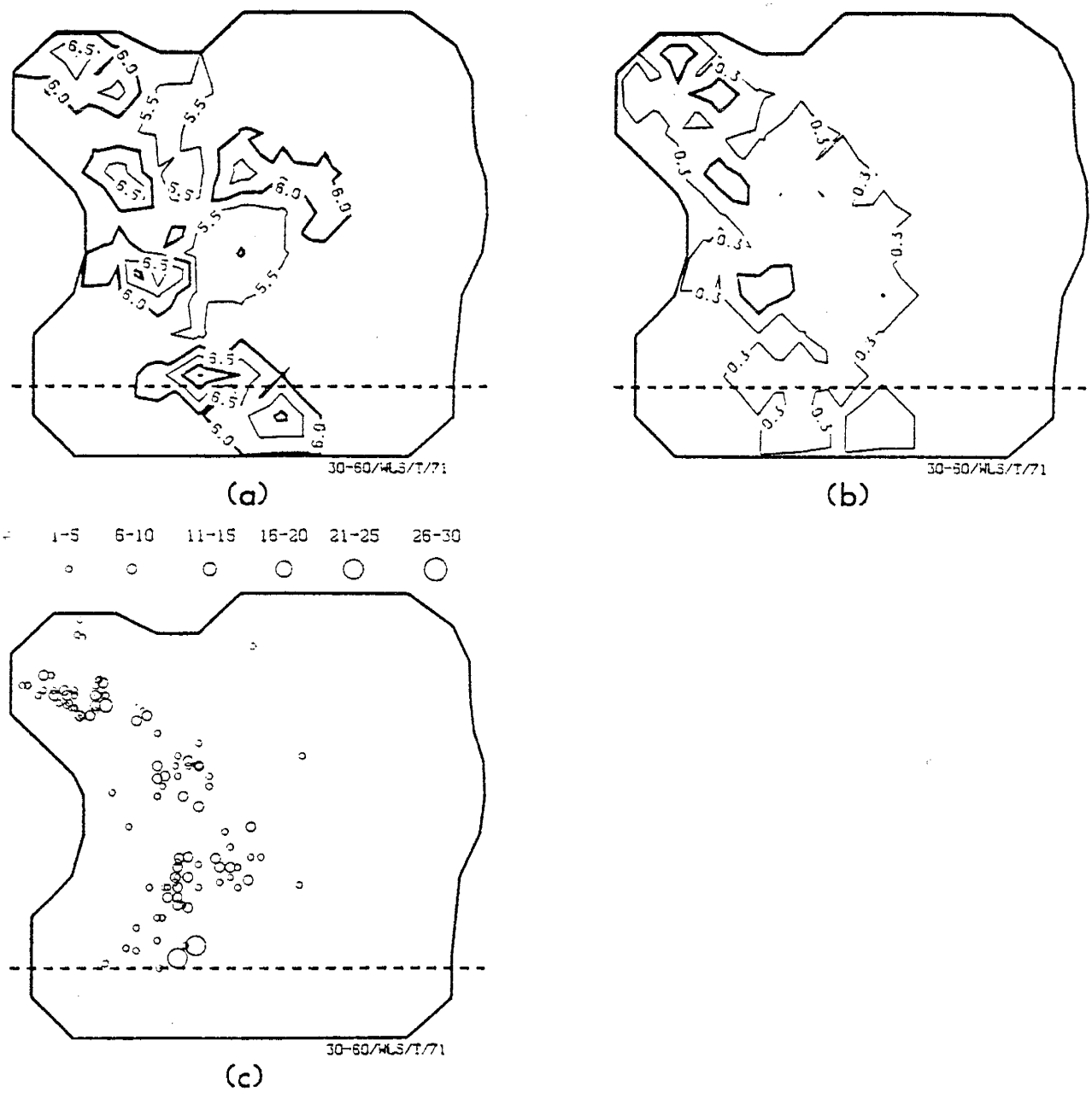

Fig. 55. Posterior log T (a) and σ_T (b) fields and location and frequency of observed head data for run 71.

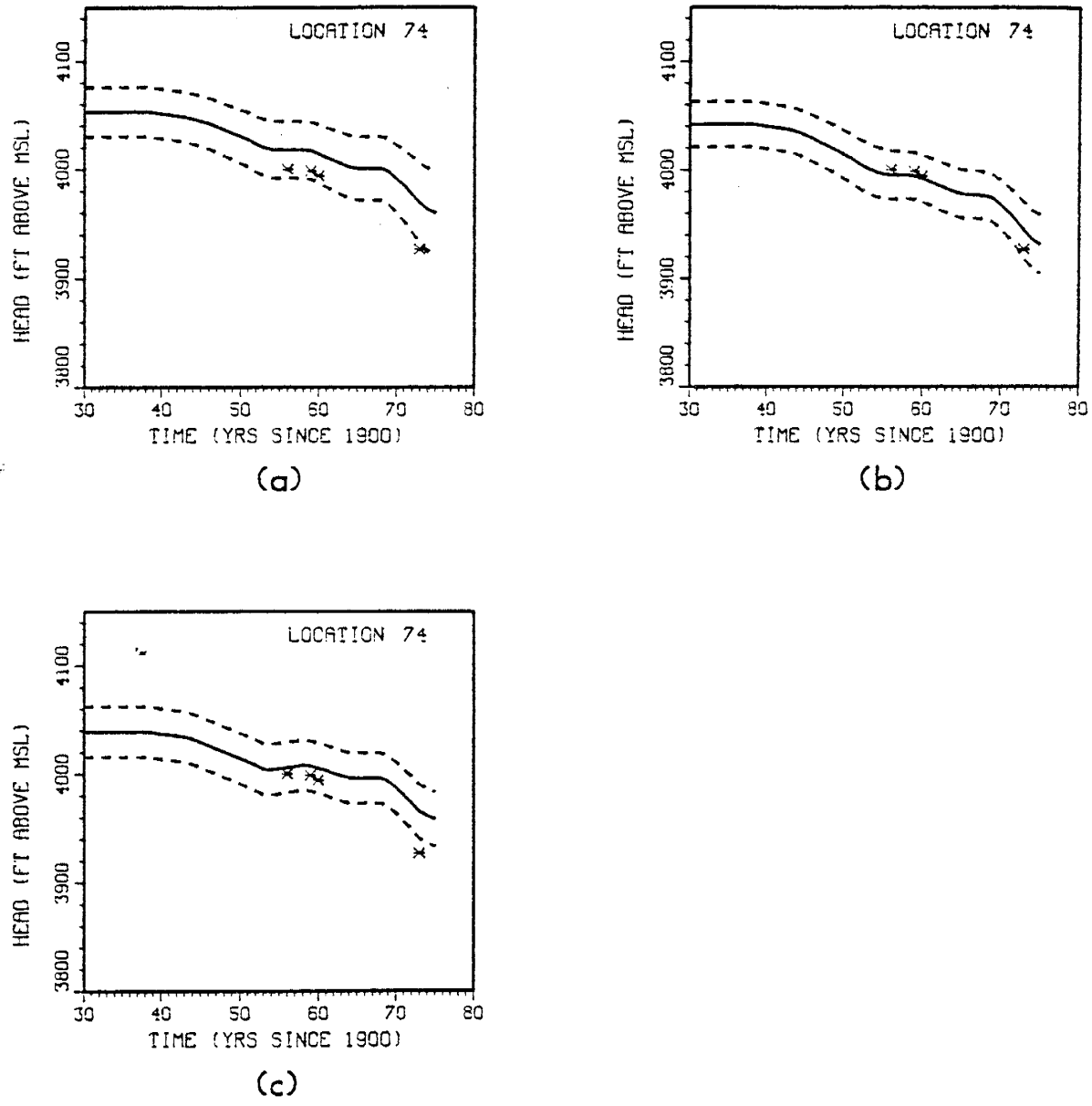

Fig. 56. Model heads (solid line), observed heads (asterisks) and $\pm 2\sigma_h$ bounds (dashed lines) at measurement location 74 for runs 88 (a), 93 (b) and 79 (c).

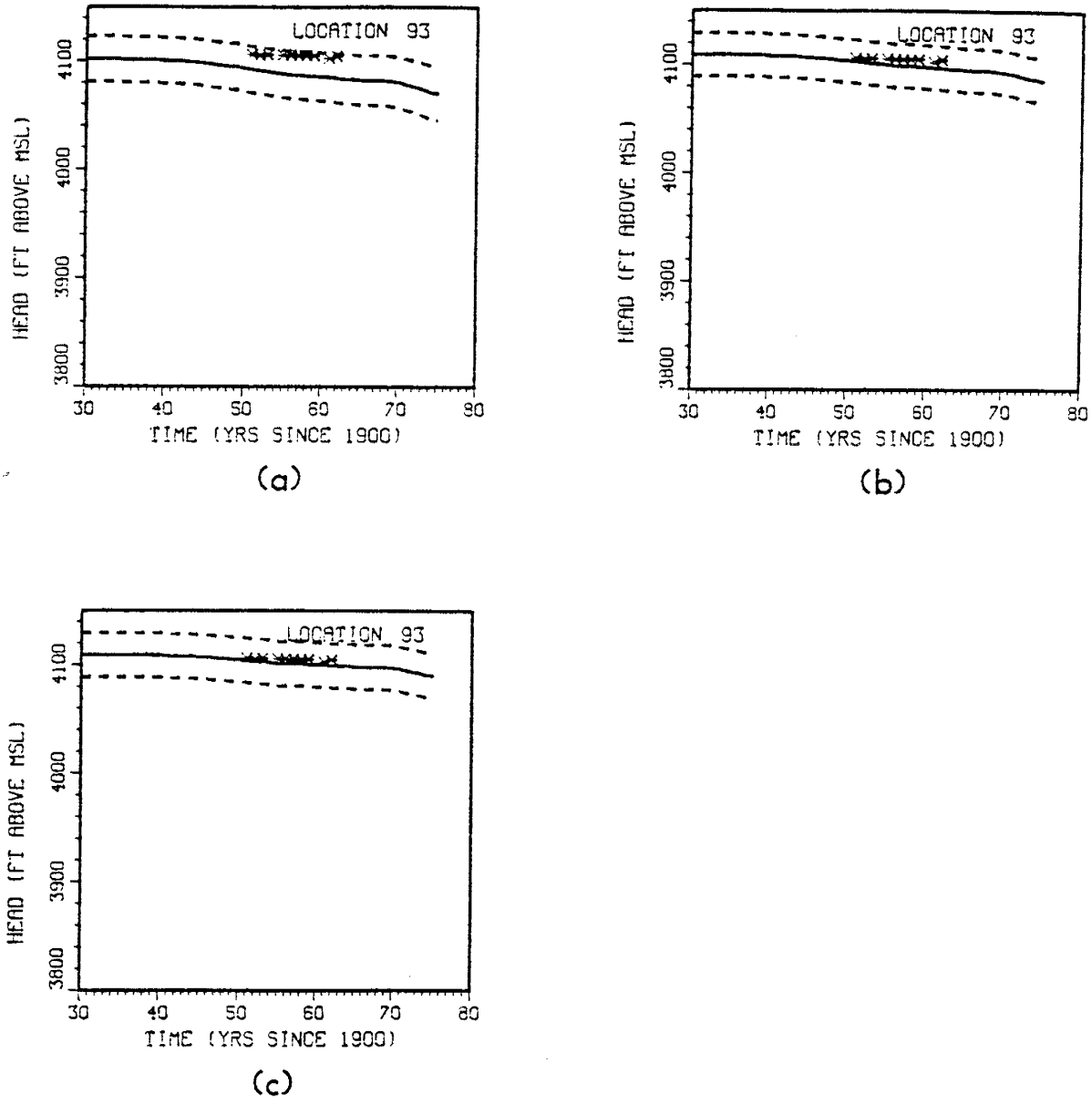

Fig. 57. Model heads (solid line), observed heads (asterisks) and $\pm 2\sigma_h$ bounds (dashed lines) at measurement location 93 for runs 88 (a), 93 (b) and 79 (c).

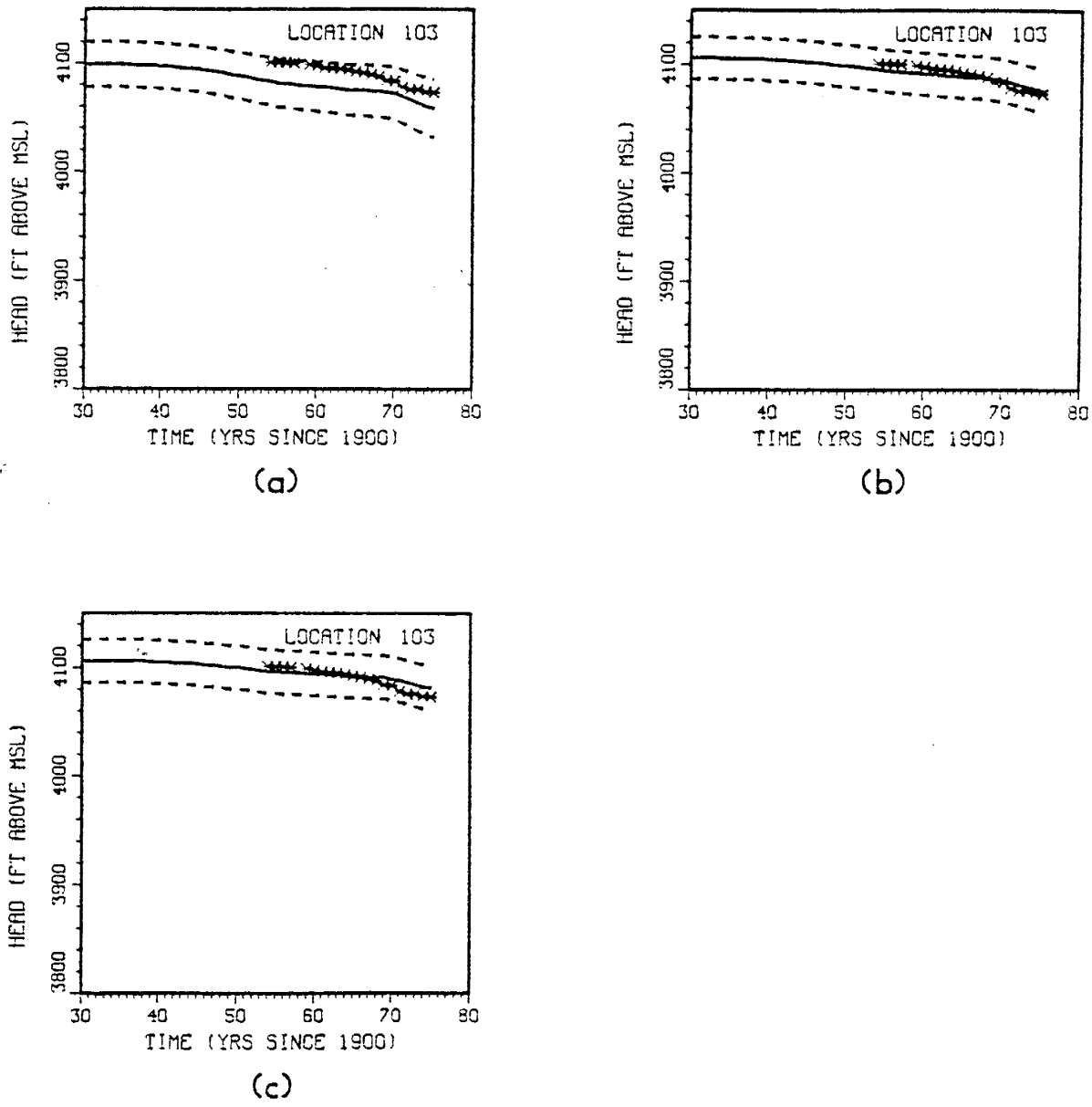

Fig. 58. Model heads (solid line), observed heads (asterisks) and $\pm 2\sigma_h$ bounds (dashed lines) at measurement location 103 for runs 88 (a), 93 (b) and 79 (c).

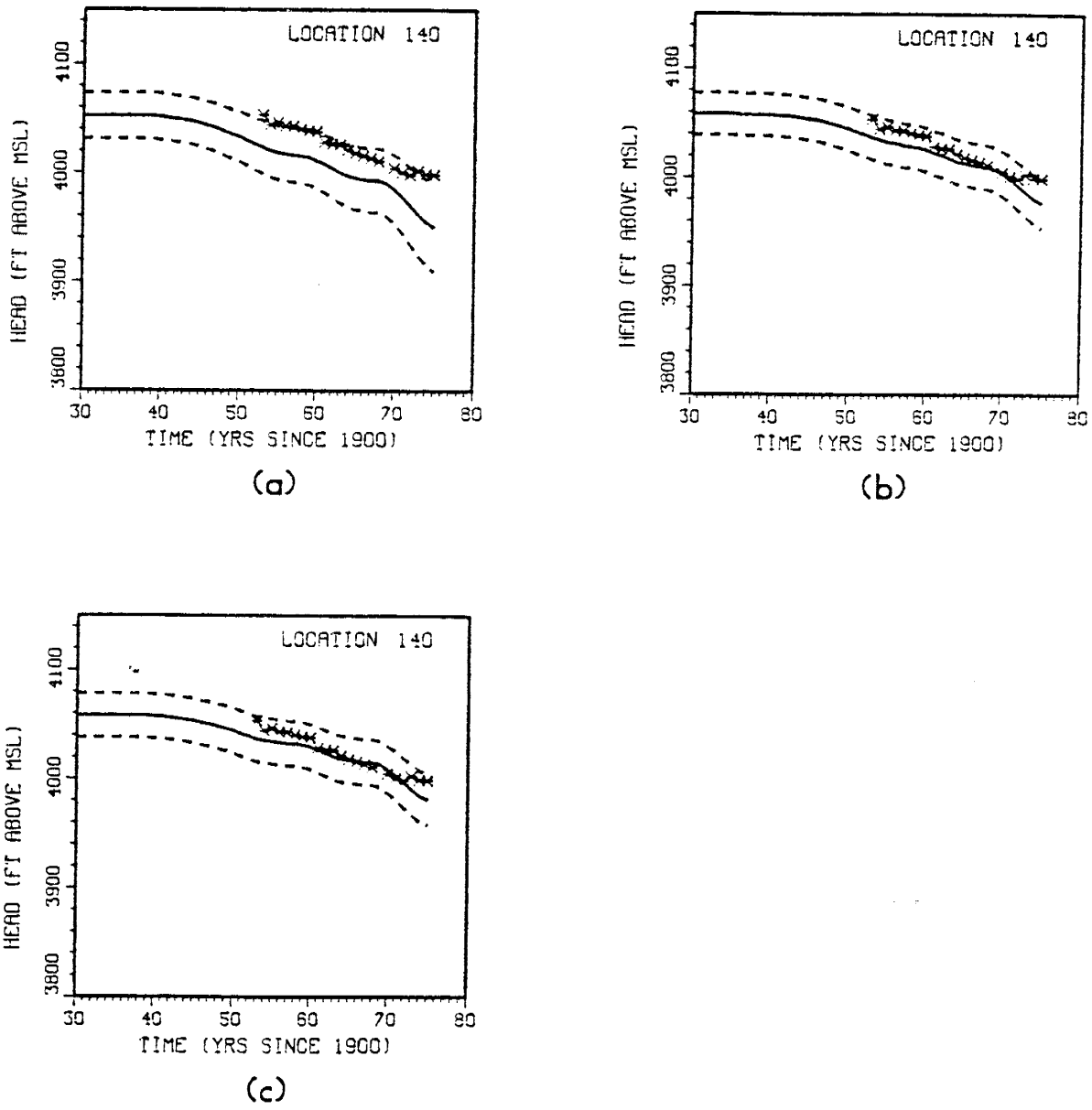

Fig. 59. Model heads (solid line), observed heads (asterisks) and $\pm 2\sigma_h$ bounds (dashed lines) at measurement location 140 for runs 88 (a), 93 (b) and 79 (c).

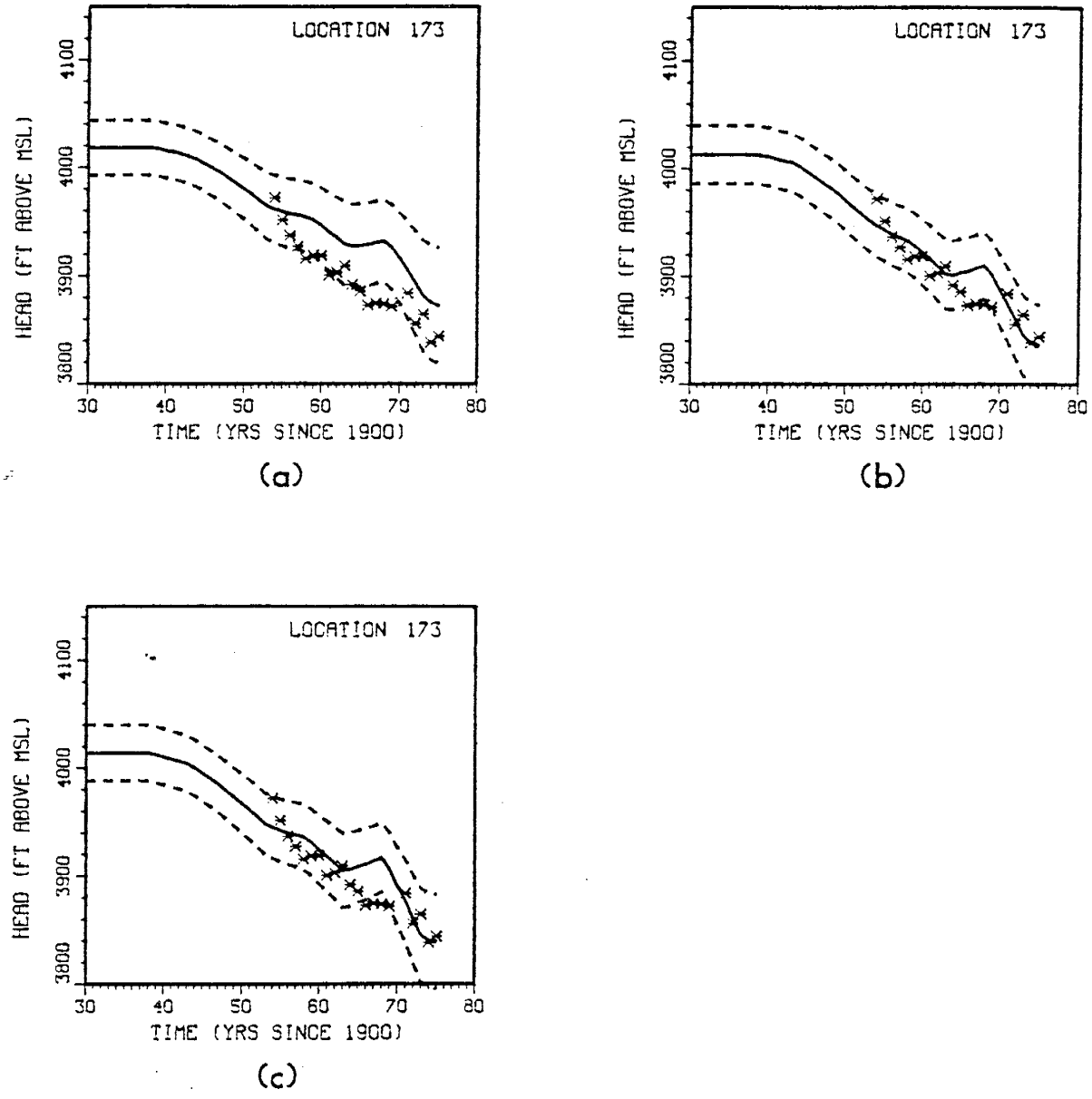

Fig. 60. Model heads (solid line), observed heads (asterisks) and $\pm 2\sigma_h$ bounds (dashed lines) at measurement location 173 for runs 88 (a), 93 (b) and 79 (c).

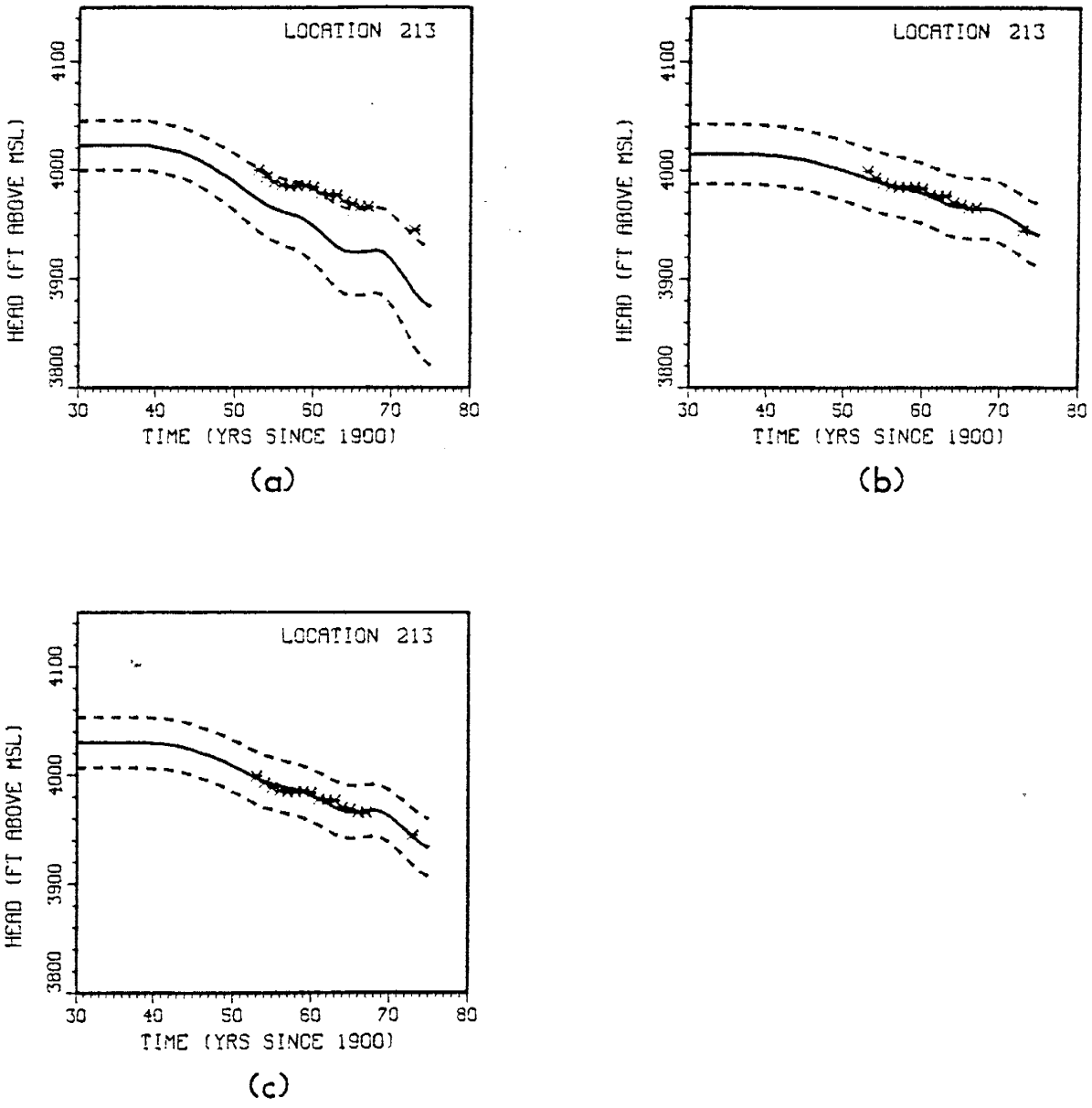

Fig. 61. Model heads (solid line), observed heads (asterisks) and $\pm 2\sigma_h$ bounds (dashed lines) at measurement location 213 for runs 88 (a), 93 (b) and 79 (c).

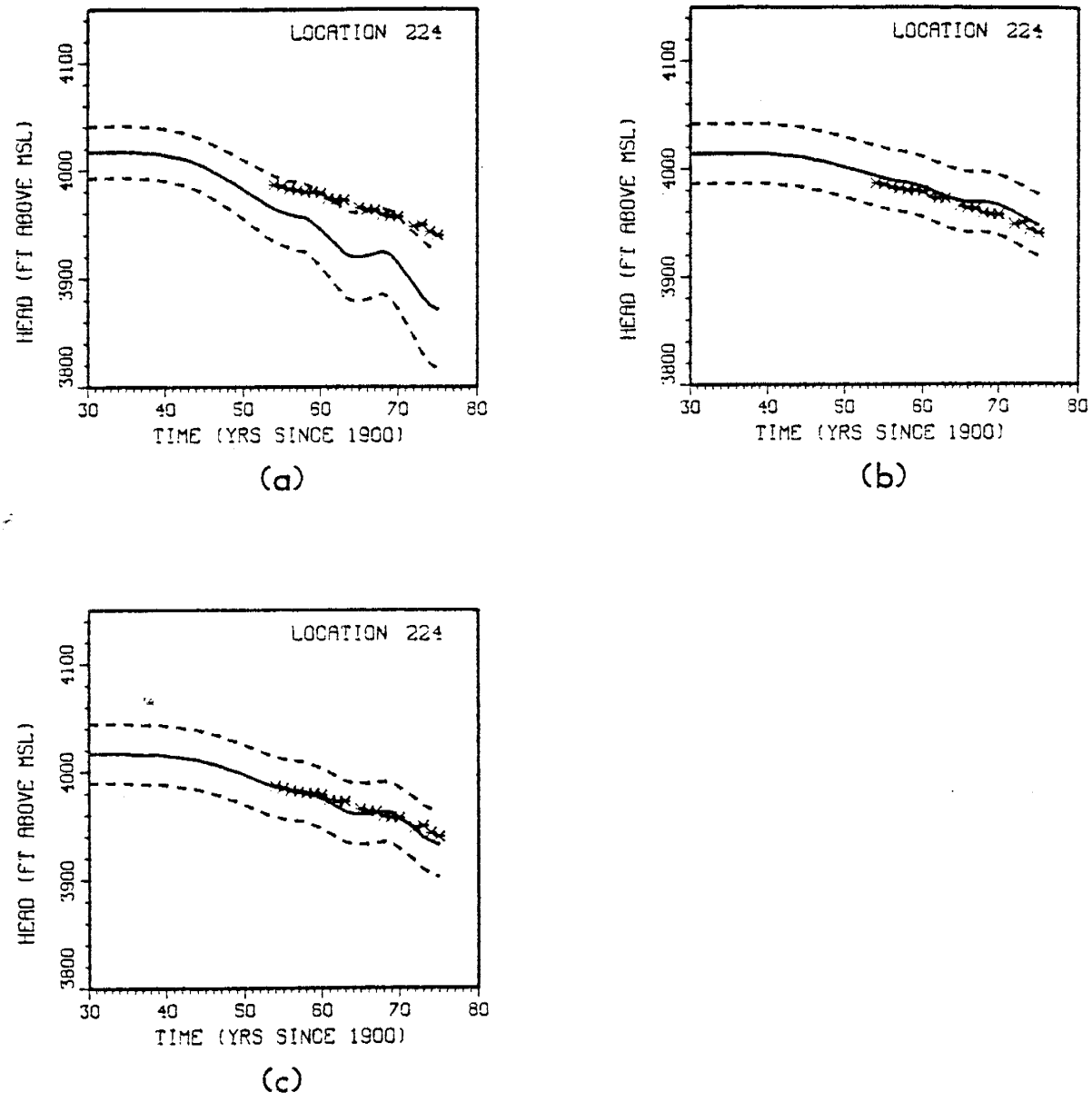

Fig. 62. Model heads (solid line), observed heads (asterisks) and $\pm 2\sigma_h$ bounds (dashed lines) at measurement location 224 for runs 88 (a), 93 (b) and 79 (c).

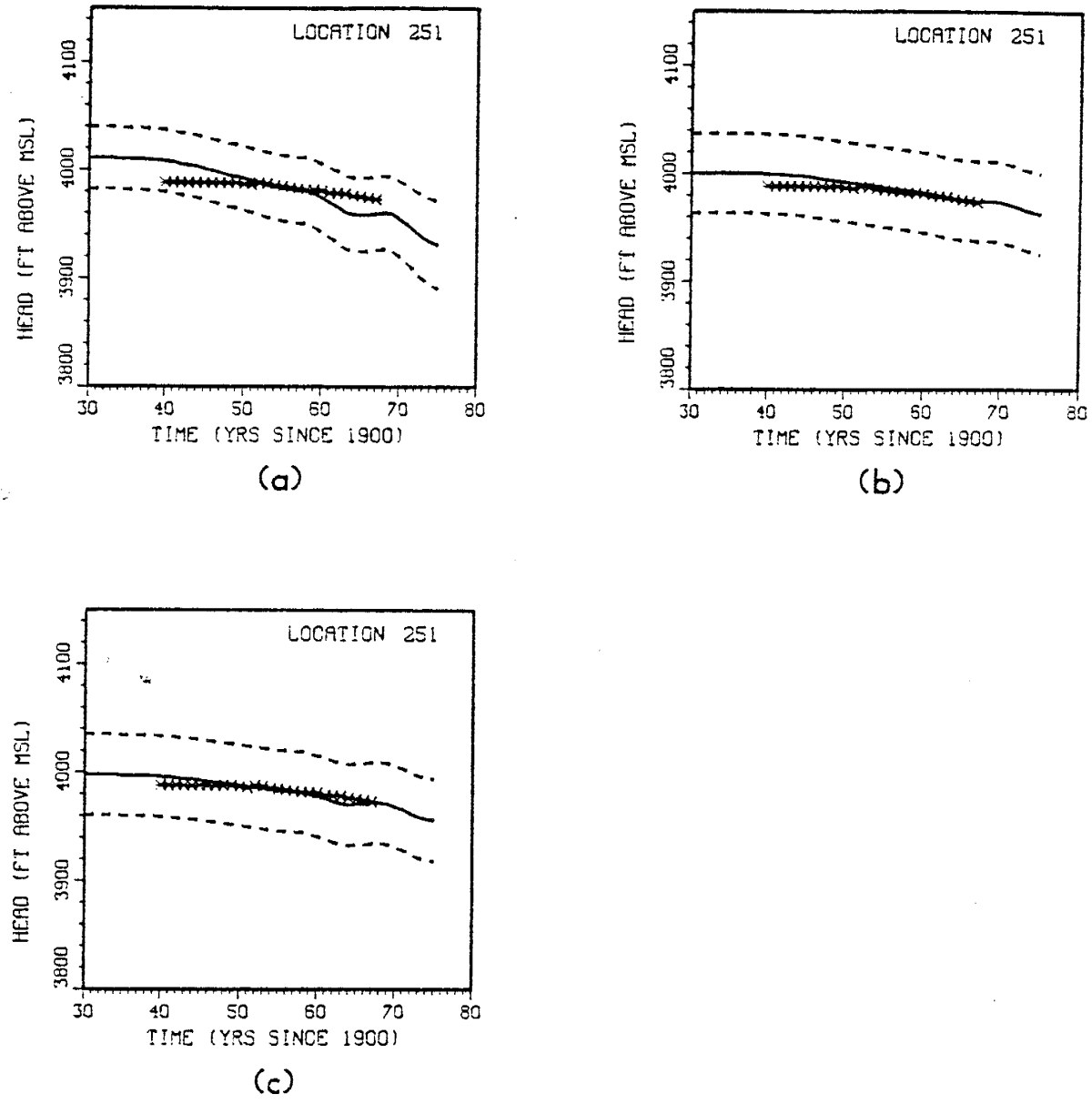

Fig. 63. Model heads (solid line), observed heads (asterisks) and $\pm 2\sigma_h$ bounds (dashed lines) at measurement location 251 for runs 88 (a), 93 (b) and 79 (c).

encouraging result, since it shows that log T estimates found using the 1930 to 1960 data set are a very good approximation of log T for the following time period 1960 to 1975.

It was not surprising that at some locations the results of run 79 displayed a better fit than did the results of run 93. This is because as more head data is used during the WLS procedure, the log T estimates must increasingly become a "compromise" to satisfy all of the available measurements in an optimal way. Therefore, at locations where run 79 produced a better fit than run 93, it can be deduced that some of the additional measurements used in run 92 "forced" the log T parameters to be slightly different from the optimum at that location. The same effect also occurred during run 71 but to a lesser extent.

Most of the observation locations showed a very good match between observed and calculated heads. Location 173 and several nearby locations not shown, however, do not show such a good match; the first portion of the downward trend of the observed head data was simply missed (figure 49). Location 173 was near the pumping center (figure 41), as were the other locations which missed this trend. These facts indicated that the pumping (B) parameters needed to be adjusted as well as log T for a satisfactory fit to be obtained at these locations. One parameter type constant through time (log T) could not be expected to account for all of the head variability in the basin, particularly in the areas of greatest drawdown.

Almost all of the observed heads were within the $\pm 2\sigma_h$ bands which roughly define 95 percent confidence intervals for a normal distribution. The exceptions were at locations 74 and 173, where one and three measurements respectively lie below the $-2\sigma_h$ line. For location 74 (figure 45), this result may be partially explained by poor conditioning of log T since the point does not lie below the $-2\sigma_h$ line for run 93. At this

particular location, the log T's conditioned on the 1930 to 1960 head data were simply not good enough to predict reasonable head values 15 years later. This poor match could be partially explained by uncertain pumping parameters also. Perhaps pumping in the vicinity of location 74 should have been greater than the SEO estimates.

The outlying heads at location 173, however, were most likely exclusively due to poor pumping estimates (figure 60). The four head observations which lie below the $-2\sigma_h$ line were taken during the time interval 1965 to 1970. This is the same time period that model heads increased due to a decrease in the SEO pumping estimates (figures 60 and 15). The observed head data did not support the decrease in pumping estimated by the SEO, and the decrease probably did not exist. If such were the case, the hump in the model calculated heads would have been smoothed, and consequently the $\pm 2\sigma_h$ lines would have dropped to enclose all of the observed heads.

Predicted water levels and the associated head uncertainties for run 79 are shown in figures 43 and 44 for the years 1940, 1960, 1973 and 1975. The increase in σ_h with time as the cone of depression expands is clearly evident from these figures.

Model Validation in Space

Log T Estimated. The observed head data set was divided in space by separating the long and short observation records. Measurement locations with less than 10 measurements were used to condition the log T estimates during WLS run 82, the results of which are shown in figure 64. The estimates from run 82 were then used as input to UP run 86, in which S, T and B were considered uncertain.

Measurement locations with more than 10 measurements were used to condition log T during WLS run 84, the results of which are shown in figure

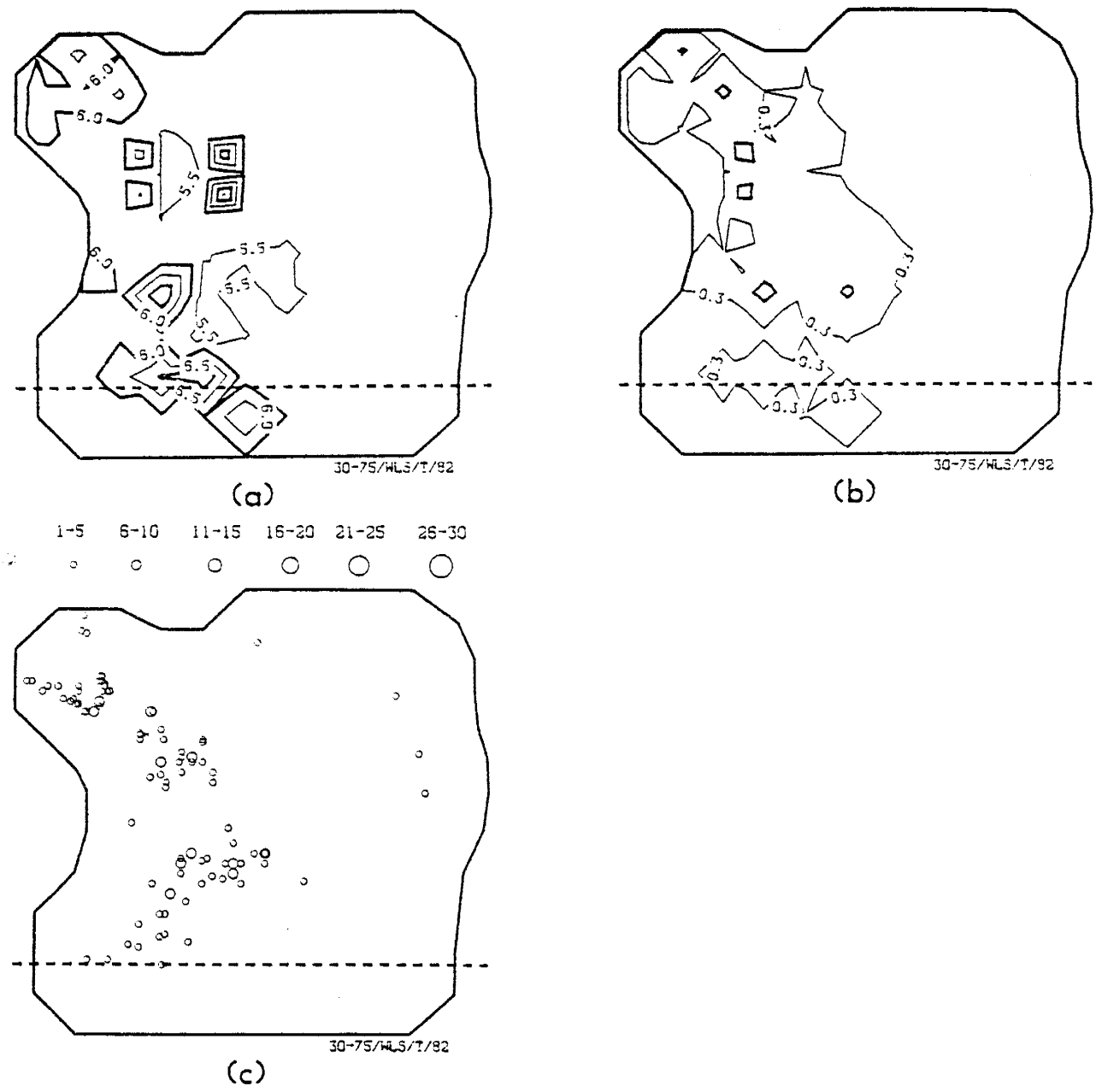

Fig. 64. Posterior log T (a) and σ_T (b) fields and location and frequency of observed head data for run 82.

65. The estimated parameters from run 84 were used as input to UP run 87, where again S, T and B were considered uncertain.

The results of runs 86 and 87 are presented in figures 66 through 76. Again the a and b sub-figures represent the "worst" and "best" fit cases respectively. Sub-figure c is output from run 86, and sub-figure d is output from run 87.

Several general comments can be made concerning figures 66 through 76. As noted in the previous section, a great deal of conditioning occured using the partial data sets, whether they consisted of locations with more or less than 10 observations. Also, as expected, model heads showed a better fit with observed heads at locations which were used to condition the log T estimates. Examples include locations 93, 103, 140, 173 and 251 (figures 68, 69, 71, 72 and 76). However, it was not uncommon for modeled heads to match well with observed heads at locations which were not used in the WLS procedure. Locations 205 and 213 (figures 73 and 74) are examples of this.

The model results at location 87 (figure 67) are interesting because the conditioned log T estimates produced a worse fit between computed and observed heads than did the prior (mean) log T values. The log T parameter estimates in the vicinity of location 87 must have been affected by additional nearby head measurements which forced the log T values away from the mean value. This example reinforces the fact that WLS parameter estimates will not necessarily produce an optimal fit at any one location in an area, but an optimal fit may be obtained for multiple locations in a region.

At location 132 (figure 70), the estimated heads did not change with conditioning. At this location the post log T estimates remained very close to their priors. This indicated that the sensitivities of heads to

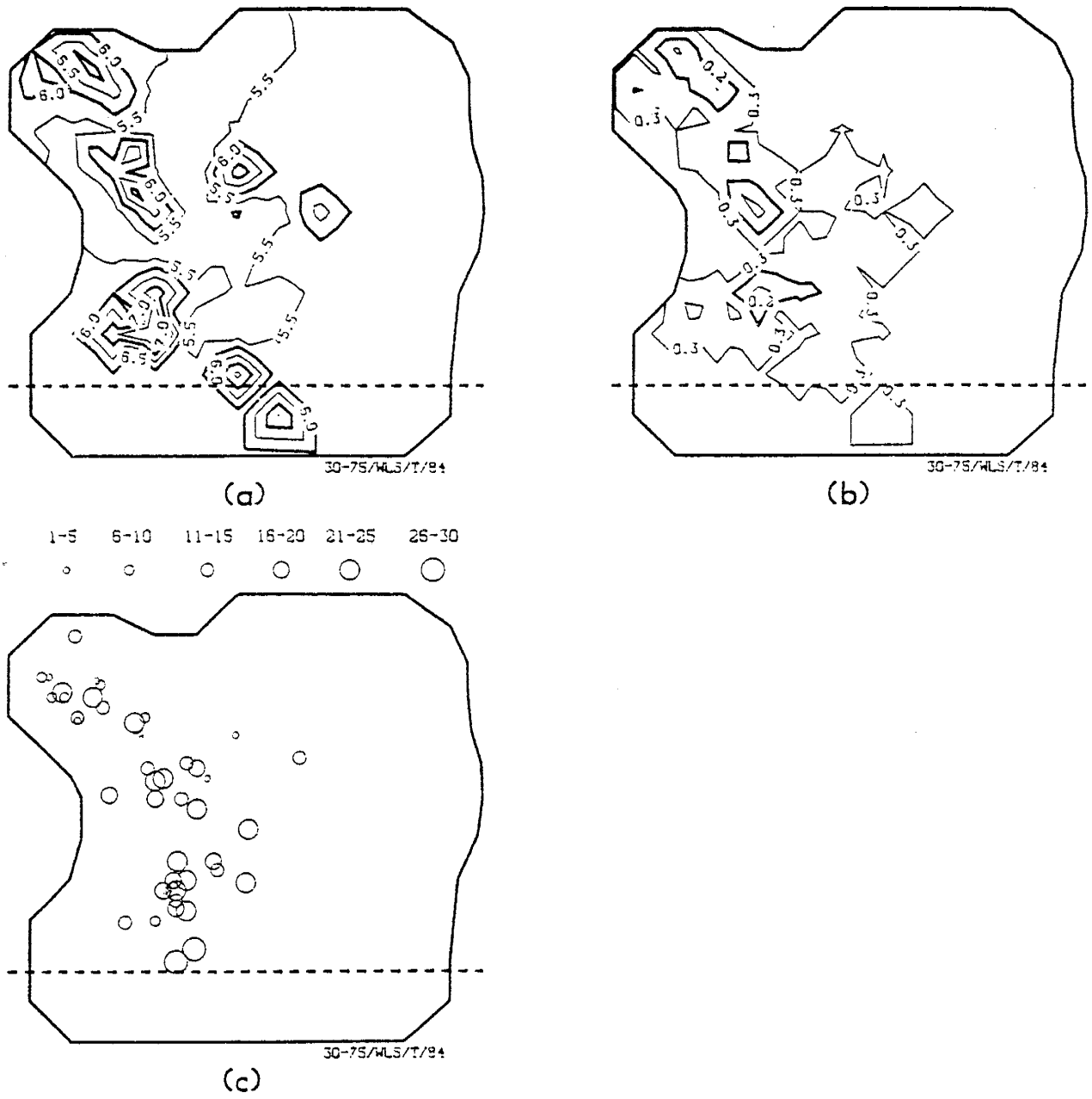

Fig. 65. Posterior log T (a) and σ_T (b) fields and location and frequency of observed head data for run 84.

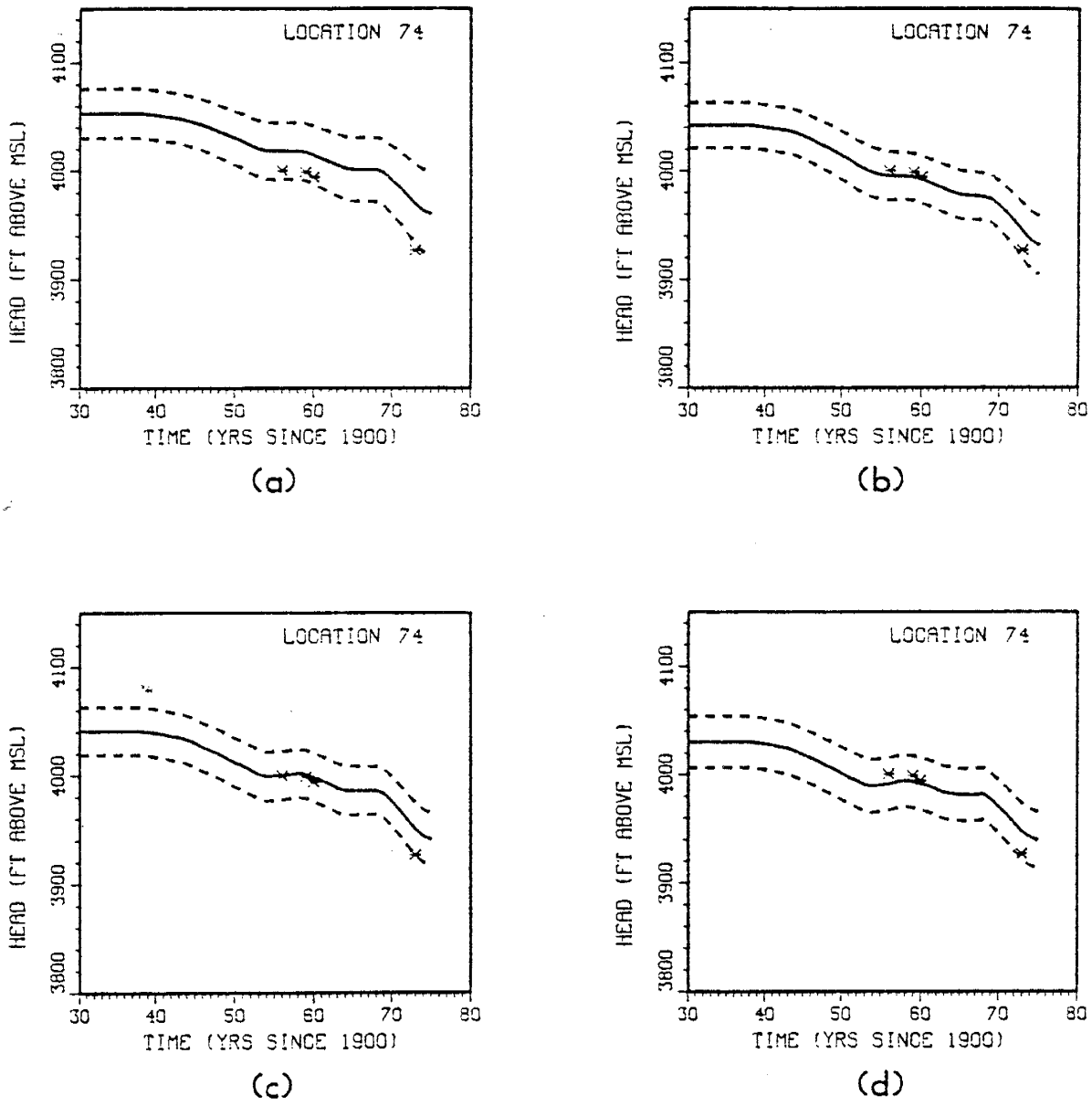

Fig. 66. Model heads (solid line), observed heads (asterisks) and $\pm 2\sigma_h$ bounds (dashed lines) at measurement location 74 for runs 88 (a), 93 (b), 86 (c) and 87 (d).

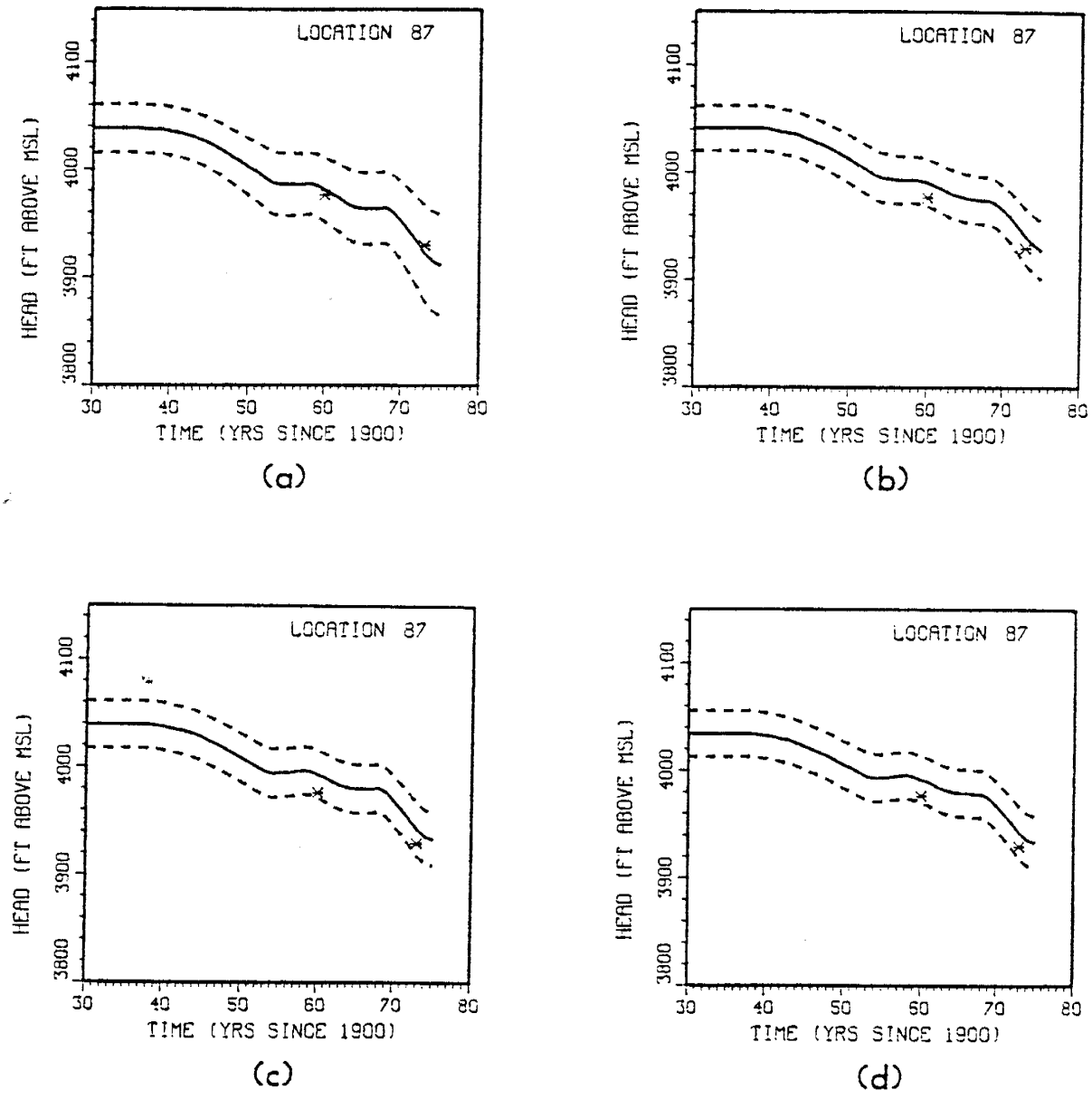

Fig. 67. Model heads (solid line), observed heads (asterisks) and $\pm 2\sigma_h$ bounds (dashed lines) at measurement location 87 for runs 88 (a), 93 (b), 86 (c) and 87 (d).

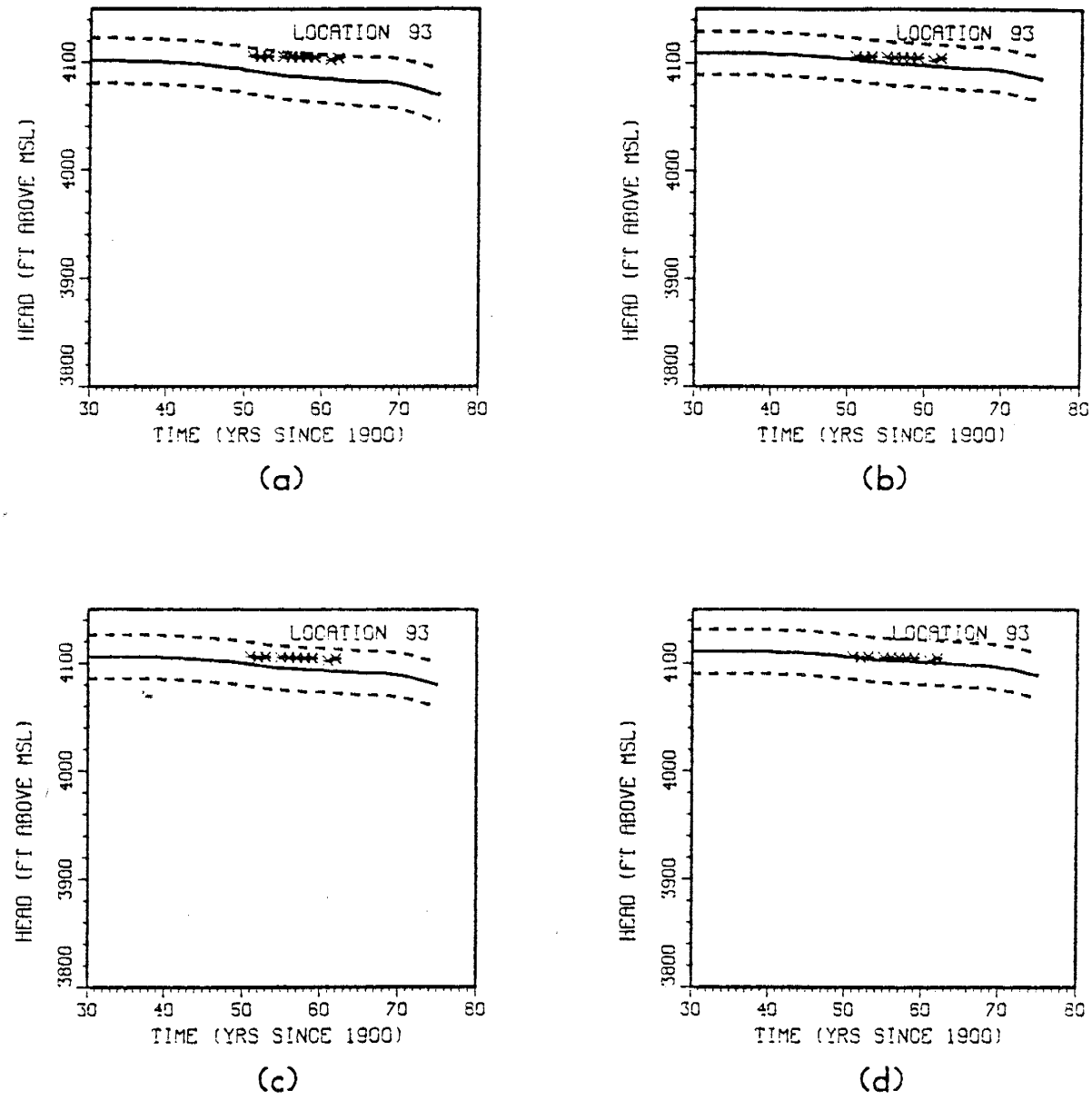

Fig. 68. Model heads (solid line), observed heads (asterisks) and $\pm 2\sigma_h$ bounds (dashed lines) at measurement location 93 for runs 88 (a), 93 (b), 86 (c) and 87 (d).

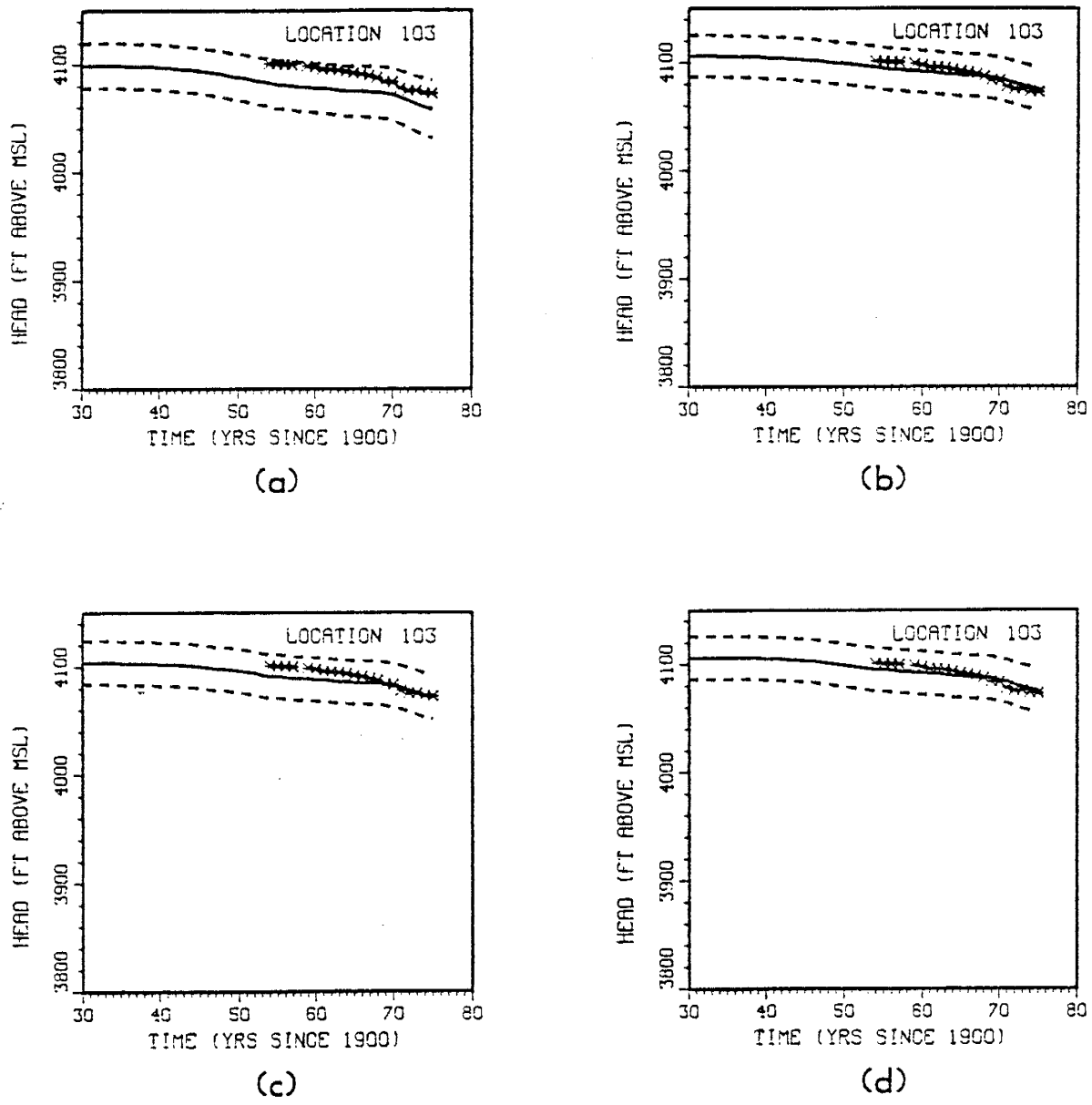

Fig. 69. Model heads (solid line), observed heads (asterisks) and $\pm 2\sigma_h$ bounds (dashed lines) at measurement location 103 for runs 88 (a), 93 (b), 86 (c) and 87 (d).

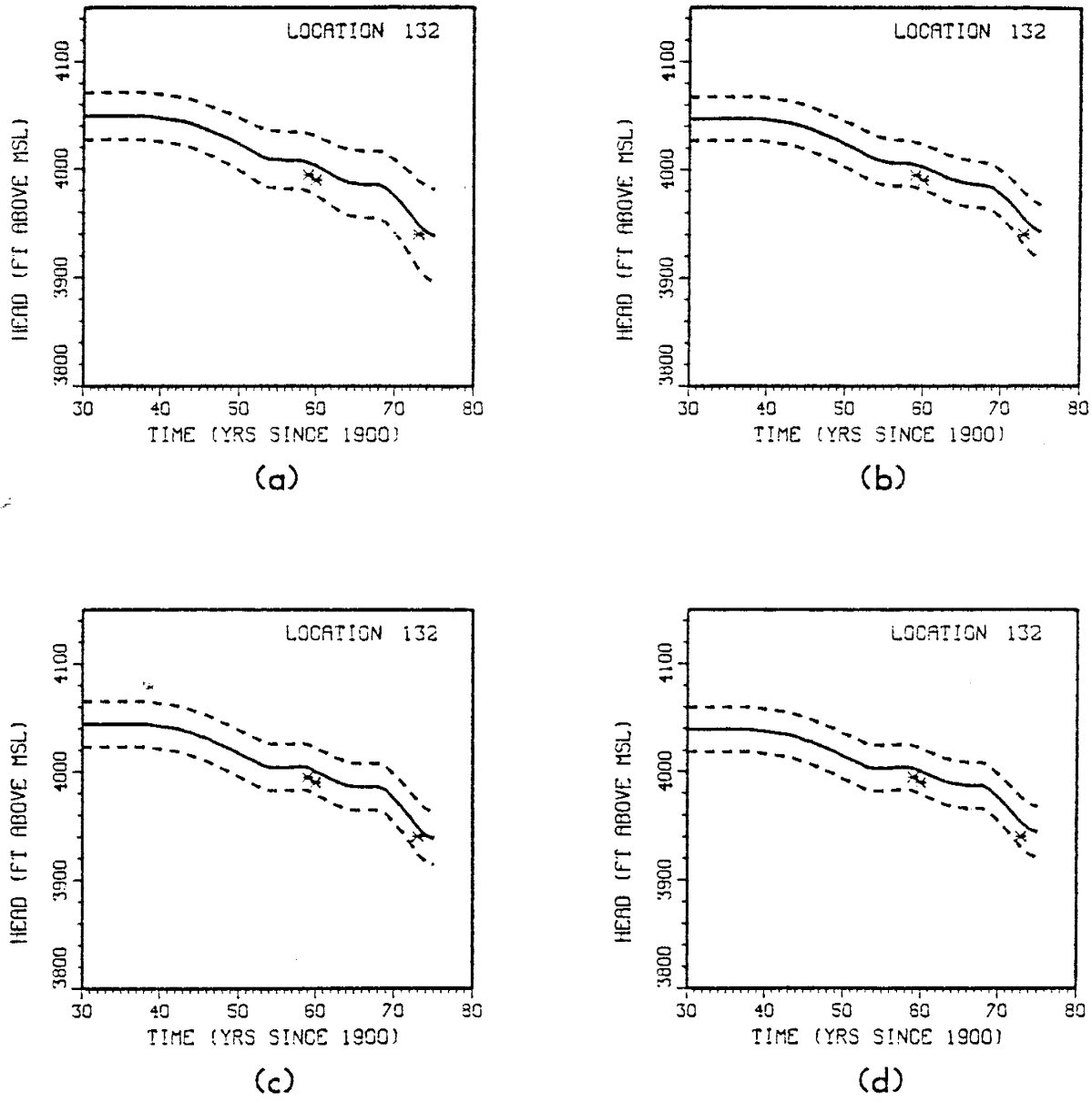

Fig. 70. Model heads (solid line), observed heads (asterisks) and $\pm 2\sigma_h$ bounds (dashed lines) at measurement location 132 for runs 88 (a), 93 (b), 86 (c) and 87 (d).

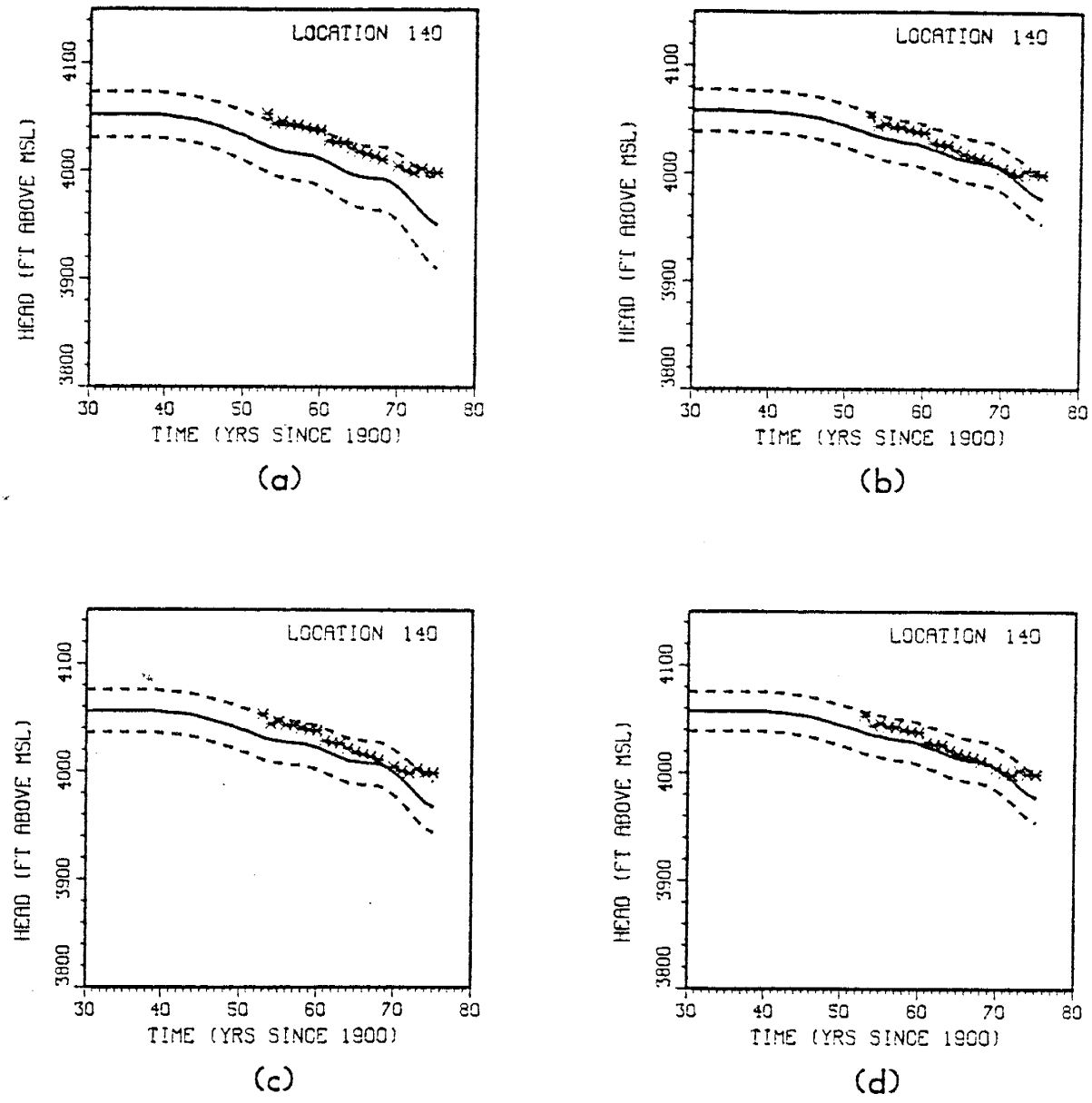

Fig. 71. Model heads (solid line), observed heads (asterisks) and $\pm 2\sigma_h$ bounds (dashed lines) at measurement location 140 for runs 88 (a), 93 (b), 86 (c) and 87 (d).

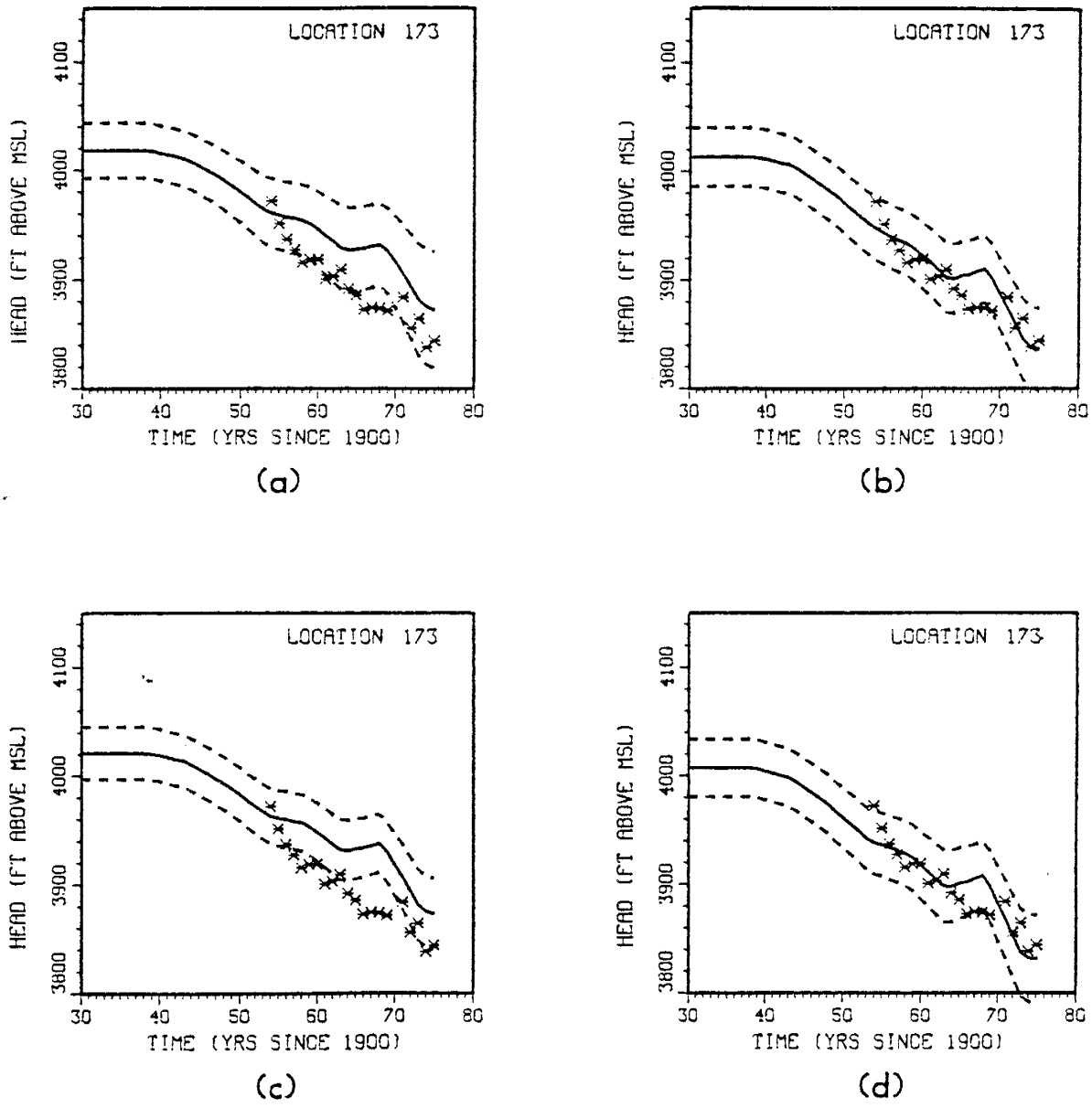

Fig. 72. Model heads (solid line), observed heads (asterisks) and $\pm 2\sigma_h$ bounds (dashed lines) at measurement location 173 for runs 88 (a), 93 (b), 86 (c) and 87 (d).

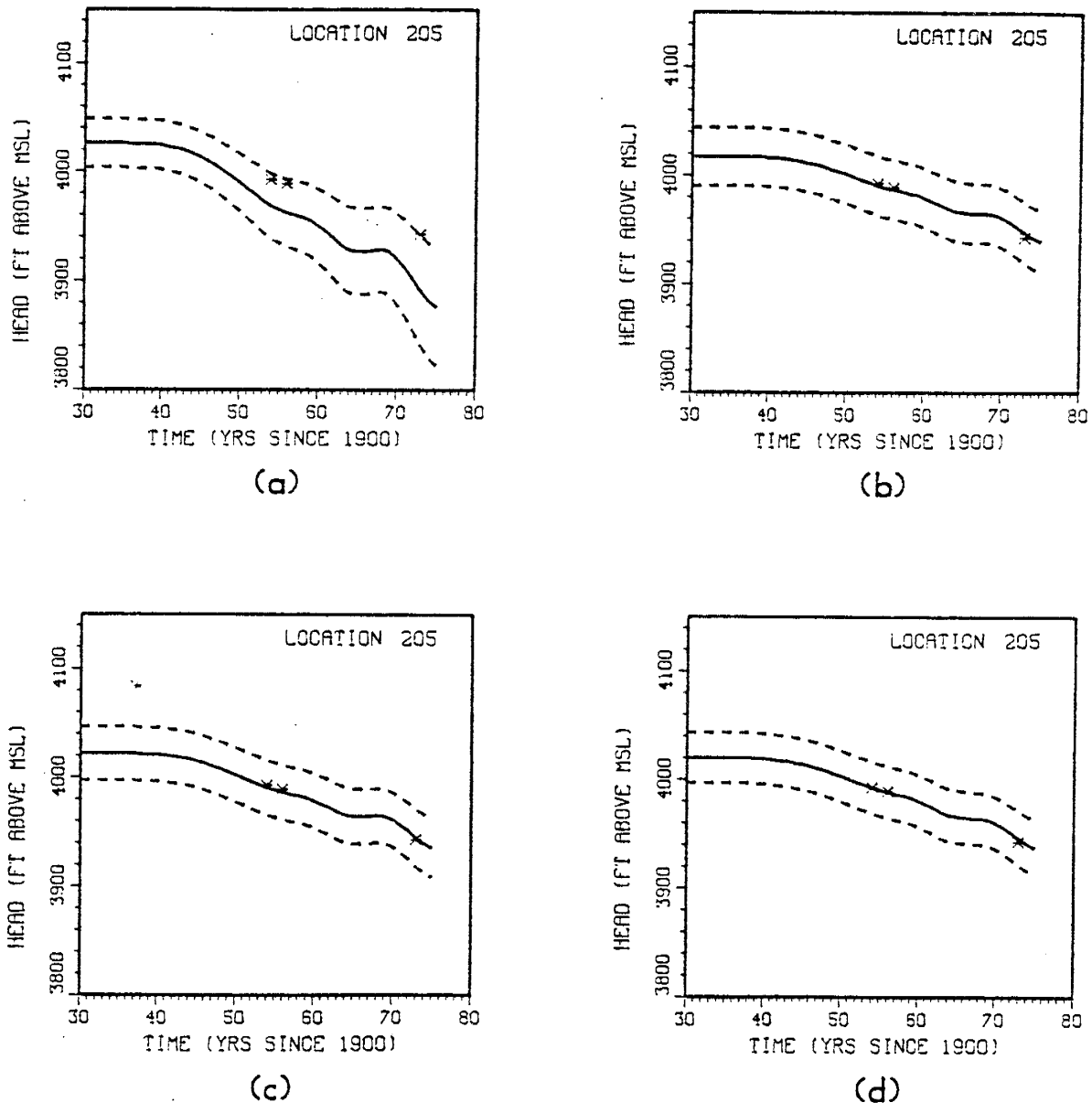

Fig. 73. Model heads (solid line), observed heads (asterisks) and $\pm 2\sigma_h$ bounds (dashed lines) at measurement location 205 for runs 88 (a), 93 (b), 86 (c) and 87 (d).

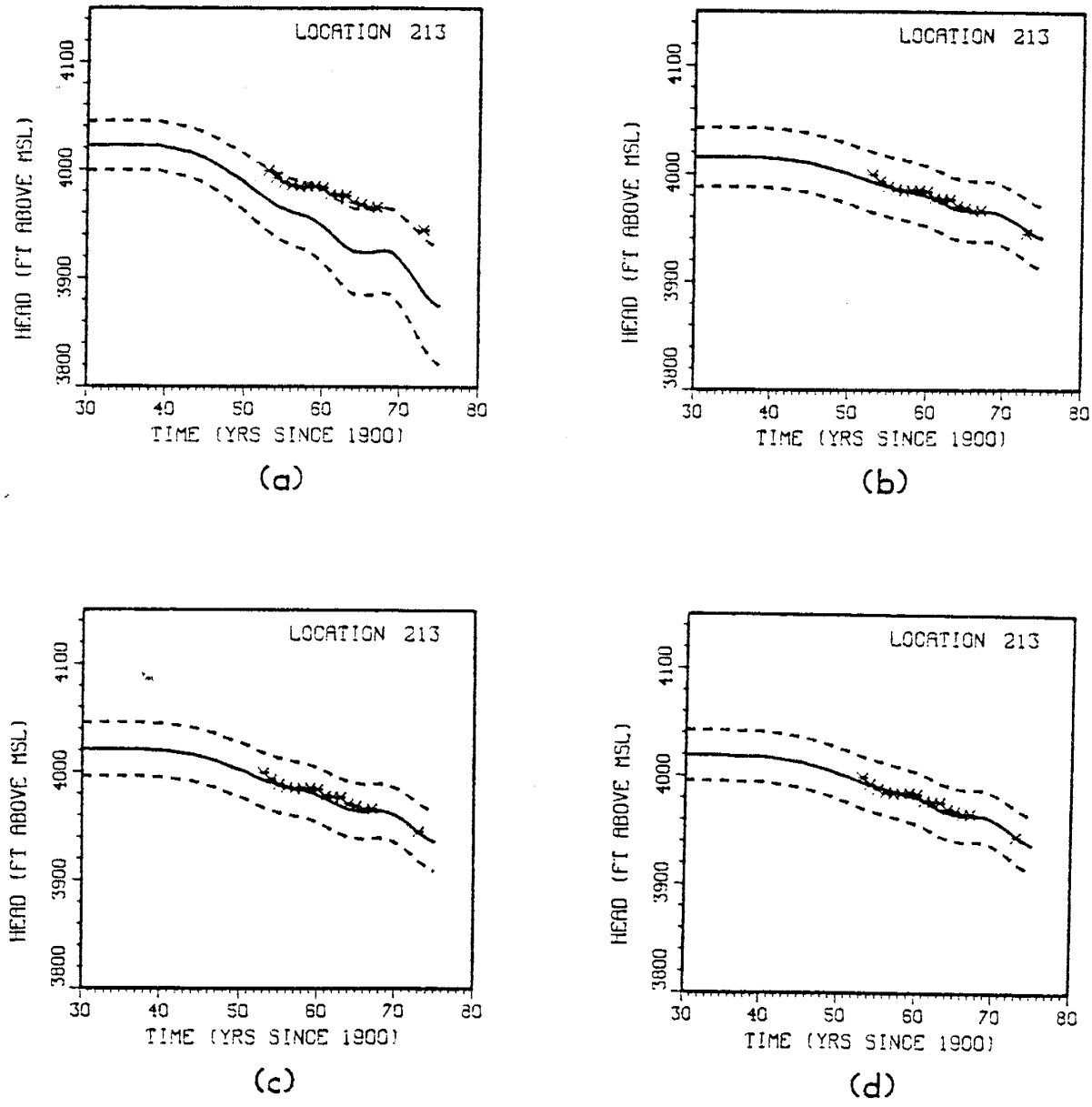

Fig. 74. Model heads (solid line), observed heads (asterisks) and $\pm 2\sigma_h$ bounds (dashed lines) at measurement location 213 for runs 88 (a), 93 (b), 86 (c) and 87 (d).

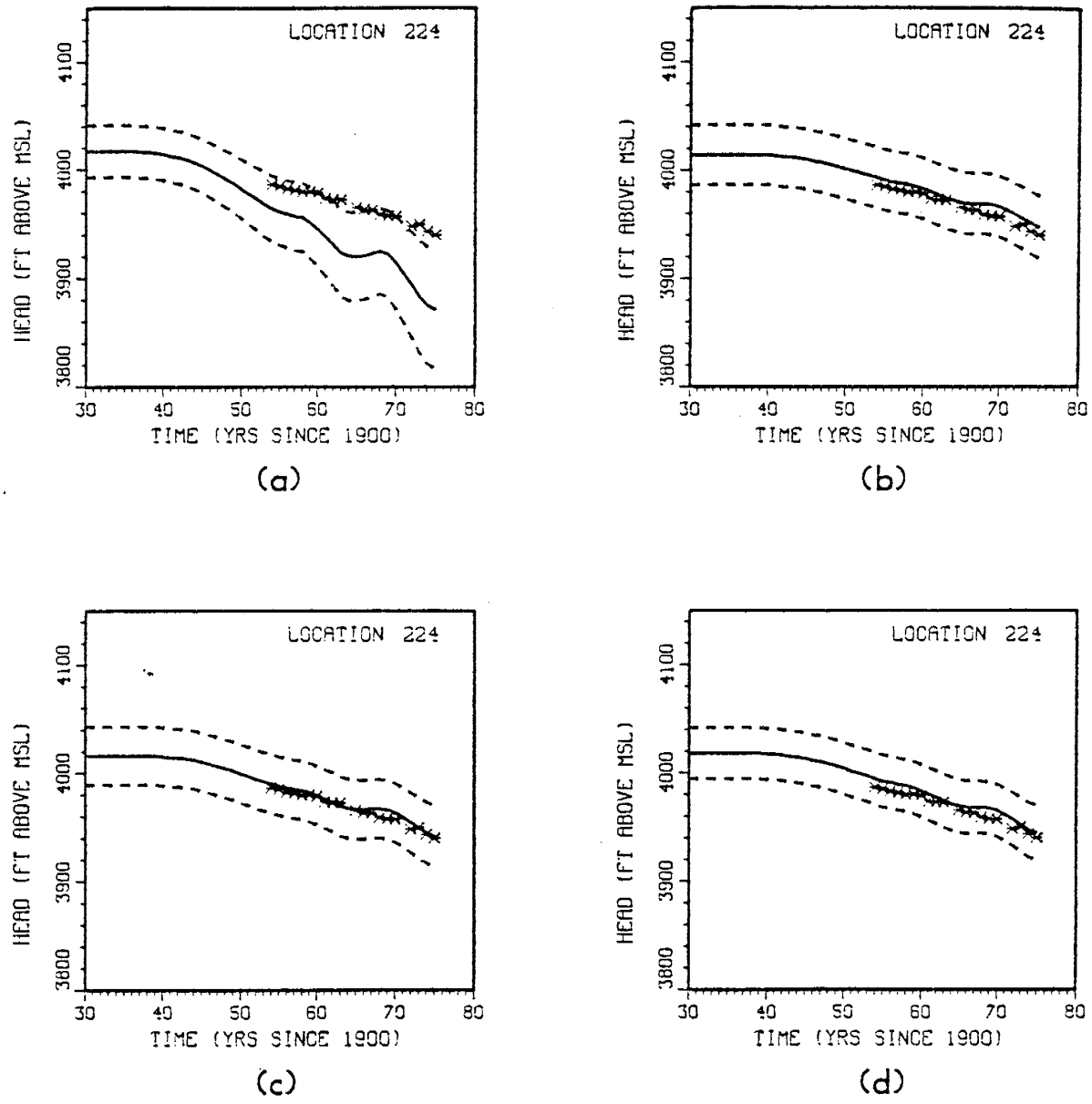

Fig. 75. Model heads (solid line), observed heads (asterisks) and $\pm 2\sigma_h$ bounds (dashed lines) at measurement location 224 for runs 88 (a), 93 (b), 86 (c) and 87 (d).

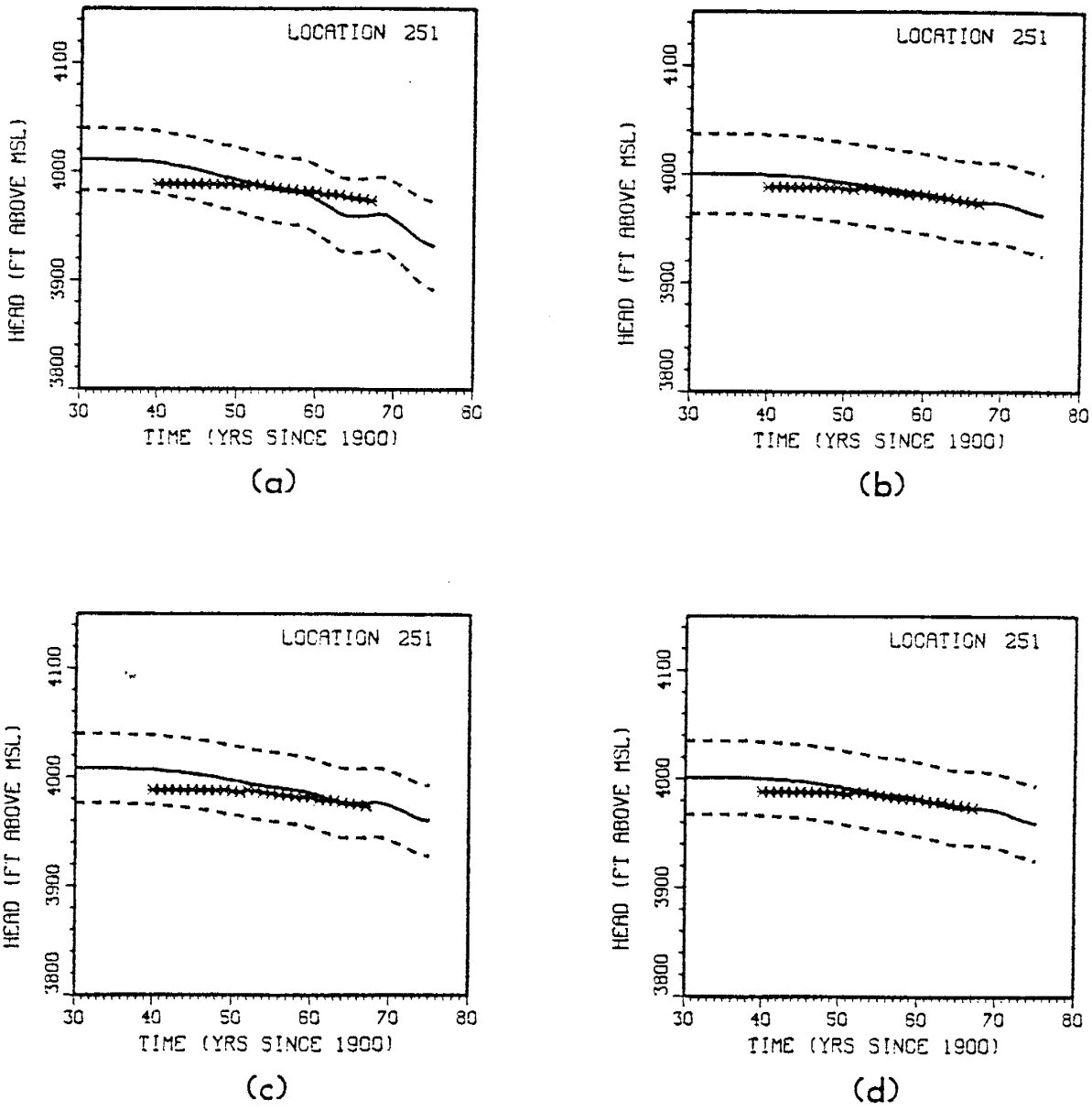

Fig. 76. Model heads (solid line), observed heads (asterisks) and $\pm 2\sigma_h$ bounds (dashed lines) at measurement location 251 for runs 88 (a), 93 (b), 86 (c) and 87 (d).

parameters in this area were small, and consequently little change in the parameters occurred during the WLS process.

Location 173 (figure 72) again shows that a major trend was missed within the cone of depression, even when the actual observations at this location were used to condition the log T estimates (figure 72d). This created even more suspicion that the mismatch could only be amended through adjustment of the pumping record.

At two locations observed heads plotted outside the calculated $\pm 2\sigma$ lines. In each instance (figures 71c and 72c) the log T parameters were not conditioned on that particular measurement location.

The model calculated head fields and the associated σ_h fields for the times 1940, 1960, 1973 and 1975 for runs 86 and 87 are shown in figures 77 through 80.

Log T and B Estimated. For the model validation in space it was logical to estimate the B (pumping) parameters as well as the log T values. WLS run 83 estimated log T and B using measurement locations with less than 10 measurements (figure 55c), and WLS run 85 estimated log T and B parameters conditioned on measurement locations with more than 10 measurements (figure 65c). The posterior log T and σ_T fields for runs 83 and 85 are shown in figure 81.

The estimated B values at four pumping nodes for runs 83 and 85 are shown in figures 82 and 83 respectively. Comparing these figures to figures 31 and 49, it is obvious that the head record used to condition the pumping estimates may significantly effect the final parameter values. The general character of the posterior estimates is, however, at many times quite similar.

UP runs 94 and 95 used as input the results from WLS runs 83 and 85 respectively. The results of these UP runs are shown in figures 84 through

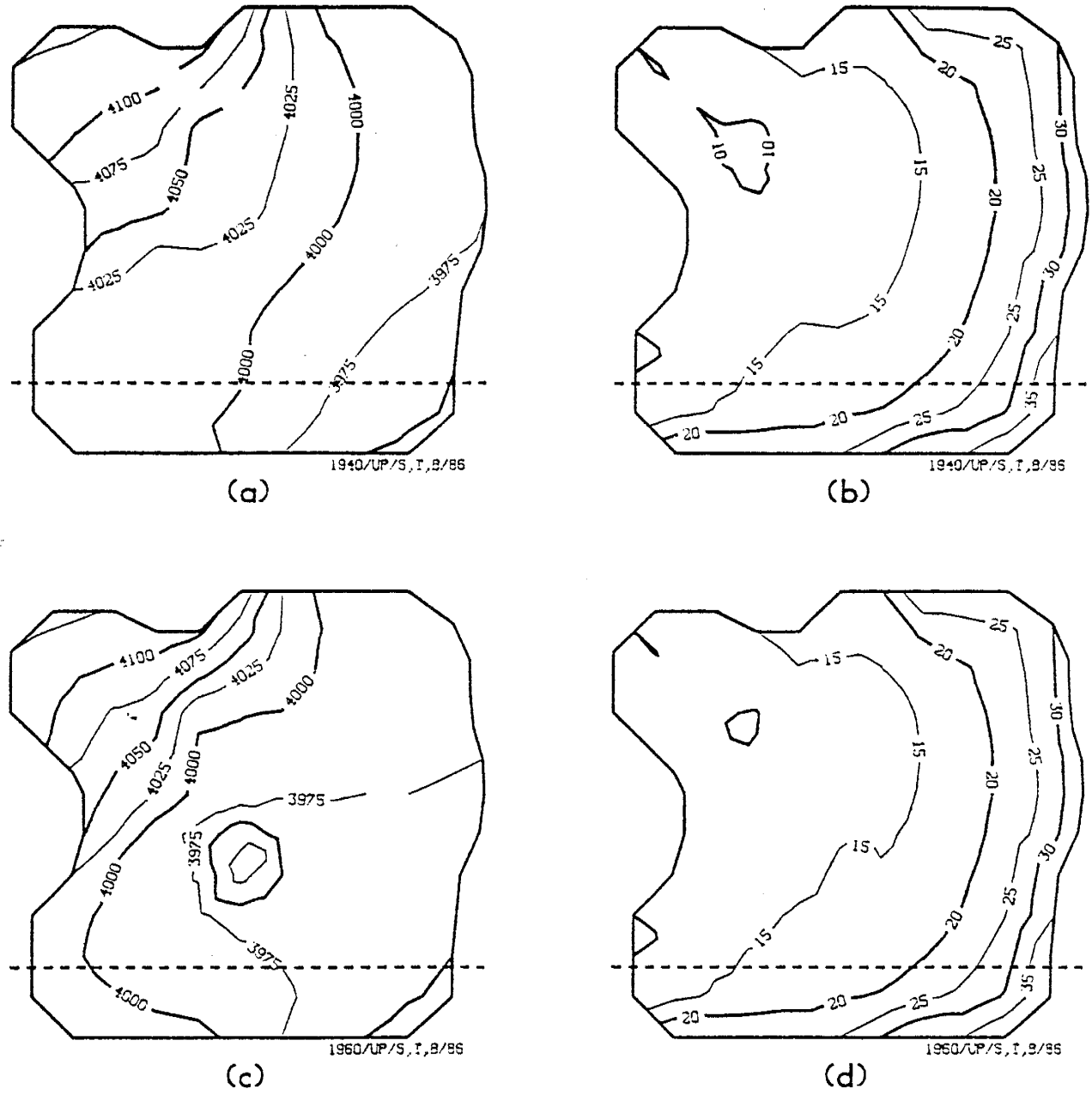

Fig. 77. Head fields (ft above MSL) and associated σ_h fields (ft) for run 86 for 1940 (a and b) and 1960 (c and d).

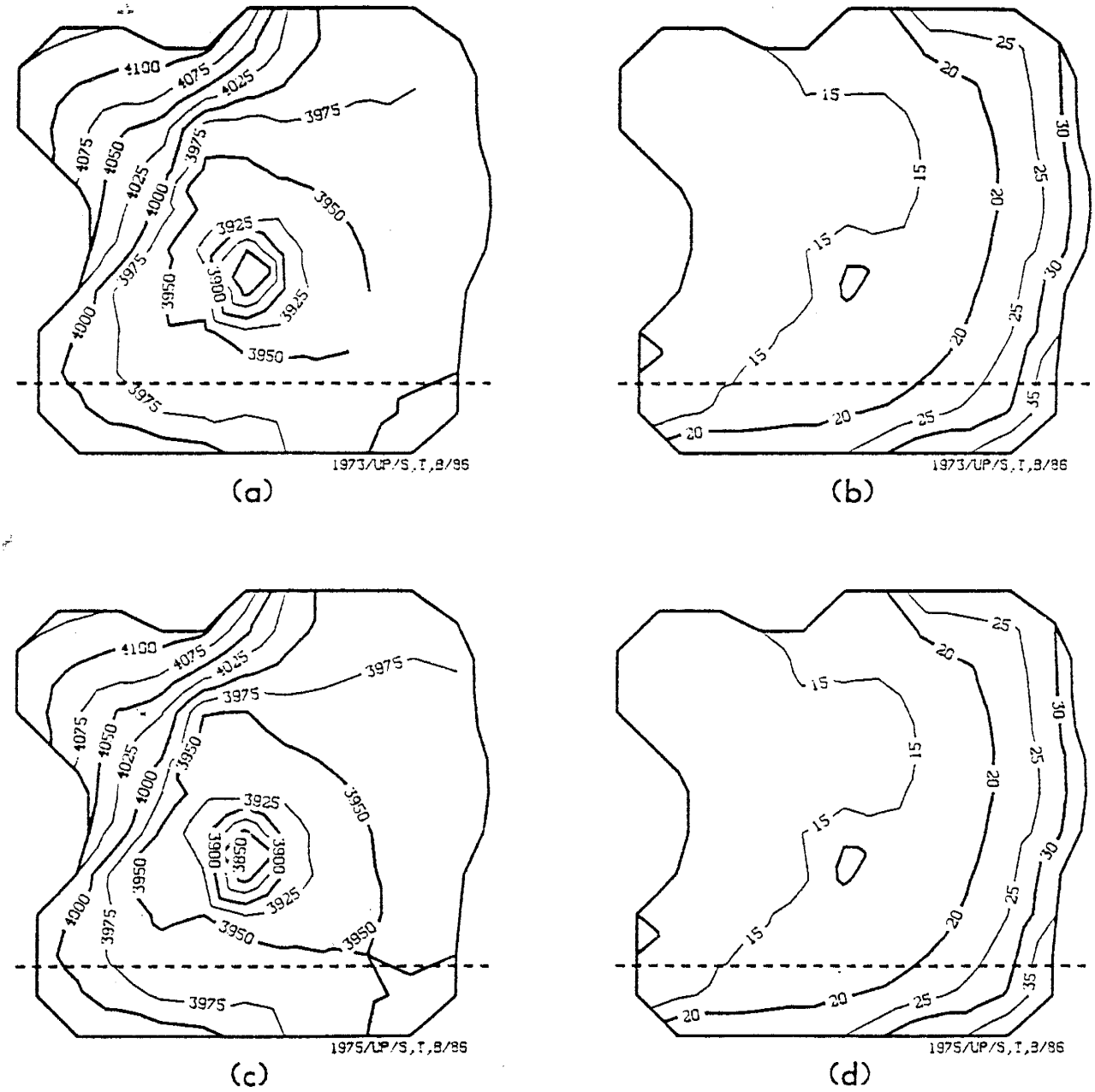

Fig. 78. Head fields (ft above MSL) and associated σ_h fields (ft) for run 86 for 1973 (a and b) and 1975 (c and d).

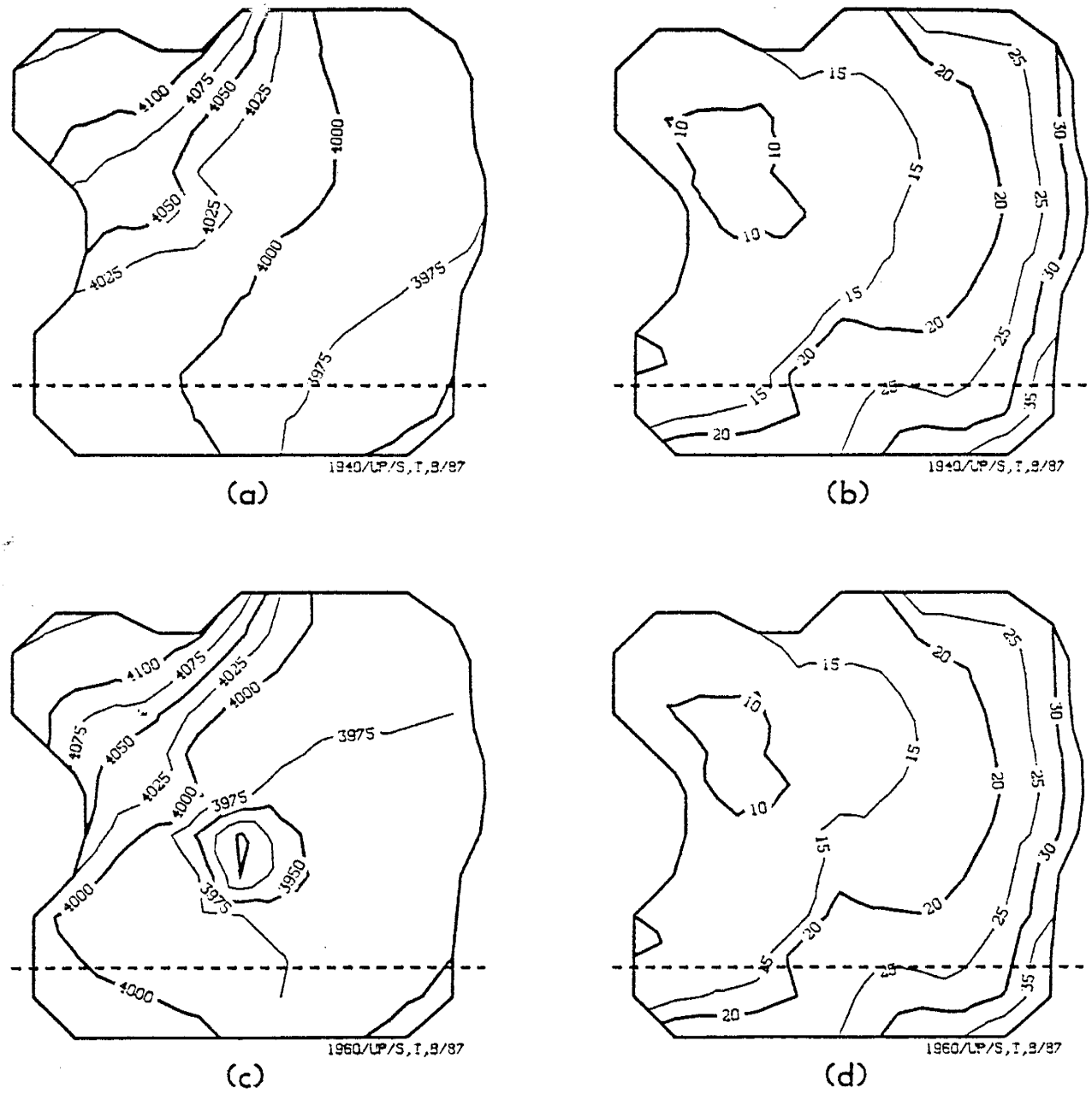

Fig. 79. Head fields (ft above MSL) and associated σ_h fields (ft) for run 87 for 1940 (a and b) and 1960 (c and d).

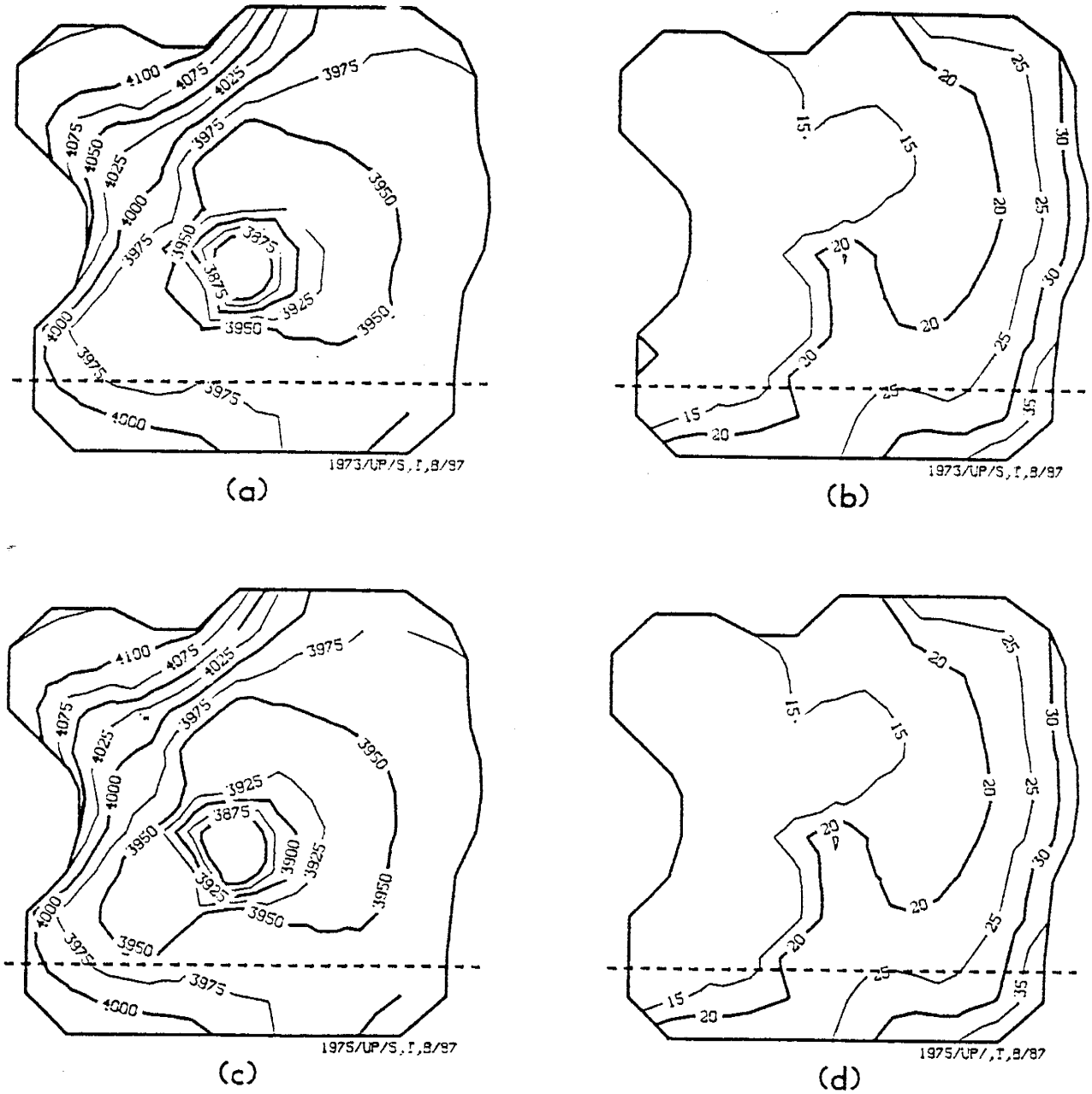

Fig. 80. Head fields (ft above MSL) and associated σ_h fields (ft) for run 87 for 1973 (a and b) and 1975 (c and d).

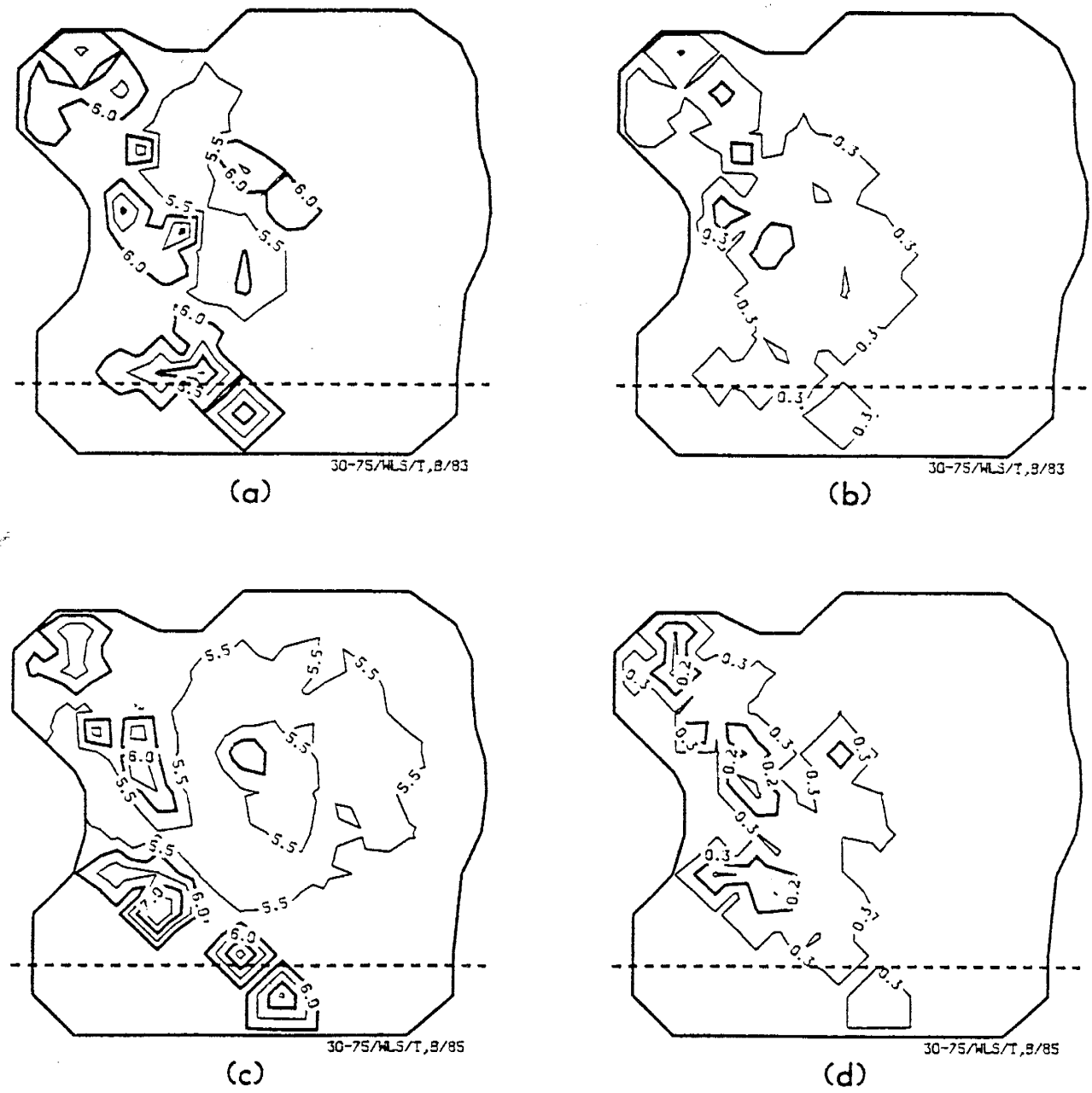

Fig. 81. Posterior log T and σ_T fields for run 83 (a and b) and run 85 (c and d).

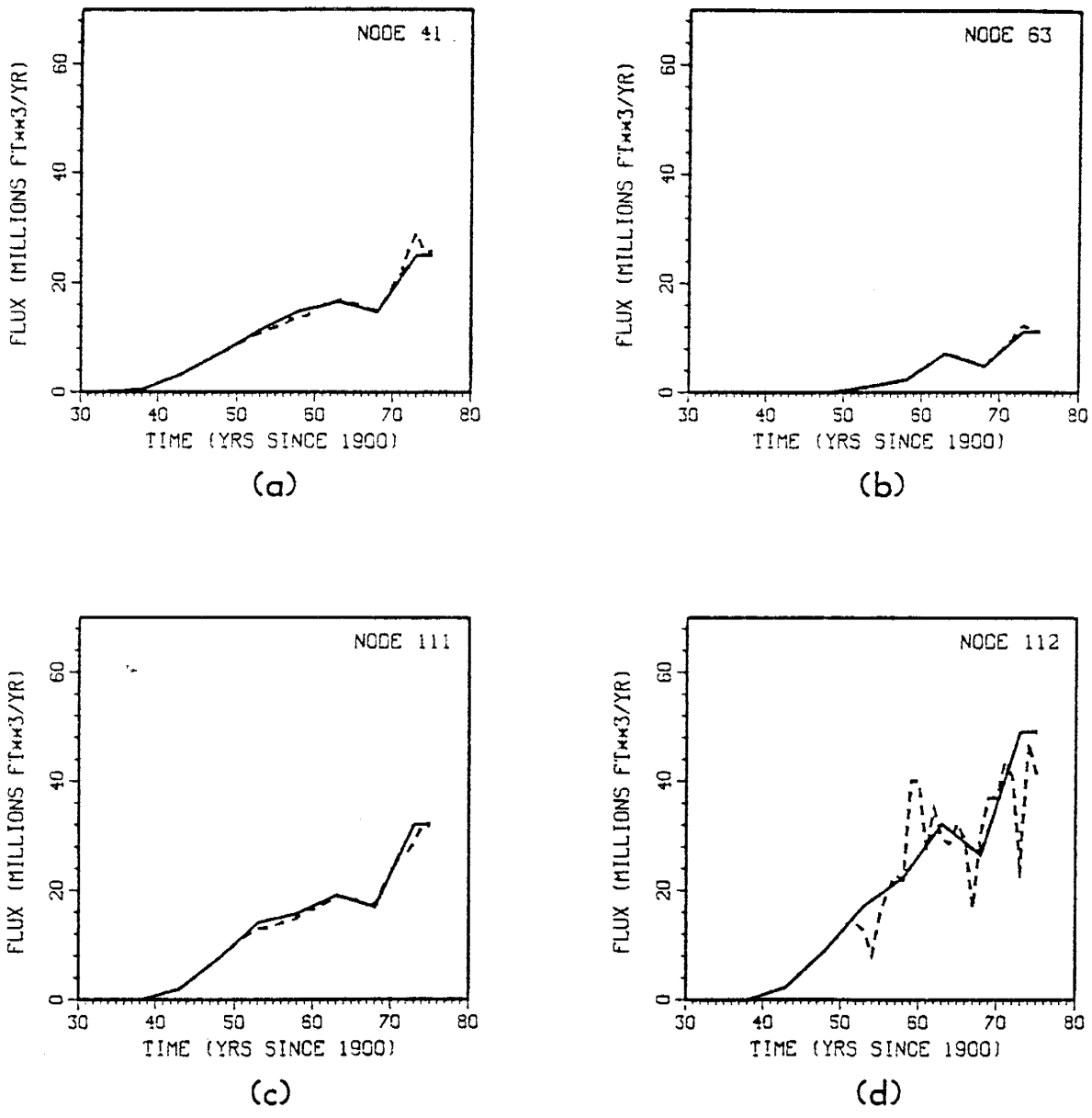

Fig. 82. Prior (solid) and post (dashed) pumping estimates at four nodes for run 83.

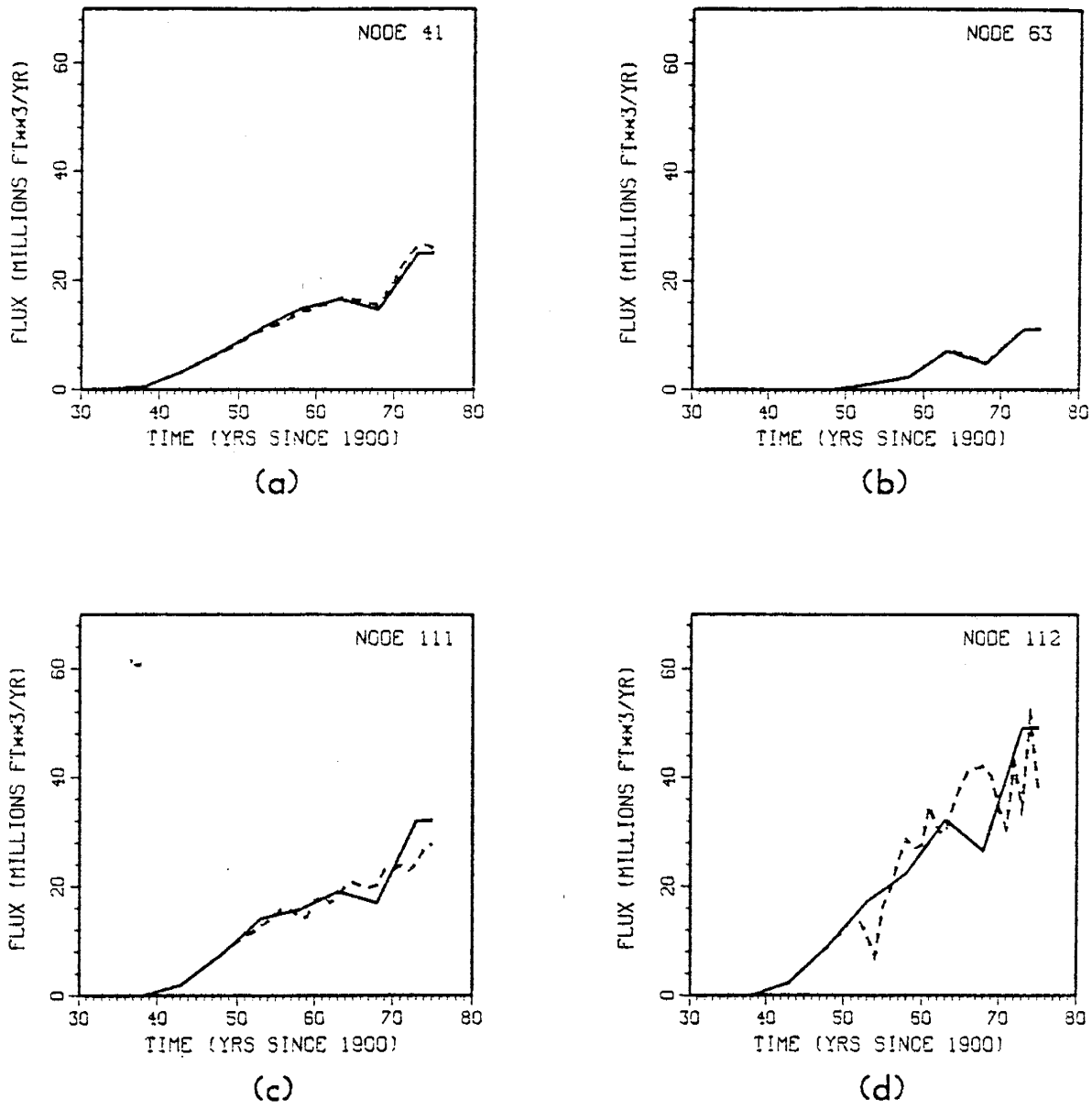

Fig. 83. Prior (solid) and post (dashed) pumping estimates at four nodes for run 85.

94 for 11 measurement locations. As before the a and b sub-figures represent the worst and best fit cases respectively, while the c and d sub-figures represent the output from UP runs 94 and 95 respectively.

The predicted heads and observed heads match very well for this set of runs. In only two cases observed heads fall outside the $\pm 2\sigma_h$ lines (figures 84d and 90c). In both of these instances, the measured heads which fell outside the certainty bounds were not used during the WLS parameter estimation.

The drawdown trend at location 173 was simulated much better than was possible for the validation runs where log T was the only estimated parameter. The drawdown trend was still missed somewhat during run 83, but this run did not use estimated log T and B values conditioned on this measurement location.

The 1940, 1960, 1973 and 1975 simulated head fields and σ_h fields for runs 94 and 95 are shown in figures 95 through 98.

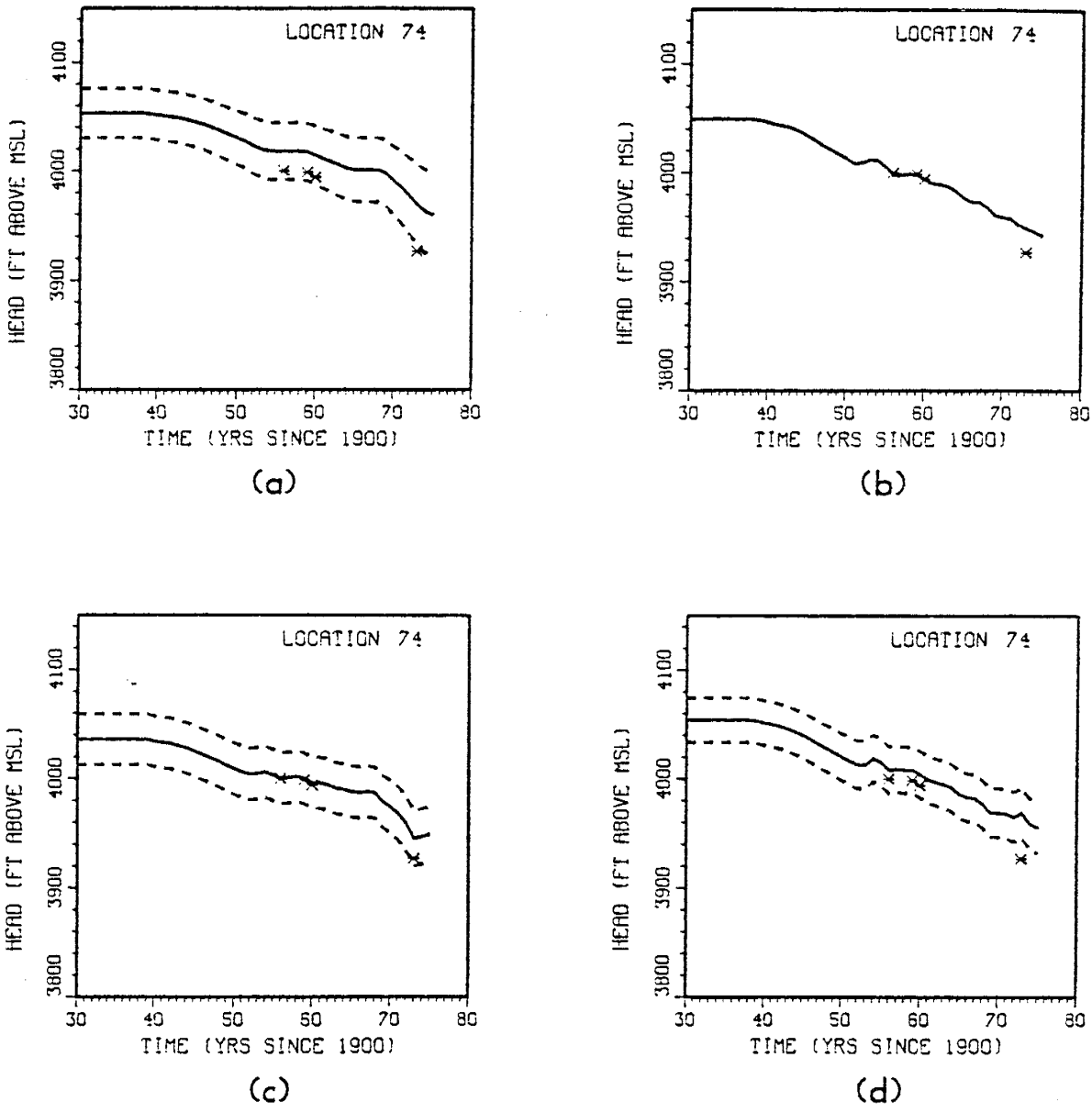

Fig. 84. Model heads (solid line), observed heads (asterisks) and $\pm 2\sigma_h$ bounds (dashed lines) at measurement location 74 for runs 88 (a), 89 (b), 94 (c) and 95 (d).

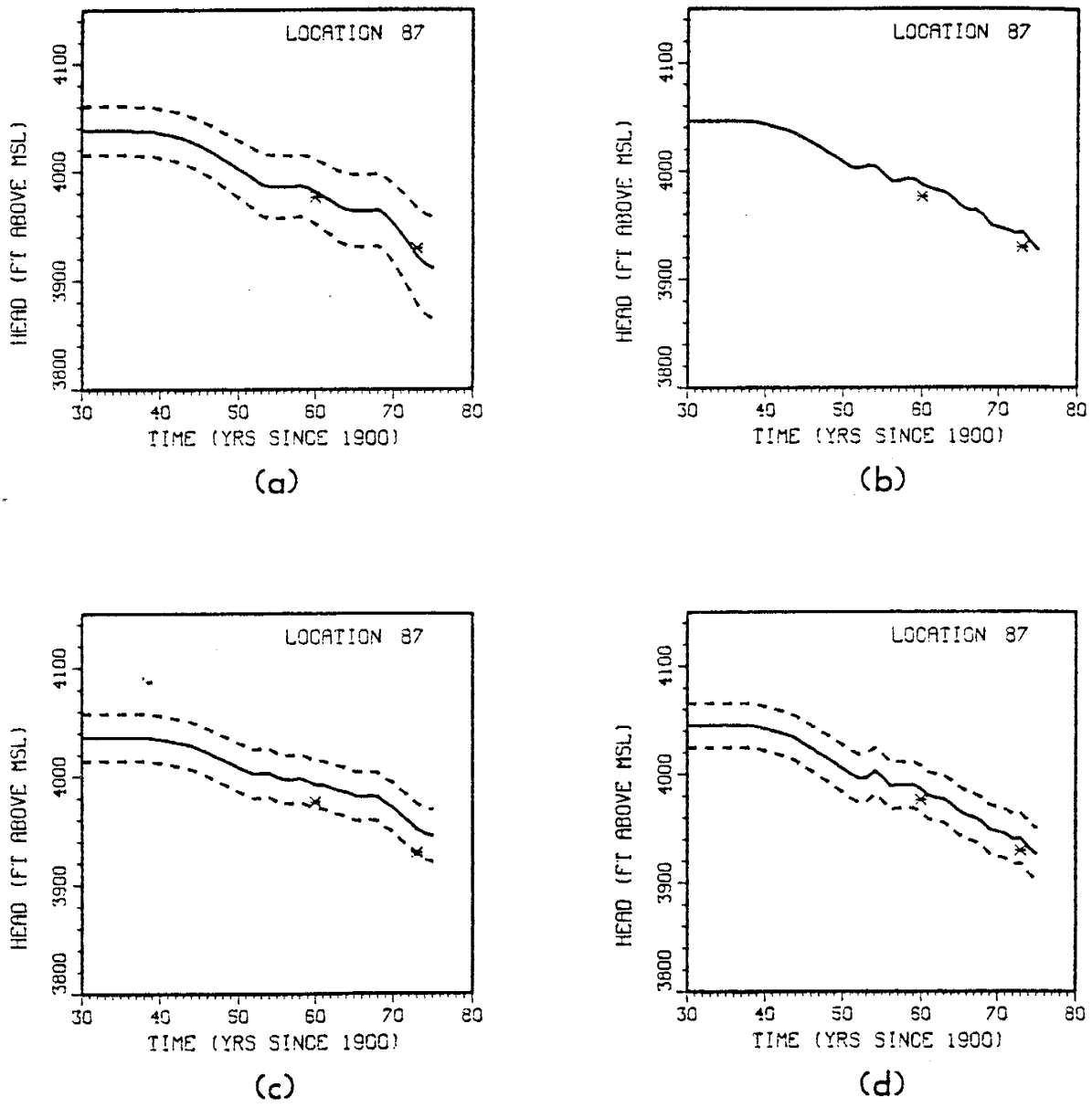

Fig. 85. Model heads (solid line), observed heads (asterisks) and $\pm 2\sigma_h$ bounds (dashed lines) at measurement location 87 for runs 88 (a), 89 (b), 94 (c) and 95 (d).

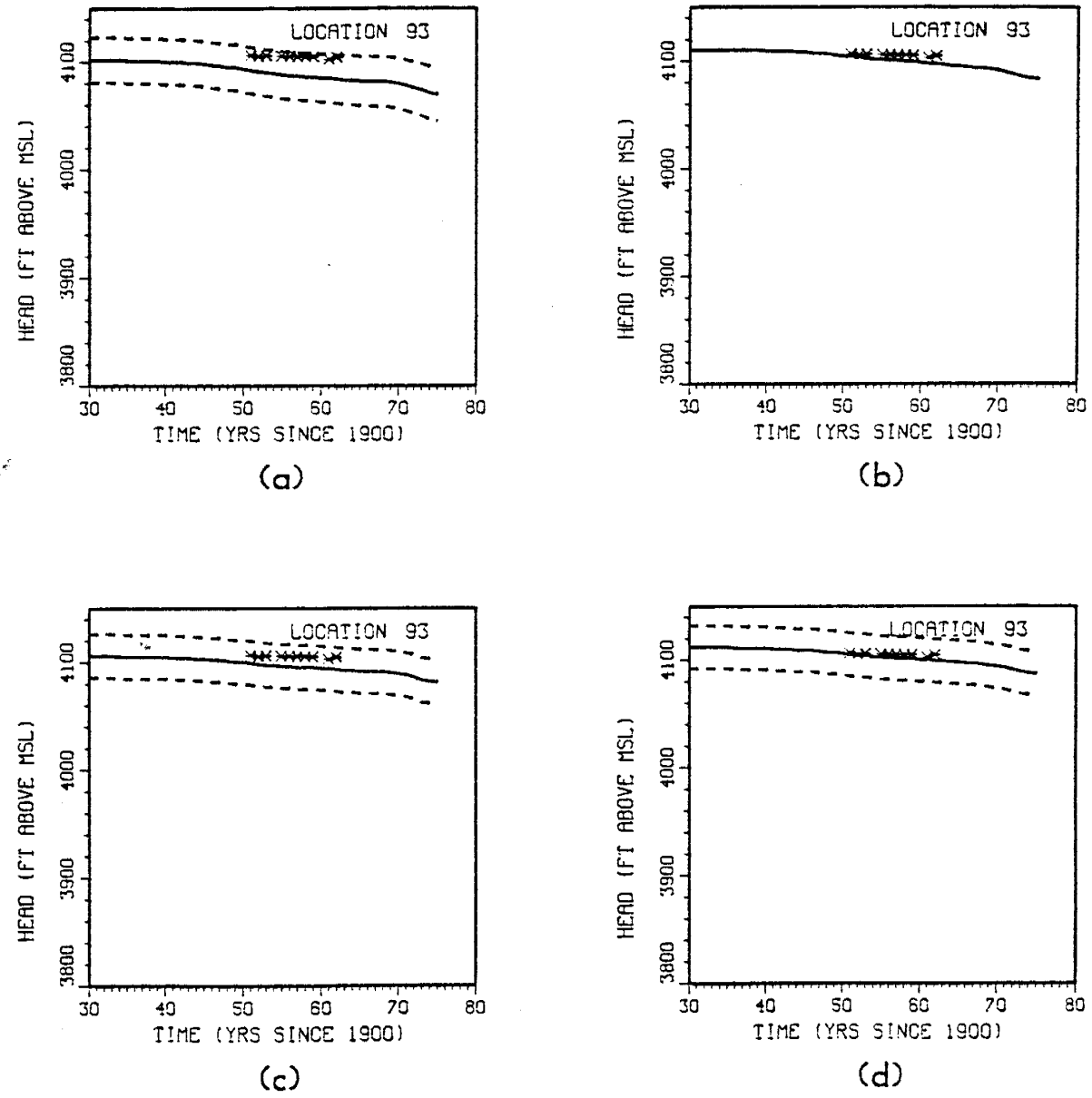

Fig. 86. Model heads (solid line), observed heads (asterisks) and $\pm 2\sigma_h$ bounds (dashed lines) at measurement location 93 for runs 88 (a), 89 (b), 94 (c) and 95 (d).

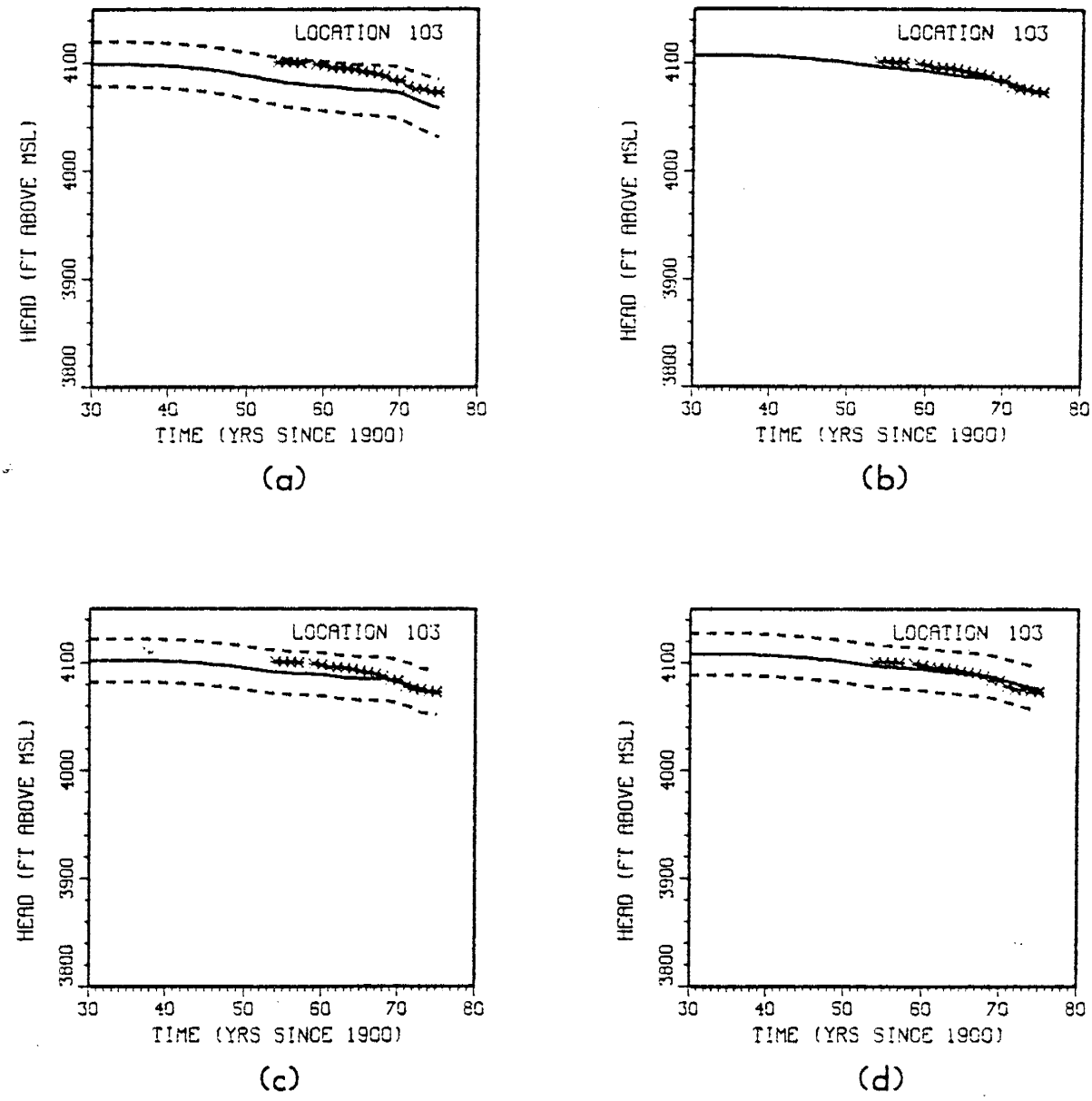

Fig. 87. Model heads (solid line), observed heads (asterisks) and $\pm 2\sigma_h$ bounds (dashed lines) at measurement location 103 for runs 88 (a), 89 (b), 94 (c) and 95 (d).

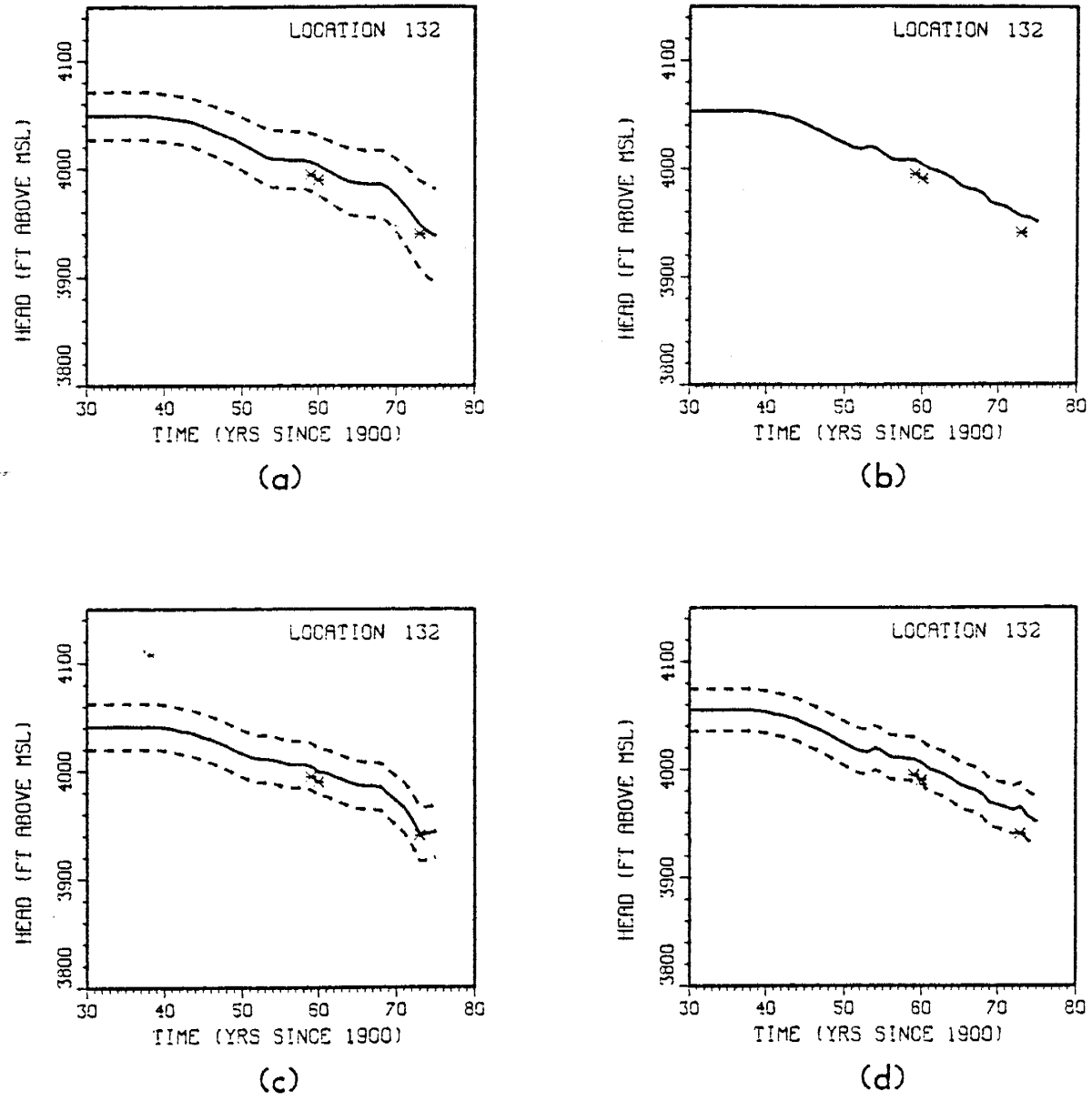

Fig. 88. Model heads (solid line), observed heads (asterisks) and $\pm 2\sigma_h$ bounds (dashed lines) at measurement location 132 for runs 88 (a), 89 (b), 94 (c) and 95 (d).

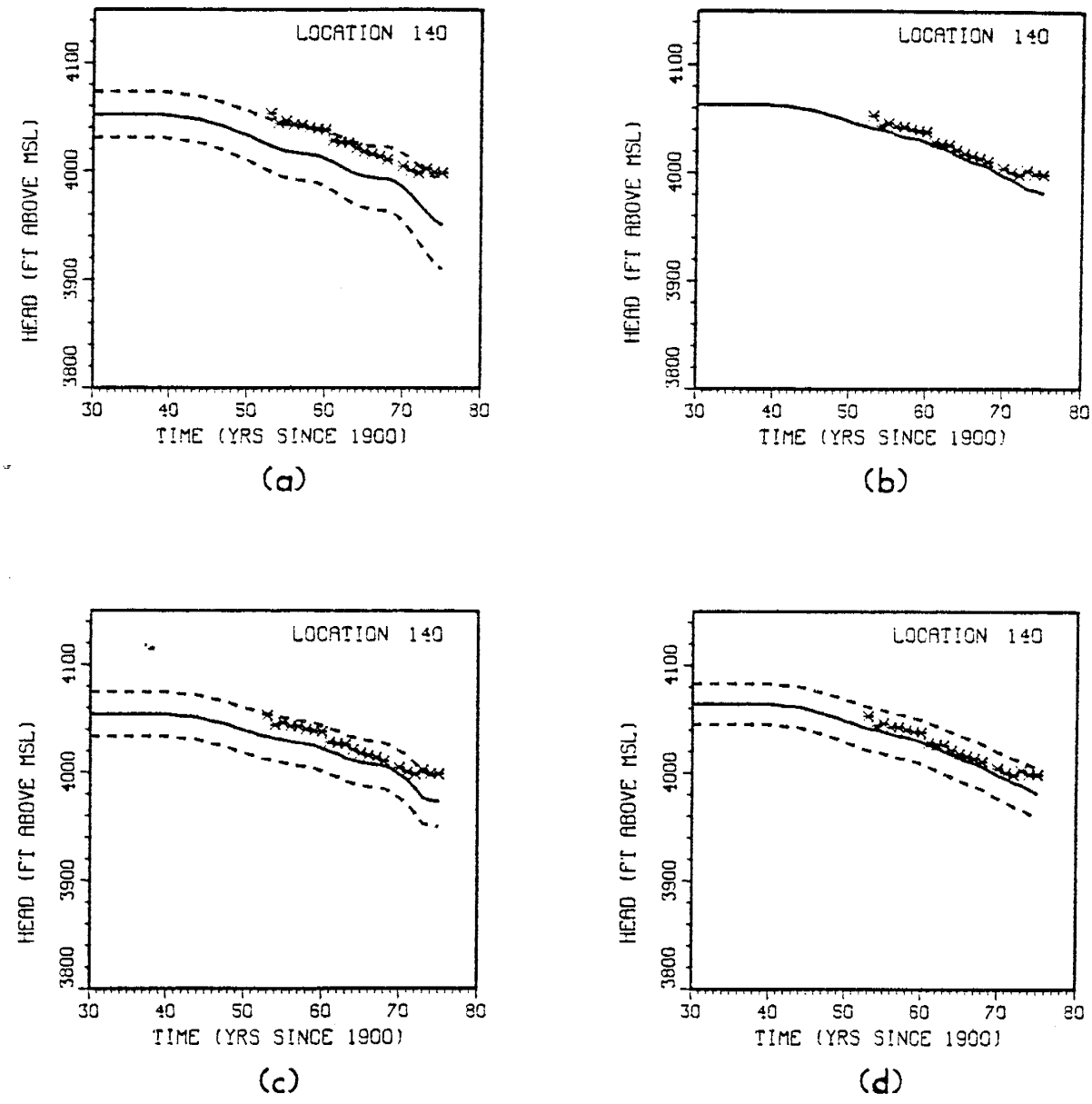

Fig. 89. Model heads (solid line), observed heads (asterisks) and $\pm 2\sigma_h$ bounds (dashed lines) at measurement location 140 for runs 88 (a), 89 (b), 94 (c) and 95 (d).

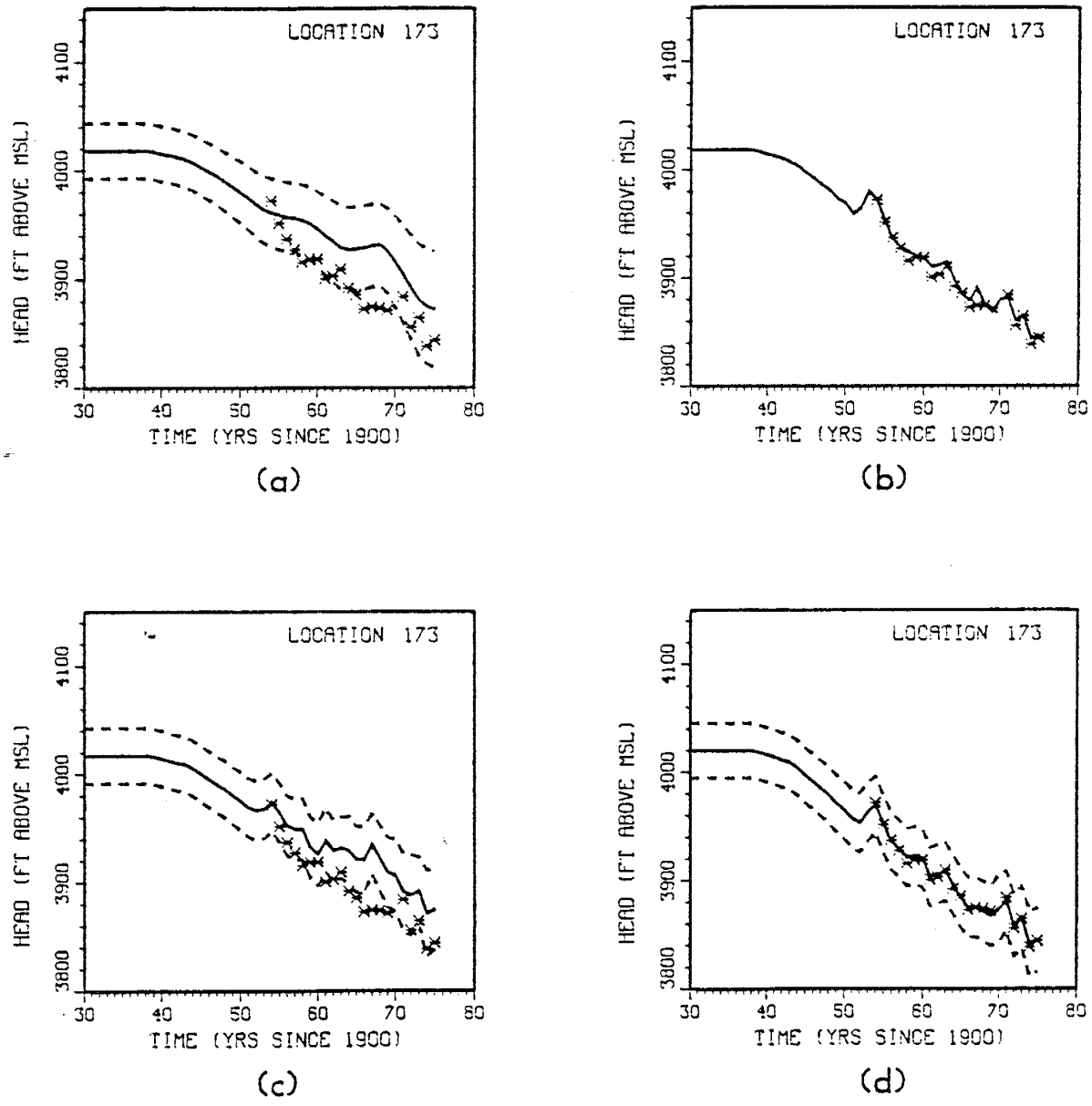

Fig. 90. Model heads (solid line), observed heads (asterisks) and $\pm 2\sigma_h$ bounds (dashed lines) at measurement location 173 for runs 88 (a), 89 (b), 94 (c) and 95 (d).

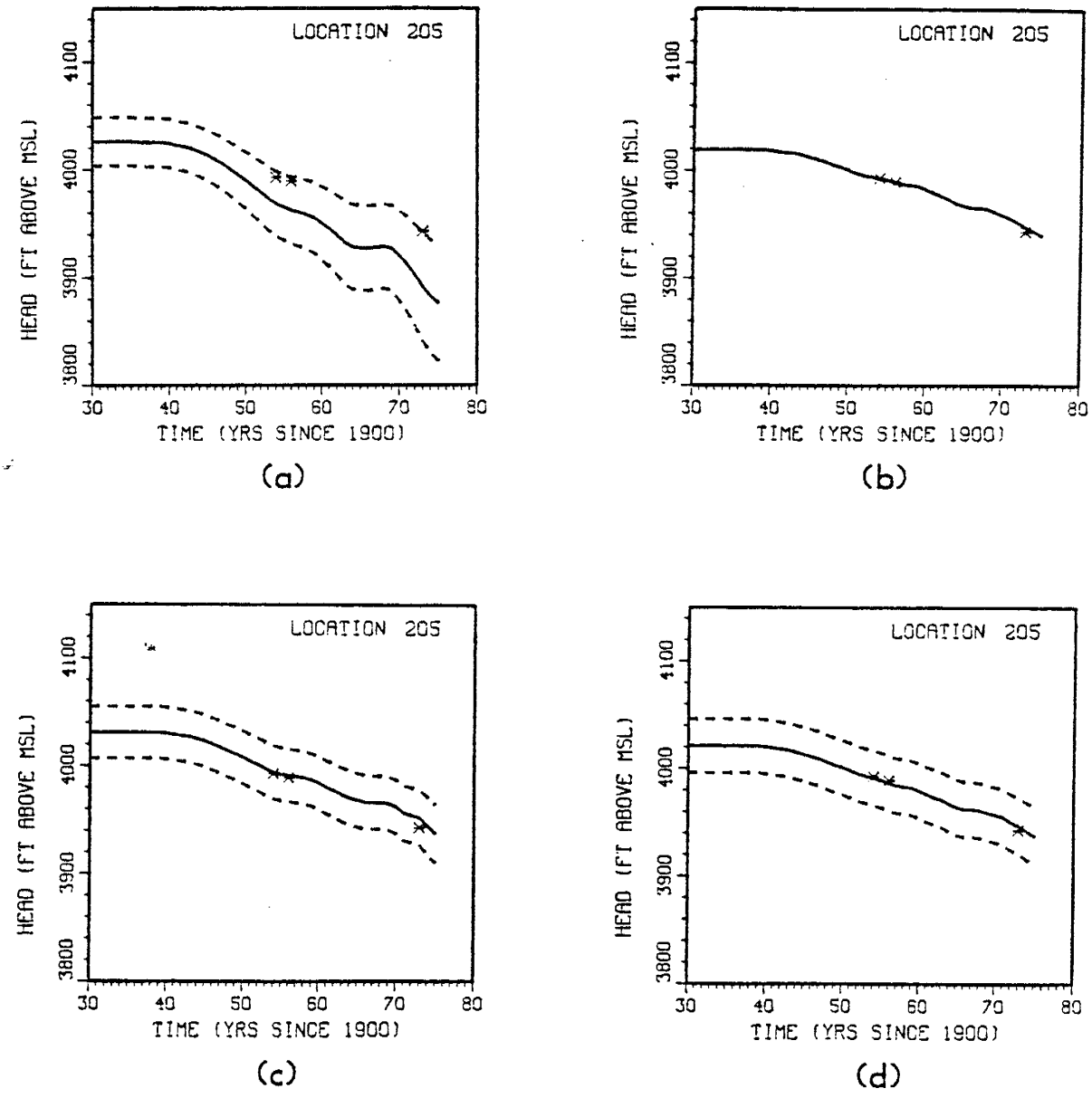

Fig. 91. Model heads (solid line), observed heads (asterisks) and $\pm 2\sigma_h$ bounds (dashed lines) at measurement location 205 for runs 88 (a), 89 (b), 94 (c) and 95 (d).

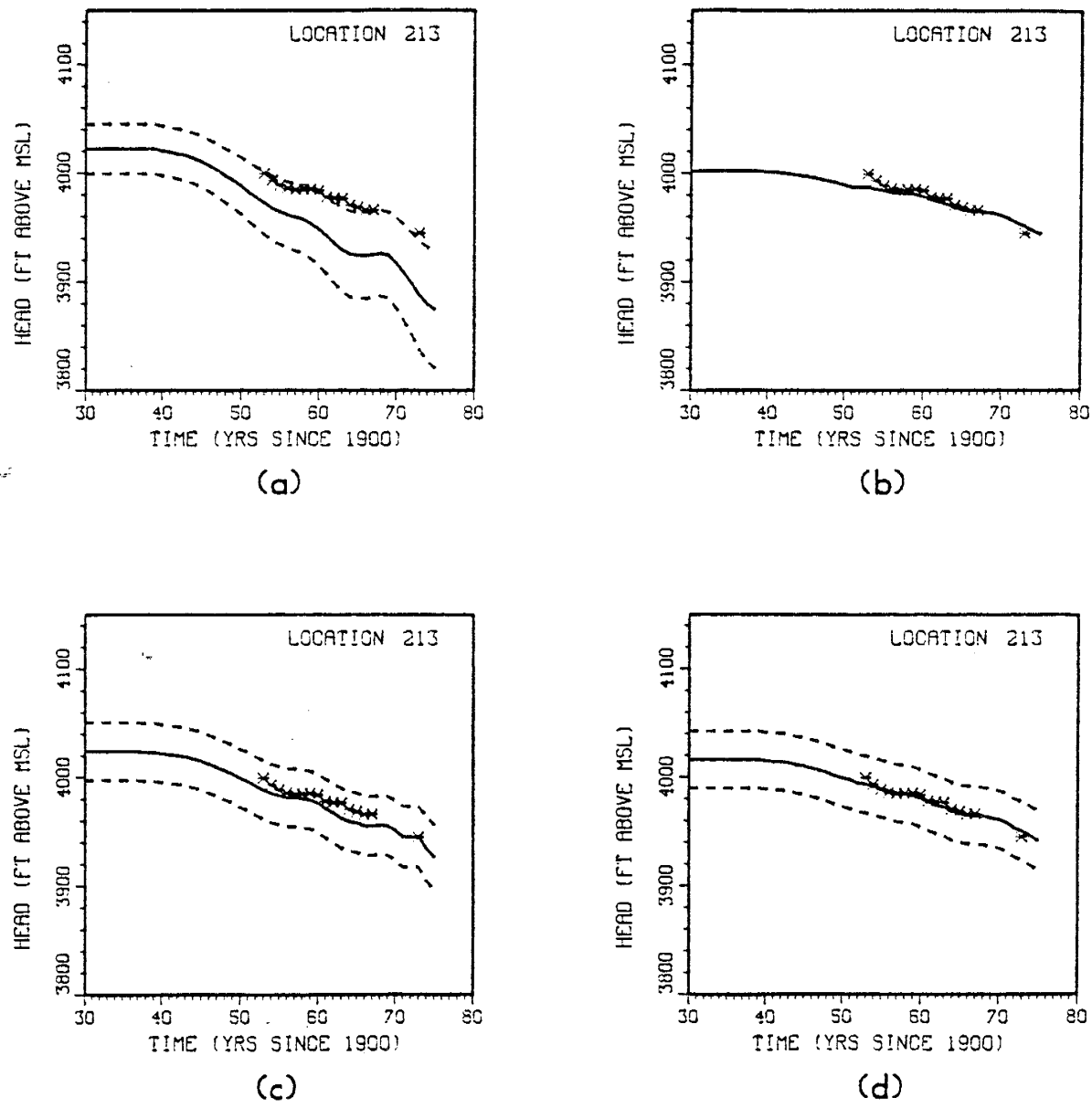

Fig. 92. Model heads (solid line), observed heads (asterisks) and $\pm 2\sigma_h$ bounds (dashed lines) at measurement location 213 for runs 88 (a), 89 (b), 94 (c) and 95 (d).

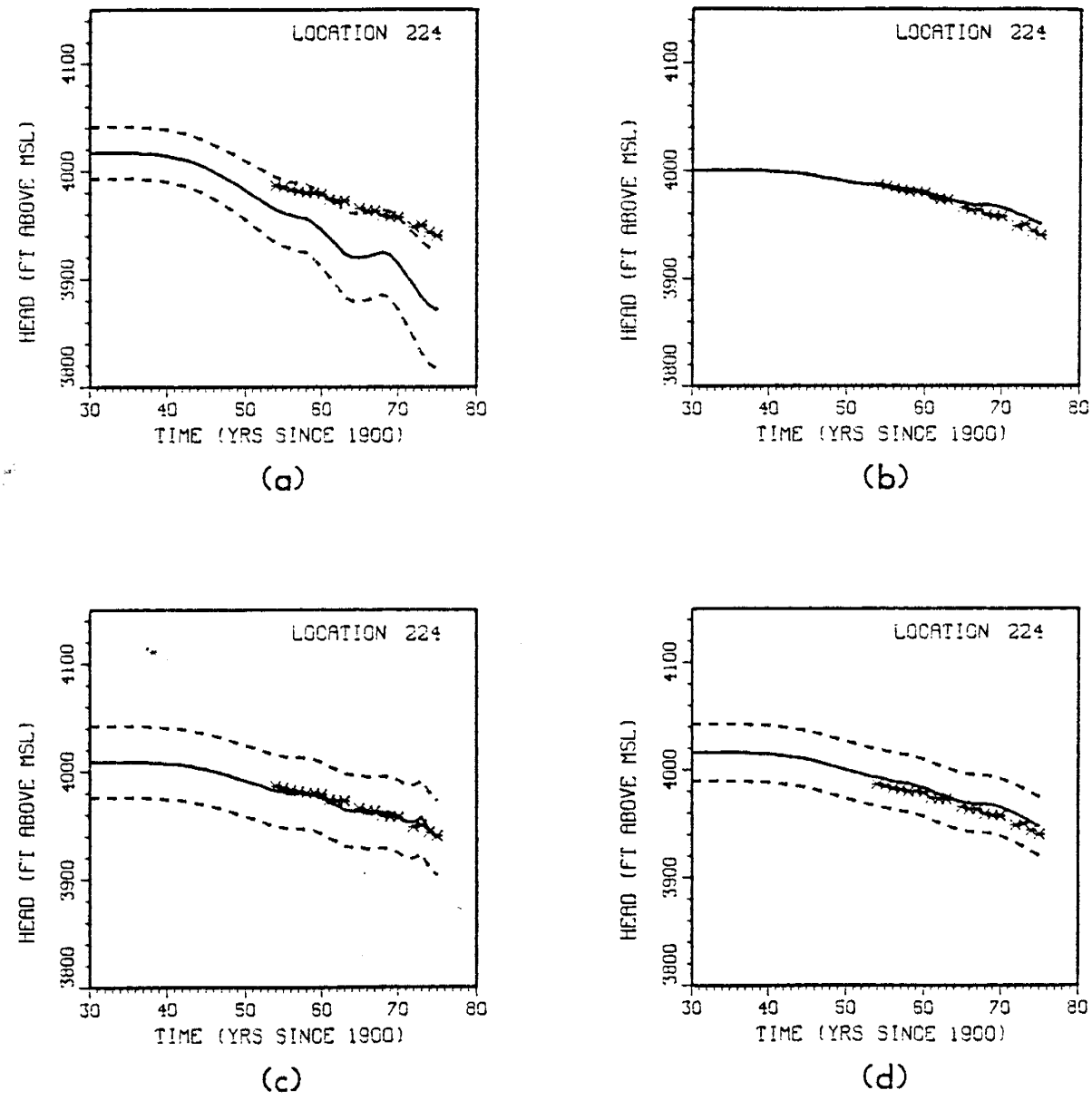

Fig. 93. Model heads (solid line), observed heads (asterisks) and $\pm 2\sigma_h$ bounds (dashed lines) at measurement location 224 for runs 88 (a), 89 (b), 94 (c) and 95 (d).

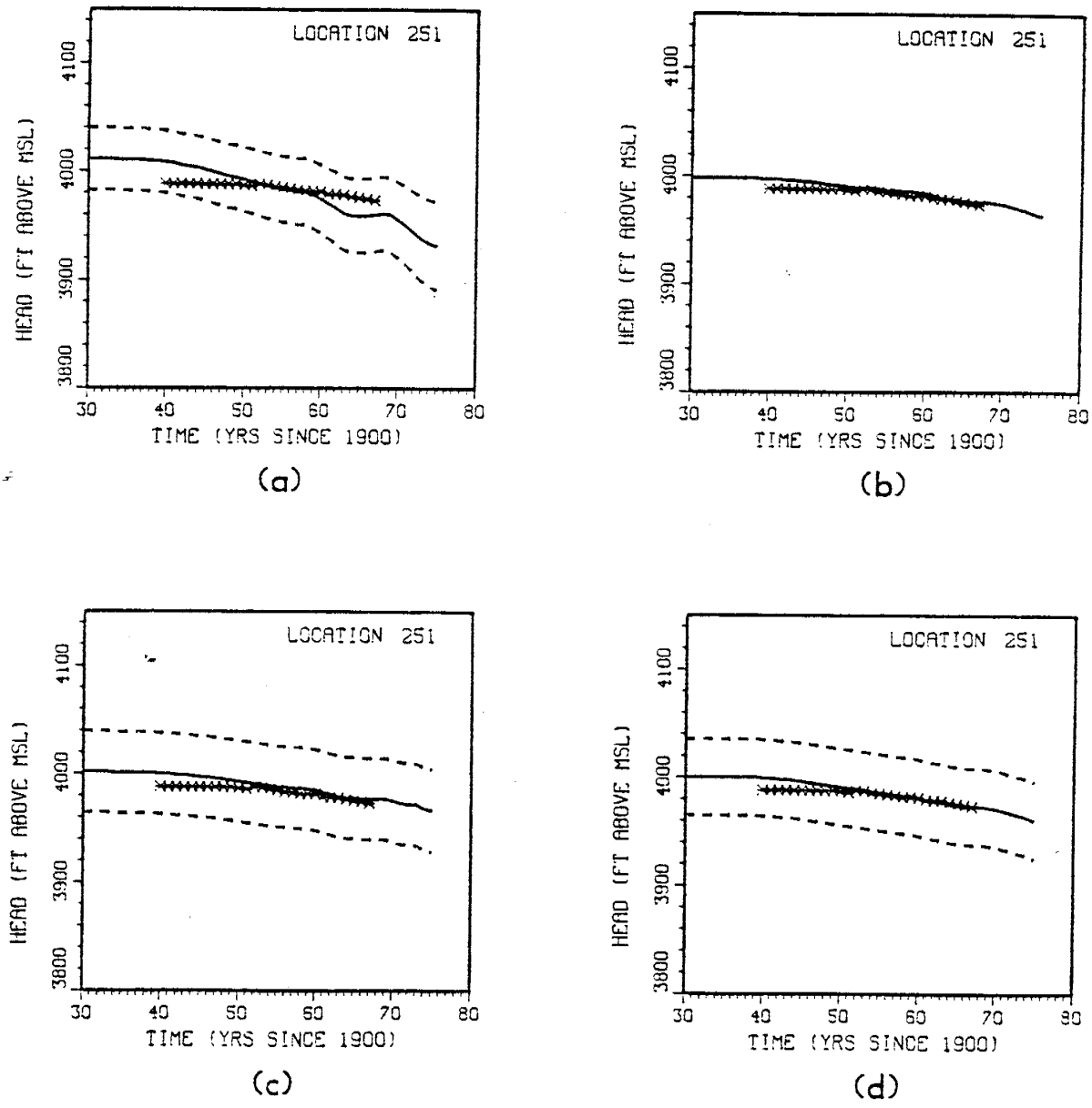

Fig. 94. Model heads (solid line), observed heads (asterisks) and $\pm 2\sigma_h$ bounds (dashed lines) at measurement location 251 for runs 88 (a), 89 (b), 94 (c) and 95 (d).

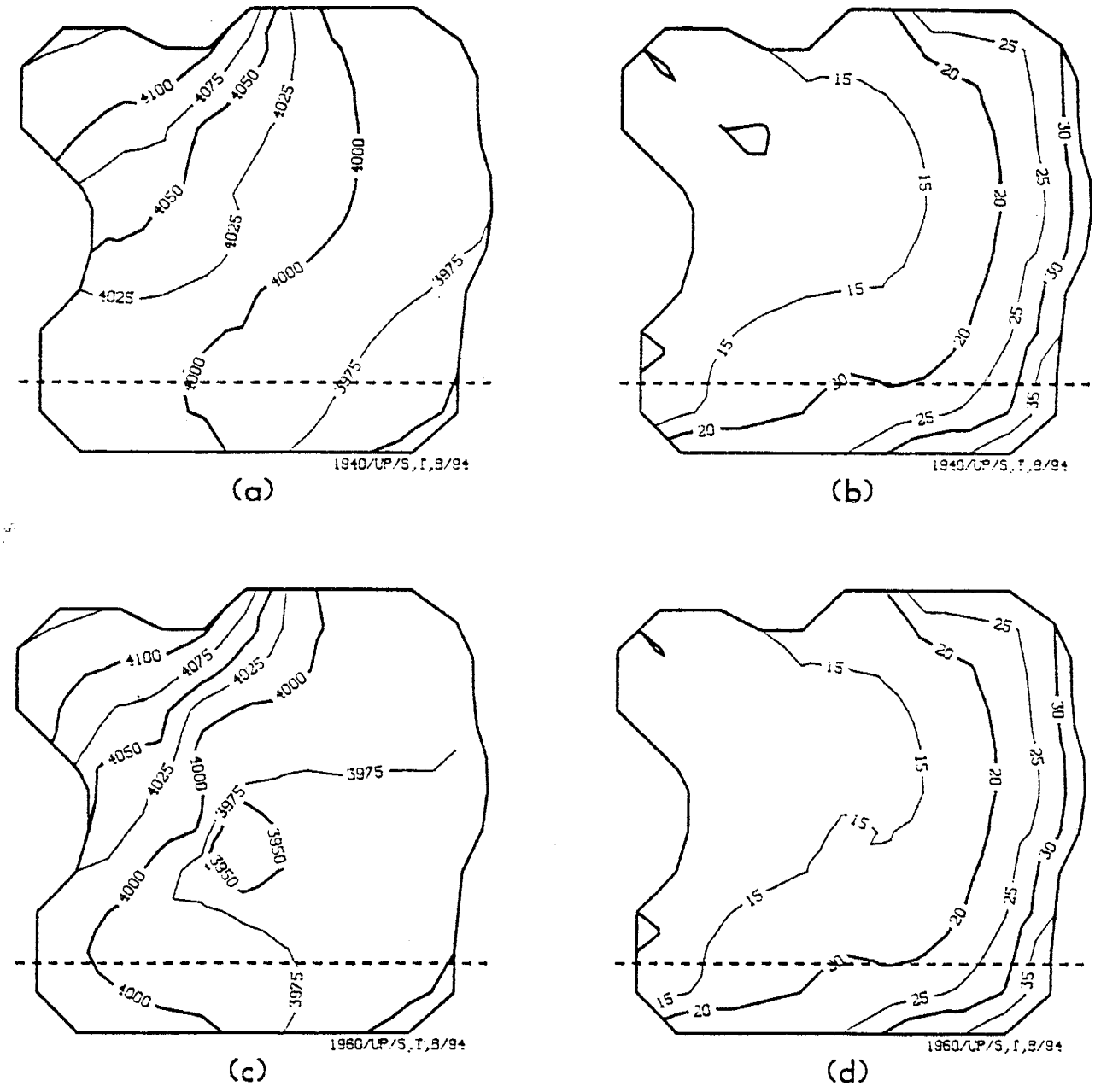

Fig. 95. Head fields (ft above MSL) and associated σ_h fields (ft) for run 94 for 1940 (a and b) and 1960 (c and d).

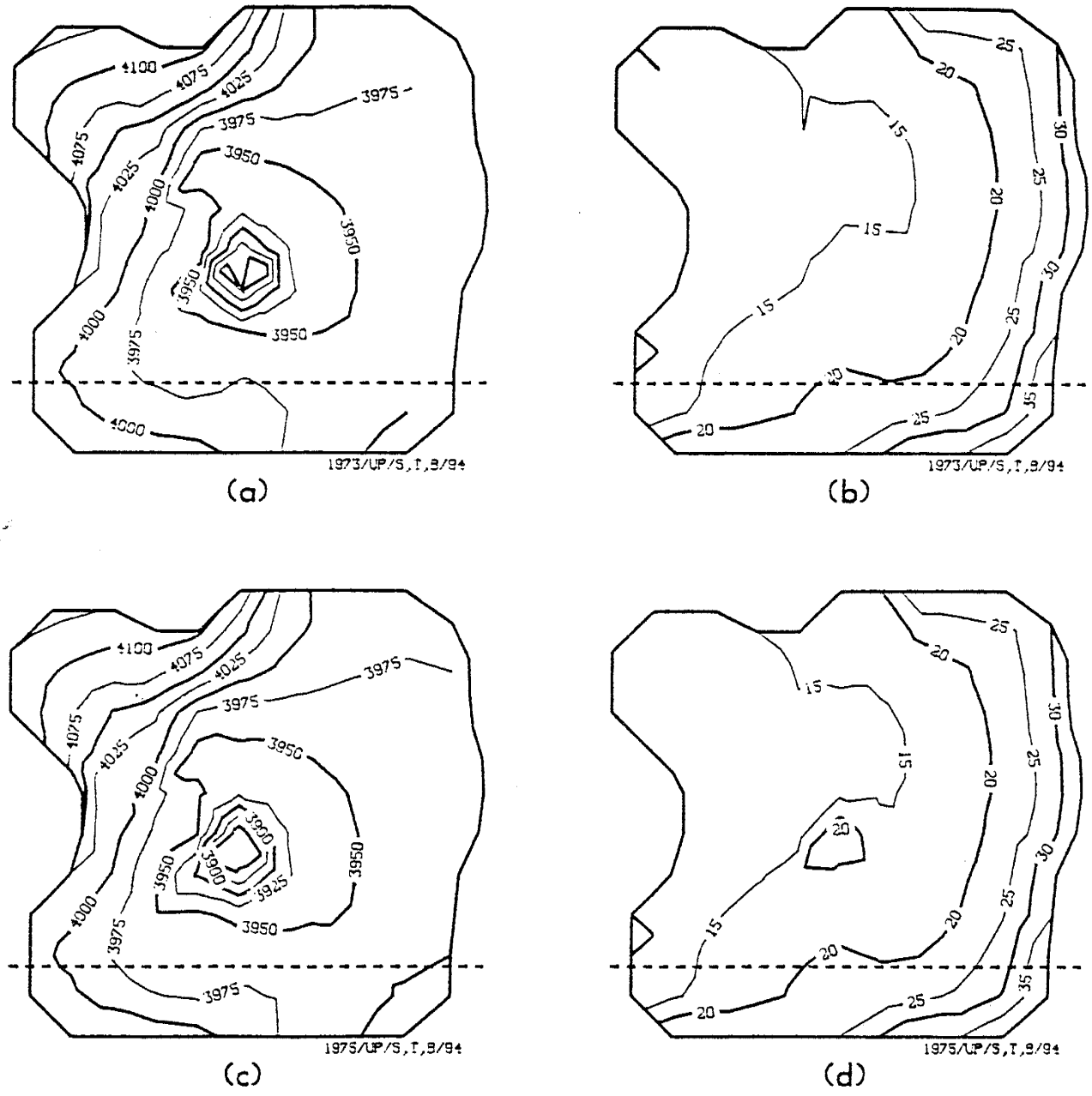

Fig. 96. Head fields (ft above MSL) and associated σ_h fields (ft) for run 94 for 1973 (a and b) and 1975 (c and d).

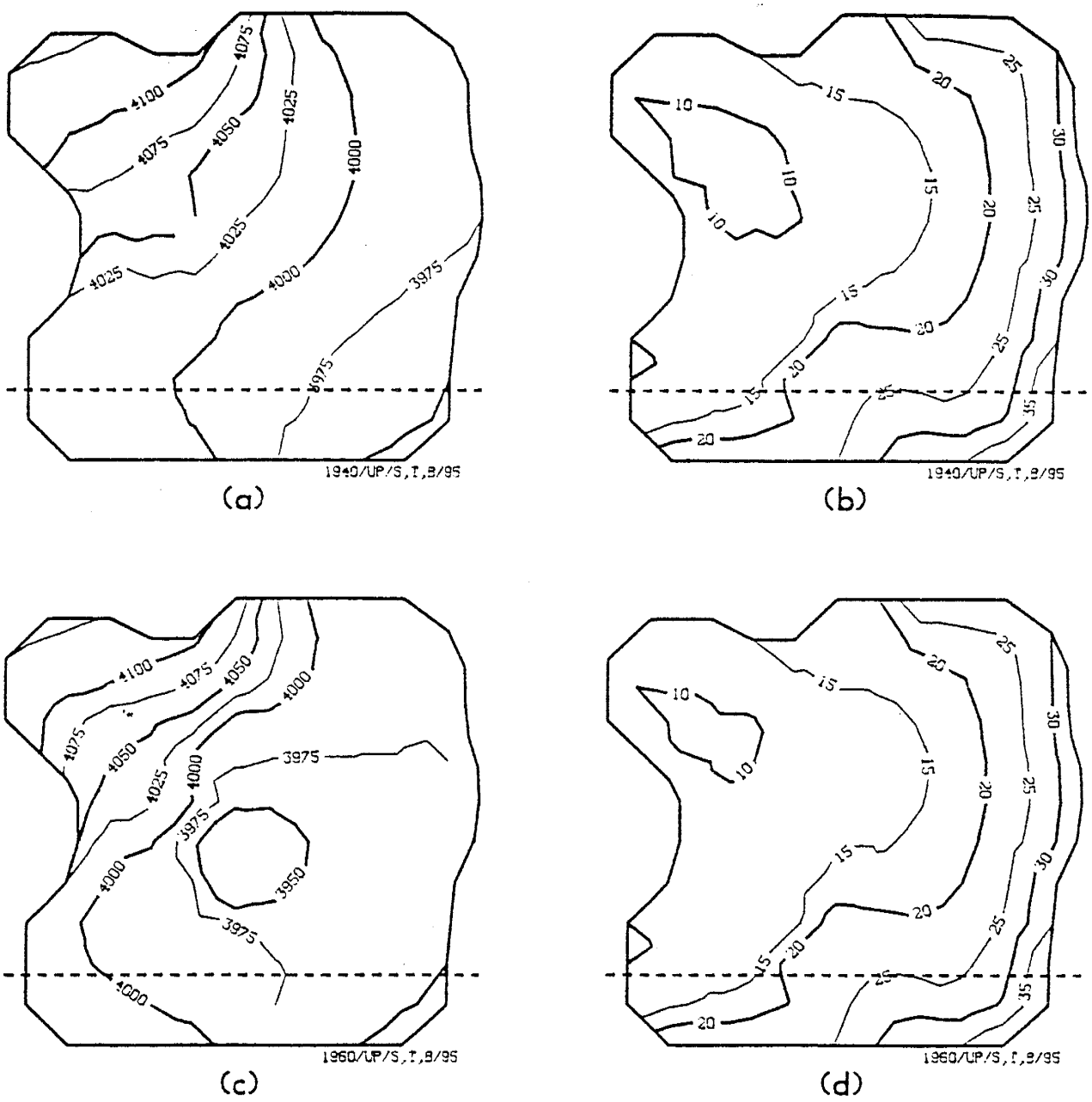

Fig. 97. Head fields (ft above MSL) and associated σ_h fields (ft) for run 95 for 1940 (a and b) and 1960 (c and d).

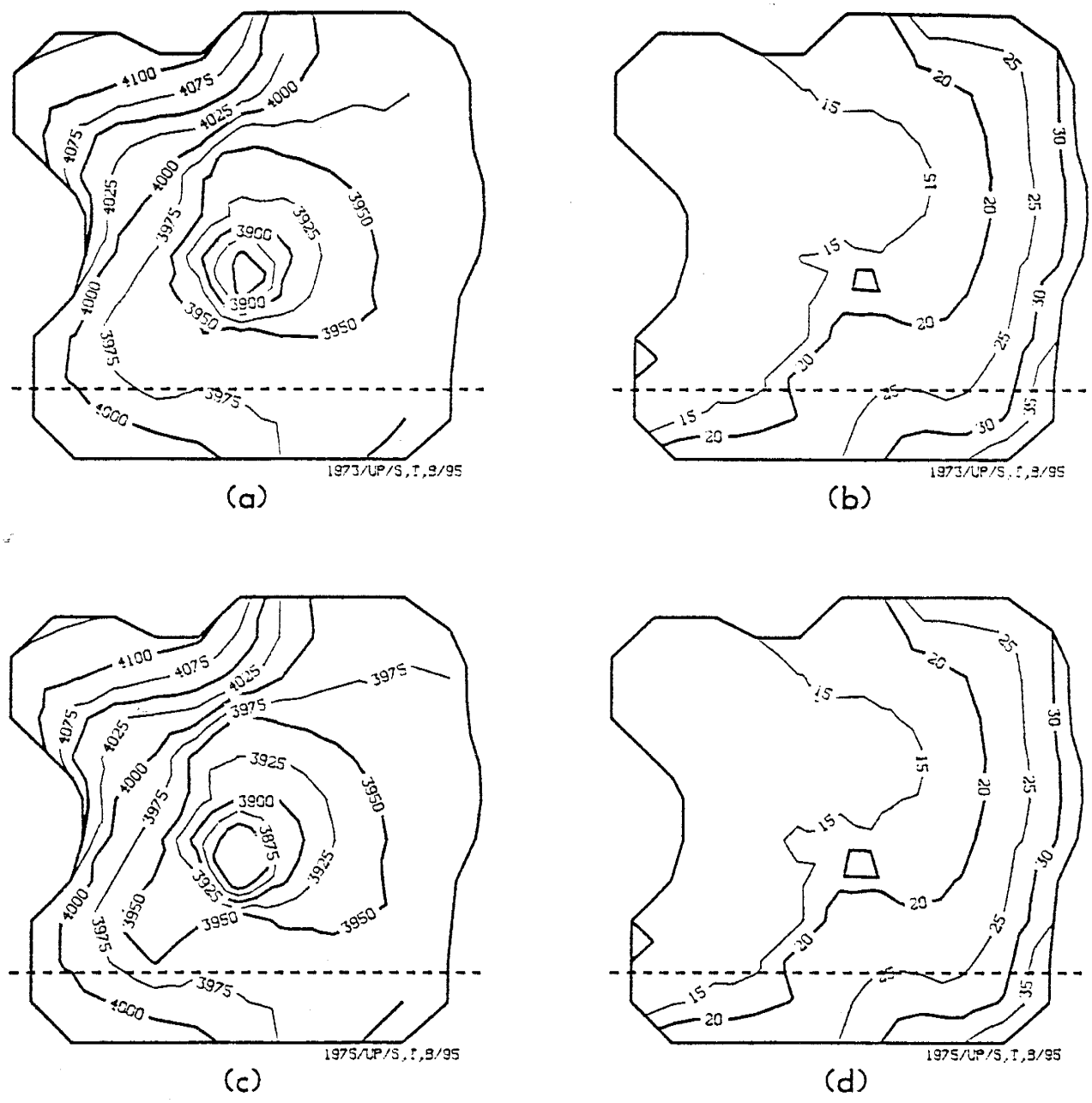

Fig. 98. Head fields (ft above MSL) and associated σ_h fields (ft) for run 95 for 1973 (a and b) and 1975 (c and d).

COMPARISON OF RESULTS TO PREVIOUS RESEARCH

The output from runs 92 and 89 was contoured so that it could be compared to the water level and drawdown maps reported by McLean (1977). McLean's figures for the Columbus Basin were digitized and replotted at the scale used in this report (figure 99). Recall that for run 92, only log T was estimated using all of the available head data for the time period 1930 to 1975. Run 89 was the same as run 92 except that the nodal pumping (B) parameters were estimated jointly with log T. The 1973 head fields for additional runs are available in the validation chapter of this report.

Comparison of Drawdowns

Drawdown maps for the time periods 1950 to 1960 and 1960 to 1970 for both runs are shown in figure 100. The cones of depression for run 92 do not match well with McLean's figures. At early time CERT estimated significant drawdown over a larger areal extent than was observed by McLean. The match was better for the period 1960 to 1970, but where CERT estimated maximum drawdowns of under 40 ft, McLean plotted drawdowns greater than 50 ft. This observation further discredits the decline in the SEO pumping estimates for 1965 to 1970 (see figure 15). Note that drawdown south of the international boundary was observed by McLean and predicted by CERT.

The drawdown maps for run 89 matched much better with those of McLean (1977). The cone of depression predicted by CERT remained larger in areal extent than that reported by McLean for 1950 to 1960. The differences, however, were primarily on the north and west sides of the pumping center as opposed to all directions in the previous run. The drawdown maps for 1960 to 1970 are very similar in general character. The two maps (figures 99b and 100d) show coincident pumping centers, a northwest-southeast trend in

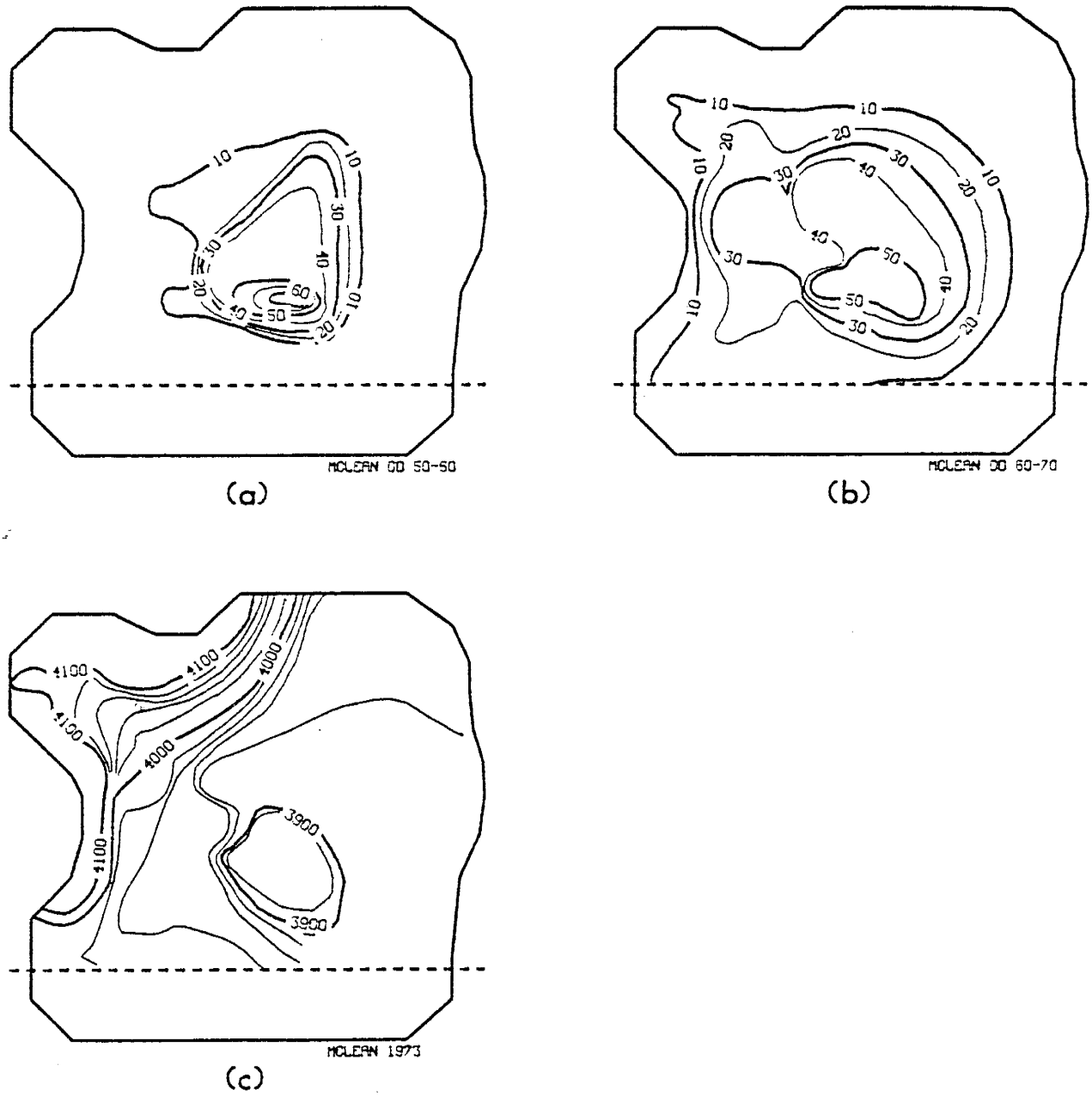

Fig. 99. Drawdown maps for 1950 - 1960 (a), 1960 - 1970 (b), and 1973 head map (c) from McLean (1977). Drawdown in feet, heads in feet above MSL.

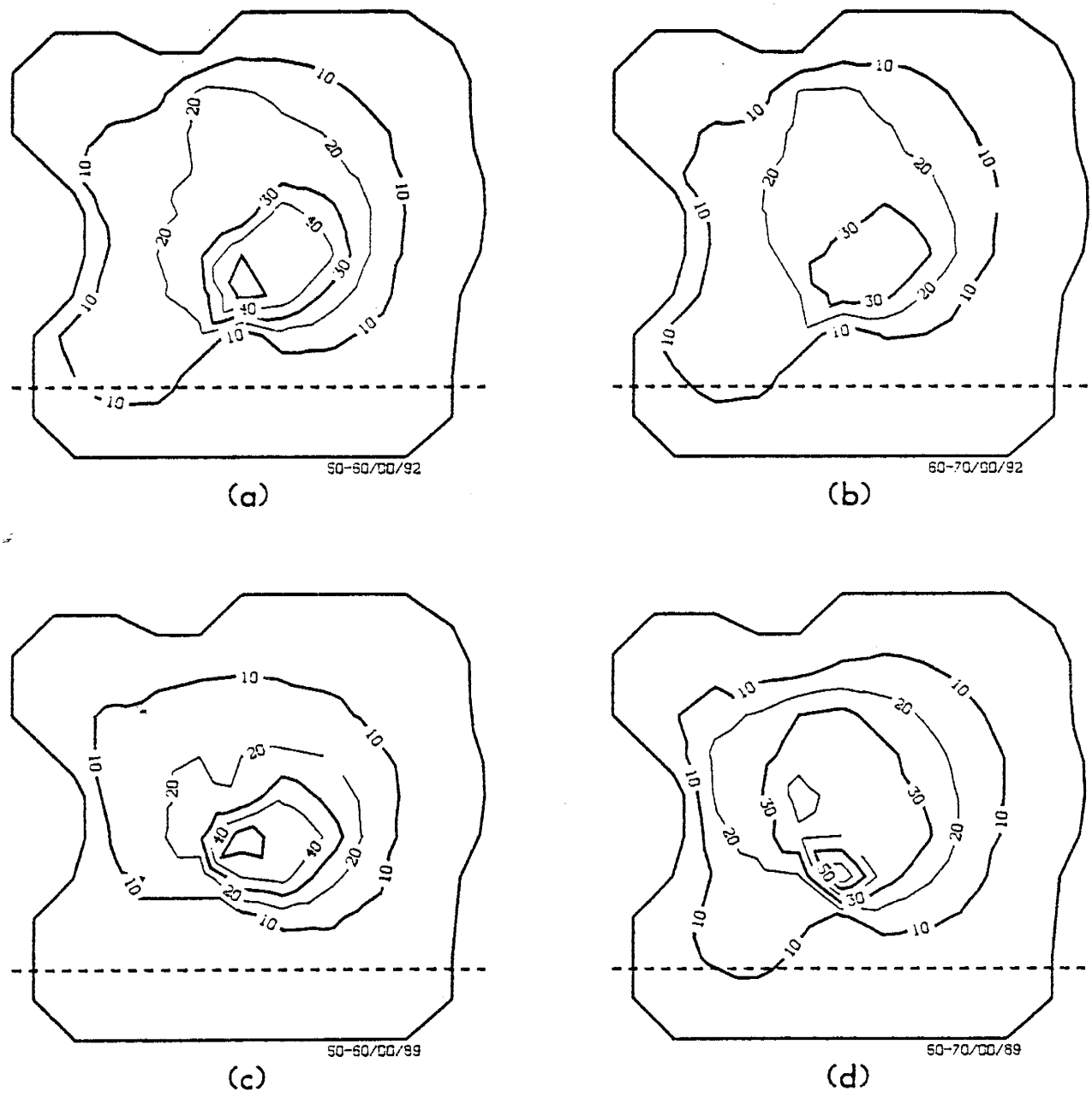

Fig. 100. Drawdown maps for run 92 for 1950 - 1960 (a), 1960 - 1970 (b), and for run 89 for 1950 - 1960 (c) and 1960 - 1970 (d). Units in feet.

the cone of depression, and similar areal extents of drawdown. CERT again predicted drawdown in Mexico due to pumping about Columbus.

Excluding the error embodied in the log T and/or B estimates for runs 92 and 89, there are several inconsistencies which contributed to the mismatch between equivalent drawdown contours. First of all, fine details in the CERT drawdown curves were not permitted because of the spatial discretization of the flow system. Secondly, contouring is a subjective procedure when done by hand (as McLean did presumably). Also, the control points which McLean used to construct his drawdown maps are unknown. In some regions of the basin he was certain to have very little data and the amount of interpretation must have been significant. It seems that for his 1973 water level map (next section) McLean may have used well control in the eastern portion of the basin which was excluded from this study due to the failure of many such wells to penetrate the confining layer. These wells showed no drawdown with time and would have led to erroneous conclusions if their observations were used in the contouring exercise. Finally, the conceptual model used during this study may be in error and the drawdowns predicted by CERT may be more extensive than they should be. This issue is discussed further in the next section.

Comparison of 1973 Head Maps

The 1973 head maps for runs 92 and 89 are plotted in figure 101. The CERT estimated heads in the western half of the basin match considerably well with McLean's contours (figure 99c). The "bulge" in the contours drawn by McLean in the gap between the Tres Hermanas and Florida mountains exists in the CERT contours but is very much subdued. Head contours for run 92 due south of the Florida Mountains appear to be artificially constricted. A linear high log T zone estimated immediately below the constricted contours

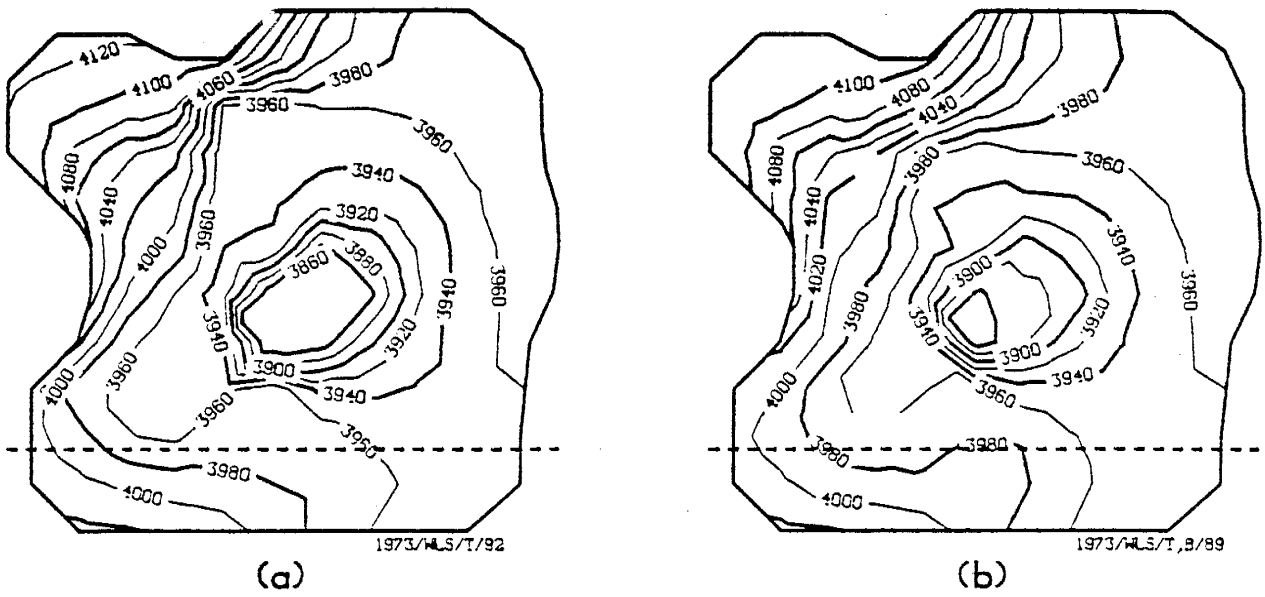

Fig. 101. Head fields (ft above MSL) for runs 92 (a) and 89 (b) for the year 1973.

probably caused this effect by forcing an abrupt gradient decrease in that region. This high log T zone may not exist in reality.

Where the head contours do not match on the grid boundaries the difference is due to the estimated constant head boundaries used in CERT. A large amount of subjectivity was involved in the boundary head estimation, and the true contours might easily be shifted one way or the other from their current location. One major difference between McLean's interpretation and that used in CERT is the configuration of the 4,000 ft to 4,100 ft head surface. McLean drew the 4,100 ft contour line encircling the north, east and south sides of the Tres Hermanas Mountains. The constant head boundaries used in CERT cause the water level contours on a gross scale to intersect the Tres Hermanas Mountains at an angle - the 4,100 ft contour is not continuous parallel to the mountain front but instead intersects the mountain front and ends.

Water levels in the eastern half of the basin were not directly comparable because it was believed that McLean used shallow wells to aid in the drawing of his contour maps. The CERT boundary conditions for the eastern half of the basin were also very uncertain. The σ_h maps presented in the validation section portray the high degree of predicted head uncertainty for the eastern half of the Columbus Basin.

Finally, a better match between observed and CERT calculated heads could have been obtained if the model had been "fine tuned" further. The boundary heads, SEO pumping estimates, and other model parameters could have been manually adjusted to produce slight changes in the predicted head contours. Such detailed model calibration, however, was not a goal of this study.

ALTERNATIVE CONCEPTUAL MODELS

At the outset of this study the Columbus Basin was conceptualized as a 2-D flow system. Geological cross sections indicated a thick confining layer over the central and eastern portions of the basin, but in the western portion of the basin the clay layers were thinner and discontinuous. The Columbus aquifer receives recharge and underflow from the mountain fronts and adjacent bolson fill aquifers to the north and northwest respectively. Outlow from the basin was originally to the south and southeast into Mexico, but this flow was decreased as basin development progressed.

Under pre-development conditions, water discharged from the primary aquifer as vertical upward leakage through the aquitard. After significant pumping began in the Columbus area, the amount of this leakage was reduced and its direction possibly reversed over large areas of the basin. The effects of vertical leakage through the aquitard were not accounted for explicitly in the Columbus Basin model.

The boundary nodes for the validation study were placed far enough from the pumping center so as not to be influenced by the cone of depression prior to 1975. Their locations were based on reported drawdown maps for the region (McLean 1977). Prescribed head boundaries were used because T and head data was non-existent in the vicinity of many of the boundary nodes.

As figures 28 and 29 indicate, the prescribed head boundary assumption was severely violated. Drawdown affected the boundary nodes as soon as major development of the basin began in the early 1950s. There was almost no time lag between increased or decreased pumping signals and the corresponding increase or decrease of boundary flux (figures 28 and 29).

There are three possible explanations for this result. First of all, the Columbus Basin may in actuality have a very small time constant, or, in

other words, the time response of the basin may resemble a large "bowl" of water. In this case the effects of pumping in the basin center propagate very rapidly towards the basin boundaries. If the Columbus Basin indeed has such a small time constant, the current model boundaries would have to be extended far beyond their current locations or a different boundary type would have to be used. If the model boundaries were extended to the west or northwest, entire adjacent groundwater basins would have to be modeled.

The alternative explanations deal with sources of water. The addition of sources of water not presently accounted for in the Columbus Basin model would restrict the growth of the cone of depression. The reduction of vertical leakage through the aquitard could be a significant source of water. The amount of reduced leakage is hard to evaluate and should be a topic for future research. Finally, there may be 3-D leakage processes occurring in the Columbus Basin which a 2-D groundwater flow code such as CERT cannot simulate. The Columbus region is primarily one of discharge (upward vertical gradients) and therefore the possibility exists of deep vertical leakage "recharging" the regional aquifer. The existence and nature of such a deep flow system would be very hard to verify.

FUTURE RESEARCH

CERT

Several problems were encountered during the Columbus Basin study which if (partially) rectified the utility of CERT would be greatly enhanced for future use. First of all, obtaining a correlation structure for the uncertain parameter types is of paramount importance for both the inverse parameter estimation and uncertainty propagation algorithms. Obtaining quantitative statistical correlations for all parameter types, however, is often very difficult if not impossible. It would be desirable therefore to investigate the accuracy and use of qualitative correlation estimates, which may be quite good when made by a professional familiar with the geographic region of interest.

CERT is not currently capable of incorporating the effects of cross-correlation between parameter types, but amending the code to do so would primarily be a matter of input and output. Because the identification of auto-correlation structures was found to be very important, the effects of cross-correlations deserve scrutiny. However, if defining auto-correlations is often difficult, defining cross-correlations is harder yet. The identification and use of cross-correlations has not been reported sufficiently in the literature.

CERT also is not currently capable of incorporating mixed parameterizations into the solution procedure. For example, if T is defined at the nodal points of the grid, S must be defined in the same manner. The capability to mix parameterizations would be very useful. For instance, a nodal parameterization could be used in areas where a lot of head and/or T data is available, and zoned parameterizations could be used where data is sparse or nonexistent.

Another problem identified during this study which is typical of the multi-dimensional search procedure and numerical model solutions in general is uniqueness. The uniqueness issue becomes apparent when log T contour maps for the different WLS runs are compared. The contour maps may look significantly different depending upon the prior parameter estimates and the head data used to condition the parameters during the optimization process. The uniqueness problem is a very complex one which will not be solved in the near future, but the accuracy of model predictions in light of the uniqueness issue needs to be examined further.

The effect of input parameter estimates on the uncertainty propagation predictions was not expected but made intuitive sense. The process of greater uncertainty propagation through high T zones would be interesting to look at in greater detail. Was this effect caused by the sensitivities in equation 9, the posterior covariance matrix, or some combination of both terms?

Finally, it would be fairly simple to add some constraint sets to CERT. A useful constraint identified during this study would be the ability to specify sign (positive or negative) of the flux at boundary nodes. Past researchers have found, however, that when constraints were specified model solutions tended to converge on the constraint boundary. This should pose less of a problem as prior parameter estimates and correlations can be specified with increased accuracy.

Columbus Basin

Several improvements could be added to the Columbus Basin model if it were to be used for predictive purposes. Additional permeability and water level measurements are always desirable, although since a large amount of conditioning occurred when a partial head record was used the utility of additional head measurements in irrigated areas is questionable. Head

measurements which could help to define boundary conditions on the north, south and east sides of the basin would be very useful however.

The existing SEO pumping estimates could also be revised. According to observed hydrographs and CERT results, the decrease in overall pumping during the time period 1965 to 1970 does not exist. Pumping estimates during this time period should be increased accordingly.

Finally, the model boundary conditions and their effect on the parameter estimates need a detailed evaluation. As mentioned earlier, this evaluation could lead to a new conceptual model for the Columbus Basin.

SUMMARY AND CONCLUSIONS

Reasonable estimates for the parameters log T and pumping (B) were obtained through the inverse procedure. Alternative parameterizations for S were evaluated by analyzing the value of the objective function, J. The attempt at estimating boundary heads (B) was unsuccessful. Realistic estimates of boundary heads might have been obtained if more water level or conductivity observations had been located in close proximity to the boundary nodes. However, this condition directly conflicts with the practice of placing model boundaries far away from the "action" so that they have lessened influence on head predictions in the region of interest.

The log T fields estimated by CERT had some consistently similar characteristics despite the fact that different covariance structures and head records were used as input. A high log T zone was consistently estimated beginning at the gap between the Tres Hermanas and Florida Mountains and trending due south through Columbus. High log T values in this region were probable due to ancestral drainages and subsurface basalt flows. It was suspected that another high permeability zone may lie on the east side of the basin in the Mimbres Graben area. CERT did not estimate such a zone, perhaps due to the paucity of data in the region. Additional head and/or permeability data in the Mimbres Graben would increase predictive capabilities for the Columbus Basin substantially.

High log T zones were also estimated within and to the north of the pumping center. These estimates were not particularly consistent, however, which indicated a problem with parameter uniqueness. These high log T zones may not exist in reality, but were estimated by CERT simply to enhance the minimization of J.

Due to parameter identifiability concerns, a series of runs was made where log T was estimated over zones of finite elements. A realistic log T field, which matched well with the estimated fields for nodal parameterizations, was obtained when log T was estimated for 25 zones of approximately equal size. When the number of zones was reduced to 13, however, unrealistic log T estimates resulted. The posterior log T fields were observed to be highly conditioned on the zoning pattern and the estimated boundary conditions.

S was found to be a relatively insensitive parameter - a result which was not surprising. An unrealistic S field was estimated by CERT when a uniform prior with a high σ_s was used. Evidently CERT provided the water needed for the prescribed outward fluxes by increasing S in the vicinity of the cone of depression, as opposed to relying upon inflow through the boundaries. Once S was zoned to provide a more realistic prior, estimated S values in each zone changed very little. These results indicated that the estimation of S in the Columbus Basin was not amenable to the inverse procedure.

The estimated pumping values seemed to be reasonable for the most part, but attempts to find a meaningful correlation between posterior B values and annual precipitation did not lead to quantitatively viable results. The extreme oscillations of pumping estimates from year to year at some nodes would not have been as pronounced if a statistical correlation in time and/or space had been found.

The uncertainty propagation results were reasonable once a qualitative boundary node correlation was derived. The values of σ_h generally increased through time in the irrigated region of the basin. For parameters which were constant in time (S and T), the increase was due to the increased sensitivities of heads to parameters. For the time-varying B parameters

(pumping) the increase was due to larger standard deviations as well as sensitivities. The portion of σ_h due to the boundary head uncertainty did not change in time.

Boundary head uncertainty was propagated through high log T zones estimated by WLS easier than through regions of lower log T. This effect may have been due to the model head sensitivities, the linearized posterior estimate of $\underline{P}_{TT}$, or some combination of these two factors.

The CERT validation results were promising because there was little difference between model calculated head values regardless of the head data set that the model parameters were conditioned on. It would seem that once some "threshold" amount of head data is obtained, additional head data has only limited use in the WLS estimation process. Simulations which used WLS estimates of log T and B (pumping) produced better fits between observed and calculated heads as opposed to simulations where only posterior estimates of log T were used. This was logical since the greater the number of uncertain parameters the more the model can be "fine tuned" to match observed heads. Whether or not the posterior B parameters were reasonable, however, is an open question.

Several important conclusions can be drawn from this research. First of all, obtaining a correlation structure for the uncertain parameter types is very important for both the inverse parameter estimation and uncertainty propagation algorithms. Large fluctuations of boundary heads and fluxes were observed at adjoining nodes and at individual nodes through time. Statistical correlation in space and time would have subdued the extreme oscillations and perhaps a more reasonable result would have been obtained. Parameter correlation also enhanced the propagation of parameter uncertainty, and if reasonable σ_h estimates are to be obtained suitable correlation must be implemented. It will always be difficult, however, to

estimate correlations between parameters such as boundary heads when they are far removed from the bulk of the data.

Secondly, users of parameter estimation models must keep in mind that the parameter estimates are inherently limited by the extent of the modeled domain and the available prior information. If insufficient information is used as model input the predicted results may not be consistent with the hydrogeology of a given situation. Parameter estimation using a code such as CERT may be less time consuming than traditional methods, but it is by no means automatic. All parameter estimates should be viewed critically and examined to find if they remain reasonable in light of information not incorporated into the inverse model. Examples of unrealistic parameter estimates were observed during this study for all of the parameter types estimated.

All of these results must be viewed in light of the prescribed head boundary constraints. Because fluxes into the Columbus aquifer through the first type boundary nodes increased with time, simulated head gradients near the boundaries were greater than they should have been. The extent to which this bias effected the parameter estimates in the basin interior is unknown, but an assessment of the problem will be made during future research.

REFERENCES

Bakr, A.A., Gelhar, L.W., Gutjahr, A.L. and MacMillan, J.R. 1978. Stochastic analysis of spatial variability in subsurface flows, 1, Comparison of one- and three-dimensional flows. Water Resour. Res., 14(2), p. 263-271.

Birch, F.S. 1980. Three-dimensional gravity modeling of basin hydrologic parameters in New Mexico. Upublished report prepared for the USGS under contract number 14-08-0001-17899.

Carrera, J. and Neuman, S.P. 1986. Estimation of aquifer parameters under transient and steady state conditions: 1. maximum likelihood method incorporating prior information. Water Resourc. Res., 22(2), p. 199-210.

Carrera, J. and Neuman, S.P. 1986. Estimation of aquifer parameters under transient and steady state conditions: 2. uniqueness, stability, and solution algorithms. Water Resourc. Res., 22(2), p. 211-227.

Carrera, J. and Neuman, S.P. 1986. Estimation of aquifer parameters under transient and steady state conditions: 3. applications to synthetic and field data. Water Resourc. Res., 22(2) p. 228-242.

Clemons, R.E., et al. 1983. Florida Mountains section of southwest New Mexico overthrust belt - a reevaluation. New Mexico Geology, p. 26-29.

Cooley, R.L. 1979. A method for estimating parameters and assessing reliability for models of steady state groundwater flow, 2, application of statistical analysis. Water Resour. Res., 15(3), p. 603-617.

Cooley, R.L. 1983. Incorporation of prior information on parameters into nonlinear regression groundwater flow models, 2, applications. Water Resour. Res., 19(3), p. 662-676.

Cooley, R.L., Konikow, L.F. and Naff, R.L. 1986. Nonlinear-regression groundwater flow modeling of a deep regional aquifer system. Water Resour. Res., 22(13), p. 1759-1778.

Cordell, L., 1979. Regional geophysical setting of the Rio Grande rift. Geological Society of American Bulletin, v. 890, p. 1073-1090, Doc. No. 80710.

Cressie, N., 1986. Kriging Nonstationary Data. Journal of the American Statistical Association, v. 81, no. 395, p. 625-634.

Darton, N.H. 1916. Geology and underground water of Luna County, New Mexico. USGS Bulletin 618.

Delfiner, P. 1976. Linear estimation of non-stationary spatial phenomena. In M. Guarascio et al., Advance Geostatistics in the Mining Industry, NATO Advanced Study Institute Series, D. Reidel Publ. Co., Boston.

Delhomme, J.P. 1978. Kriging in the Hydrosciences. Advances in Water Resources, v. 1, no. 5, p. 251-266.

Dettinger, M.D. and Wilson, J.L. 1981. First order analysis of uncertainty in numerical models of groundwater flow, Part 1. Mathematical development. Water Resour. Res., 17(1), p. 149-161.

Doty, G.C. 1969. Availability of ground water near Arena, Luna County, New Mexico. USGS open-file report, Albuquerque, New Mexico.

Gabin, V.L. and Lesperance, L.E. 1977. New Mexico climatological data: precipitation, temperature, evaporation, and wind; monthly and annual means 1850-1975. W.K. Summers and Associates, Socorro, New Mexico.

Hawley, J.W. 1975. Quaternary history of Dona Ana County region, south-central New Mexico. New Mexico Geological Society Guidebook 26, p. 139-150.

Journel, A.B. and Huijbregts, Ch.J. 1978. Mining Geostatistics. Academic, New York.

Kafritsas, J. and Bras, R.L. 1981. The practice of kriging. Technical Rpt. 263, Ralph M. Parsons Lab., Dept. of Civil Eng., Massachusetts Institute of Technology, Cambridge, Mass.

King, W.E., Hawley, J.W., Taylor, A.M. and Wilson, R.P. 1971. Geology and ground-water resources of central and western Dona Ana County, New Mexico. New Mexico Water Resources Research Institute, Hydrologic Report 1.

Kottlowski, F.E., et al. 1969. Key oil tests and stratigraphic sections in southwest New Mexico. New Mexico Geological Society, Twentieth Fuel Conference, p. 186-194.

Luenberger, D.G. 1984. Introduction to linear and non-linear programming. Addison-Wesley, Reading, Mass.

McLean, J.S. 1977. Hydrologic maps and data in the Mimbres Basin, New Mexico. Open-file report 77-314.

Neuman, S.P. 1973. Calibration of distributed parameter groundwater flow models viewed as a multiple-objective decision process under uncertainty. Water Resour. Res., 9(4), p. 1006-1021.

Neuman, S.P., Fogg, G.E. and Jacobson, E.A. 1980. A statistical approach to the inverse problem in aquifer hydrology, 2, case study. Water Resour. Res., 16(1), p. 33-58.

Neuman, S.P. and Yakowitz, S. 1979. A statistical approach to the inverse problem of aquifer hydrology, 1, theory. Water Resour. Res., 15 (4), p. 845-860.

New Mexico State Engineer Office, 1956. Progress report on the ground-water resources of the Mimbres Valley, Luna County; in the Twenty-Second Biennial Report of the State Engineer of New Mexico.

Reeves, C.C. 1969. Pluvial Lake Palomas Northwestern Chihuahua, Mexico. New Mexico Geological Society, Twentieth Field Conference, p. 143-153.

Sammis, T.W. 1979. Consumptive use and yields of crops in Dona Ana County. New Mexico Water Resources Research Institute, Technical Report No. 127, New Mexico State University, Las Cruces, New Mexico.

Seager, W.R., 1982. State Geological Highway Map, New Mexico Bureau of Mines and Mineral Resources, Socorro.

Seager, W.R. 1983. Laramide wrench faults, basement-cored uplifts, and complimentary basins in southern New Mexico. New Mexico Geology, v. 5, no. 4, p. 69-76.

Seager, W.R., et al. 1984. New K-Ar dates from basalts and the evolution of the southern Rio Grande rift. Geological Society of America Bulletin, v. 95, p. 87-99.

Swanberg, C.A., et al. 1981. Electrical exploration and geothermal gradient studies near Columbus, New Mexico. New Mexico Energy and Minerals Department and New Mexico Energy Institute at New Mexico State University, EMD proj. no. 2-68-2204.

Sykes, J.F., Wilson, J.L. and Andrews, R.W. 1985. Sensitivity analysis for steady state groundwater flow using adjoint operators. Water Resour. Res., 21(3), p. 359-371.

Townley, L.R. 1983. Numerical models of groundwater flow: prediction and parameter estimation in the presence of uncertainty. Ph.D. thesis, Dep. of Civ. Eng., Mass. Inst. Technol., Cambridge, Mass.

Townley, L.R. and Wilson, J.L. 1985. CERT documentation and user's manual. Open-file report at the New Mexico Institute of Mining and Technology, Hydrology Program. Submitted to ONWI.

Townley, L.R. and Wilson, J.L. 1985. Computational efficient algorithms for parameter estimation of uncertainty in numerical models of groundwater flow. Water Resour. Res., 21 (12), p. 1851-1860.

Walton, W.C. 1970. Groundwater resources evaluation. McGraw Hill, New York.

Wilson, J.L. and Dettinger, M. 1979. State versus transient parameter estimation in groundwater systems. In proceedings of Verification of Mathematical and Physical Models in Hydrologic Engineering, 26th Annual Hydrologic Division Conference, ASCE.

Wilson, J.L., et al. 1979. Mathematical development and verification of a finite element aquifer flow model AQUIFEM-1. Technical Report 248, p. 114, Ralph M. Parsons Lab, Mass. Inst. Tech., Cambridge, Mass.

Wilson, J.L. and Harper, W. 1983. Evaluation prediction uncertainty in performance assessment: far field flow at bedded salt sites. Proceeding of 5th Ann. Civilian Radioactive Waste Management Information. Meeting, U.S. D.O.E., Washington, D.C.

Wilson, J.W. and Metcalf, D.E. 1985. Illustration and verification of adjoint sensitivity theory for steady state groundwater flow. Water Resour. Res., 21(11), p. 1602-1610.

Yeh, W. 1986. Review of parameter identification procedures in groundwater hydrology: the inverse problem. Water Resour. Res., 22(2), p. 95-108.

APPENDIX I

Well Hydrographs

The well numbering system used in New Mexico is shown in fig. I-1. The identification numbers for the Columbus Basin wells are abbreviated. For example, well number T26S.R7W.24.424 is listed as 26.7.24.424. The abbreviation is not ambiguous because all of the wells in the Columbus Basin have South townships and West ranges.

Well hydrographs for the 139 wells used in the Columbus Basin study, plus the hydrographs of 12 additional wells that would have been used if their measurements were not post 1975, are shown on pages 216 to 241. The hydrographs shown are those which remained after the screening process explained in the "Observed Head Data" section of this report. The CERT well location number is shown in the bottom left-hand corner of each plot.

The reported depths for the Columbus Basin wells are provided in table I-1. Individual head measurements which were deleted (not shown on hydrographs) or given a higher variance are listed in table I-2. The criteria for deletion or assignment of an increased variance are listed in the next section of this appendix, following the hydrographics, on page 242.

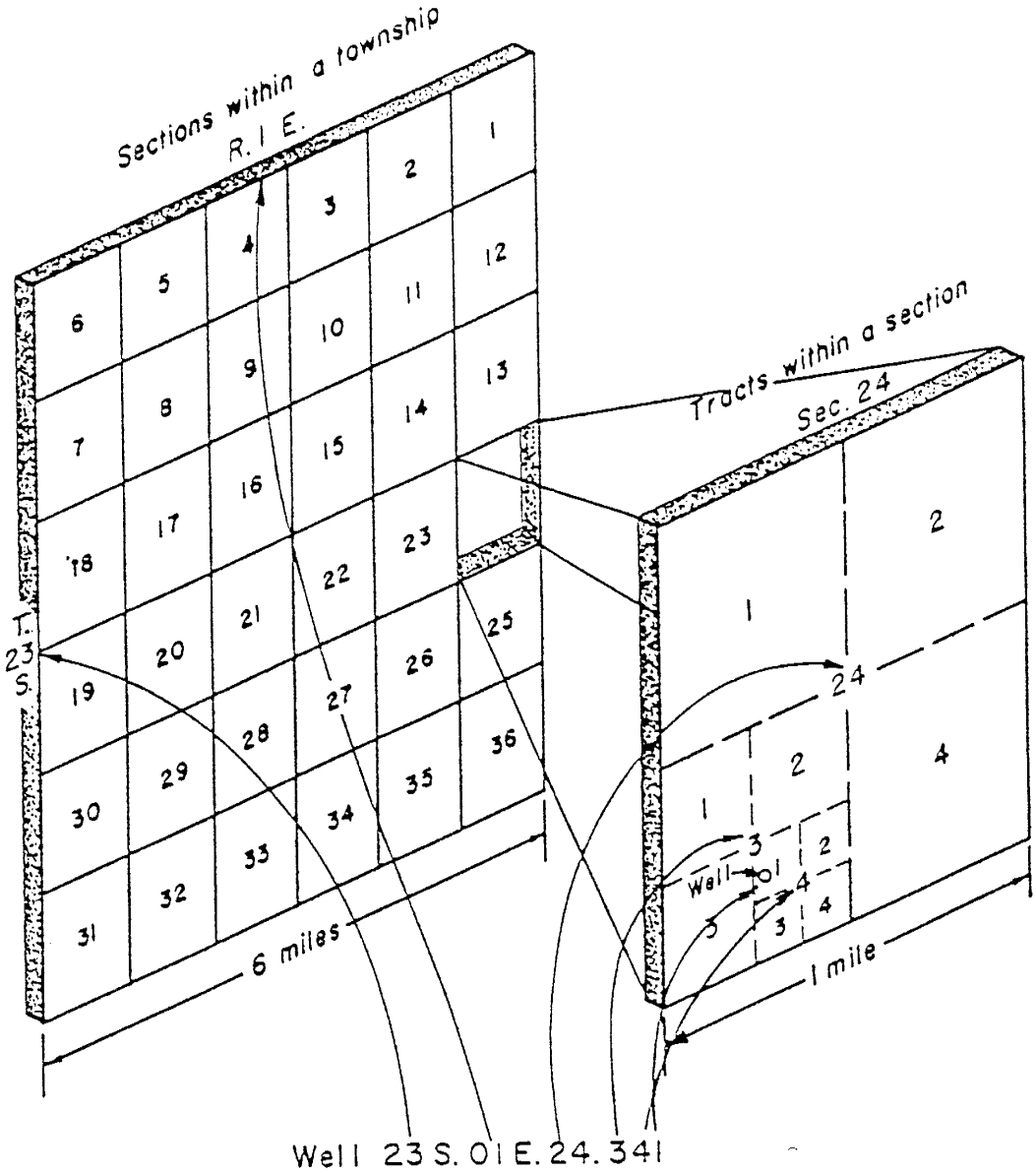

Fig. I-1. System of numbering wells in New Mexico.

Table I-1

Reported well depths for Columbus Basin study

Location No.	Depth (ft.)	Location No.	Depth (ft.)
26.6.24.111	108	27.8.15.131	510
26.7.24.424	600	27.8.15.212	495
26.7.26.244	147	27.8.18.121	186
26.8.19.141	160	27.8.18.121	200
26.8.30.112	100	27.8.18.121	186
26.8.30.112	325	27.8.18.123	207
27.5.30.223	320	27.8.22.113	480
27.6.10.100	920	27.8.22.133	406
27.6.26.120	910	27.8.25.111	650
27.6.31.333	230	27.8.25.131	530
27.7.2.111	138	27.8.25.231	614
27.7.17.444	210	27.8.25.231	668
27.2.19.133	1000	27.8.25.411	596
27.7.19.311	400	27.8.26.311	605
27.7.25.111	700	27.8.27.412	315
27.7.30.311	308	27.8.32.440	296
27.7.30.311	600	27.8.35.113	605
27.7.31.211	595	27.8.35.113	600
27.7.31.231	100	27.8.35.122	550
27.7.31.411	595	27.8.35.321	470
27.8.5.100	31	27.8.36.111	493
27.8.5.131	550	27.9.1.431	62
27.8.5.132	417	27.9.2.211	23
27.8.5.134	500	27.9.2.431	47
27.8.5.144	60	27.9.3.421	46
27.8.5.312	500	27.9.11.121	82
27.8.5.323	500	27.9.12.111	29
27.8.5.341	60	27.9.12.143	230
27.8.6.331	750	27.9.12.212	340
27.8.7.111	46	27.9.12.243	60
27.8.7.313	195	27.9.12.424	66
27.8.8.111	205	28.6.10.311	300
27.8.8.122	300	28.7.6.311	744
27.8.8.211	30	28.7.8.341	900
27.8.8.311	413	28.7.9.411	720
27.8.8.331	91	28.7.11.244	154
27.8.8.411	38	28.7.17.411	585
27.8.14.333	113	28.7.19.133	500
28.7.19.141	922	28.8.26.111	650
28.7.19.220	627	28.8.26.222	700
28.7.20.311	630	28.8.26.242	696
28.7.20.411	692	28.8.26.322	594
28.7.20.422	545	28.8.26.411	300
28.7.20.422	532	28.8.35.211	420
28.7.21.211	488	28.8.35.211	400
28.7.22.111	850	28.8.36.111	270
28.7.22.111	500	28.8.36.133	608
28.7.22.311	917	28.8.36.143	630
28.7.28.124	723	28.8.36.411	450
28.7.29.139	804	29.7.4.111	185
28.7.29.211	574	29.7.12.222	130
28.7.29.211	610	29.7.18.211	180
28.7.29.422	825	29.8.2.111	711
28.7.30.213	1000	29.8.3.311	266
28.7.30.411	815	29.8.4.210	190
28.7.30.443	1000	29.8.9.411	400
28.8.1.121	750	29.8.9.411	96
28.8.2.111	503	29.8.10.422	500
28.8.9.412	240	29.8.11.113	132
28.8.24.110	628	29.8.11.121	200
28.8.24.131	602	29.8.12.244	180
28.8.24.211	711	29.8.13.111	180
28.8.24.311	628	29.8.14.312	408
28.8.25.111	775	29.8.17.231	325
28.8.25.211	529	29.8.18.231	312
28.8.25.311	605		

Table I-2

Head measurments deleted (asterisks) or assigned an increased variance for Columbus Basin study

Well Location No.	Time of Measurment	Criterion for Deletion
26.8.30.112	73,74,75,76	3, possibly 4
27.7.30.311	*73	4
27.8.8.111	*82	4
27.8.25.231	53,59	4
27.8.26.422	82	3, possibly 4
27.8.35.113	*79	4
28.7.17.411	60	3, possibly 4
28.7.22.111	62,63	3, possibly 4
28.7.29.211	82	3, possibly 4
28.8.2.111	*79,82	4
28.8.25.211	*77	4
28.8.25.311	*77	4
28.8.26.322	77,78,79,80,81,82	3

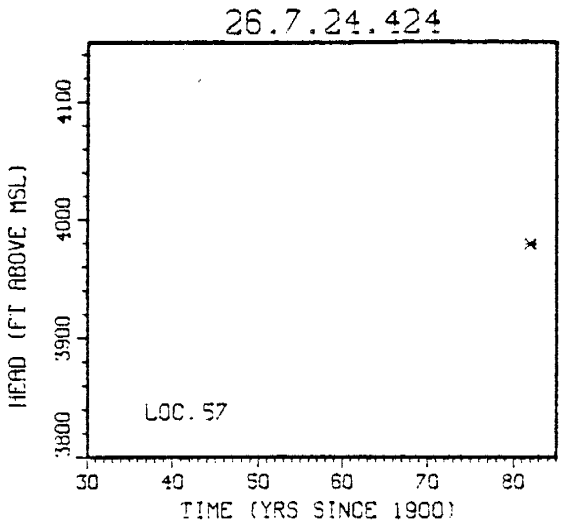
26.7.24.424
HEAD (FT ABOVE MSL)
4100
4000
3900
3800
LOC.57
30
40
50
60
70
80
TIME (YRS SINCE 1900)

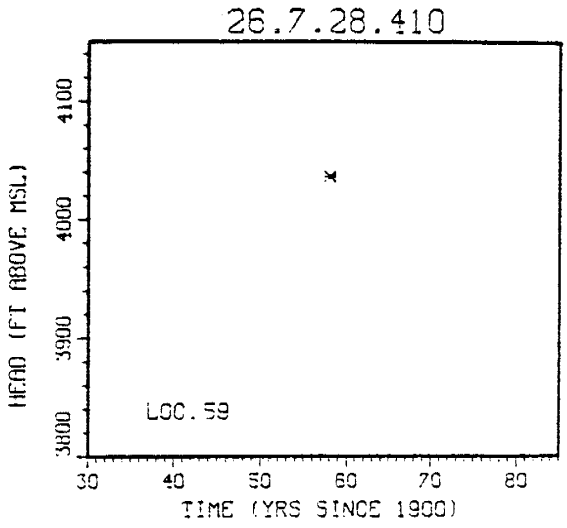
26.7.28.410
HEAD (FT ABOVE MSL)
4100
4000
3900
3800
LOC.59
30
40
50
60
70
80
TIME (YRS SINCE 1900)

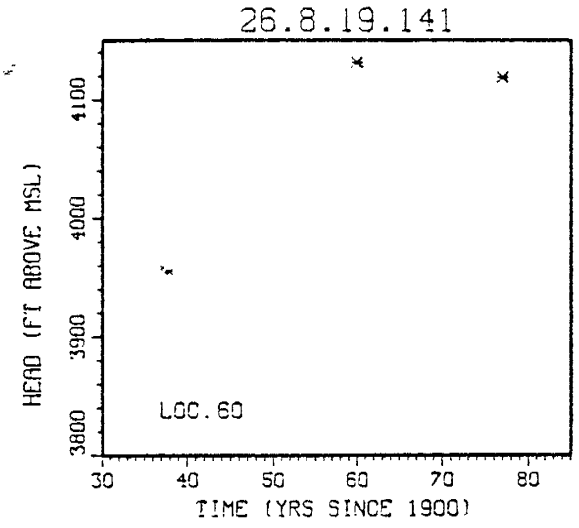
26.8.19.141
HEAD (FT ABOVE MSL)
4100
4000
3900
3800
LOC.60
30
40
50
60
70
80
TIME (YRS SINCE 1900)

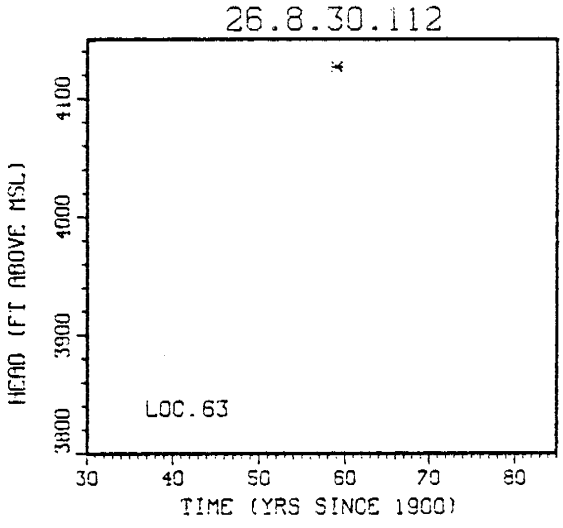
26.8.30.112
HEAD (FT ABOVE MSL)
4100
4000
3900
3800
LOC.63
30
40
50
60
70
80
TIME (YRS SINCE 1900)

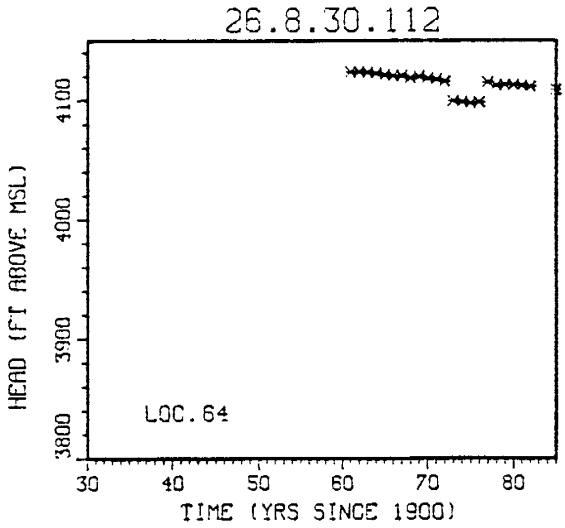
26.8.30.112
HEAD (FT ABOVE MSL)
4100
4000
3900
3800
LOC.64
30
40
50
60
70
80
TIME (YRS SINCE 1900)

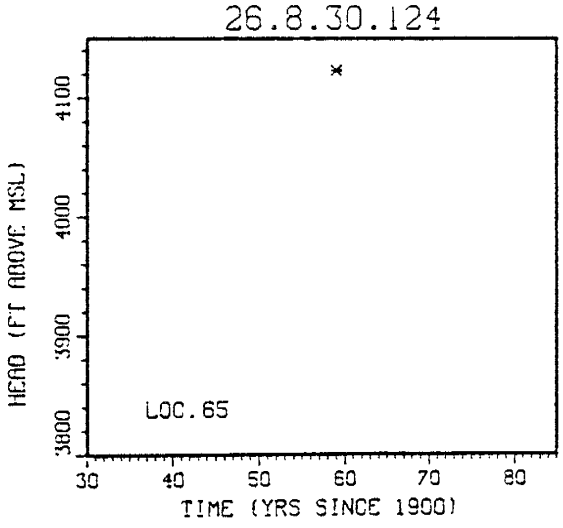
26.8.30.124
HEAD (FT ABOVE MSL)
4100
4000
3900
3800
LOC.65
30
40
50
60
70
80
TIME (YRS SINCE 1900)

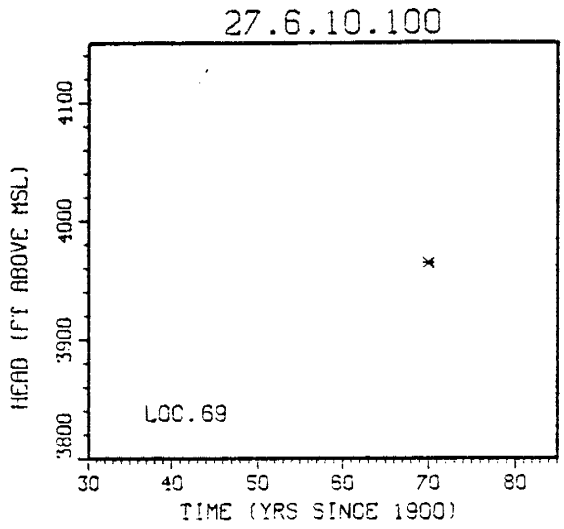
27.6.10.100
HEAD (FT ABOVE MSL)
4100
4000
3900
3800
LOC.69
30
40
50
60
70
80
TIME (YRS SINCE 1900)

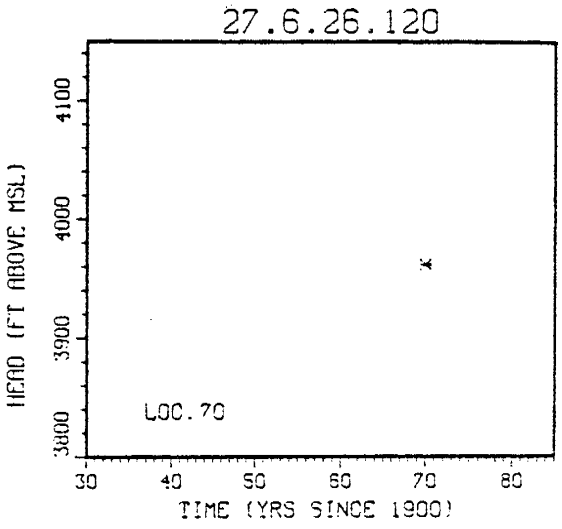
27.6.26.120
HEAD (FT ABOVE MSL)
4100
4000
3900
3800
LOC.70
30
40
50
60
70
80
TIME (YRS SINCE 1900)

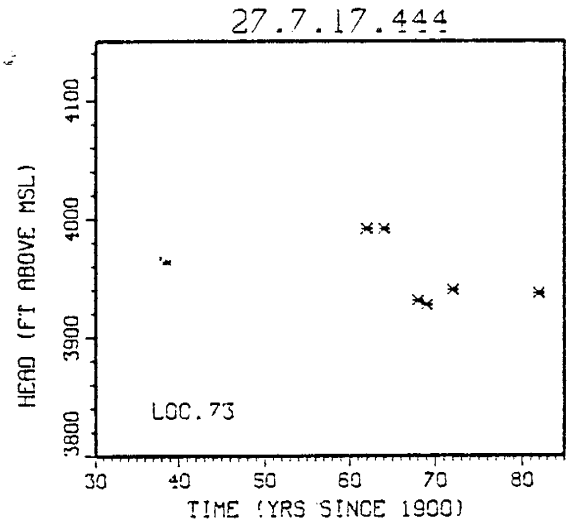
27.7.17.444
HEAD (FT ABOVE MSL)
4100
4000
3900
3800
LOC.73
30
40
50
60
70
80
TIME (YRS SINCE 1900)

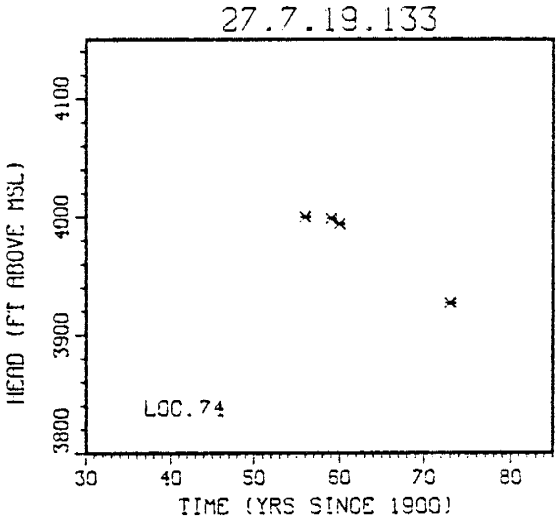
27.7.19.133
HEAD (FT ABOVE MSL)
4100
4000
3900
3800
LOC.74
30
40
50
60
70
80
TIME (YRS SINCE 1900)

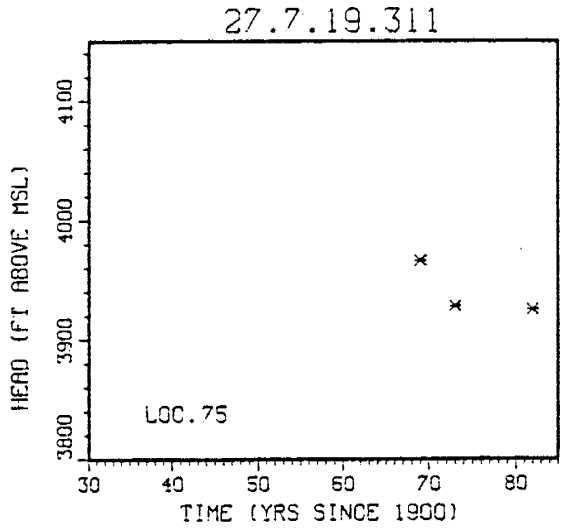
27.7.19.311
HEAD (FT ABOVE MSL)
4100
4000
3900
3800
LOC.75
30
40
50
60
70
80
TIME (YRS SINCE 1900)

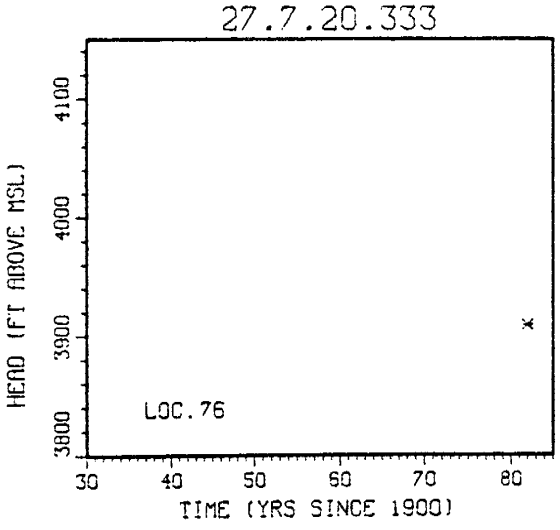
27.7.20.333
HEAD (FT ABOVE MSL)
4100
4000
3900
3800
LOC.76
30
40
50
60
70
80
TIME (YRS SINCE 1900)

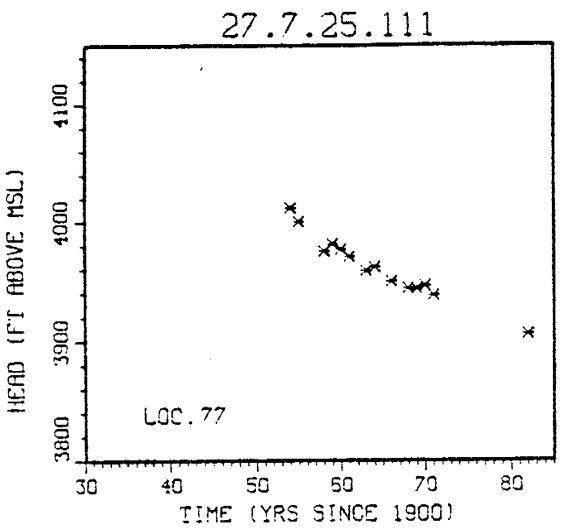
27.7.25.111
HEAD (FT ABOVE MSL)
4100
4000
3900
3800
LOC.77
30
40
50
60
70
80
TIME (YRS SINCE 1900)

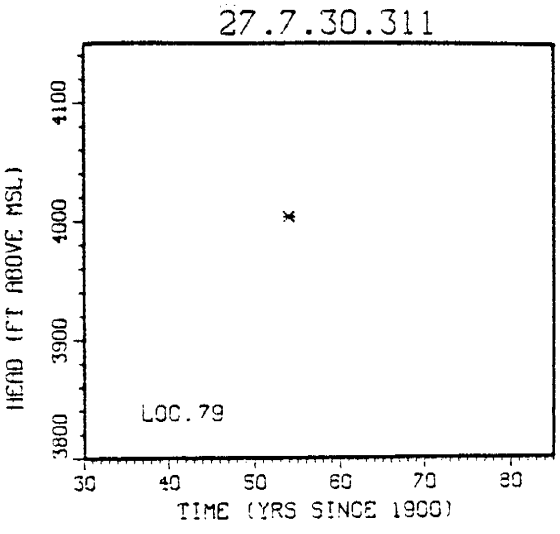
27.7.30.311
HEAD (FT ABOVE MSL)
4100
4000
3900
3800
LOC.79
30
40
50
60
70
80
TIME (YRS SINCE 1900)

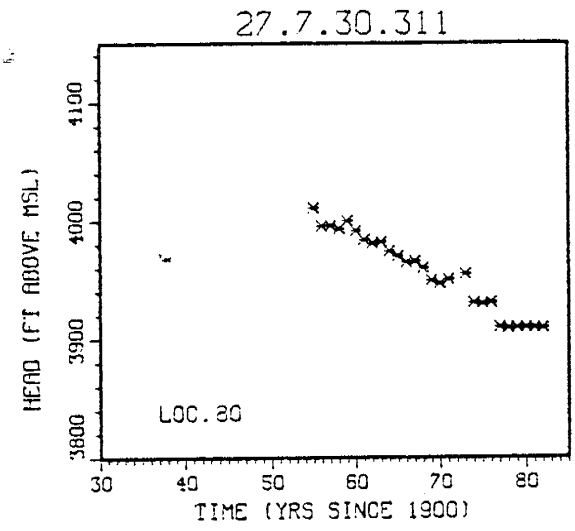
27.7.30.311
HEAD (FT ABOVE MSL)
4100
4000
3900
3800
LOC.80
30
40
50
60
70
80
TIME (YRS SINCE 1900)

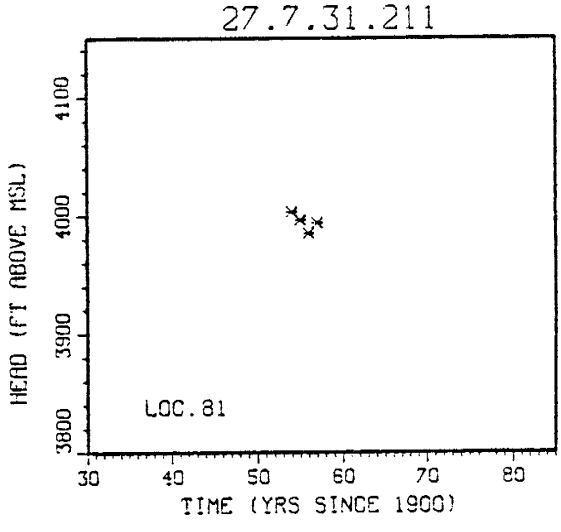
27.7.31.211
HEAD (FT ABOVE MSL)
4100
4000
3900
3800
LOC.81
30
40
50
60
70
80
TIME (YRS SINCE 1900)

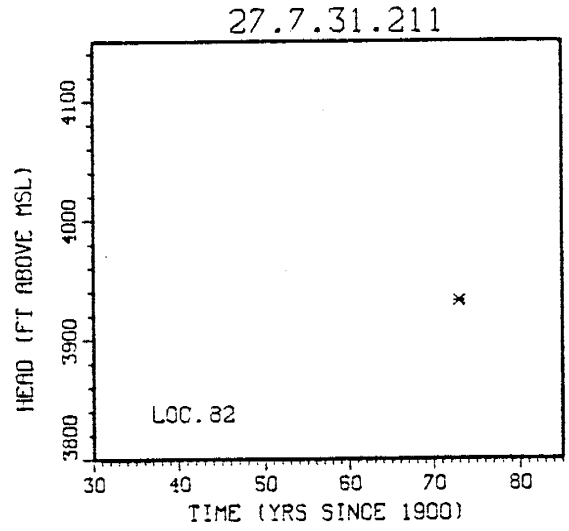
27.7.31.211
HEAD (FT ABOVE MSL)
4100
4000
3900
3800
LOC.82
30
40
50
60
70
80
TIME (YRS SINCE 1900)

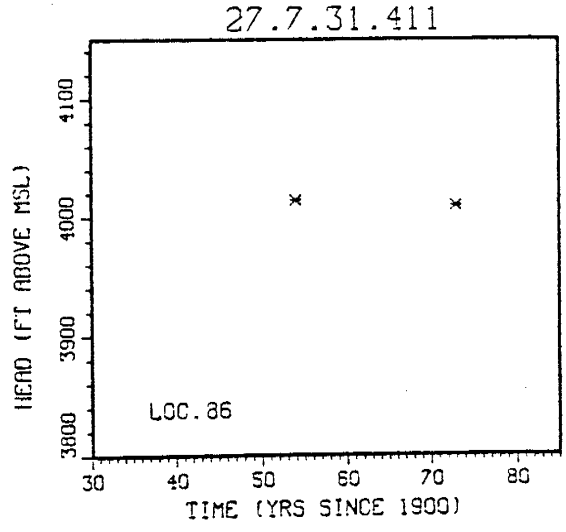
27.7.31.411
HEAD (FT ABOVE MSL)
4100
4000
3900
3800
LOC.86
30
40
50
60
70
80
TIME (YRS SINCE 1900)

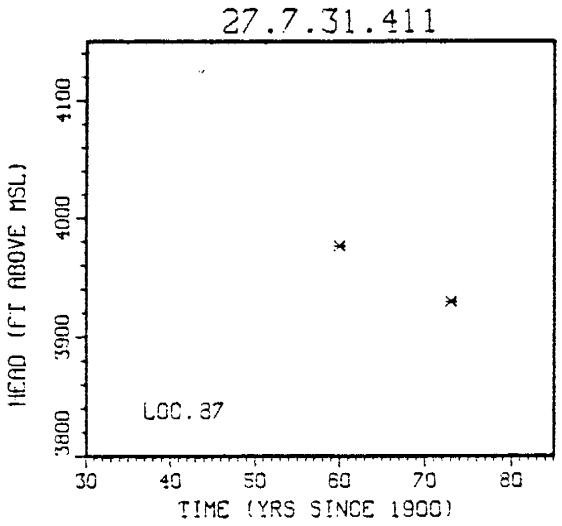
27.7.31.411
HEAD (FT ABOVE MSL)
4100
4000
3900
3800
LOC.87
30
40
50
60
70
80
TIME (YRS SINCE 1900)

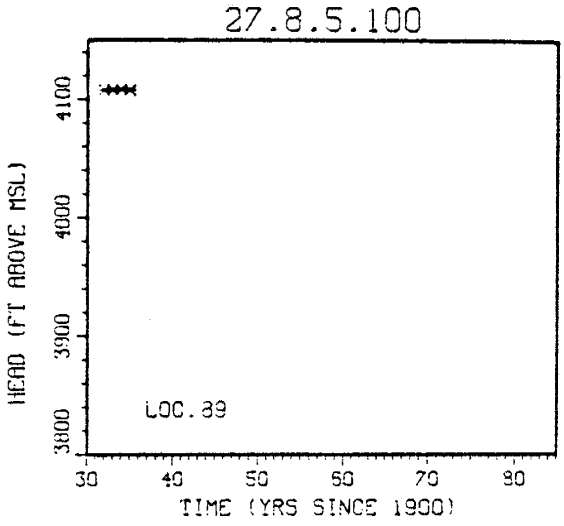
27.8.5.100
HEAD (FT ABOVE MSL)
4100
4000
3900
3800
LOC.89
30
40
50
60
70
80
TIME (YRS SINCE 1900)

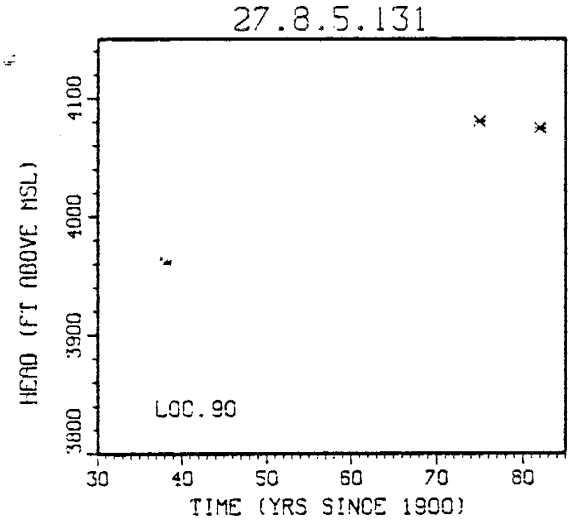
27.8.5.131
HEAD (FT ABOVE MSL)
4100
4000
3900
3800
LOC.90
30
40
50
60
70
80
TIME (YRS SINCE 1900)

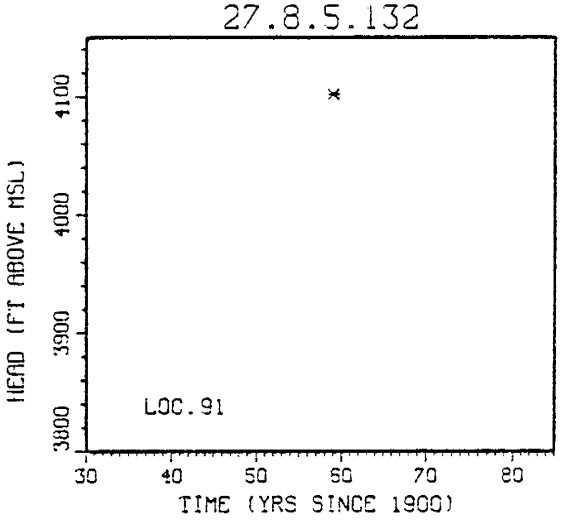
27.8.5.132
HEAD (FT ABOVE MSL)
4100
4000
3900
3800
LOC.91
30
40
50
60
70
80
TIME (YRS SINCE 1900)

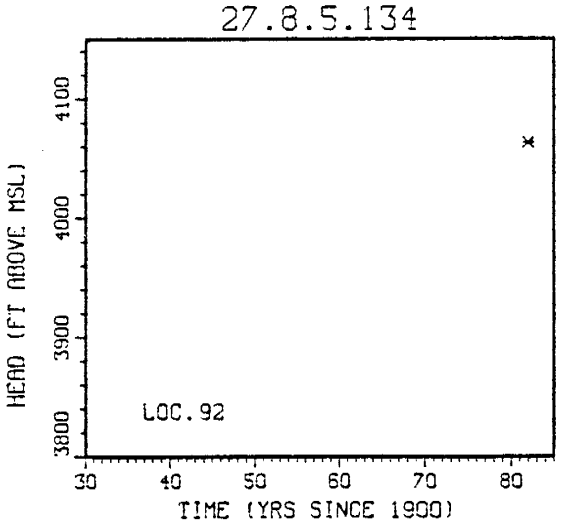
27.8.5.134
HEAD (FT ABOVE MSL)
4100
4000
3900
3800
LOC.92
30
40
50
60
70
80
TIME (YRS SINCE 1900)

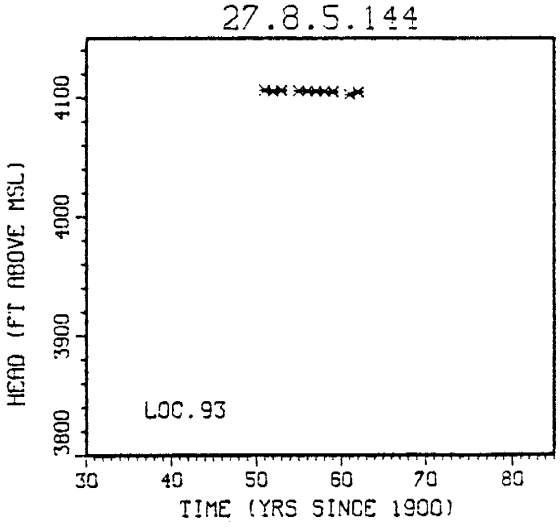
27.8.5.144
HEAD (FT ABOVE MSL)
4100
4000
3900
3800
LOC.93
30
40
50
60
70
80
TIME (YRS SINCE 1900)

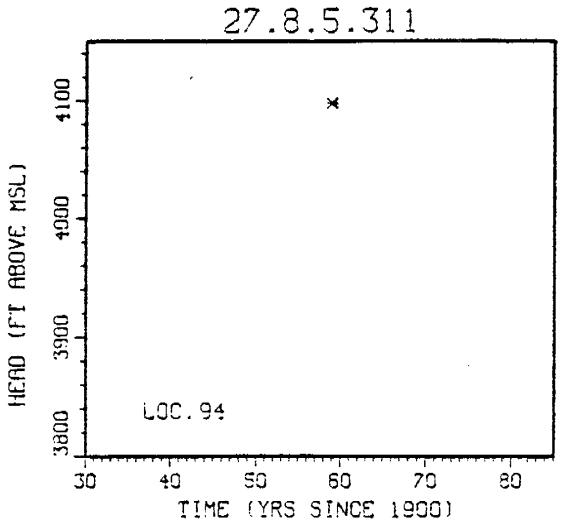
27.8.5.311
HEAD (FT ABOVE MSL)
4100
4000
3900
3800
LOC.94
30
40
50
60
70
80
TIME (YRS SINCE 1900)

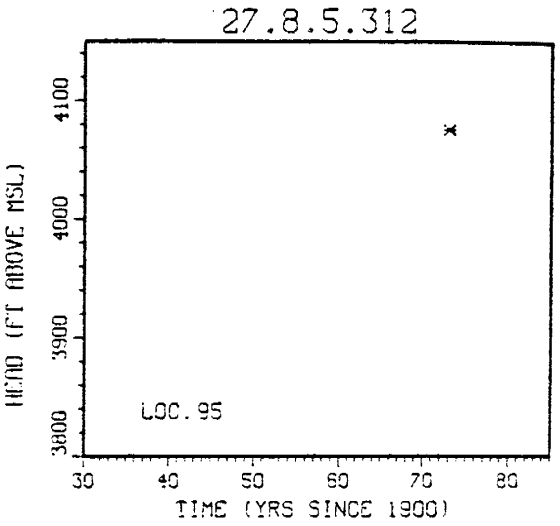
27.8.5.312
HEAD (FT ABOVE MSL)
4100
4000
3900
3800
LOC.95
30
40
50
60
70
80
TIME (YRS SINCE 1900)

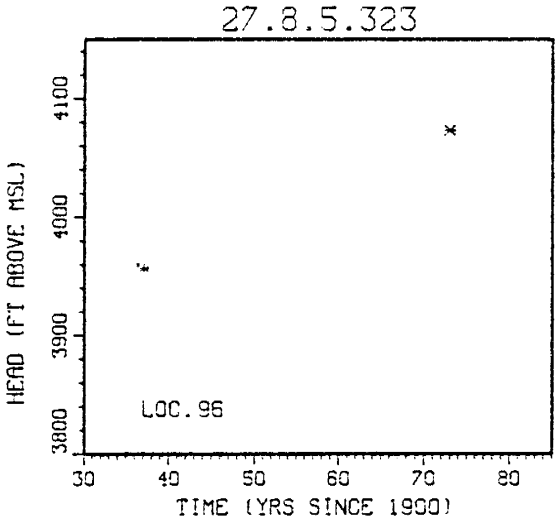
27.8.5.323
HEAD (FT ABOVE MSL)
4100
4000
3900
3800
LOC.96
30
40
50
60
70
80
TIME (YRS SINCE 1900)

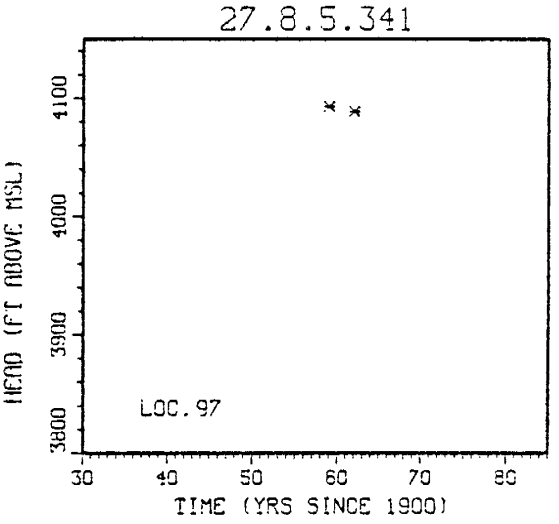
27.8.5.341
HEAD (FT ABOVE MSL)
4100
4000
3900
3800
LOC.97
30
40
50
60
70
80
TIME (YRS SINCE 1900)

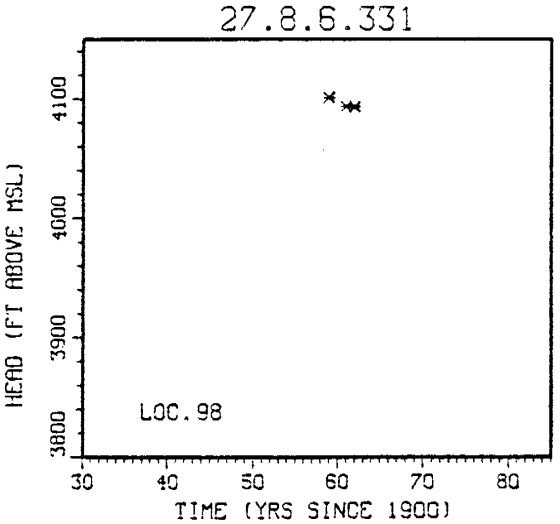
27.8.6.331
HEAD (FT ABOVE MSL)
4100
4000
3900
3800
LOC.98
30
40
50
60
70
80
TIME (YRS SINCE 1900)

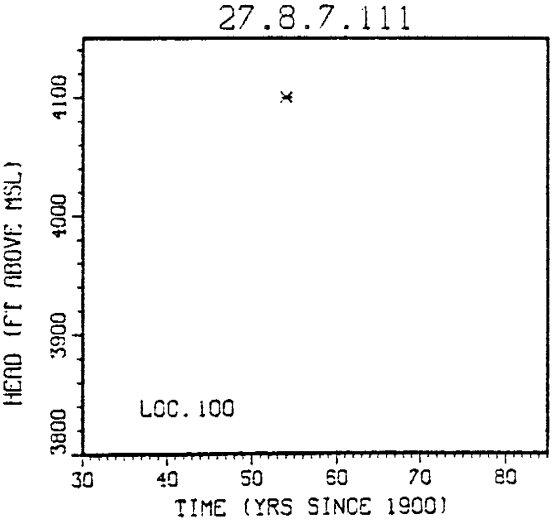
27.8.7.111
HEAD (FT ABOVE MSL)
4100
4000
3900
3800
LOC.100
30
40
50
60
70
80
TIME (YRS SINCE 1900)

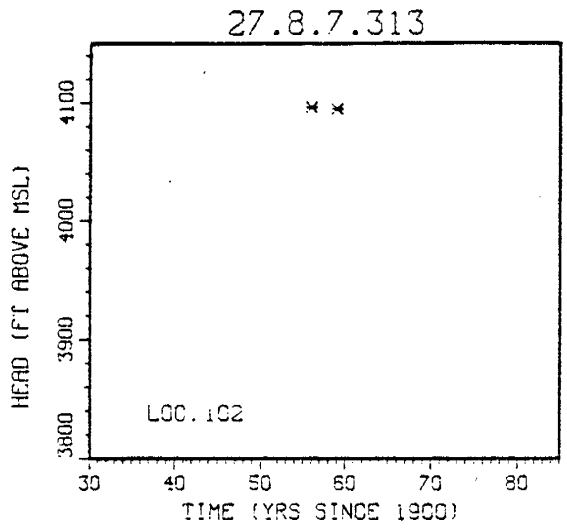
27.8.7.313
HEAD (FT ABOVE MSL)
4100
4000
3900
3800
LOC.102
30
40
50
60
70
80
TIME (YRS SINCE 1900)

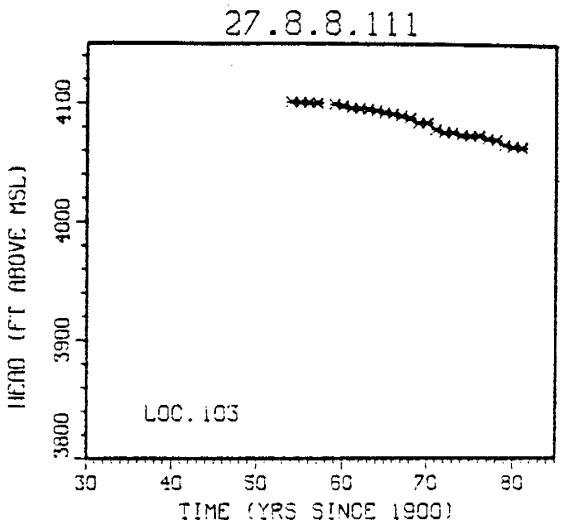
27.8.8.111
HEAD (FT ABOVE MSL)
4100
4000
3900
3800
LOC.103
30
40
50
60
70
80
TIME (YRS SINCE 1900)

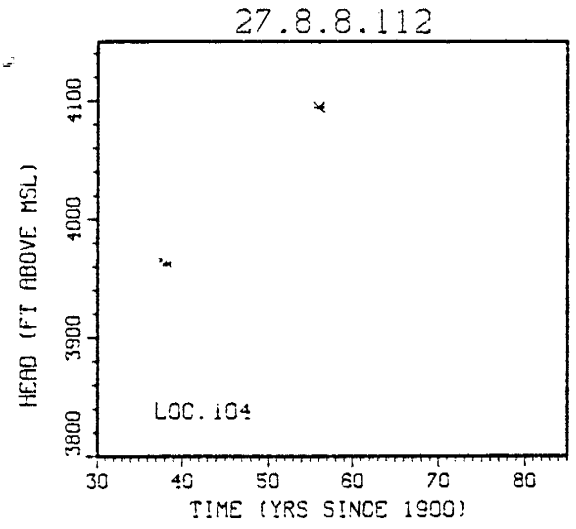
27.8.8.112
HEAD (FT ABOVE MSL)
4100
4000
3900
3800
LOC.104
30
40
50
60
70
80
TIME (YRS SINCE 1900)

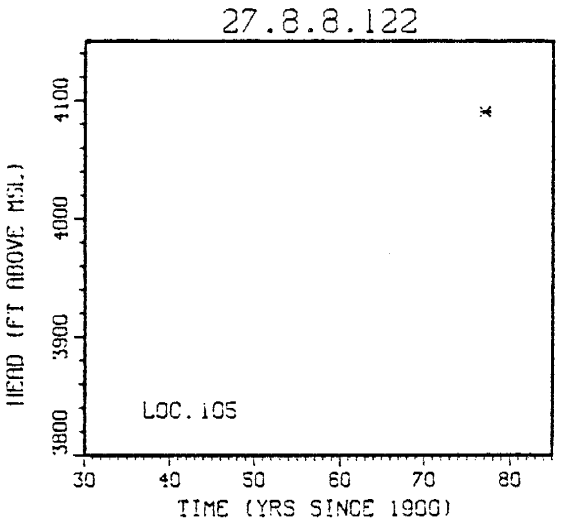
27.8.8.122
HEAD (FT ABOVE MSL)
4100
4000
3900
3800
LOC.105
30
40
50
60
70
80
TIME (YRS SINCE 1900)

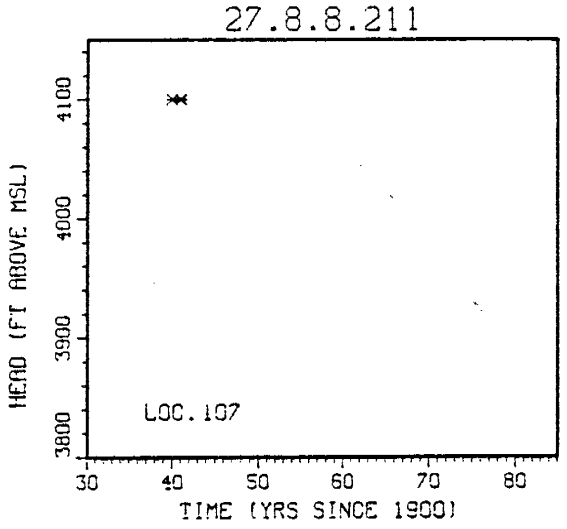
27.8.8.211
HEAD (FT ABOVE MSL)
4100
4000
3900
3800
LOC.107
30
40
50
60
70
80
TIME (YRS SINCE 1900)

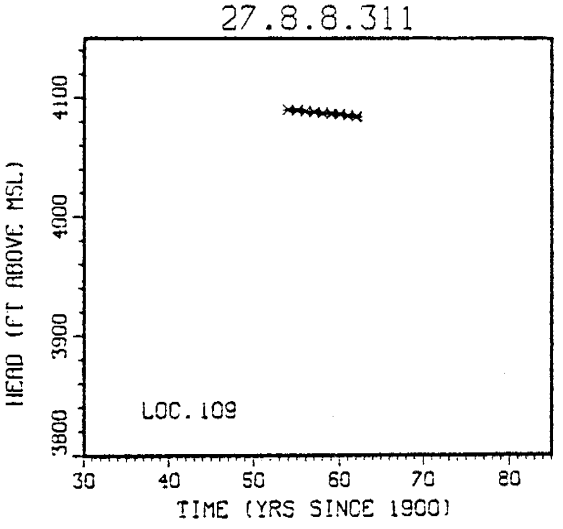
27.8.8.311
HEAD (FT ABOVE MSL)
4100
4000
3900
3800
LOC.109
30
40
50
60
70
80
TIME (YRS SINCE 1900)

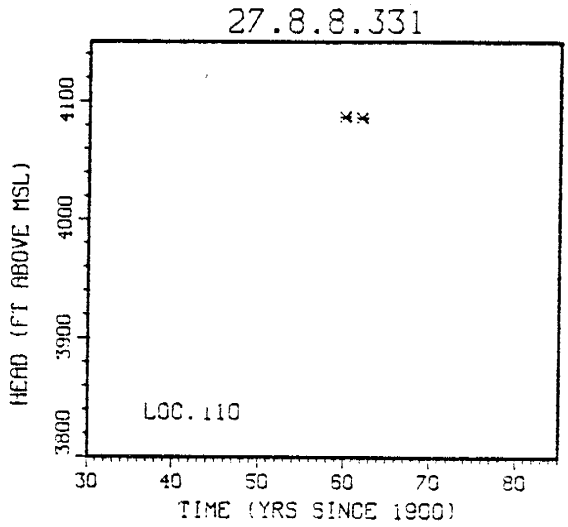
27.8.8.331
HEAD (FT ABOVE MSL)
4100
4000
3900
3800
LOC. 110
30
40
50
60
70
80
TIME (YRS SINCE 1900)

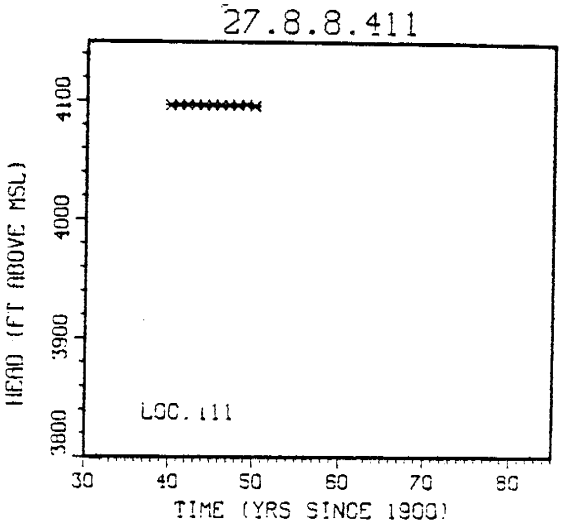
27.8.8.411
HEAD (FT ABOVE MSL)
4100
4000
3900
3800
LOC. 111
30
40
50
60
70
80
TIME (YRS SINCE 1900)

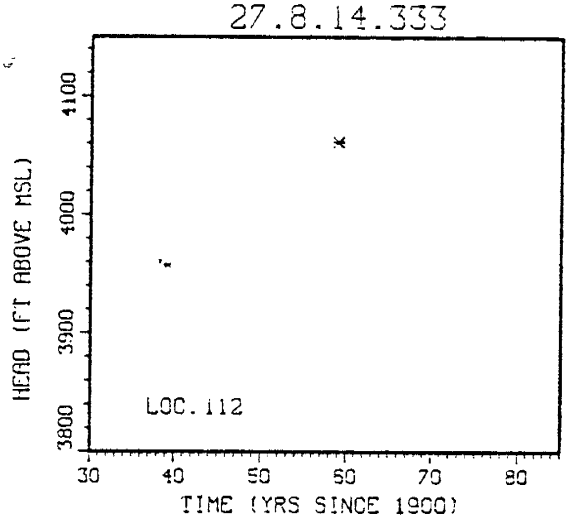
27.8.14.333
HEAD (FT ABOVE MSL)
4100
4000
3900
3800
LOC. 112
30
40
50
60
70
80
TIME (YRS SINCE 1900)

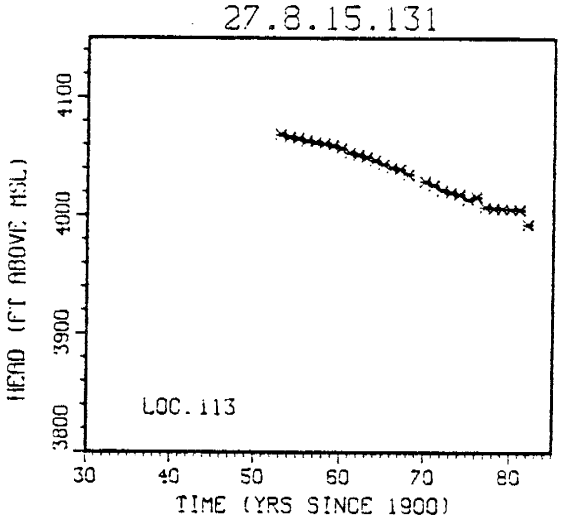
27.8.15.131
HEAD (FT ABOVE MSL)
4100
4000
3900
3800
LOC. 113
30
40
50
60
70
80
TIME (YRS SINCE 1900)

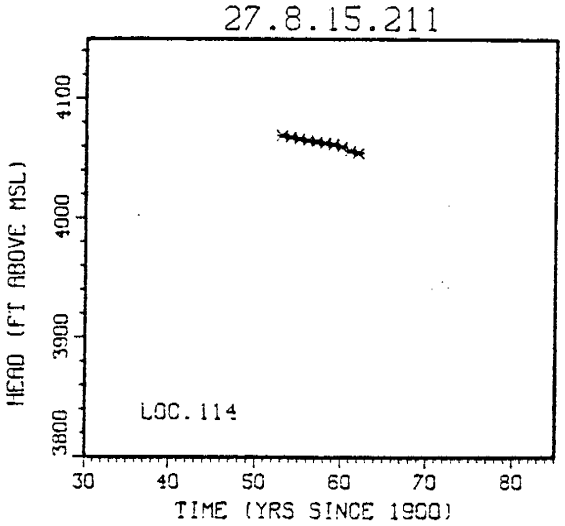
27.8.15.211
HEAD (FT ABOVE MSL)
4100
4000
3900
3800
LOC. 114
30
40
50
60
70
80
TIME (YRS SINCE 1900)

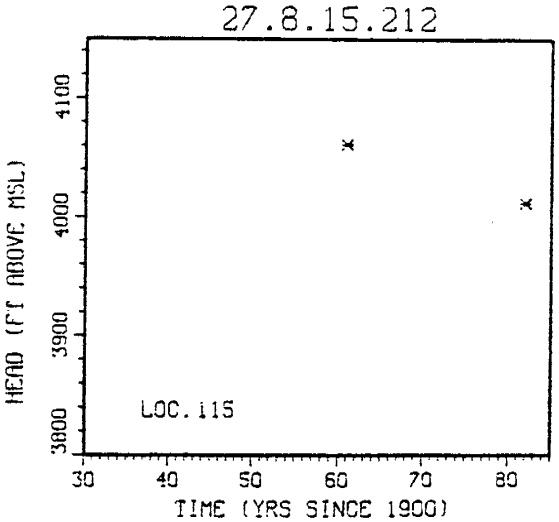
27.8.15.212
HEAD (FT ABOVE MSL)
4100
4000
3900
3800
LOC. 115
30
40
50
60
70
80
TIME (YRS SINCE 1900)

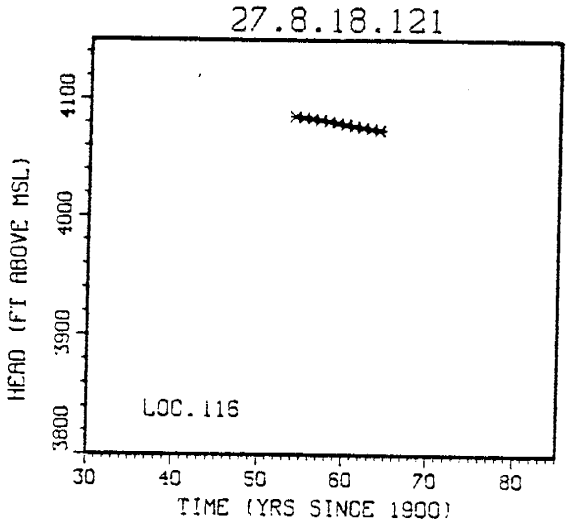
27.8.18.121
HEAD (FT ABOVE MSL)
4100
4000
3900
3800
LOC. 116
30
40
50
60
70
80
TIME (YRS SINCE 1900)

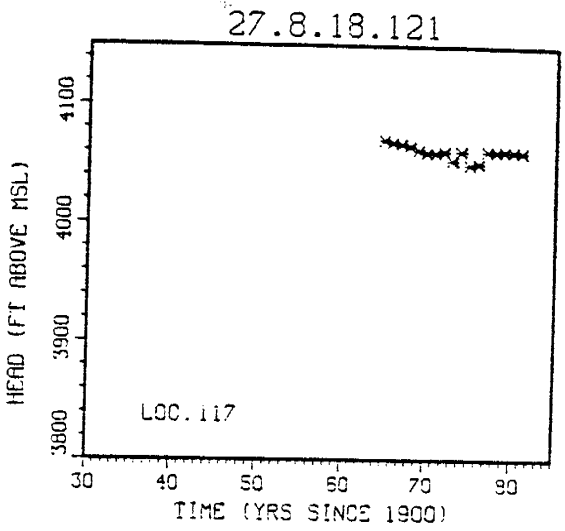
27.8.18.121
HEAD (FT ABOVE MSL)
4100
4000
3900
3800
LOC. 117
30
40
50
60
70
80
TIME (YRS SINCE 1900)

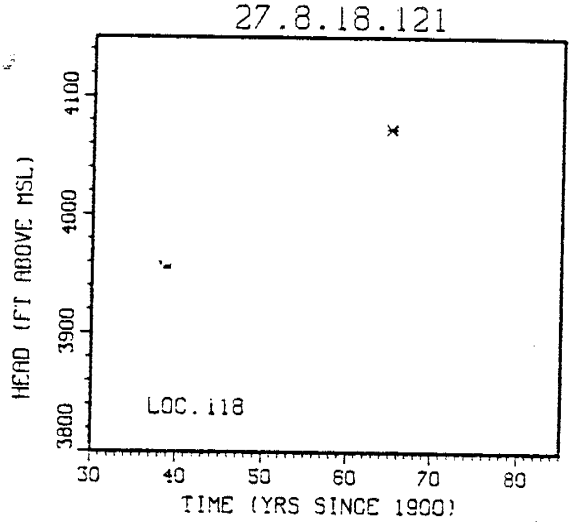
27.8.18.121
HEAD (FT ABOVE MSL)
4100
4000
3900
3800
LOC. 118
30
40
50
60
70
80
TIME (YRS SINCE 1900)

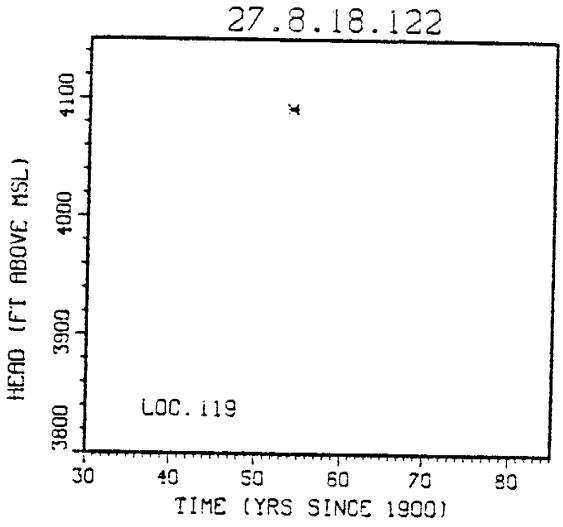
27.8.18.122
HEAD (FT ABOVE MSL)
4100
4000
3900
3800
LOC. 119
30
40
50
60
70
80
TIME (YRS SINCE 1900)

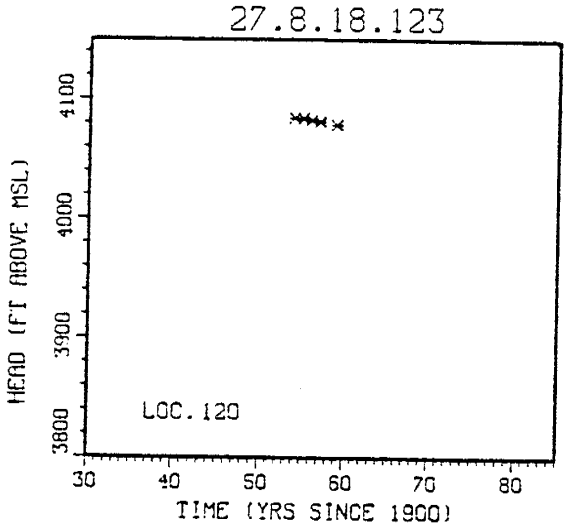
27.8.18.123
HEAD (FT ABOVE MSL)
4100
4000
3900
3800
LOC. 120
30
40
50
60
70
80
TIME (YRS SINCE 1900)

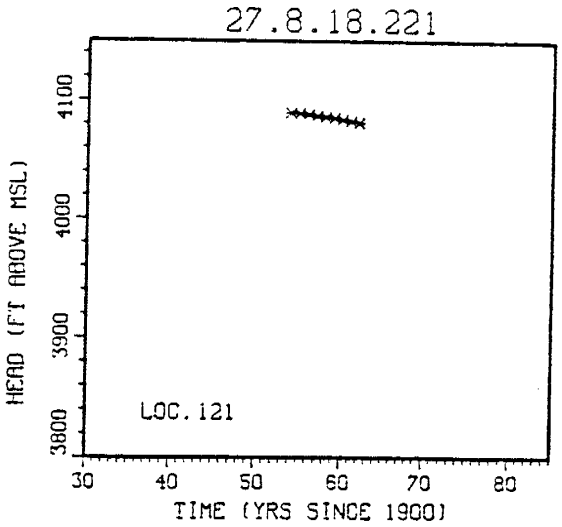
27.8.18.221
HEAD (FT ABOVE MSL)
4100
4000
3900
3800
LOC. 121
30
40
50
60
70
80
TIME (YRS SINCE 1900)

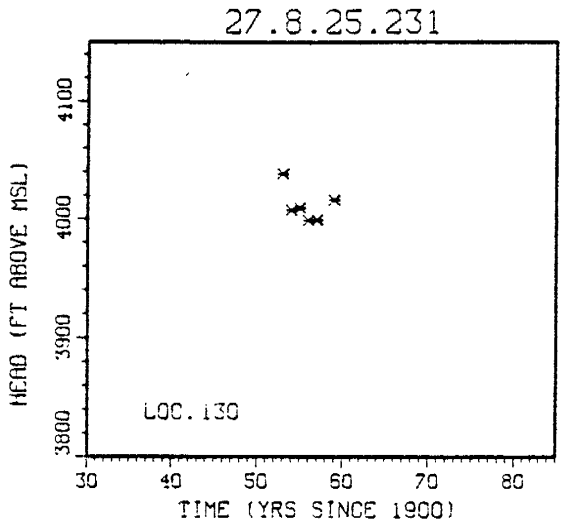
27.8.25.231
HEAD (FT ABOVE MSL)
4100
4000
3900
3800
LOC. 130
30
40
50
60
70
80
TIME (YRS SINCE 1900)

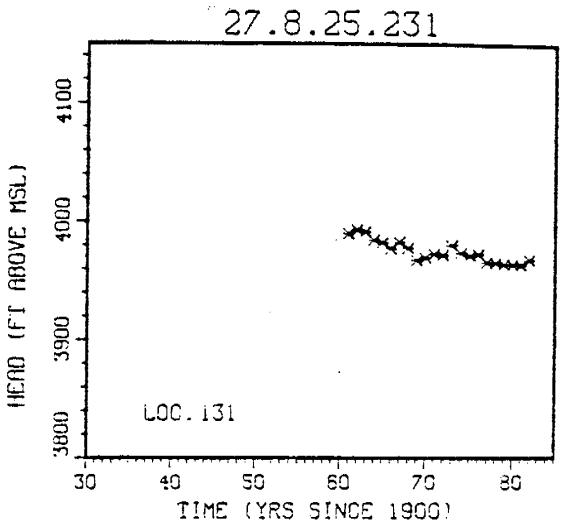
27.8.25.231
HEAD (FT ABOVE MSL)
4100
4000
3900
3800
LOC. 131
30
40
50
60
70
80
TIME (YRS SINCE 1900)

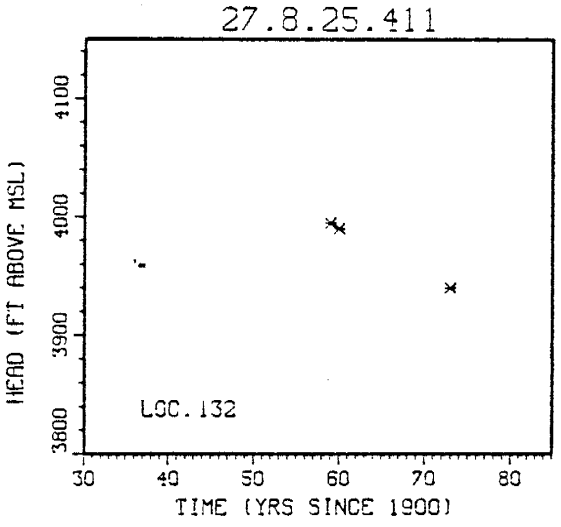
27.8.25.411
HEAD (FT ABOVE MSL)
4100
4000
3900
3800
LOC. 132
30
40
50
60
70
80
TIME (YRS SINCE 1900)

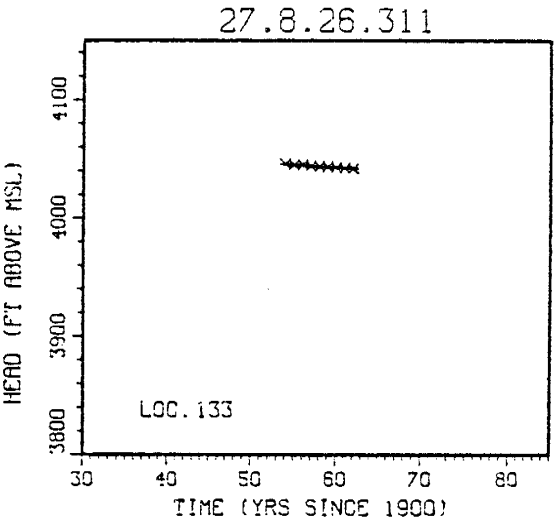
27.8.26.311
HEAD (FT ABOVE MSL)
4100
4000
3900
3800
LOC. 133
30
40
50
60
70
80
TIME (YRS SINCE 1900)

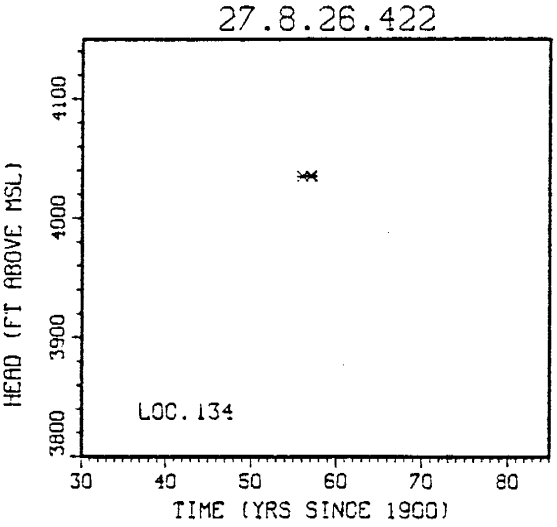
27.8.26.422
HEAD (FT ABOVE MSL)
4100
4000
3900
3800
LOC. 134
30
40
50
60
70
80
TIME (YRS SINCE 1900)

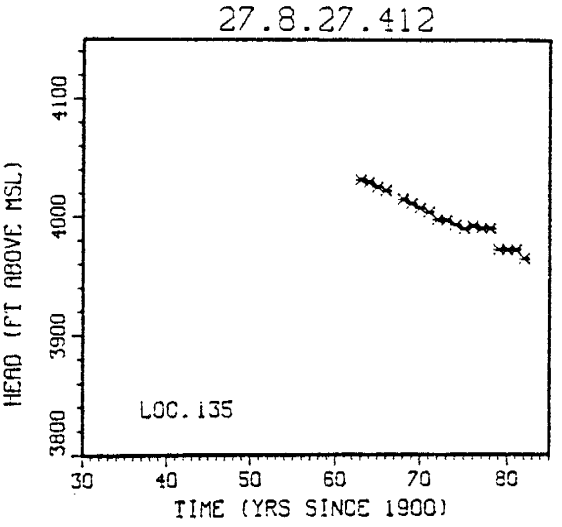
27.8.27.412
HEAD (FT ABOVE MSL)
4100
4000
3900
3800
LOC. 135
30
40
50
60
70
80
TIME (YRS SINCE 1900)

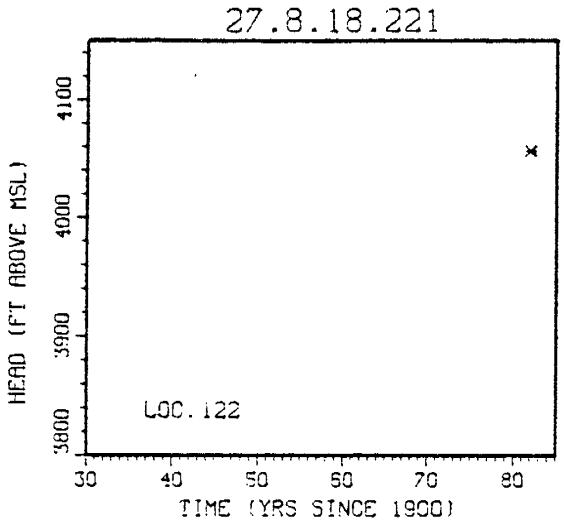
27.8.18.221
HEAD (FT ABOVE MSL)
4100
4000
3900
3800
LOC.122
30
40
50
60
70
80
TIME (YRS SINCE 1900)

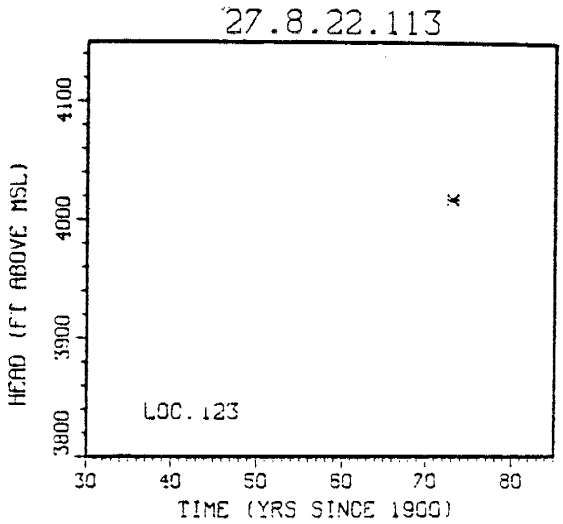
27.8.22.113
HEAD (FT ABOVE MSL)
4100
4000
3900
3800
LOC.123
30
40
50
60
70
80
TIME (YRS SINCE 1900)

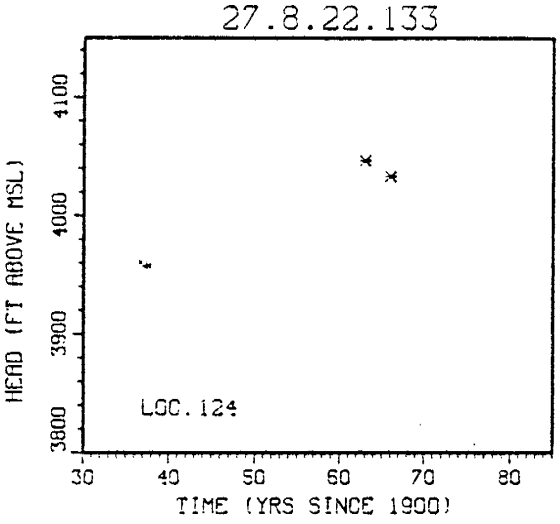
27.8.22.133
HEAD (FT ABOVE MSL)
4100
4000
3900
3800
LOC.124
30
40
50
60
70
80
TIME (YRS SINCE 1900)

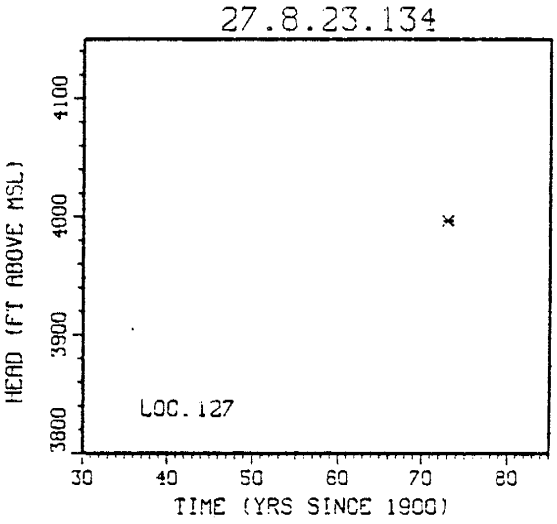
27.8.23.134
HEAD (FT ABOVE MSL)
4100
4000
3900
3800
LOC.127
30
40
50
60
70
80
TIME (YRS SINCE 1900)

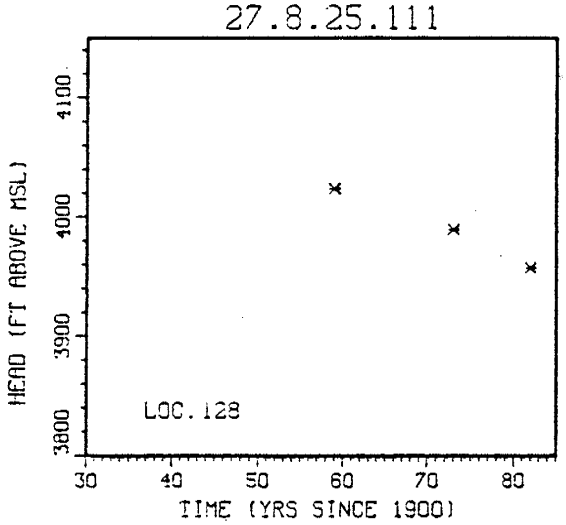
27.8.25.111
HEAD (FT ABOVE MSL)
4100
4000
3900
3800
LOC.128
30
40
50
60
70
80
TIME (YRS SINCE 1900)

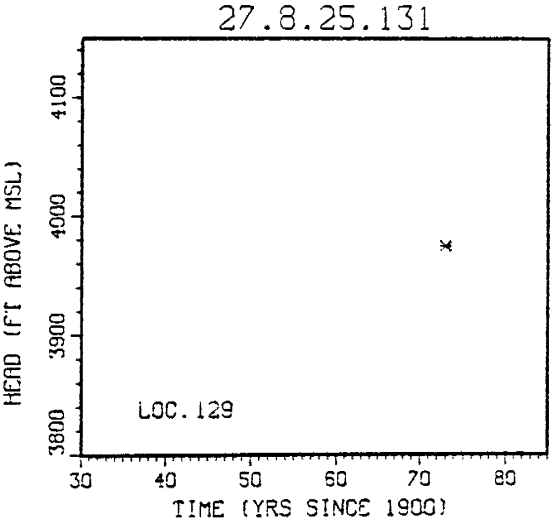
27.8.25.131
HEAD (FT ABOVE MSL)
4100
4000
3900
3800
LOC.129
30
40
50
60
70
80
TIME (YRS SINCE 1900)

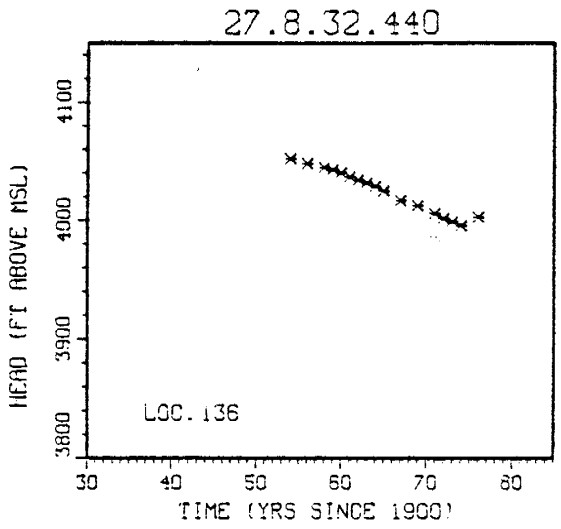
27.8.32.440
HEAD (FT ABOVE MSL)
4100
4000
3900
3800
LOC.136
30
40
50
60
70
80
TIME (YRS SINCE 1900)

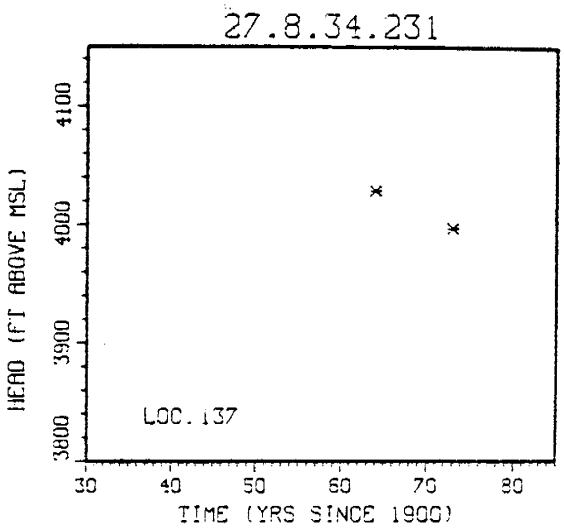
27.8.34.231
HEAD (FT ABOVE MSL)
4100
4000
3900
3800
LOC.137
30
40
50
60
70
80
TIME (YRS SINCE 1900)

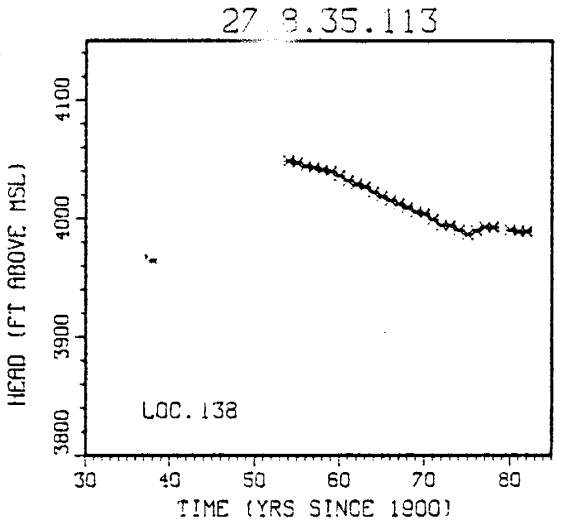
27.8.35.113
HEAD (FT ABOVE MSL)
4100
4000
3900
3800
LOC.138
30
40
50
60
70
80
TIME (YRS SINCE 1900)

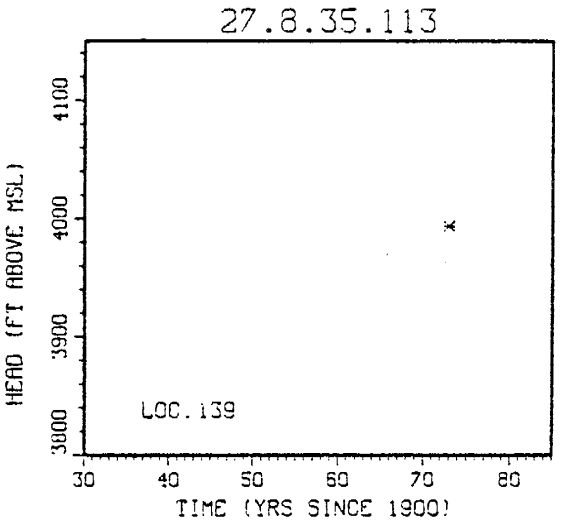
27.8.35.113
HEAD (FT ABOVE MSL)
4100
4000
3900
3800
LOC.139
30
40
50
60
70
80
TIME (YRS SINCE 1900)

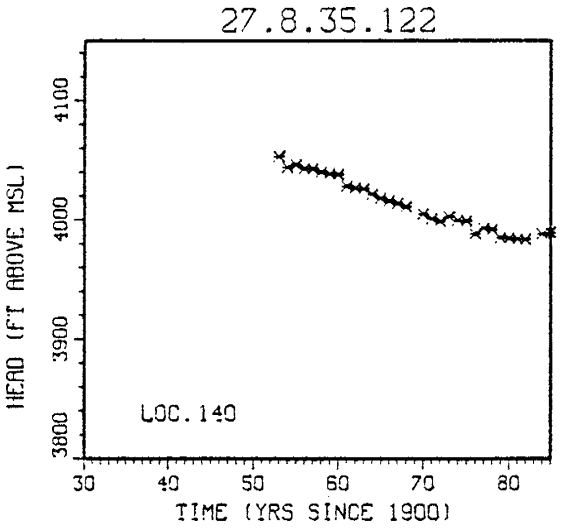
27.8.35.122
HEAD (FT ABOVE MSL)
4100
4000
3900
3800
LOC.140
30
40
50
60
70
80
TIME (YRS SINCE 1900)

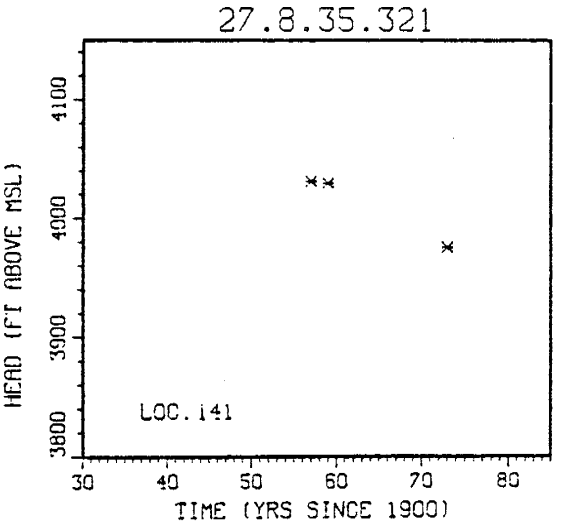
27.8.35.321
HEAD (FT ABOVE MSL)
4100
4000
3900
3800
LOC.141
30
40
50
60
70
80
TIME (YRS SINCE 1900)

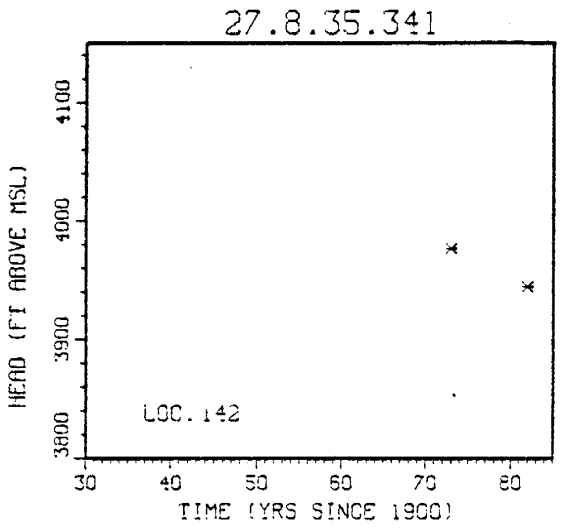
27.8.35.341
HEAD (FT ABOVE MSL)
4100
4000
3900
3800
LOC.142
30
40
50
60
70
80
TIME (YRS SINCE 1900)

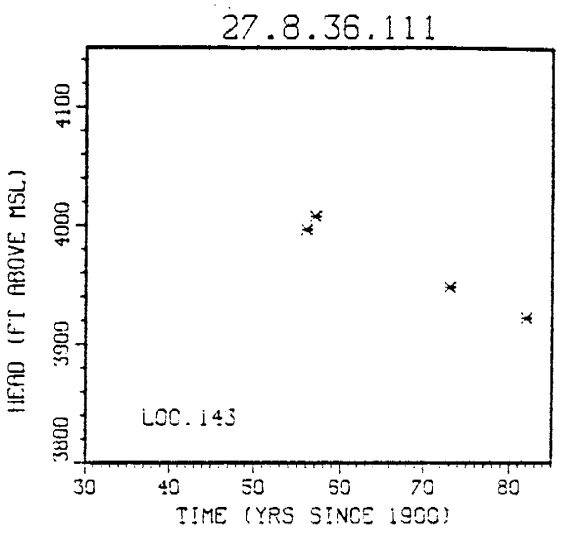
27.8.36.111
HEAD (FT ABOVE MSL)
4100
4000
3900
3800
LOC.143
30
40
50
60
70
80
TIME (YRS SINCE 1900)

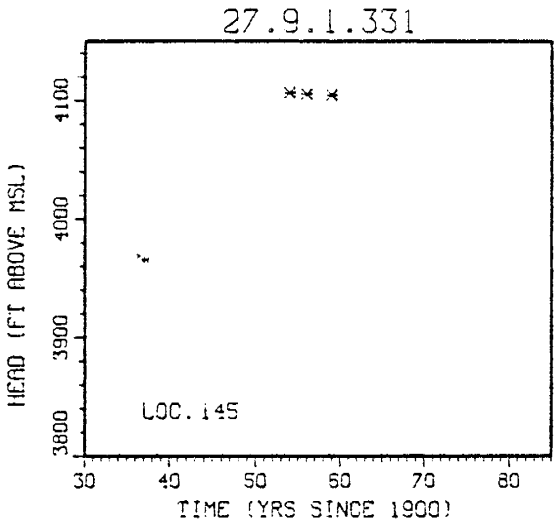
27.9.1.331
HEAD (FT ABOVE MSL)
4100
4000
3900
3800
LOC.145
30
40
50
60
70
80
TIME (YRS SINCE 1900)

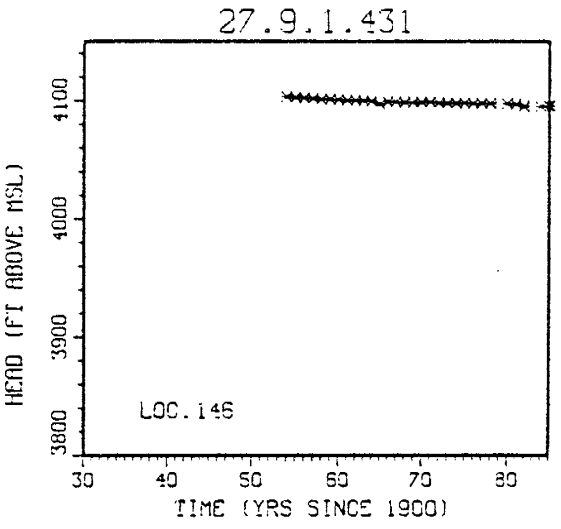
27.9.1.431
HEAD (FT ABOVE MSL)
4100
4000
3900
3800
LOC.146
30
40
50
60
70
80
TIME (YRS SINCE 1900)

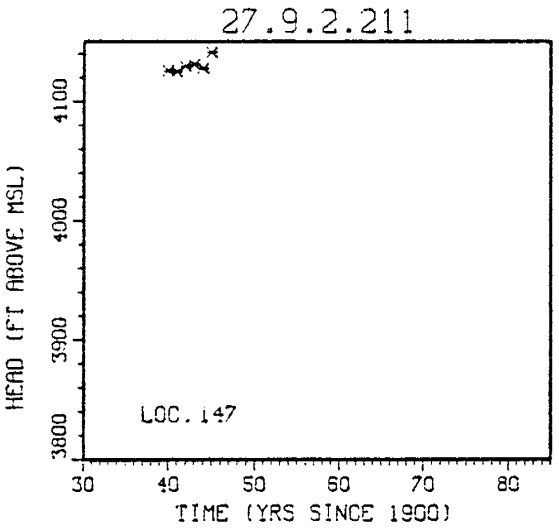
27.9.2.211
HEAD (FT ABOVE MSL)
4100
4000
3900
3800
LOC.147
30
40
50
60
70
80
TIME (YRS SINCE 1900)

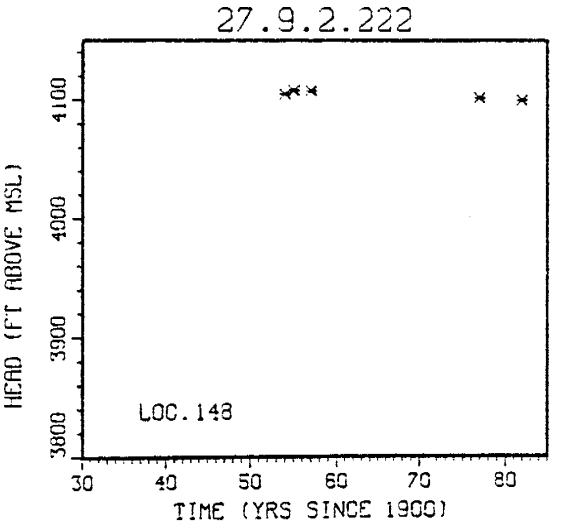
27.9.2.222
HEAD (FT ABOVE MSL)
4100
4000
3900
3800
LOC.148
30
40
50
60
70
80
TIME (YRS SINCE 1900)

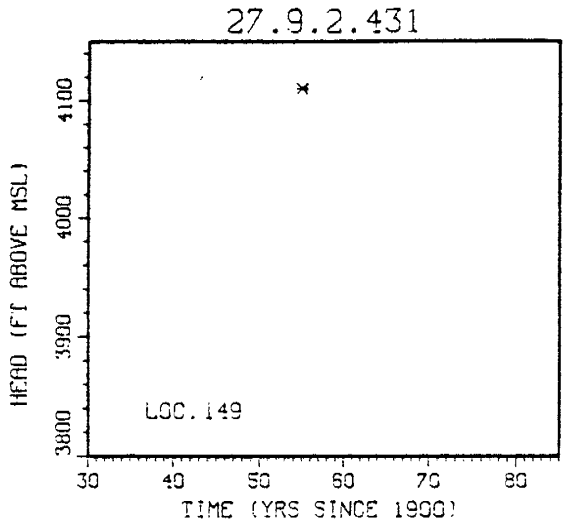
27.9.2.431
HEAD (FT ABOVE MSL)
4100
4000
3900
3800
LOC.149
30
40
50
60
70
80
TIME (YRS SINCE 1900)

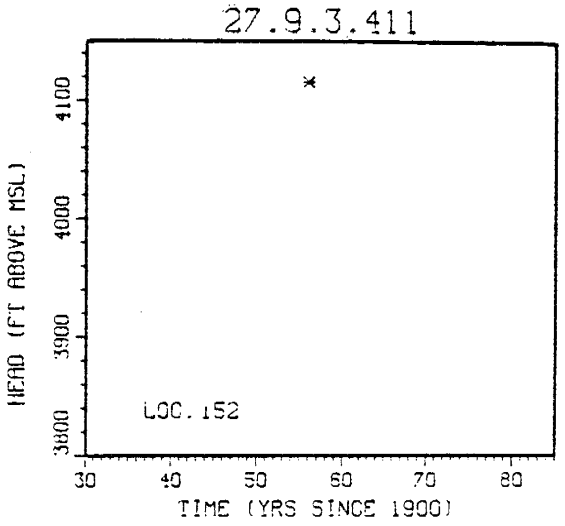
27.9.3.411
HEAD (FT ABOVE MSL)
4100
4000
3900
3800
LOC.152
30
40
50
60
70
80
TIME (YRS SINCE 1900)

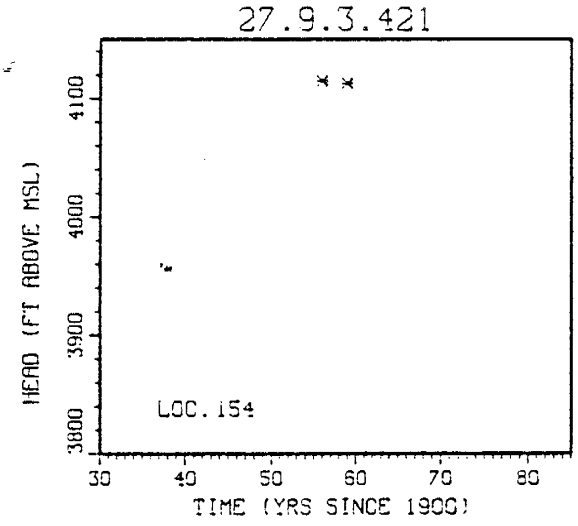
27.9.3.421
HEAD (FT ABOVE MSL)
4100
4000
3900
3800
LOC.154
30
40
50
60
70
80
TIME (YRS SINCE 1900)

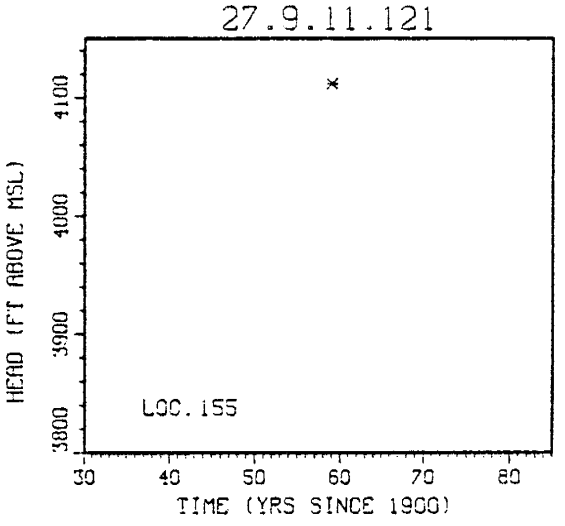
27.9.11.121
HEAD (FT ABOVE MSL)
4100
4000
3900
3800
LOC.155
30
40
50
60
70
80
TIME (YRS SINCE 1900)

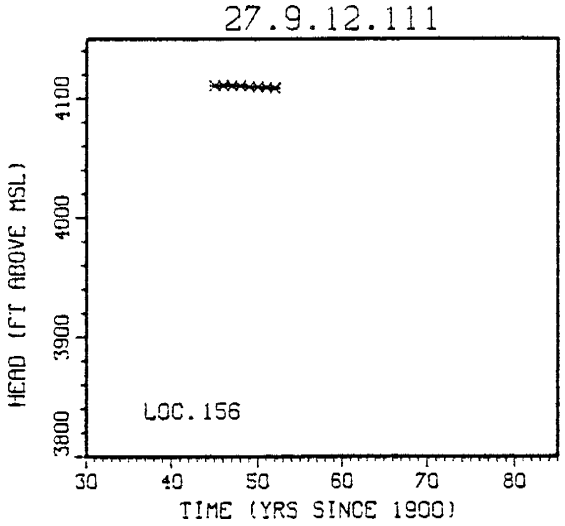
27.9.12.111
HEAD (FT ABOVE MSL)
4100
4000
3900
3800
LOC.156
30
40
50
60
70
80
TIME (YRS SINCE 1900)

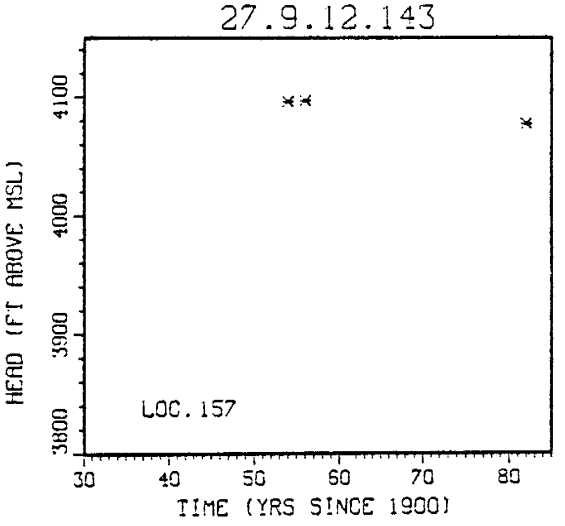
27.9.12.143
HEAD (FT ABOVE MSL)
4100
4000
3900
3800
LOC.157
30
40
50
60
70
80
TIME (YRS SINCE 1900)

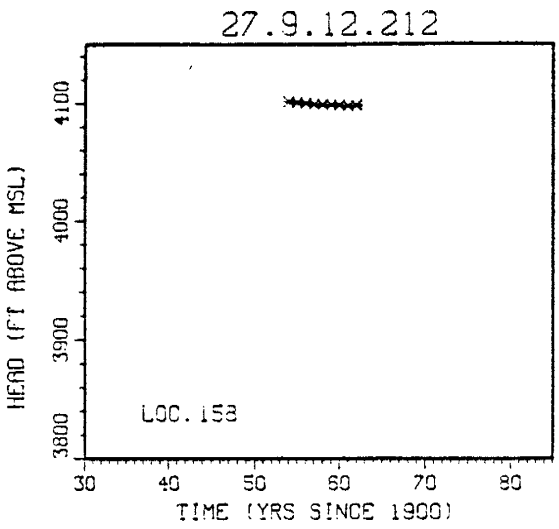
27.9.12.212
HEAD (FT ABOVE MSL)
4100
4000
3900
3800
LOC.158
30
40
50
60
70
80
TIME (YRS SINCE 1900)

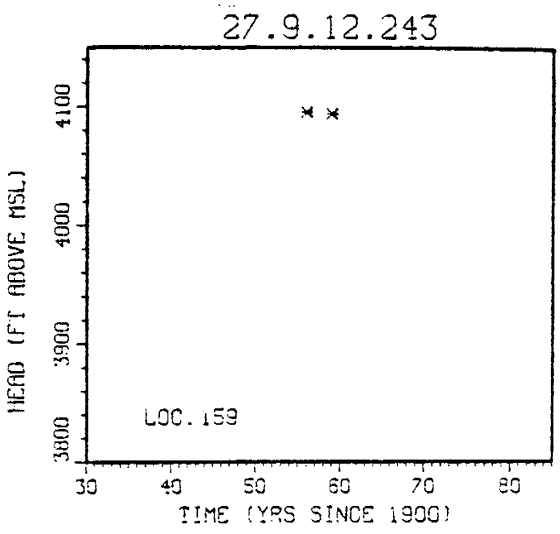
27.9.12.243
HEAD (FT ABOVE MSL)
4100
4000
3900
3800
LOC.159
30
40
50
60
70
80
TIME (YRS SINCE 1900)

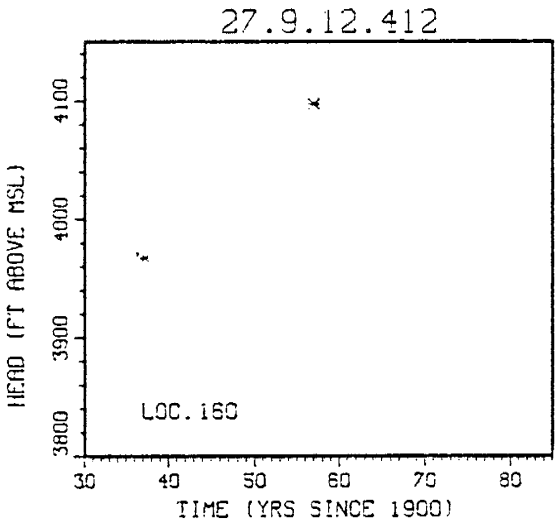
27.9.12.412
HEAD (FT ABOVE MSL)
4100
4000
3900
3800
LOC.160
30
40
50
60
70
80
TIME (YRS SINCE 1900)

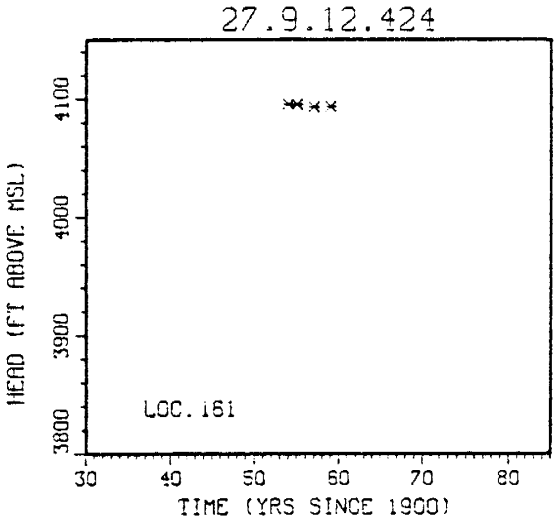
27.9.12.424
HEAD (FT ABOVE MSL)
4100
4000
3900
3800
LOC.161
30
40
50
60
70
80
TIME (YRS SINCE 1900)

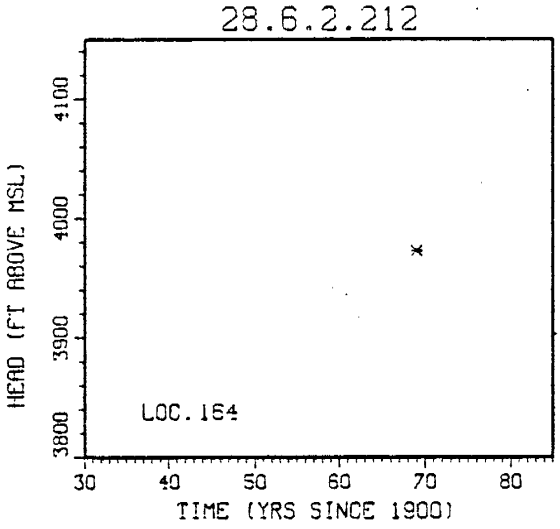
28.6.2.212
HEAD (FT ABOVE MSL)
4100
4000
3900
3800
LOC.164
30
40
50
60
70
80
TIME (YRS SINCE 1900)

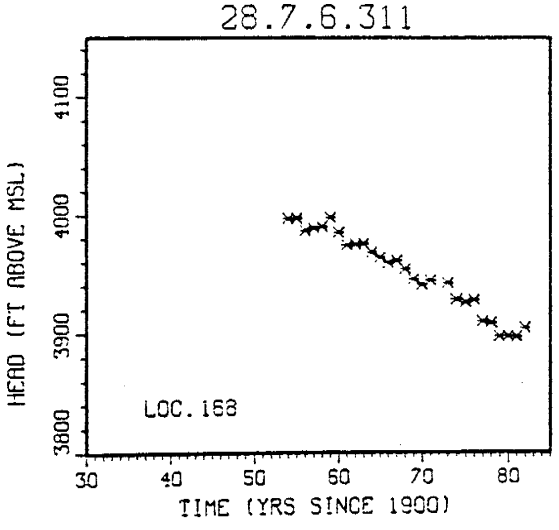
28.7.6.311
HEAD (FT ABOVE MSL)
4100
4000
3900
3800
LOC.168
30
40
50
60
70
80
TIME (YRS SINCE 1900)

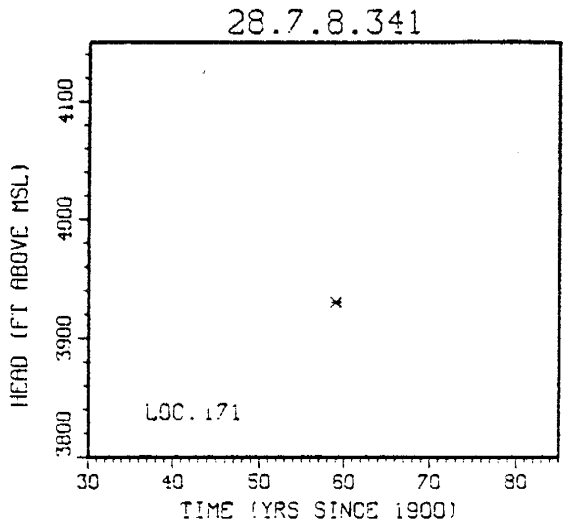
28.7.8.341
HEAD (FT ABOVE MSL)
4100
4000
3900
3800
LOC.171
30
40
50
60
70
80
TIME (YRS SINCE 1900)

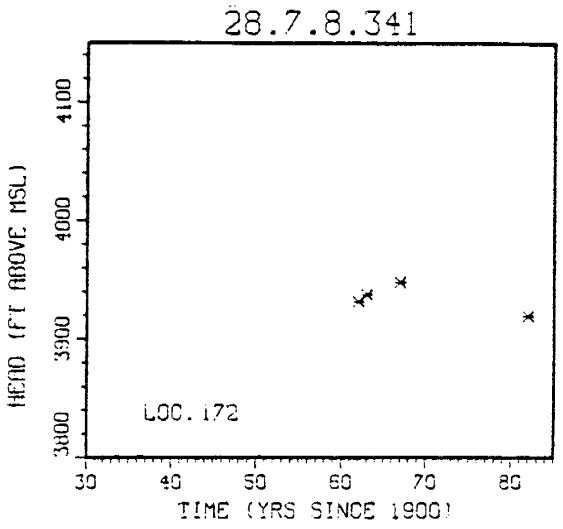
28.7.8.341
HEAD (FT ABOVE MSL)
4100
4000
3900
3800
LOC.172
30
40
50
60
70
80
TIME (YRS SINCE 1900)

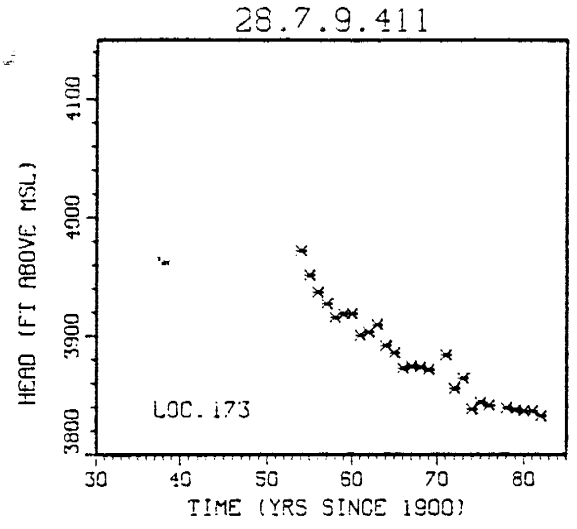
28.7.9.411
HEAD (FT ABOVE MSL)
4100
4000
3900
3800
LOC.173
30
40
50
60
70
80
TIME (YRS SINCE 1900)

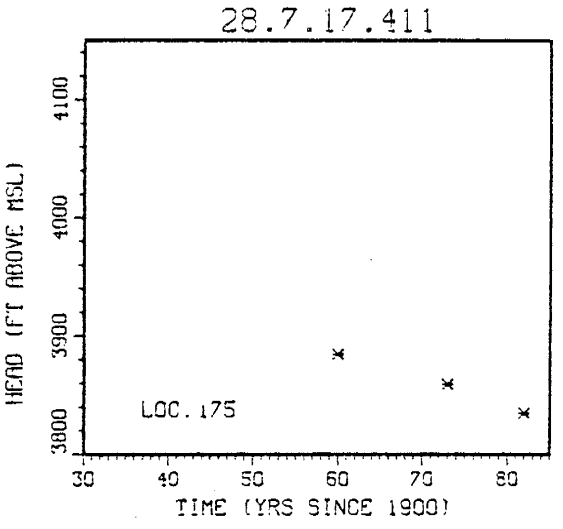
28.7.17.411
HEAD (FT ABOVE MSL)
4100
4000
3900
3800
LOC.175
30
40
50
60
70
80
TIME (YRS SINCE 1900)

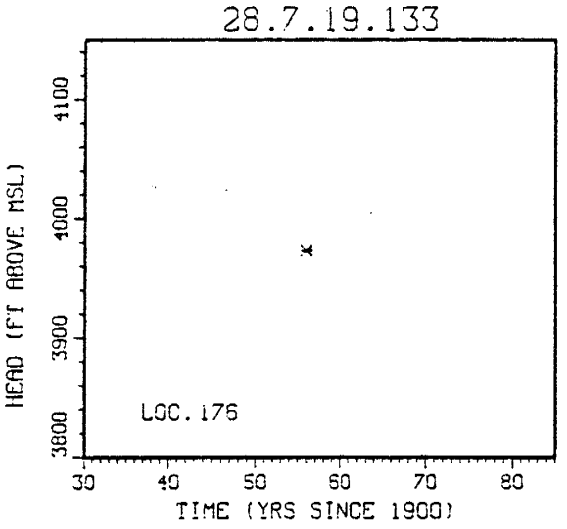
28.7.19.133
HEAD (FT ABOVE MSL)
4100
4000
3900
3800
LOC.176
30
40
50
60
70
80
TIME (YRS SINCE 1900)

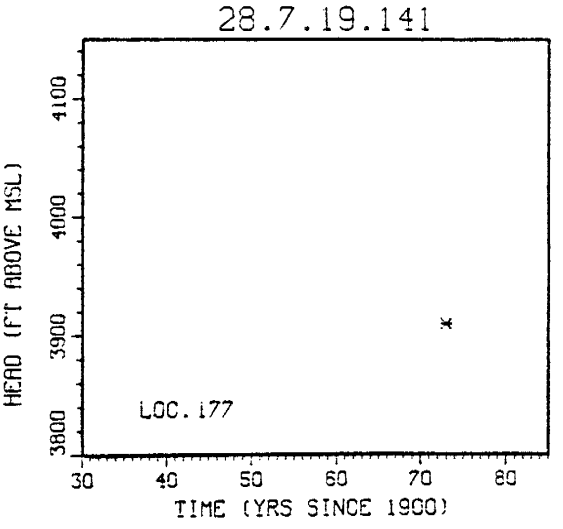
28.7.19.141
HEAD (FT ABOVE MSL)
4100
4000
3900
3800
LOC.177
30
40
50
60
70
80
TIME (YRS SINCE 1900)

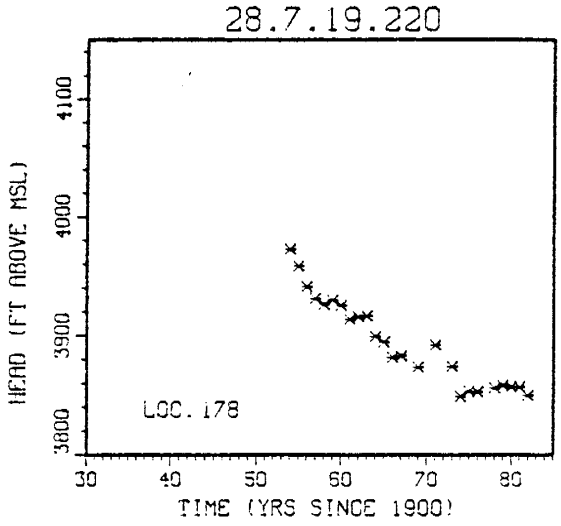
28.7.19.220
HEAD (FT ABOVE MSL)
4100
4000
3900
3800
LOC. 178
30
40
50
60
70
80
TIME (YRS SINCE 1900)

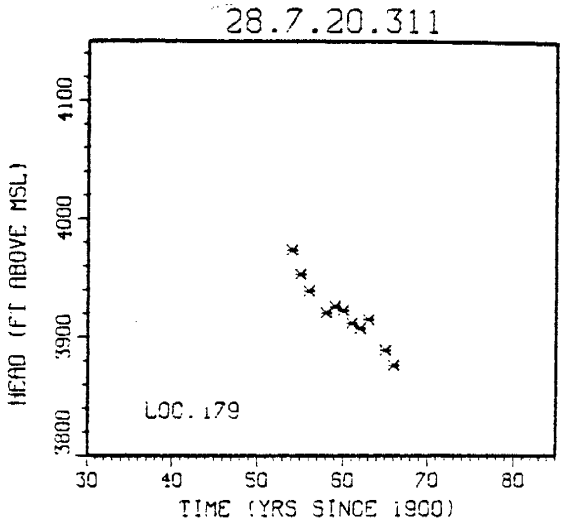
28.7.20.311
HEAD (FT ABOVE MSL)
4100
4000
3900
3800
LOC. 179
30
40
50
60
70
80
TIME (YRS SINCE 1900)

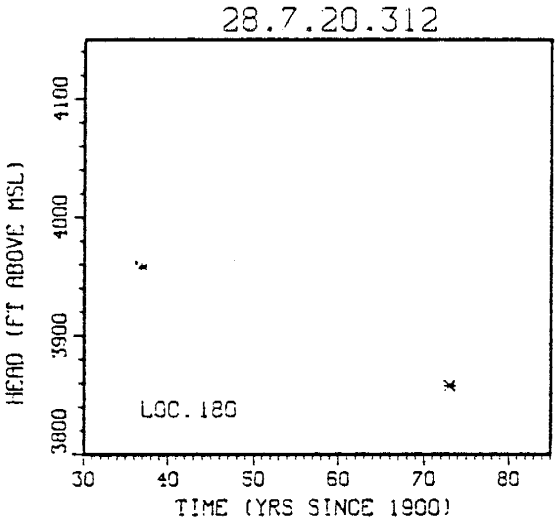
28.7.20.312
HEAD (FT ABOVE MSL)
4100
4000
3900
3800
LOC. 180
30
40
50
60
70
80
TIME (YRS SINCE 1900)

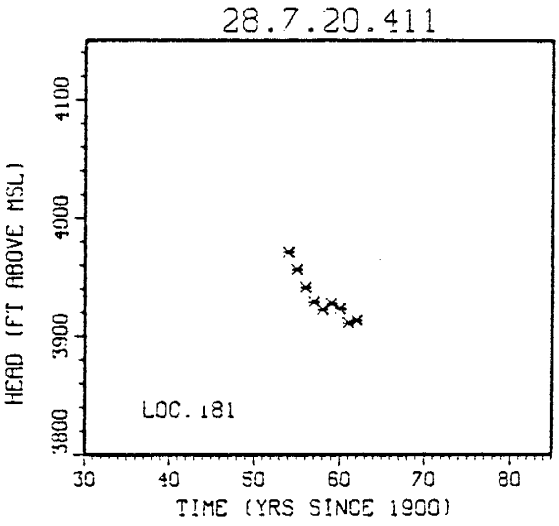
28.7.20.411
HEAD (FT ABOVE MSL)
4100
4000
3900
3800
LOC. 181
30
40
50
60
70
80
TIME (YRS SINCE 1900)

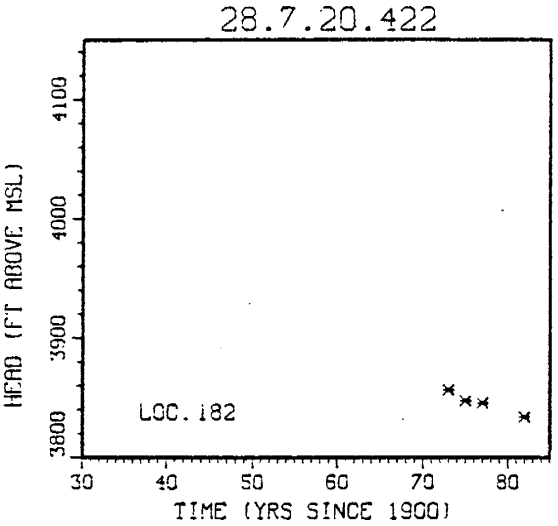
28.7.20.422
HEAD (FT ABOVE MSL)
4100
4000
3900
3800
LOC. 182
30
40
50
60
70
80
TIME (YRS SINCE 1900)

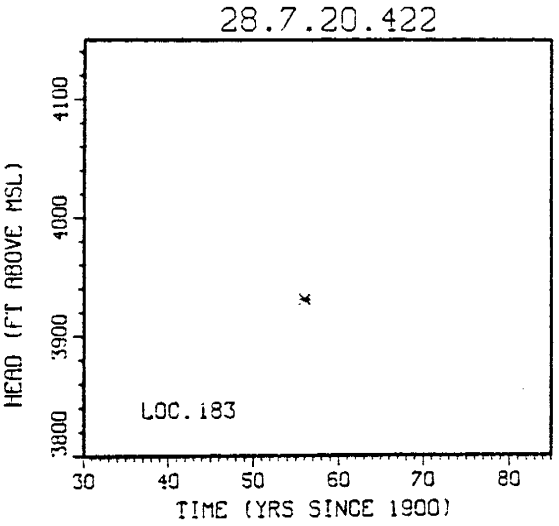
28.7.20.422
HEAD (FT ABOVE MSL)
4100
4000
3900
3800
LOC. 183
30
40
50
60
70
80
TIME (YRS SINCE 1900)

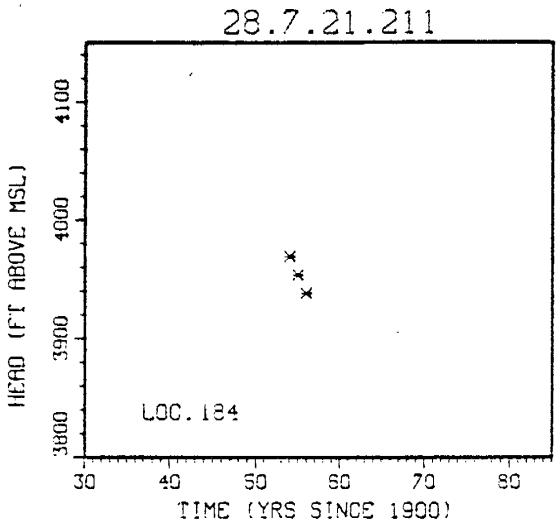
28.7.21.211
HEAD (FT ABOVE MSL)
4100
4000
3900
3800
LOC.184
30
40
50
60
70
80
TIME (YRS SINCE 1900)

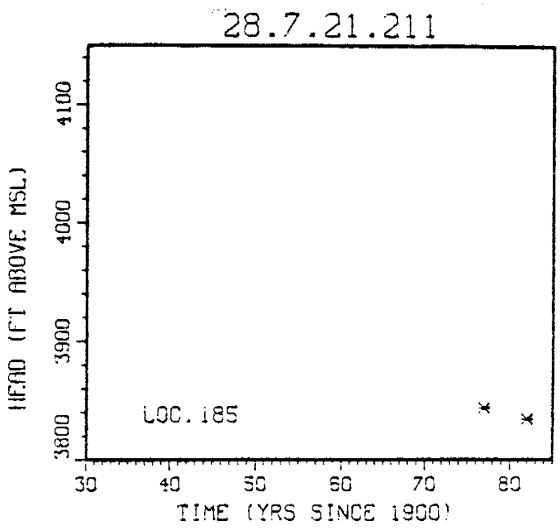
28.7.21.211
HEAD (FT ABOVE MSL)
4100
4000
3900
3800
LOC.185
30
40
50
60
70
80
TIME (YRS SINCE 1900)

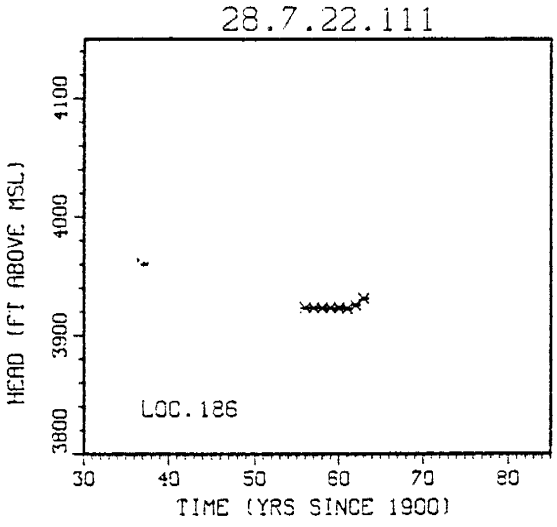
28.7.22.111
HEAD (FT ABOVE MSL)
4100
4000
3900
3800
LOC.186
30
40
50
60
70
80
TIME (YRS SINCE 1900)

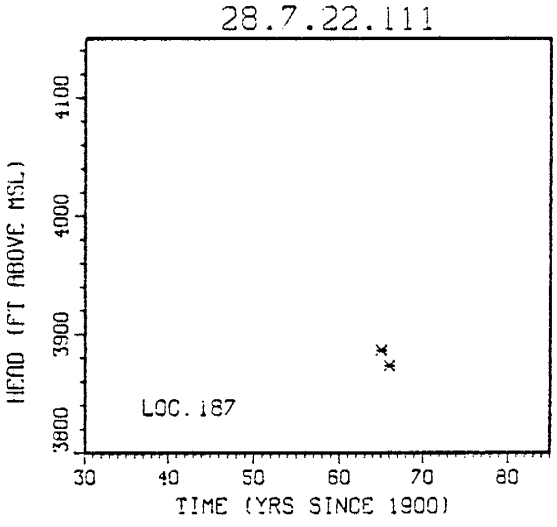
28.7.22.111
HEAD (FT ABOVE MSL)
4100
4000
3900
3800
LOC.187
30
40
50
60
70
80
TIME (YRS SINCE 1900)

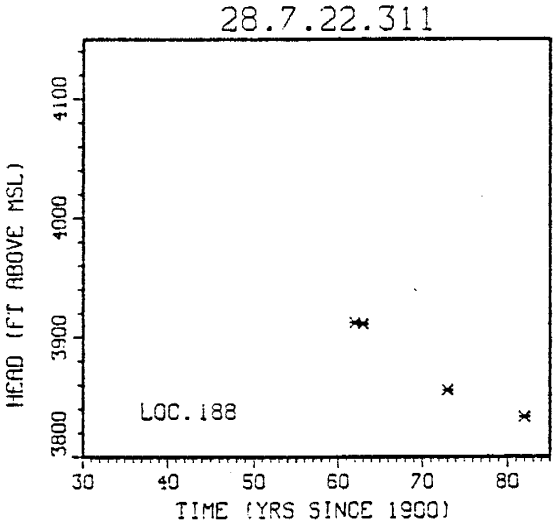
28.7.22.311
HEAD (FT ABOVE MSL)
4100
4000
3900
3800
LOC.188
30
40
50
60
70
80
TIME (YRS SINCE 1900)

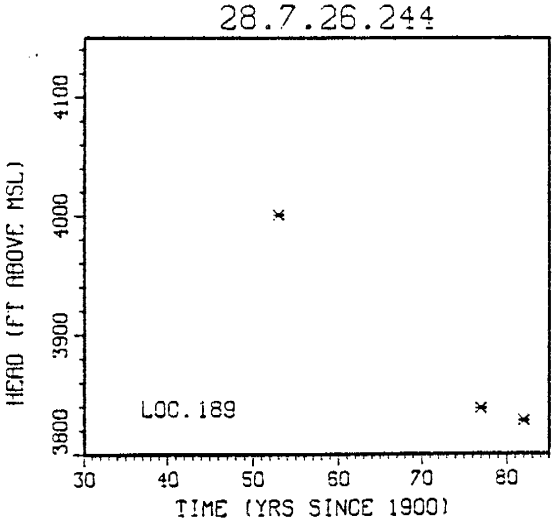
28.7.26.244
HEAD (FT ABOVE MSL)
4100
4000
3900
3800
LOC.189
30
40
50
60
70
80
TIME (YRS SINCE 1900)

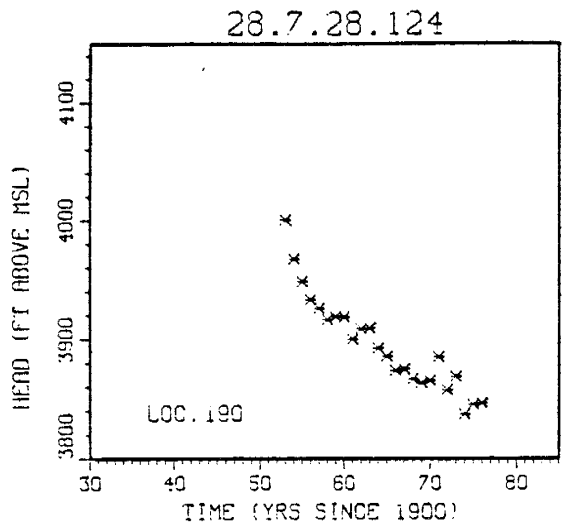
28.7.28.124
HEAD (FT ABOVE MSL)
4100
4000
3900
3800
LOC.190
30
40
50
60
70
80
TIME (YRS SINCE 1900)

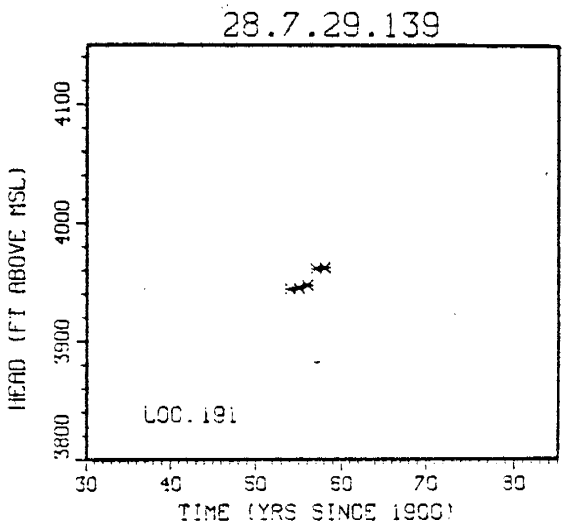
28.7.29.139
HEAD (FT ABOVE MSL)
4100
4000
3900
3800
LOC.191
30
40
50
60
70
80
TIME (YRS SINCE 1900)

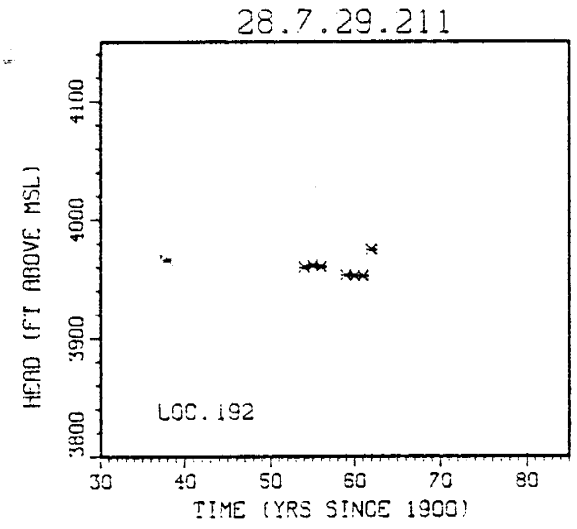
28.7.29.211
HEAD (FT ABOVE MSL)
4100
4000
3900
3800
LOC.192
30
40
50
60
70
80
TIME (YRS SINCE 1900)

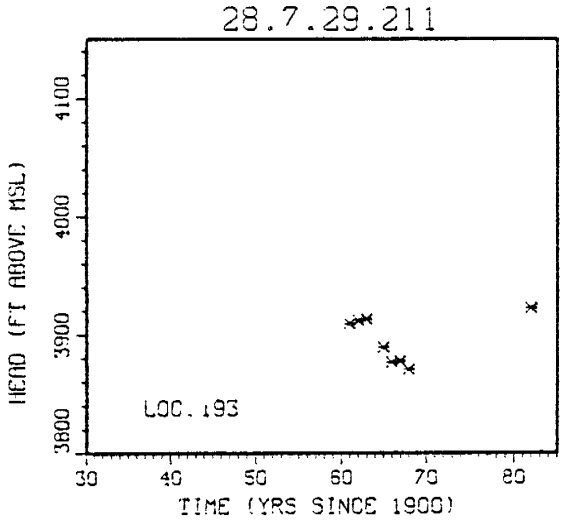
28.7.29.211
HEAD (FT ABOVE MSL)
4100
4000
3900
3800
LOC.193
30
40
50
60
70
80
TIME (YRS SINCE 1900)

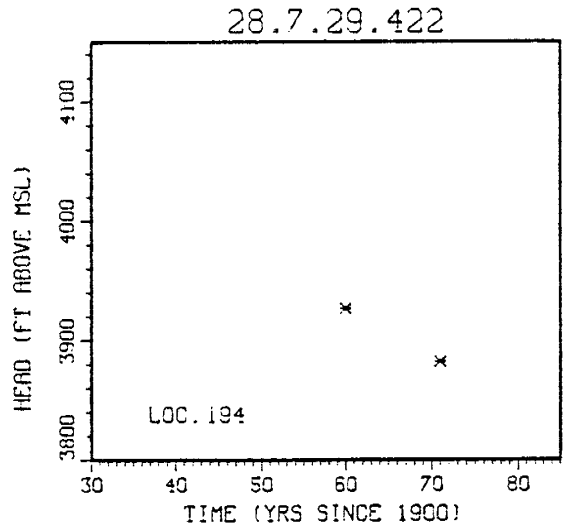
28.7.29.422
HEAD (FT ABOVE MSL)
4100
4000
3900
3800
LOC.194
30
40
50
60
70
80
TIME (YRS SINCE 1900)

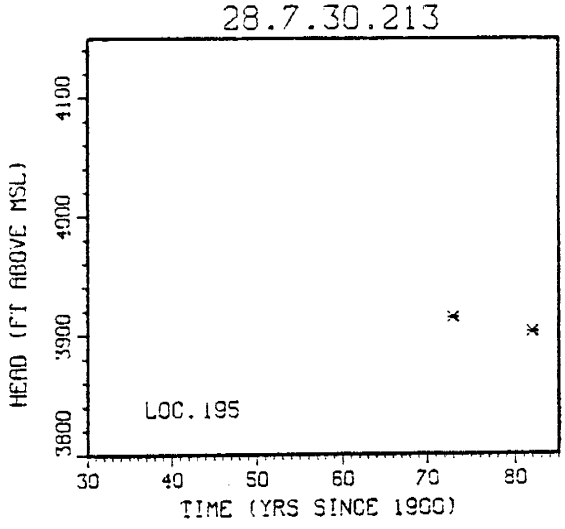
28.7.30.213
HEAD (FT ABOVE MSL)
4100
4000
3900
3800
LOC.195
30
40
50
60
70
80
TIME (YRS SINCE 1900)

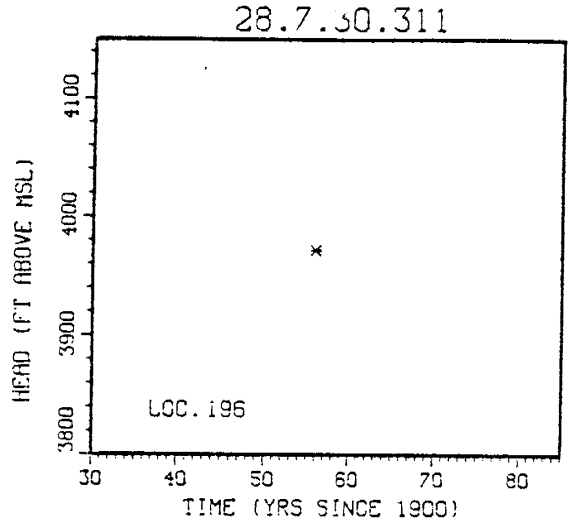
28.7.30.311
HEAD (FT ABOVE MSL)
4100
4000
3900
3800
LOC. 196
30
40
50
60
70
80
TIME (YRS SINCE 1900)

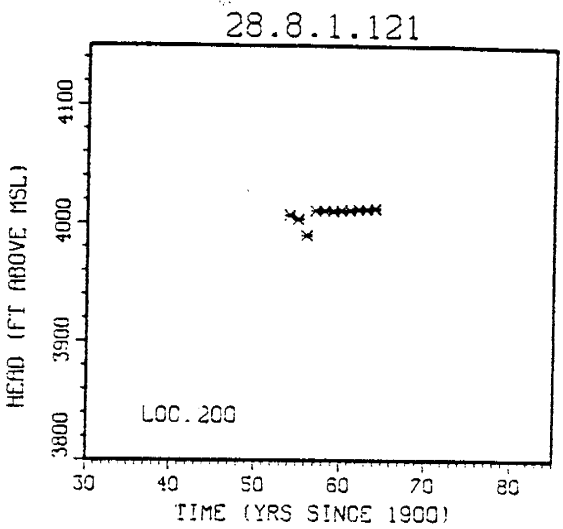
28.8.1.121
HEAD (FT ABOVE MSL)
4100
4000
3900
3800
LOC. 200
30
40
50
60
70
80
TIME (YRS SINCE 1900)

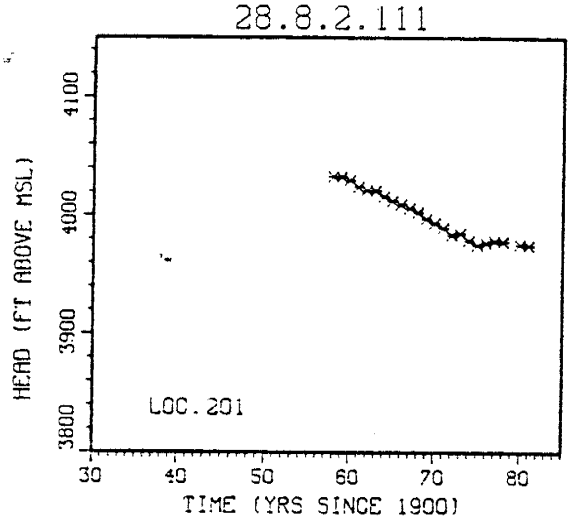
28.8.2.111
HEAD (FT ABOVE MSL)
4100
4000
3900
3800
LOC. 201
30
40
50
60
70
80
TIME (YRS SINCE 1900)

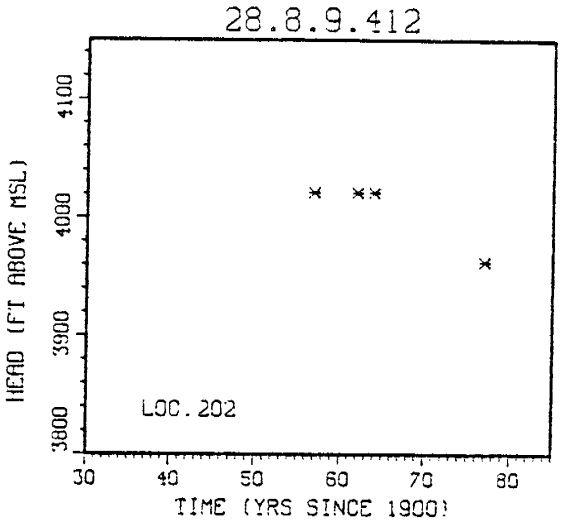
28.8.9.412
HEAD (FT ABOVE MSL)
4100
4000
3900
3800
LOC. 202
30
40
50
60
70
80
TIME (YRS SINCE 1900)

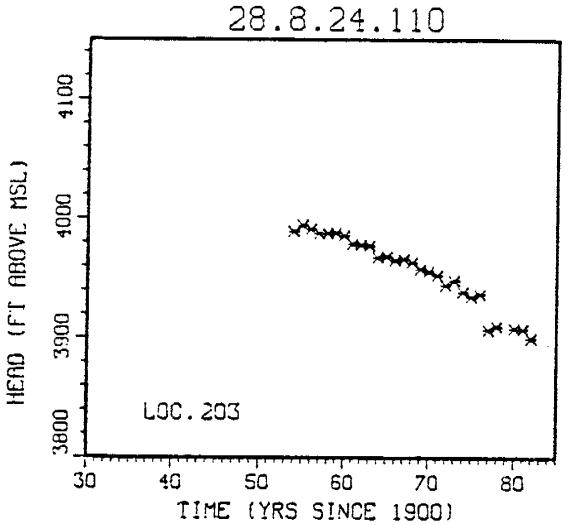
28.8.24.110
HEAD (FT ABOVE MSL)
4100
4000
3900
3800
LOC. 203
30
40
50
60
70
80
TIME (YRS SINCE 1900)

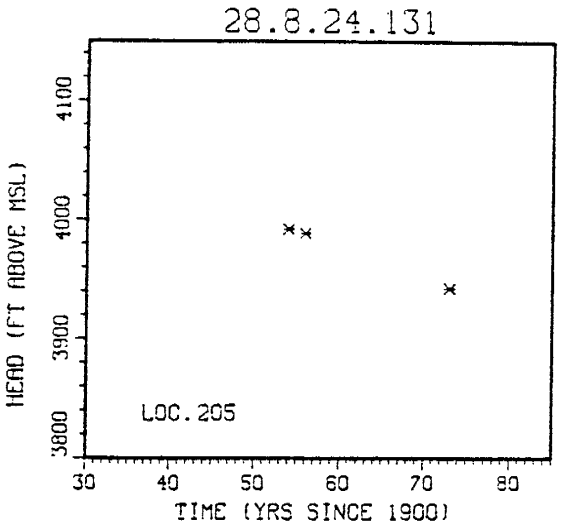
28.8.24.131
HEAD (FT ABOVE MSL)
4100
4000
3900
3800
LOC. 205
30
40
50
60
70
80
TIME (YRS SINCE 1900)

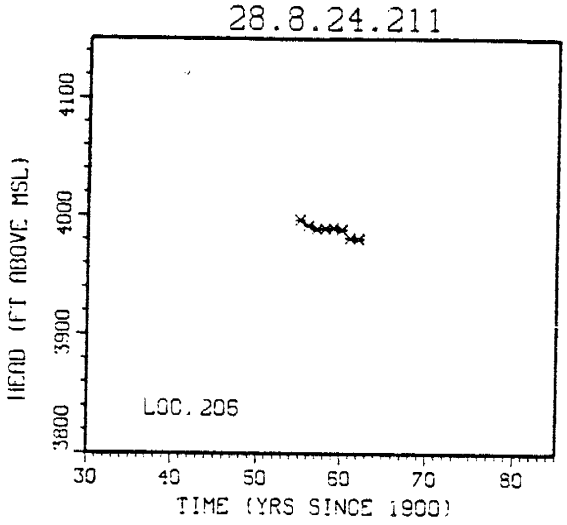
28.8.24.211
HEAD (FT ABOVE MSL)
4100
4000
3900
3800
LOC. 206
30
40
50
60
70
80
TIME (YRS SINCE 1900)

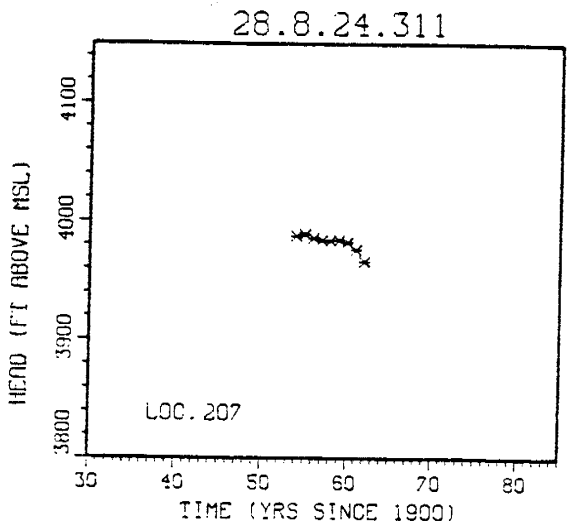
28.8.24.311
HEAD (FT ABOVE MSL)
4100
4000
3900
3800
LOC. 207
30
40
50
60
70
80
TIME (YRS SINCE 1900)

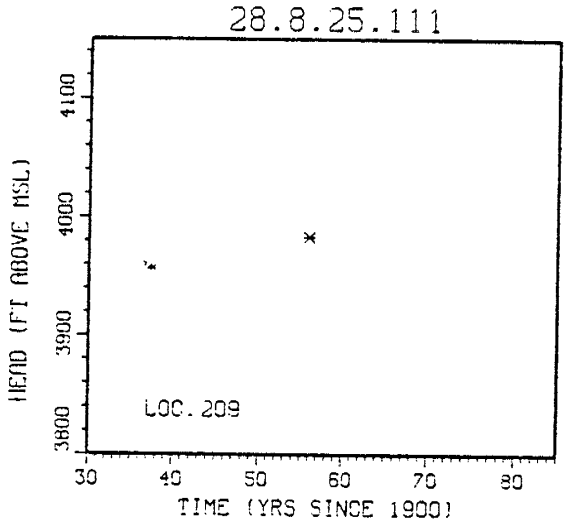
28.8.25.111
HEAD (FT ABOVE MSL)
4100
4000
3900
3800
LOC. 209
30
40
50
60
70
80
TIME (YRS SINCE 1900)

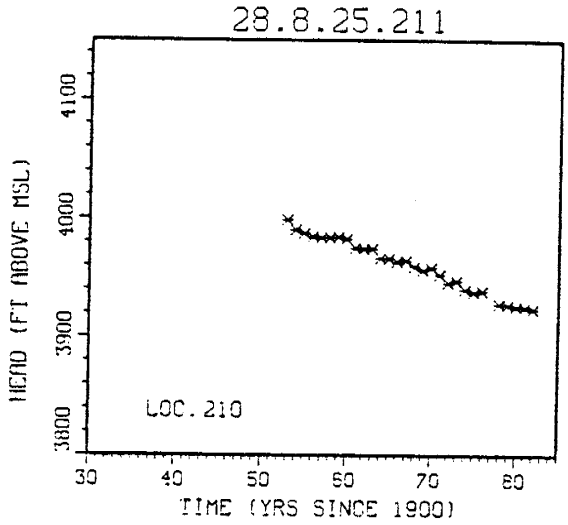
28.8.25.211
HEAD (FT ABOVE MSL)
4100
4000
3900
3800
LOC. 210
30
40
50
60
70
80
TIME (YRS SINCE 1900)

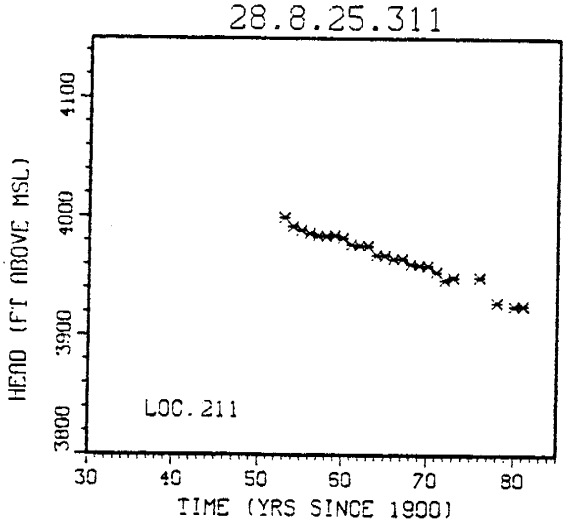
28.8.25.311
HEAD (FT ABOVE MSL)
4100
4000
3900
3800
LOC. 211
30
40
50
60
70
80
TIME (YRS SINCE 1900)

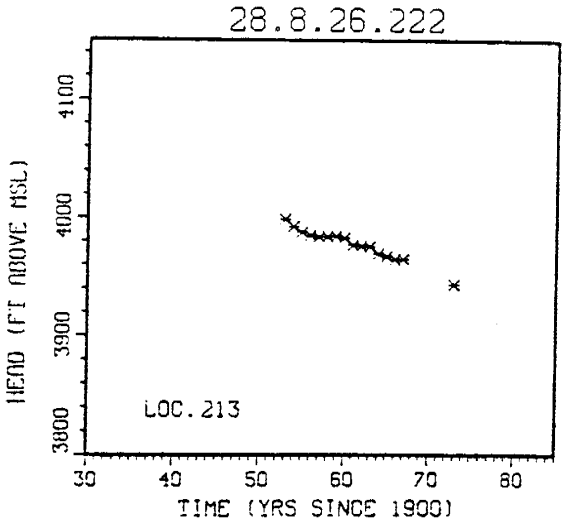
28.8.26.222
HEAD (FT ABOVE MSL)
4100
4000
3900
3800
LOC. 213
30
40
50
60
70
80
TIME (YRS SINCE 1900)

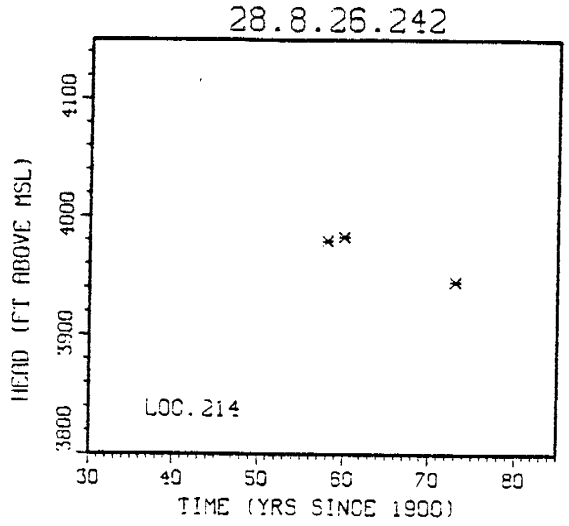
28.8.26.242
HEAD (FT ABOVE MSL)
4100
4000
3900
3800
LOC. 214
30
40
50
60
70
80
TIME (YRS SINCE 1900)

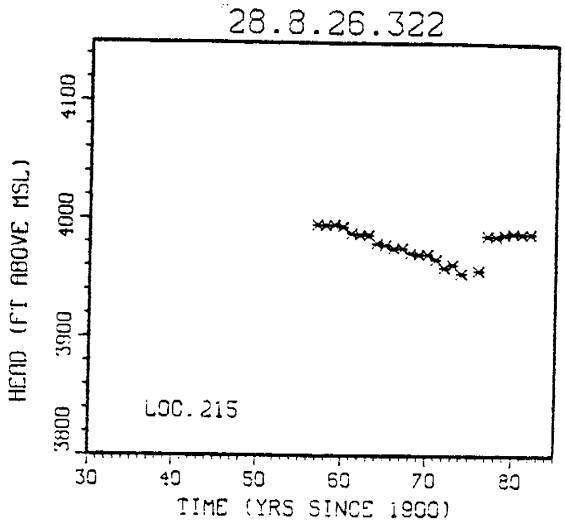
28.8.26.322
HEAD (FT ABOVE MSL)
4100
4000
3900
3800
LOC. 215
30
40
50
60
70
80
TIME (YRS SINCE 1900)

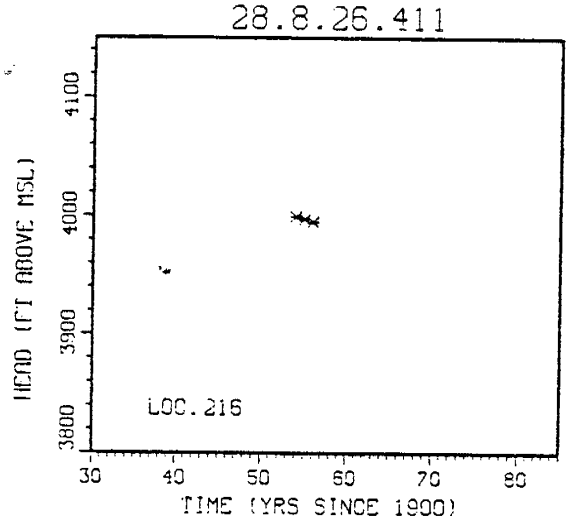
28.8.26.411
HEAD (FT ABOVE MSL)
4100
4000
3900
3800
LOC. 216
30
40
50
60
70
80
TIME (YRS SINCE 1900)

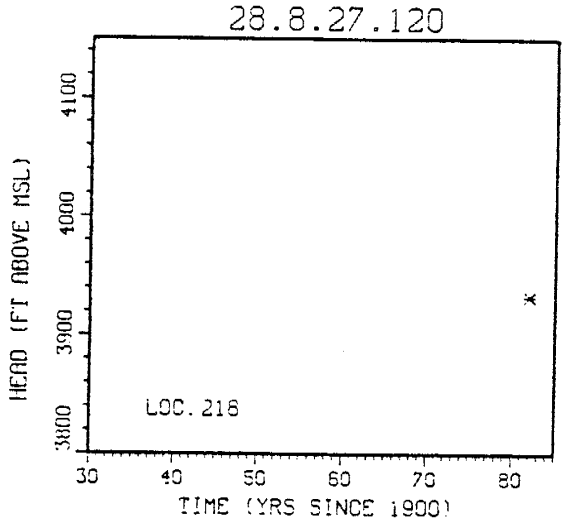
28.8.27.120
HEAD (FT ABOVE MSL)
4100
4000
3900
3800
LOC. 218
30
40
50
60
70
80
TIME (YRS SINCE 1900)

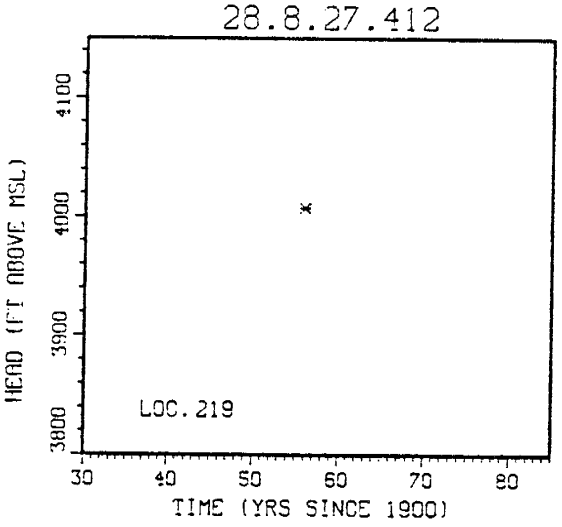
28.8.27.412
HEAD (FT ABOVE MSL)
4100
4000
3900
3800
LOC. 219
30
40
50
60
70
80
TIME (YRS SINCE 1900)

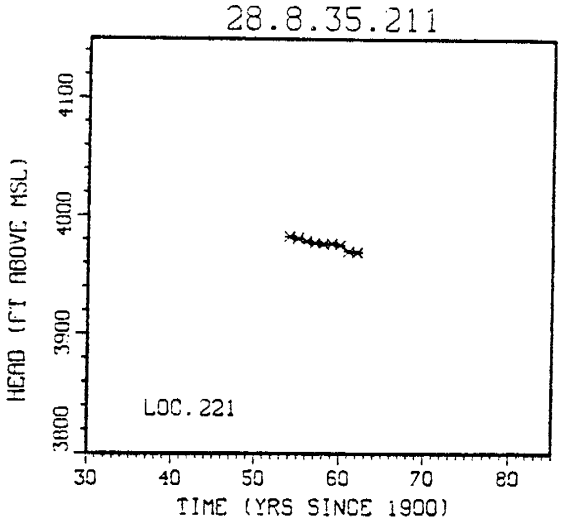
28.8.35.211
HEAD (FT ABOVE MSL)
4100
4000
3900
3800
LOC. 221
30
40
50
60
70
80
TIME (YRS SINCE 1900)

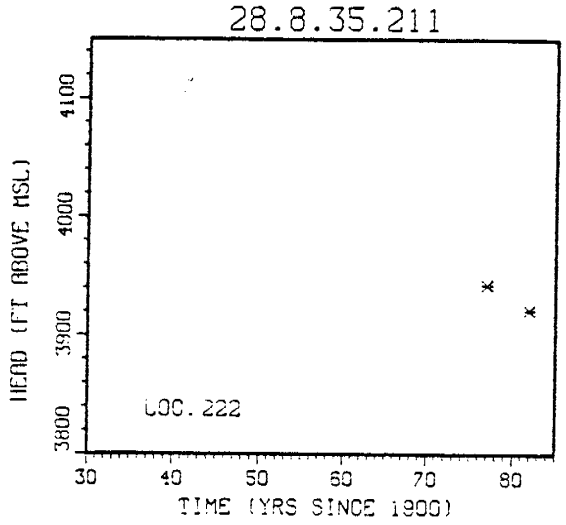
28.8.35.211
HEAD (FT ABOVE MSL)
4100
4000
3900
3800
LOC. 222
30
40
50
60
70
80
TIME (YRS SINCE 1900)

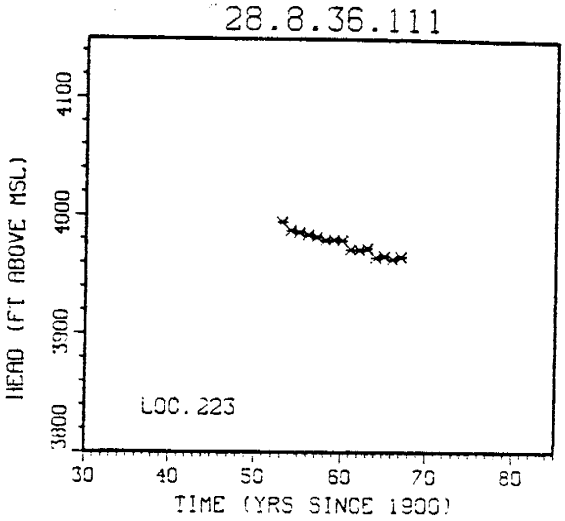
28.8.36.111
HEAD (FT ABOVE MSL)
4100
4000
3900
3800
LOC. 223
30
40
50
60
70
80
TIME (YRS SINCE 1900)

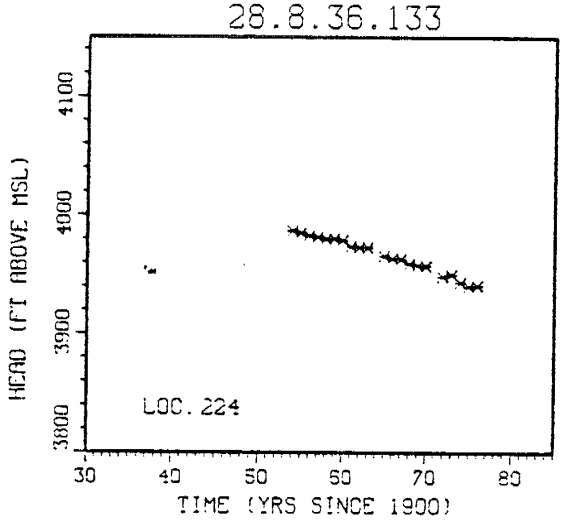
28.8.36.133
HEAD (FT ABOVE MSL)
4100
4000
3900
3800
LOC. 224
30
40
50
60
70
80
TIME (YRS SINCE 1900)

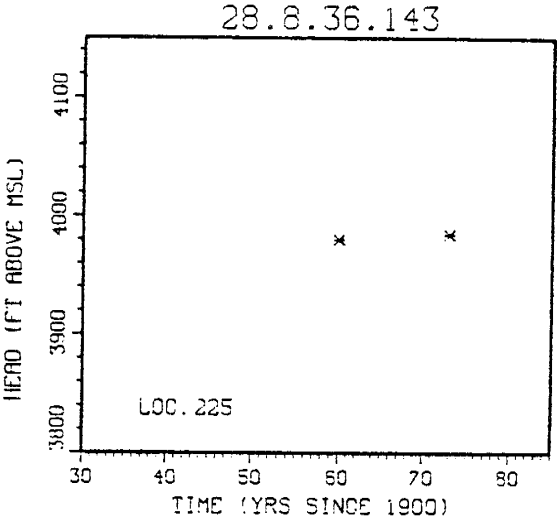
28.8.36.143
HEAD (FT ABOVE MSL)
4100
4000
3900
3800
LOC. 225
30
40
50
60
70
80
TIME (YRS SINCE 1900)

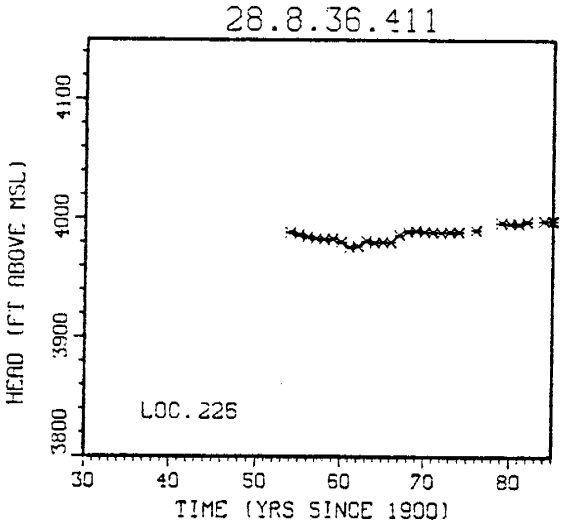
28.8.36.411
HEAD (FT ABOVE MSL)
4100
4000
3900
3800
LOC. 226
30
40
50
60
70
80
TIME (YRS SINCE 1900)

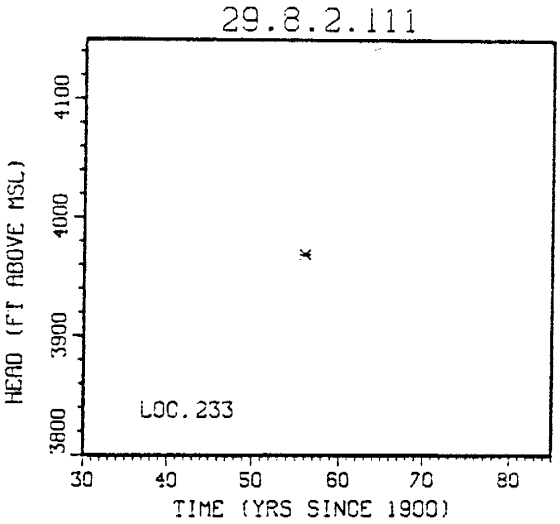
29.8.2.111
HEAD (FT ABOVE MSL)
4100
4000
3900
3800
LOC. 233
30
40
50
60
70
80
TIME (YRS SINCE 1900)

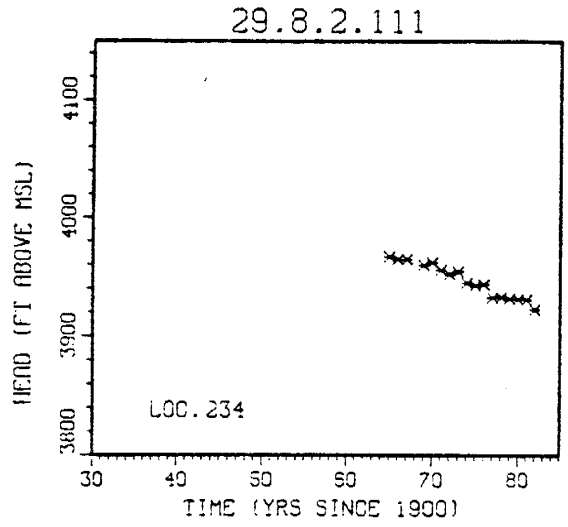
29.8.2.111
HEAD (FT ABOVE MSL)
4100
4000
3900
3800
LOC. 234
30
40
50
60
70
80
TIME (YRS SINCE 1900)

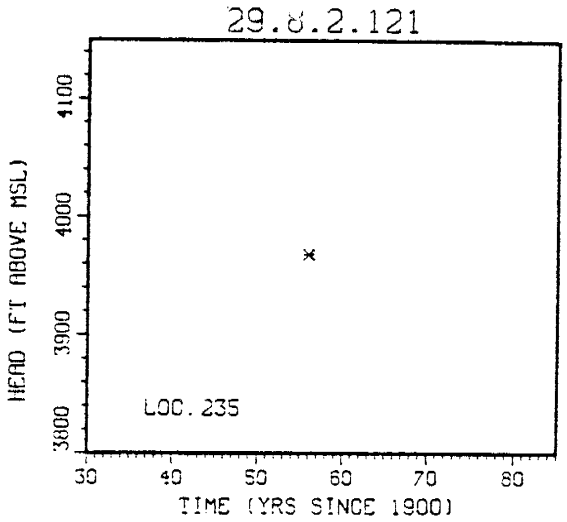
29.8.2.121
HEAD (FT ABOVE MSL)
4100
4000
3900
3800
LOC. 235
30
40
50
60
70
80
TIME (YRS SINCE 1900)

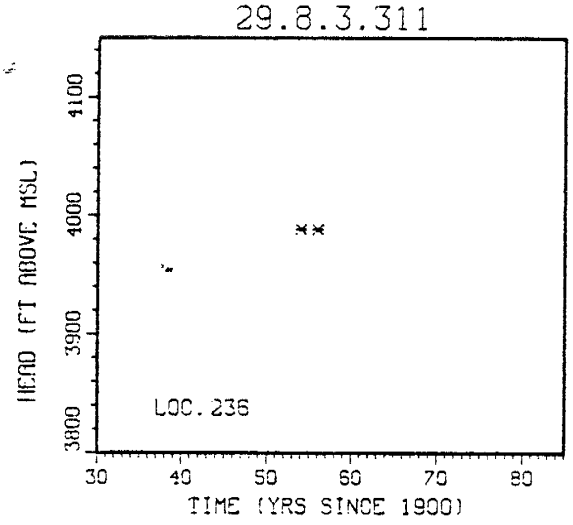
29.8.3.311
HEAD (FT ABOVE MSL)
4100
4000
3900
3800
LOC. 236
30
40
50
60
70
80
TIME (YRS SINCE 1900)

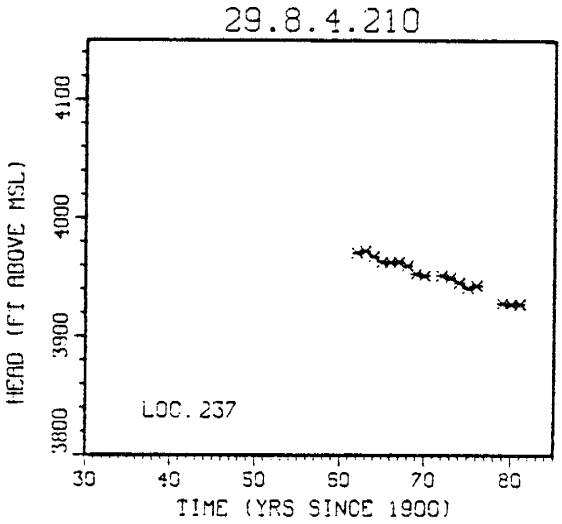
29.8.4.210
HEAD (FT ABOVE MSL)
4100
4000
3900
3800
LOC. 237
30
40
50
60
70
80
TIME (YRS SINCE 1900)

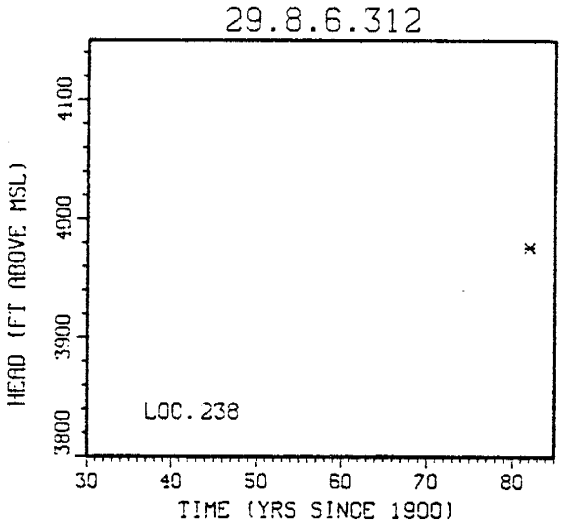
29.8.6.312
HEAD (FT ABOVE MSL)
4100
4000
3900
3800
LOC. 238
30
40
50
60
70
80
TIME (YRS SINCE 1900)

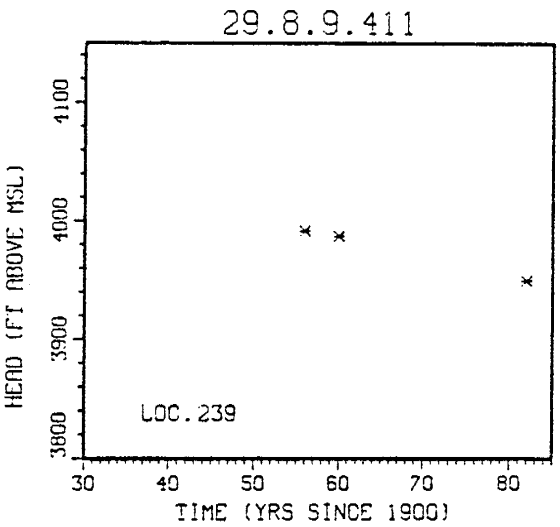
29.8.9.411
HEAD (FT ABOVE MSL)
4100
4000
3900
3800
LOC. 239
30
40
50
60
70
80
TIME (YRS SINCE 1900)

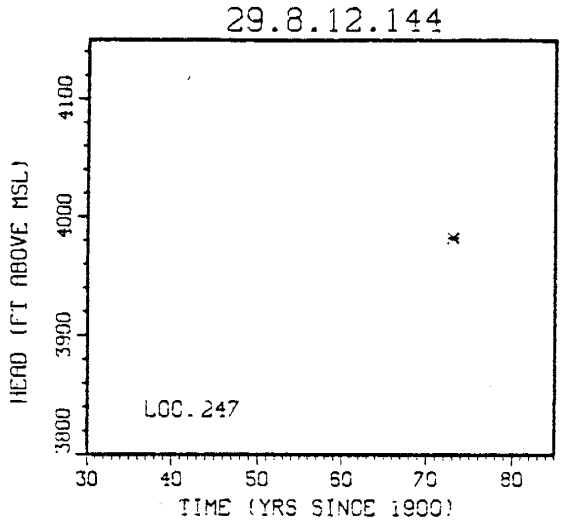
29.8.12.144
HEAD (FT ABOVE MSL)
4100
4000
3900
3800
LOC. 247
30
40
50
60
70
80
TIME (YRS SINCE 1900)

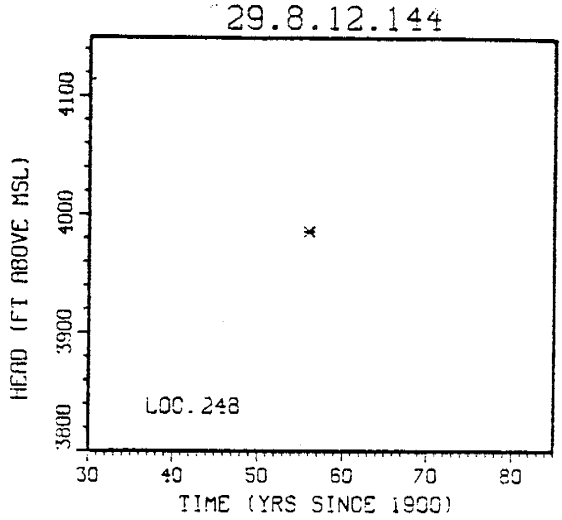
29.8.12.144
HEAD (FT ABOVE MSL)
4100
4000
3900
3800
LOC. 248
30
40
50
60
70
80
TIME (YRS SINCE 1900)

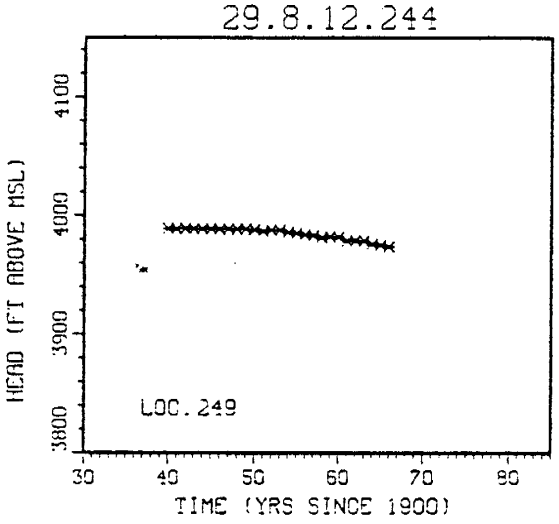
29.8.12.244
HEAD (FT ABOVE MSL)
4100
4000
3900
3800
LOC. 249
30
40
50
60
70
80
TIME (YRS SINCE 1900)

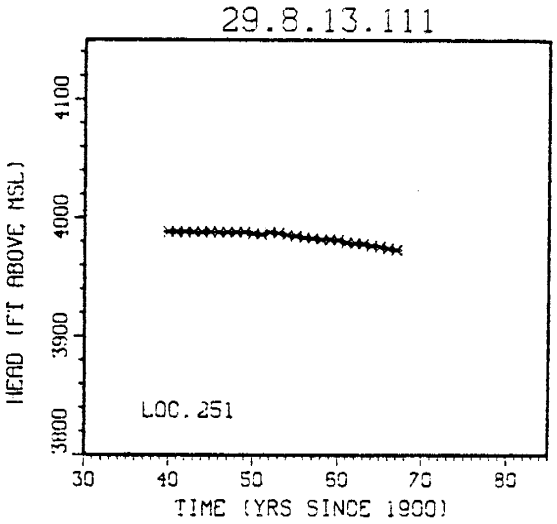
29.8.13.111
HEAD (FT ABOVE MSL)
4100
4000
3900
3800
LOC. 251
30
40
50
60
70
80
TIME (YRS SINCE 1900)

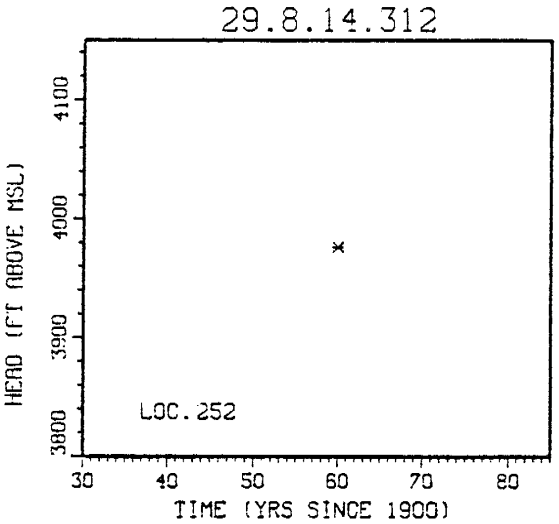
29.8.14.312
HEAD (FT ABOVE MSL)
4100
4000
3900
3800
LOC. 252
30
40
50
60
70
80
TIME (YRS SINCE 1900)

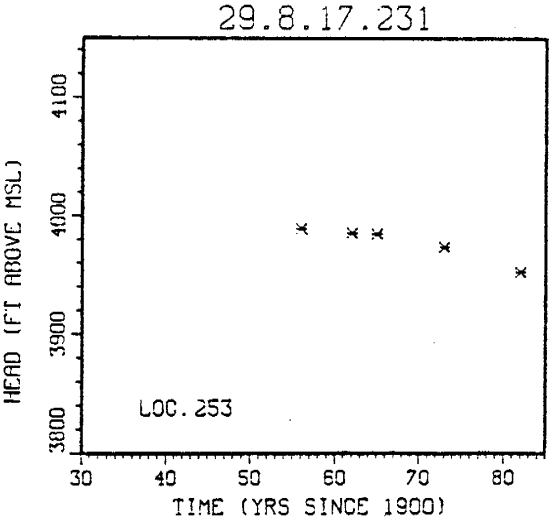
29.8.17.231
HEAD (FT ABOVE MSL)
4100
4000
3900
3800
LOC. 253
30
40
50
60
70
80
TIME (YRS SINCE 1900)

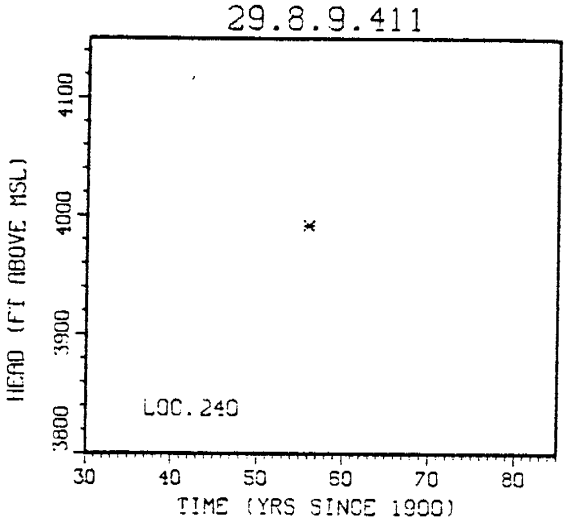
29.8.9.411
HEAD (FT ABOVE MSL)
4100
4000
3900
3800
LOC.240
30
40
50
60
70
80
TIME (YRS SINCE 1900)

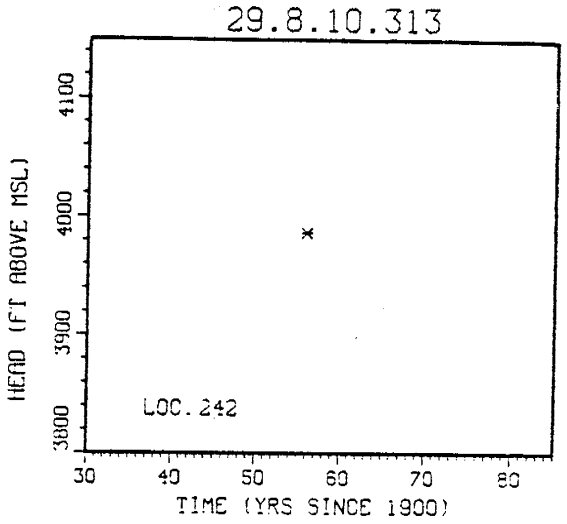
29.8.10.313
HEAD (FT ABOVE MSL)
4100
4000
3900
3800
LOC.242
30
40
50
60
70
80
TIME (YRS SINCE 1900)

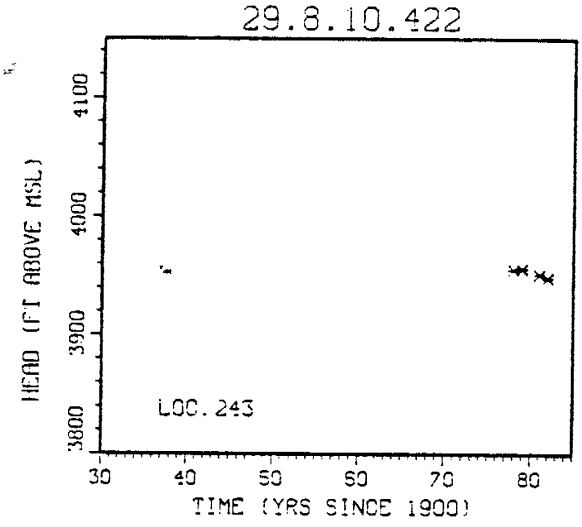
29.8.10.422
HEAD (FT ABOVE MSL)
4100
4000
3900
3800
LOC.243
30
40
50
60
70
80
TIME (YRS SINCE 1900)

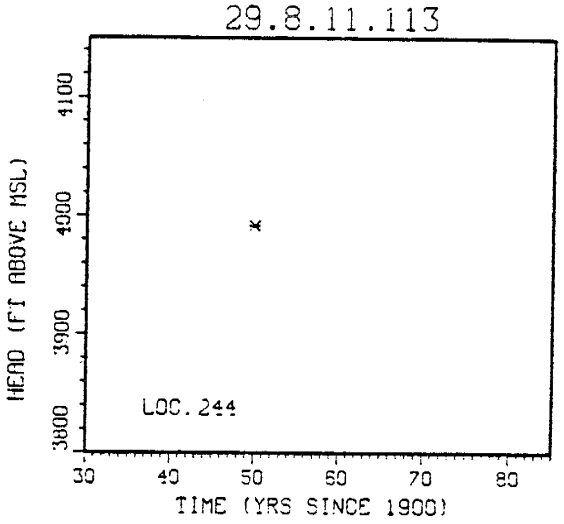
29.8.11.113
HEAD (FT ABOVE MSL)
4100
4000
3900
3800
LOC.244
30
40
50
60
70
80
TIME (YRS SINCE 1900)

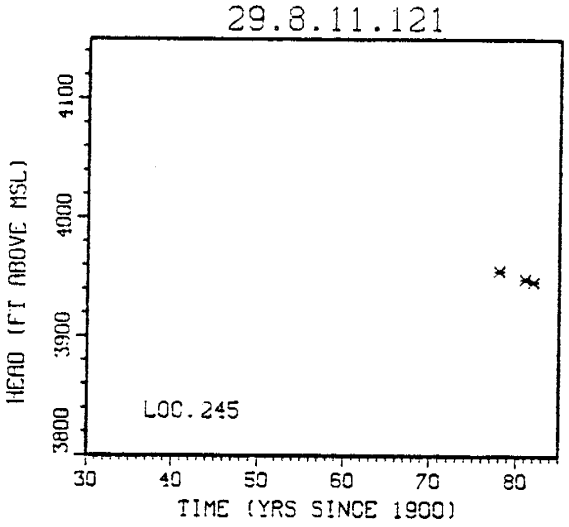
29.8.11.121
HEAD (FT ABOVE MSL)
4100
4000
3900
3800
LOC.245
30
40
50
60
70
80
TIME (YRS SINCE 1900)

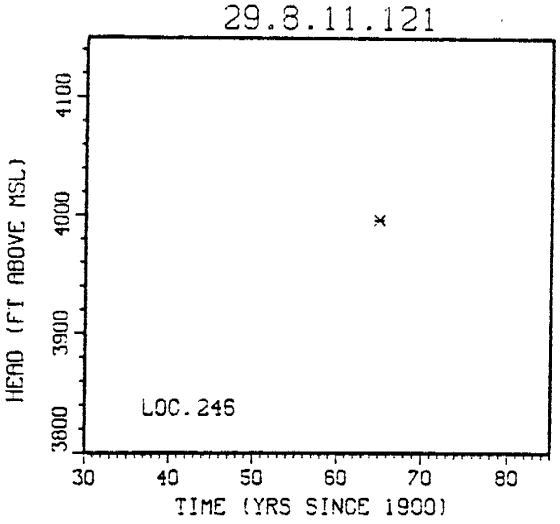
29.8.11.121
HEAD (FT ABOVE MSL)
4100
4000
3900
3800
LOC.246
30
40
50
60
70
80
TIME (YRS SINCE 1900)

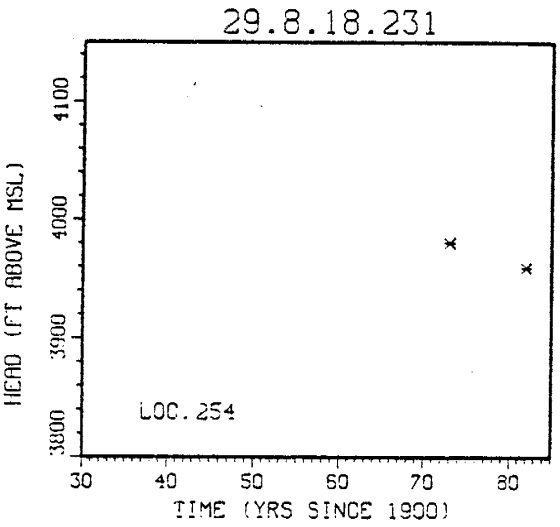
29.8.18.231
HEAD (FT ABOVE MSL)
4100
4000
3900
3800
LOC.254
30
40
50
60
70
80
TIME (YRS SINCE 1900)

Deleted Wells

The well locations deleted from the Columbus Basin study are provided in table I-3. The hydrographs of the deleted wells follow on pages 244 to 247. The depths of some of these wells can be found in table I-1. The deletion of wells or measurements from the Columbus Basin study was justified through one of the following criteria:

1. Well was believed to be screened in the shallow aquifer or aquitard overlying the main Columbus Basin aquifer. Very common for wells located in the western half of the basin.
2. Well was believed to be in poor connection with the aquifer. Water level in well was static while nearby wells showed drawdown.
3. Well was believed to be sampling a localized flow system, possibly 3-D, which was not indicative of the regional system. Possibly had effects due to local recharge, clay lenses, etc.
4. Human error either with measurement or record of measurement.

Table I-3

Well locations deleted for Columbus Basin study

Well Location No.	Criterion for Deletion
26.6.20.323	1
26.6.24.111	1
26.7.26.224	1
27.5.30.223	1
27.7.2.111	1
27.6.31.333	1
27.7.31.231	1
27.9.3.411	1 or 3
27.9.3.414	1 or 3
28.5.19.431	1
28.6.10.311	1
28.6.23.311	1
28.7.5.131	1, possibly 2
28.7.11.244	1, possibly 2
28.7.30.411	4, possibly 3
28.7.30.443	2
28.8.26.111	4
29.7.4.111	1, possibly 2
29.7.8.424	1, possibly 4
29.7.12.222	1
29.7.18.211	1

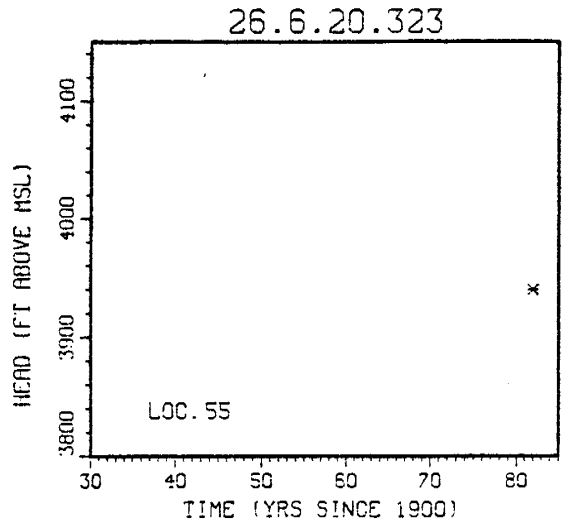
26.6.20.323
HEAD (FT ABOVE MSL)
4100
4000
3900
3800
LOC. 55
30
40
50
60
70
80
TIME (YRS SINCE 1900)

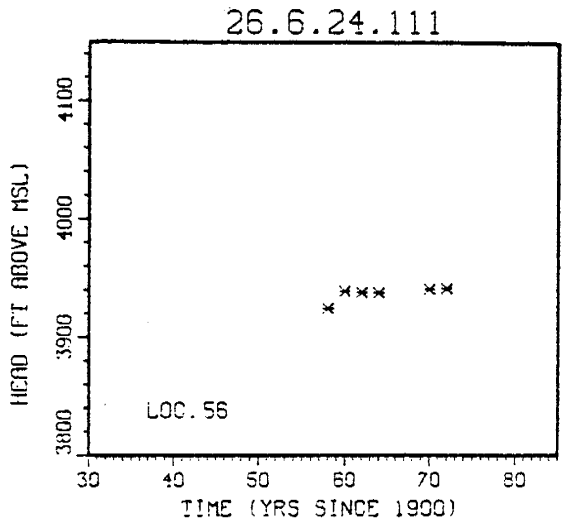
26.6.24.111
HEAD (FT ABOVE MSL)
4100
4000
3900
3800
LOC. 56
30
40
50
60
70
80
TIME (YRS SINCE 1900)

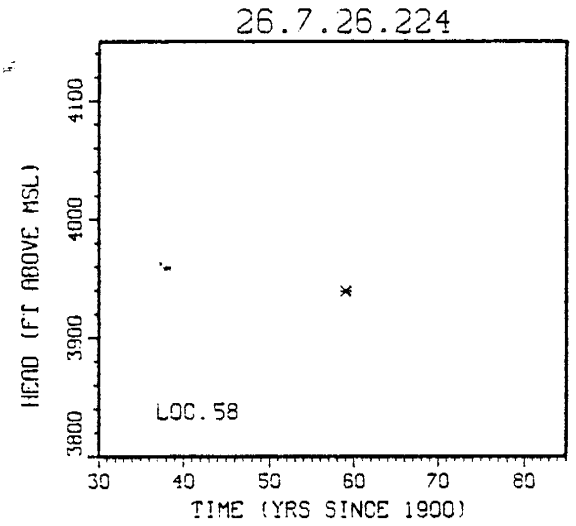
26.7.26.224
HEAD (FT ABOVE MSL)
4100
4000
3900
3800
LOC. 58
30
40
50
60
70
80
TIME (YRS SINCE 1900)

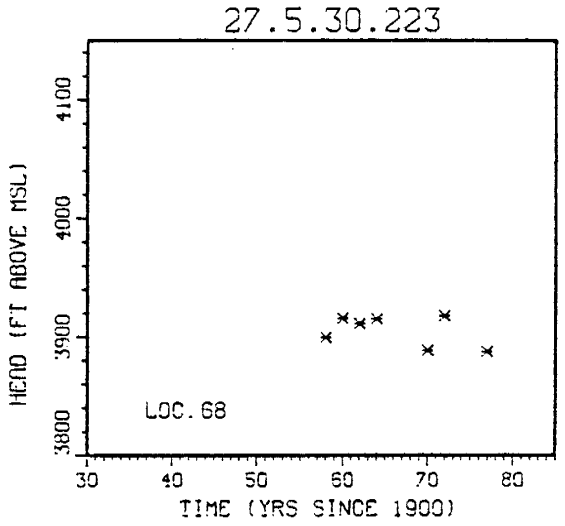
27.5.30.223
HEAD (FT ABOVE MSL)
4100
4000
3900
3800
LOC. 68
30
40
50
60
70
80
TIME (YRS SINCE 1900)

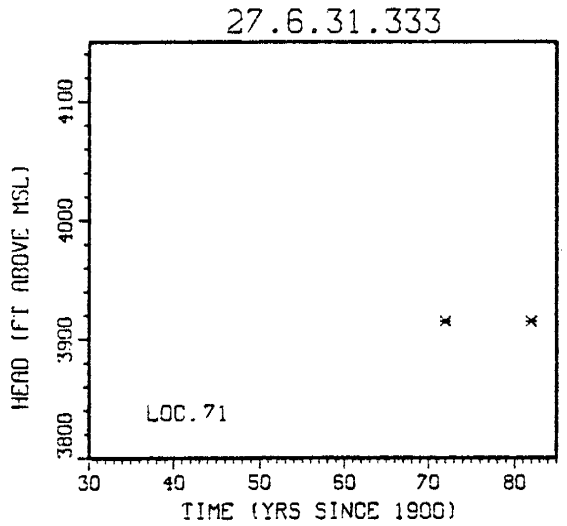
27.6.31.333
HEAD (FT ABOVE MSL)
4100
4000
3900
3800
LOC. 71
30
40
50
60
70
80
TIME (YRS SINCE 1900)

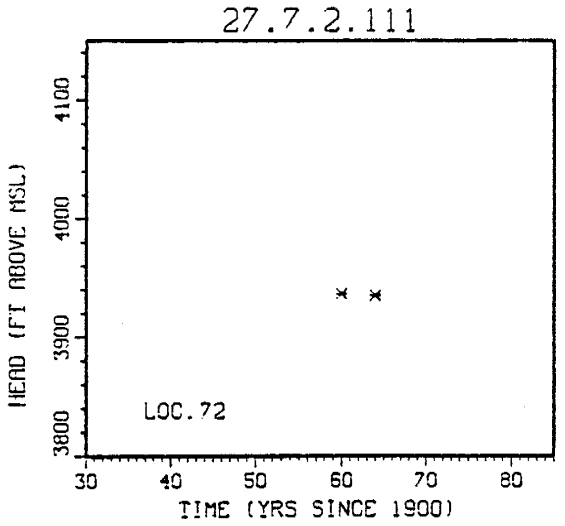
27.7.2.111
HEAD (FT ABOVE MSL)
4100
4000
3900
3800
LOC. 72
30
40
50
60
70
80
TIME (YRS SINCE 1900)

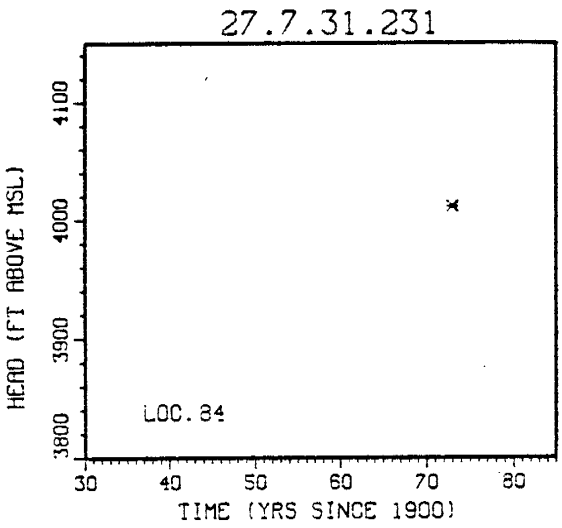
27.7.31.231
HEAD (FT ABOVE MSL)
4100
4000
3900
3800
LOC. 84
30
40
50
60
70
80
TIME (YRS SINCE 1900)

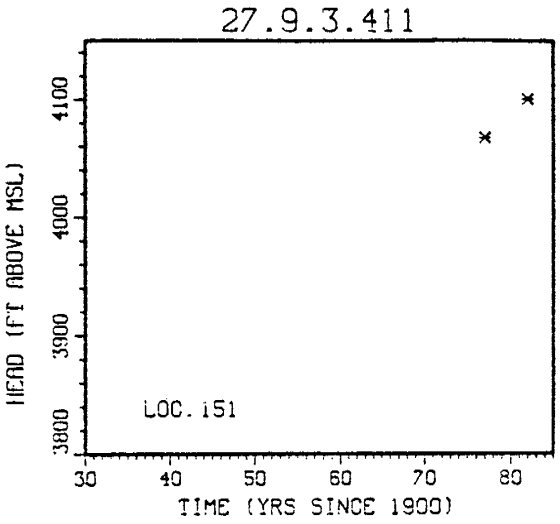
27.9.3.411
HEAD (FT ABOVE MSL)
4100
4000
3900
3800
LOC. 151
30
40
50
60
70
80
TIME (YRS SINCE 1900)

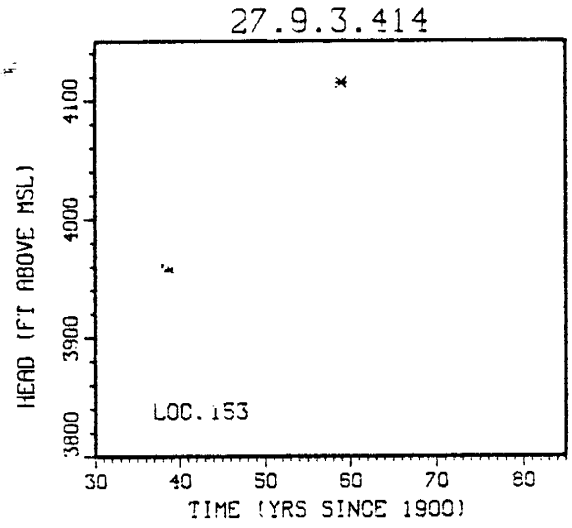
27.9.3.414
HEAD (FT ABOVE MSL)
4100
4000
3900
3800
LOC. 153
30
40
50
60
70
80
TIME (YRS SINCE 1900)

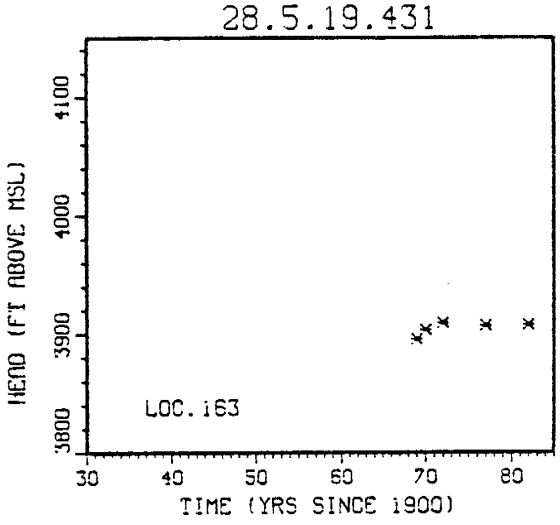
28.5.19.431
HEAD (FT ABOVE MSL)
4100
4000
3900
3800
LOC. 163
30
40
50
60
70
80
TIME (YRS SINCE 1900)

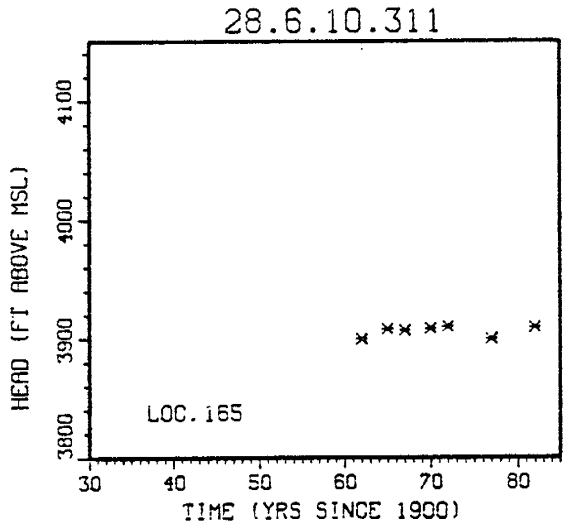
28.6.10.311
HEAD (FT ABOVE MSL)
4100
4000
3900
3800
LOC. 165
30
40
50
60
70
80
TIME (YRS SINCE 1900)

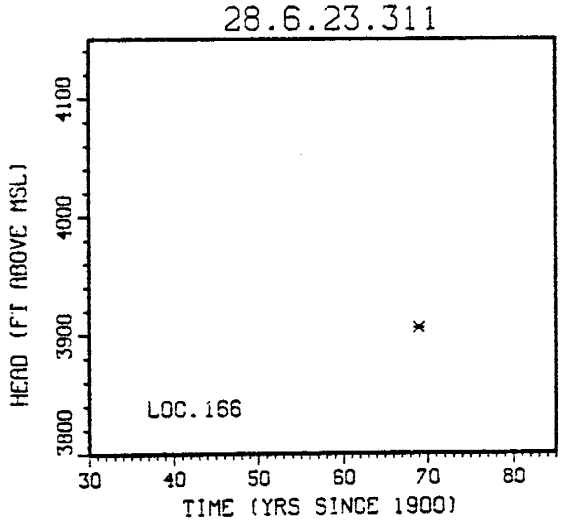
28.6.23.311
HEAD (FT ABOVE MSL)
4100
4000
3900
3800
LOC. 166
30
40
50
60
70
80
TIME (YRS SINCE 1900)

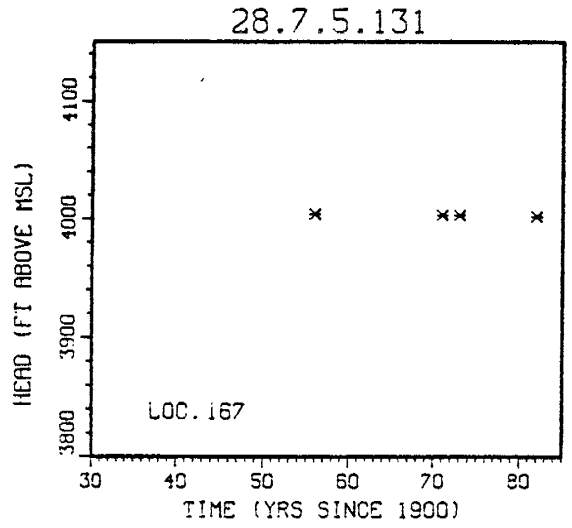
28.7.5.131
HEAD (FT ABOVE MSL)
4100
4000
3900
3800
LOC.167
30
40
50
60
70
80
TIME (YRS SINCE 1900)

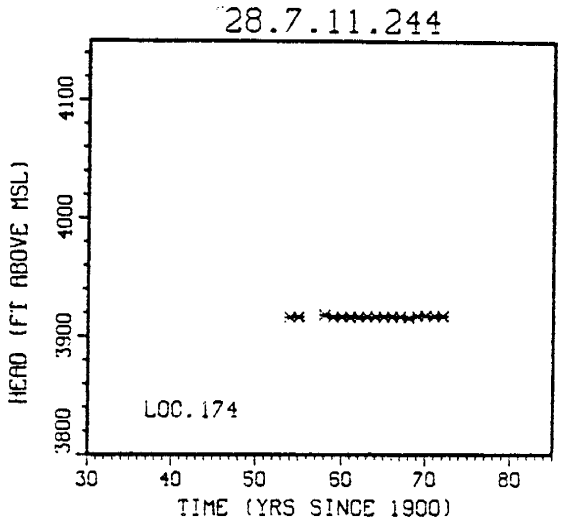
28.7.11.244
HEAD (FT ABOVE MSL)
4100
4000
3900
3800
LOC.174
30
40
50
60
70
80
TIME (YRS SINCE 1900)

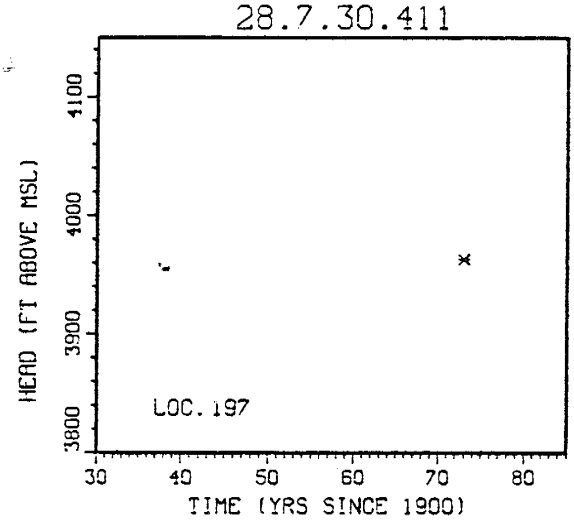
28.7.30.411
HEAD (FT ABOVE MSL)
4100
4000
3900
3800
LOC.197
30
40
50
60
70
80
TIME (YRS SINCE 1900)

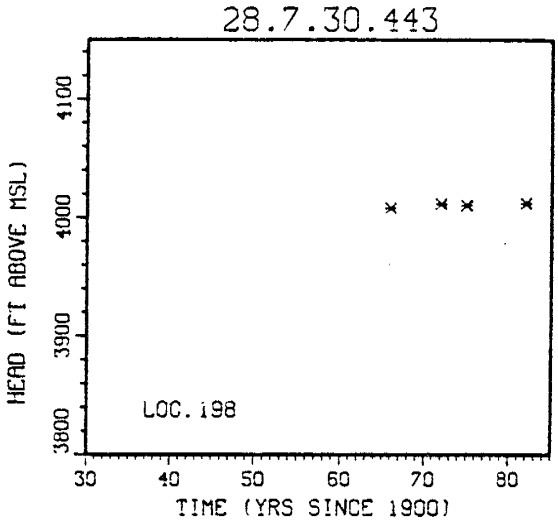
28.7.30.443
HEAD (FT ABOVE MSL)
4100
4000
3900
3800
LOC.198
30
40
50
60
70
80
TIME (YRS SINCE 1900)

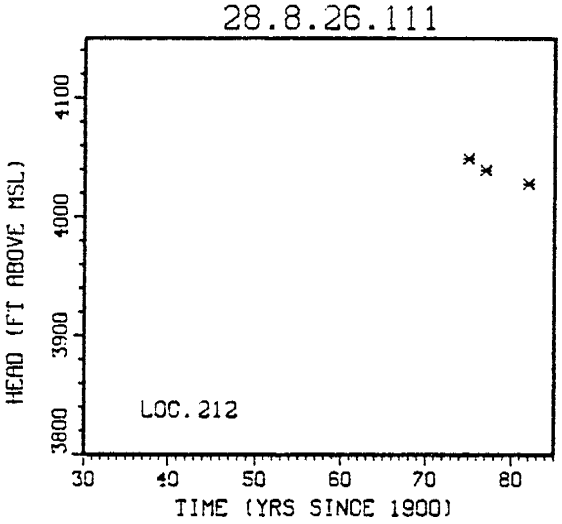
28.8.26.111
HEAD (FT ABOVE MSL)
4100
4000
3900
3800
LOC.212
30
40
50
60
70
80
TIME (YRS SINCE 1900)

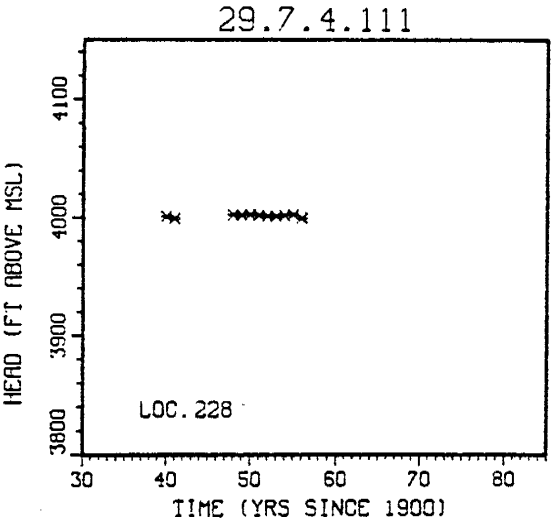
29.7.4.111
HEAD (FT ABOVE MSL)
4100
4000
3900
3800
LOC.228
30
40
50
60
70
80
TIME (YRS SINCE 1900)

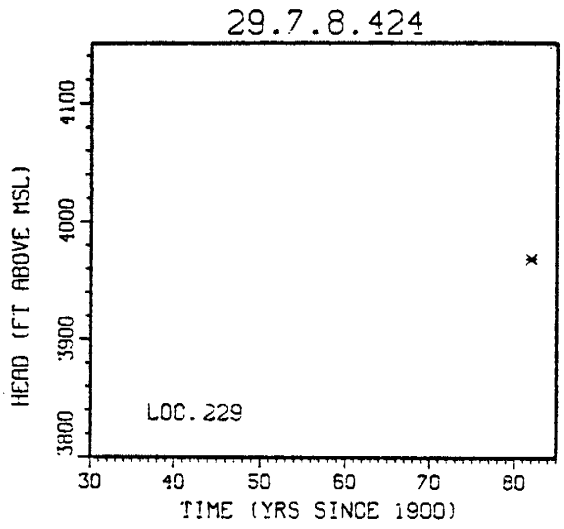
29.7.8.424
HEAD (FT ABOVE MSL)
4100
4000
3900
3800
LOC. 229
30
40
50
60
70
80
TIME (YRS SINCE 1900)

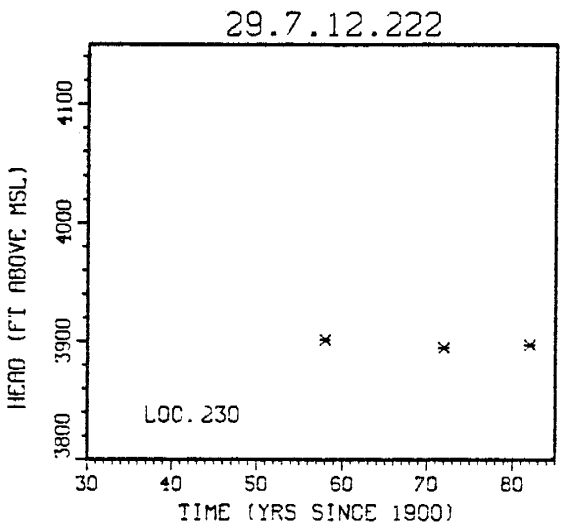
29.7.12.222
HEAD (FT ABOVE MSL)
4100
4000
3900
3800
LOC. 230
30
40
50
60
70
80
TIME (YRS SINCE 1900)

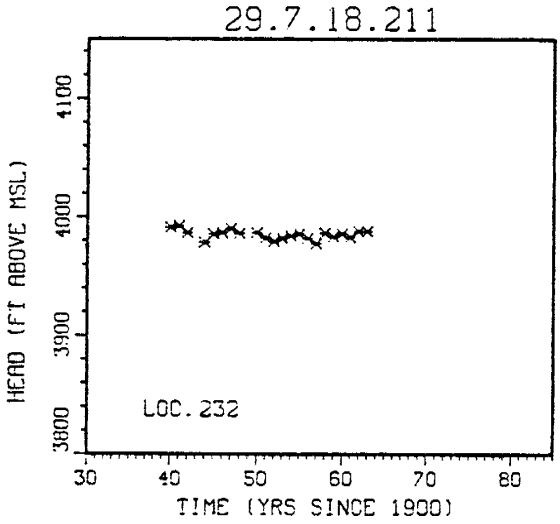
29.7.18.211
HEAD (FT ABOVE MSL)
4100
4000
3900
3800
LOC. 232
30
40
50
60
70
80
TIME (YRS SINCE 1900)